Durability and Adhesion of a Model Epoxy Adhesive Bonded to Modified Silicon Substrates

Dingying Xu

Dissertation submitted to the Faculty of the
Virginia Polytechnic Institute and State University
in partial fulfillment of the requirements for the degree of

Doctor of Philosophy
in
Chemistry

John G. Dillard, Chairman
David A. Dillard
Alan R. Esker
Thomas C. Ward
James E. McGrath

June 10, 2004
Blacksburg, VA

Keywords: epoxy, silicon surface modification, silane coupling agent, probe test, durability, adhesion, plasma treatment, X-ray photoelectron spectroscopy, failure analysis

Durability and Adhesion of a Model Epoxy Adhesive Bonded to Modified Silicon Substrates

Dingying Xu

Abstract

The adhesion and durability of model epoxy/silane/SiO_2/Si bonded systems were investigated under various conditions, including the type of surface preparation, pH of the environmental media, temperature, cyclic thermal stress, and external applied stress. The fundamental debond mechanism was studied for bonded systems exposed to selected environments. The bond failure mode was characterized by examining the failed bond surfaces using X-ray photoelectron spectroscopy.

The effectiveness of combining the oxygen plasma treatment and silane coupling agent (SCA) derivatization in adhesion promotion for an epoxy bonded to a silicon surface was evaluated in this research. SCAs with different amine functionalities were studied. The oxygen plasma treatment time was varied systematically to achieve a different extent of oxidation on the Si wafer. The surface chemistry/composition of various silane derivatized Si surfaces was investigated. The studies revealed that SCA interaction with the Si surface was enhanced by the oxygen plasma pre-treatment of the Si substrates. XPS surface analysis results showed that the SCA/SiO_2 ratio did not correlate strongly with the increase in oxygen plasma pretreatment time. However, for Si surfaces treated for longer oxygen plasma pretreatment times, more silanol groups may be available to interact with the hydrolyzed silanol groups on silane, resulting in a stronger SCA-Si attachment.

Three different tests were employed to determine adhesion and durability of the model epoxy/SCA/SiO_2/Si bonded specimens. The immersion test qualitatively evaluates the bond durability for various systems exposed to different chemical and thermal conditions. Second, a novel probe test was used to quantitatively determine adhesion under critical debonding conditions for bonded specimens with different SCA preparations. A general trend of bond durability varied in the manner SCA-2 > SCA-3 > SCA-1 > no silane. Bond durability also increased for samples: model epoxy/SCA modified/O_2 plasma treated/Si as the oxygen plasma pre-treatment time increased. Third, bond durability was studied using the wedge DCB (double cantilever beam) test under subcritical debonding conditions with environment-assisted crack growth as a function of applied strain energy release rate. Higher crack velocity and the absence of a $G_{threshold}$ value were noted in tests at 70 ^{o}C. The $G_{threshold}$ value increased as the strength of the interface increased and as the chemical aggressiveness of the environment decreased. For tests involving 25 ^{o}C -70 ^{o}C thermal cycling, only limited crack growth was found.

DEDICATION

to

My parents

Peiyuan and Fengmei Xu

ACKNOWLEDGEMENTS

Much gratitude is owed to my committee members for their help with this endeavor. I would like to thank Dr. John Dillard, Dr. David Dillard, Dr. Thomas Ward, Dr. James McGrath, and Dr. Alan Esker for all that they have taught me through my graduate studies at Virginia Tech. I especially thank my advisor, Dr. John Dillard, for his guidance and support; knowing him has improved me as a researcher and as a person.

Many thanks are expressed to the Hewlett-Packard Corporation for the financial support to fund my graduate research. Support from HP also allowed me to attend many outstanding conferences, from which I have benefited personally and professionally. I would also like to thank Dr. Paul Reboa and Dr. Ellen Chappell at HP who provided the necessary materials for the research, as well as for meaningful discussions and suggestions. Thanks also go to members of the VT-HP project, Dr. M. Sankarapandian, Dr. Kai-tak Wan, Dr. Zuo Sun, and Dr. Shu Guo, for their help with various aspects of my research. In addition, I wish to thank Greg Fritz, who conducted the cyclic temperature studies in the summer 2003 as a summer undergraduate research student.

Special thanks go to Mr. Frank Cromer, whose patience and help with surface analytical instrumentation and data analysis has been invaluable. Mr. Jim Coulter in the electronics shop is also acknowledged for his help with a number of electronics-related issues. The members of the Physics Machine Shop, Melvin Shaver, Fred Blair, John Miller, are much appreciated for many fabrication related needs. The secretaries, Esther Brann, Laurie Good, Tammy Jo Hiner, Sheila Collins, Agness Chandler, and Roberta Gilbert are thanked for their help over the years.

I would like to express thanks to many former and current colleagues, who have not only provided help with my research, but also made my time in Blacksburg most enjoyable. For some, their friendship will be forever remembered. Thanks go to (in no particular order): Dr. Ronald DiFelice, Dr. Sumitra Subrahmanyan, Dr. Qin Lin, Dr. Sandra Henderson, Dr. Emmett O'Brien, Ms. Elizabeth Neyman, Ms. Lei Zeng, Mr. Jianjun Deng, Dr. ChangHui Lui, Mr. Min Mao, Mr. Zengyu Huang, and Mr. Hitendra Singh.

Next to last, but certainly not the least, I express the utmost thanks to my parents, Dr. Peiyuan and Fengmei Xu who believed in me, encouraged me and supported me through good and bad times. Also, I would like to thank my girl friend, Ms. Xiaodong (Jane) Wang for her support for the past two years as we both worked toward the final goal.

Finally, I would like to thank the fabulous New River that provided me with many memorable fishing moments which I will miss dearly.

TABLE OF CONTENTS

LIST OF FIGURES

LIST OF TABLES

1. Introduction

Epoxy based polymer networks have been widely used in microelectronics as encapsulation materials for semiconductor devices because of excellent heat, moisture, solvent, chemical resistance, superior adhesion, electrical and mechanical properties[1-3]. To achieve optimum adhesive durability, it is often necessary to modify the as-received substrate. Silane coupling agents (SCAs) improve bonding between polymers and inorganic oxide surfaces, resulting in greater durability and resistance to water attack at the interface[4]. In this work, the effect of surface modification of silicon wafers on adhesion to epoxy polymers has been studied. The surface modification was accomplished by pretreating the Si substrates in an oxygen plasma to enhance the silane deposition. The silane coupling agents included SCA-1 (a trialkoxy silane with primary amine functionality), SCA-2 (a trialkoxy silane with secondary amine functionality), and SCA-3 (a trialkoxy silane with two secondary amine functionalities). Silylation reactions using such silanes have been reported previously for surfaces such as silica or glass[4]. The interactions of the organofunctional groups in these silanes with epoxy polymers were also documented[5-8]. The current study focused on the adhesion and durability of epoxy-silicon bonded systems immersed in water-solute mixtures maintained at various temperatures up to 70 ^{o}C (static) and cyclical immersion at 25 ^{o}C and 70 ^{o}C.

Two types of surface modification methods were investigated. Sol-gel reactions of organosilanes on silicon surfaces occur *via* the formation of a Si-O-Si bond between the hydrolyzed silane molecules and the surface silanol groups[9]. A silane-modified surface exhibited improved wetting characteristics if polar functionalities such as amino groups were present[10]. However, the sol-gel reaction suffered in that the siloxane bonds between silane and the inorganic oxide surfaces were hydrolyzed in the presence of water. The hydrolysis of siloxane silicon bonds was reversible, and some indirect evidence suggested that hydrolysis and siloxane formation were in a true equilibrium at different pH values[10].

Surface modification by plasma polymerization also improves adhesion between polymers and metal substrates[11]. Given the choices, a wide variety of vinyl monomers, saturated hydrocarbons or organosilanes, coupled with optimized plasma reaction conditions, may be polymerized to yield highly crosslinked, and coherent thin films. These films act as adhesion promoters as demonstrated in certain systems[12,13].

1.1 Surface, Interface, and Interphase

It is important to address three questions before discussing adhesion principles. What is a surface? What is an interface? or What is an interphase? The first two terms can be defined together. The most comprehensive statement is to say that a surface or interface exists in a system in any case where there is an abrupt change in the system properties with distance[14]. Such properties can be density, crystal structure, crystal orientation, chemical composition, etc. The degree of abruptness of the change in system properties defines the interface. The interface can be viewed in two extreme cases. One, is a crystalline solid in contact with its own vapor at low temperature. In this case, the interface is effectively one atomic or molecular layer thick. Second, is a liquid in contact with its own vapor at high temperature and pressure. In this case, the thickness of the interface approaches infinity as the critical point is approached. A real surface or interface exists along a predetermined plane of atoms with relaxation allowed to reach its equilibrium configuration[15].

Consider the interphase. An interphase may be defined as a region of materials whose chemical or physical structures have been modified because of contact between two phases[16]. In the realm related to adhesives and adhesion, Sharpe[17] defined the interphase as a transition zone between the surface of a substrate (adherend) and the bulk of a polymer (adhesive) that is in contact with the substrate. Unfortunately, the boundaries and thickness of the interphase are difficult to define. Perhaps, it is more appropriate to state that an interphase is a gradient away from the surface of a bulk phase or between two bulk phases.

1.2 Adhesion Theories

Five contemporary theories of adhesion are physical and chemical adsorption, diffusion, electrostatic, and mechanical interlocking[18]. The physical adsorption theory states that molecular forces arising from primary and secondary interactions are responsible for adhesion[18]. Furthermore, materials adhere because of the interatomic and intermolecular forces that are established between the substrate and the adhesive[19]. Assuming that there is intimate interfacial contact, good adhesion is often the result of van der Waals interactions[20].

The adsorption theory invokes the formation of covalent, ionic or hydrogen bonds across the interface[18]. The use of adhesion promoters best illustrates this theory in that they improve adhesion between organic and inorganic substrates by forming primary chemical bonds with the surface. Acid-base interactions, especially electron donor (Lewis base)-electron acceptor (Lewis acid) interactions also play an important role in interfacial energy and adhesion.

The diffusion theory applies principally to polymer-polymer adhesive bonds. It asserts that adhesion is a result of the interdiffusion of the chains of one polymer into the chains of another[21]. Such interdiffusion will occur only if the polymer chains are mobile (i.e. the temperature must be above the glass transition temperature of the polymer) and compatible.

The electrostatic theory contends that if two metals are placed in contact, electrons will be transferred from one to the other thus forming an electrical double layer, which gives the force of attraction[18]. Because most polymers are insulators, this theory accounts for adhesion in only a few special cases.

The mechanical interlocking theory asserts that adhesion is a result of an adhesive interlocking into the irregularities of the adherend surface. Improvements in adhesion result from increased interfacial area[18]. Mechanical interlocking on a micro scale is

evident *via* the penetration of adhesive into the porous oxide of an anodized aluminum surface[22].

1.3 Surface Cleaning of Semiconductor Materials

Surface cleaning of semiconductor surfaces is of paramount importance for adhesion in these systems. Cleaning is needed because the semiconductor oxide surface rapidly absorbs hydrocarbons[23] and other gaseous substances. These organic contaminants create a weak boundary layer on the oxide surface and lower the surface energy. Surface cleaning, that is, the removal of organic contamination as well as particles from the surface, is essential for improving adhesion. In some cases, it is also necessary to remove the native oxide surface layer to expose a virgin substrate material to ensure success in subsequent surface modification steps. A large body of literature describes various methods and processes for cleaning semiconductor substrates[24-27]. Basic aqueous solutions with the addition of oxidizers are used to remove organic surface contaminants[28]. Acidic formulations also work effectively[24]. To remove the native oxide on silicon, fluorine-containing reagents are used for etching in aqueous solution or in the gas phase[25-27]. However, wet chemical cleaning methods suffer from environmental concerns with materials handling and disposal, and the fact that such cleaning procedures often leave trace amounts of residue on the surface presents additional problems for downstream processes.

Ablation, or plasma etching, is distinguished from cleaning only by the amount of material that is removed. Plasma etching using oxygen or fluorine-containing gases or gas mixtures is an effective way to remove surface organic contaminants and the native oxide layer in a controlled fashion[29]. On the other hand, plasma treatments can be used to modify the surface chemistry. For example, oxygen atoms and high energy oxygenated radical species can react with the surface, yielding a surface with high surface energy and improved wettability.

1.4 Use of Epoxy Polymers in Microelectronic Devices

Epoxy resins are widely used for coating and encapsulating electric circuit components and electronic devices. The epoxy serves to isolate a device from adverse environmental effects such as moisture, solvents, microorganisms, and mechanical stresses which often lead to adhesion failure that causes device failure. In the past 10 to 20 years, epoxy resins have been widely used in microelectronics packaging. Epoxies provide isolation between closely packed (less than micron spacing between features) and usually fragile electrical elements with good adhesion, stress and thermal expansion properties to either the substrates or other elements[1].

Epoxy resins possess a number of physical properties suitable for electrical and microelectronics applications, including good adhesion to metals and silicon, low permeability or water absorption (typically 0.1% to 0.25%), great stability against harsh chemicals and solvents, and the ability to inhibit corrosion at the surface and interface[2]. Epoxy resins also fulfill other requirements for microelectronics packaging, namely their low viscosity prior to curing, low stress resistance that develops between the electronic components and the epoxy resin, low heat of reaction (i.e., curing) and high thermal conductivity to prevent possible damage to the device under protection, and minimum effects of aging[2]. All of these make epoxy resins ideal candidates for encapsulating materials and packaging for microelectronics devices. In addition, the highly crosslinked nature of some epoxy systems allows the development of high aspect ratio features with sharp lines when used as photoresists for sub-micron features[30].

1.5 Plasma Surface Modification

1.5.1 Plasma Parameters

The term plasma describes the state of ionized gas (e.g., glow discharge), which consists of positively charged molecules and atoms, negatively charged ions, and electrons[31]. The plasma state can be created in a number of ways. The term hot plasma

refers to the gaseous complex of ionized molecules and atoms at temperatures greater than 10,000 K. Cold plasmas are created by a form of excitation energy such as an electric glow discharge. The commonly used plasma generation devices include low-pressure electrical discharges, Penning plasma discharges, microwave generated plasmas, radio frequency (RF) capacitive discharges, and RF inductively coupled (IC) plasma devices.

The major advantages of RF plasma generators are that no internal electrodes are needed, the plasma is easily sustained at a low pressure (< 50 mTorr) and the plasma achieves high ionization efficiencies[32]. A schematic illustration of a RF plasma reactor is shown in Figure 1-1. Because there are no internal electrodes, no impurities are sputtered from the electrodes to become incorporated into the growing deposited film. Within the plasma generator, energy from the radio frequency source is transferred by the electric field to free electrons, which collide with molecules, atoms, and surfaces. Inelastic electron collisions with molecules generate more electrons, ions, free radicals, and molecules in excited states. Charged species generation is possible because each electron carries an energy of 1-10 eV. This energy is sufficient to induce ionization and to break most covalent bonds[33]. The electrons do not achieve thermodynamic equilibrium with gas molecules in low-pressure cold plasmas. As a result the temperature of the gas molecules is near ambient. Some representative types of electron-atom/molecule reactions in plasmas are given below.

Excitation: $e + A \rightarrow e + A^*$ $e + A_2 \rightarrow A_2^* + e$ $e + AB \rightarrow e + AB^*$

Dissociative Attachment: $e + AB \rightarrow A + B^-$ $e + A_2 \rightarrow A^+ + A^- + e$ $e + AB \rightarrow A^+ + B^- + e$

Dissociation: $e + A_2 \rightarrow 2A + e$ $e + AB \rightarrow e + A + B$

Ionization: $e + A_2 \rightarrow A^+ + A + 2e$ $e + AB \rightarrow 2e + A^+ + B$

Ion-Ion Reaction: $A^+ + B^- \rightarrow AB + h\nu$ $A^+ + B^- \rightarrow A^* + B^* + h\nu$

Ion-Molecule Reaction: $A^+ + B \rightarrow AB^+$ or $A + B^{+\cdot}$ $A + B^- \rightarrow AB^-$ or $A^- + B$

Each of the energetic species is very reactive with other species, and with any surface exposed to the plasma.

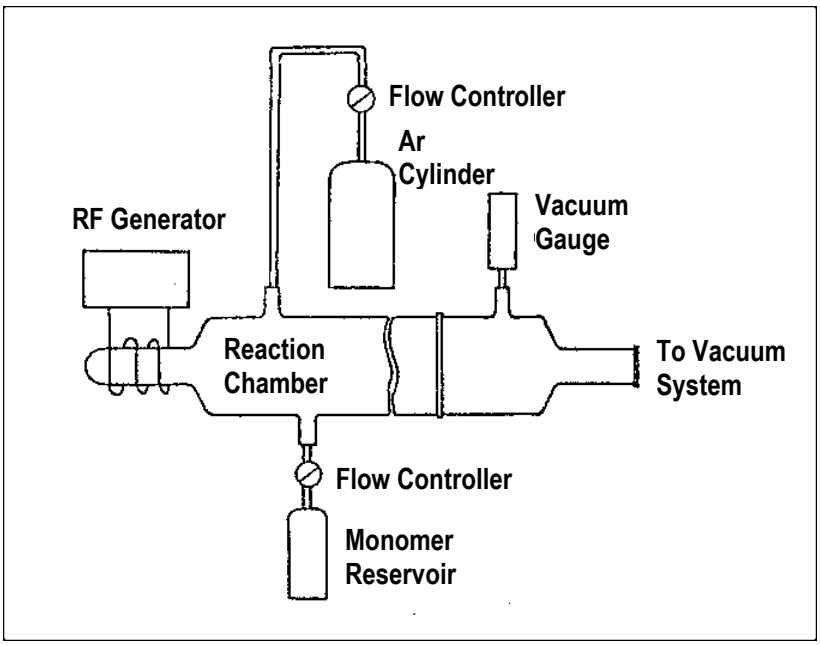

Figure 1-1. A schematic illustration of a common RF plasma reactor (adapted from reference 34).

1.6 Sol-Gel Surface Modification

Organosilanes have been widely used in the coatings and microelectronics industry because of their unique electronic, optical and adhesion promoting properties[35]. Surface modification reactions with organosilanes utilize the sol-gel processing technique. Thin films of silanes are deposited onto various metal or semiconductor surfaces in their hydrolyzed sol form *via* processes such as spin coating or dip coating. These procedures require volatile organic solvents in the reaction media.

1.6.1 Sol-Gel Science and Technology Overview

Much of the emergence of sol-gel technology over the past half-century is related to the application of wet chemical methods in the synthesis of ceramics[36-38]. However, this technology can be traced to the dawn of man, as glass production is depicted on the walls of ancient Egyptian tombs near Thebes (1700-3000 B.C.). Today, sol-gel processing is actively studied in both academia and industry, as a new and potentially powerful technique for the preparation of high performance materials. In the past 10 to 20 years, all types of thin films and coatings with novel optical and electrical properties, silica glass, organic-inorganic hybrid materials, as well as nanocomposites, have been prepared *via* sol-gel processing of different precursor materials[39].

To appreciate all of these technological developments, one must understand what sol-gel encompasses. Brinker and Scherer defined sol-gel as "the preparation of ceramic materials by preparation of a sol, gelation of the sol, and the removal of the solvent."[40] A sol is a fluid, a colloidal dispersion of solid particles in a liquid phase where the particles are sufficiently small to remain suspended by Brownian motion. A gel is a solid consisting of at least two phases wherein a solid phase forms a network that entraps and immobilizes a liquid phase. This definition mirrors the statement by Flory[41], that for a polymer system, the gel point occurs at a critical extent of (a network) reaction when there exists at least one large molecule of macroscopic dimensions and "infinite" molecular weight. Further reaction may occur beyond the gel point in which crosslink density may increase and molecules remaining in the sol fraction may react into the network structure. The term "sol-gel" has become much more broadly applied in the literature and refers to systems containing neither true sols nor true gels[40].

In the sol-gel process, the aqueous or alcoholic reaction solution usually contains precursors such as metal alkoxides, metal salts, or metal complexes. Metal alkoxides are employed as high purity solution precursors in the sol-gel process. Many metal alkoxide molecules can react with water through a series of hydrolysis and condensation steps in the presence of a catalyst to yield metal oxide or oxy-hydroxide gel. Sol-gel processing

allows the formation of fibers, films or composites and is commonly accompanied by techniques such as spinning[42], dip-coating[43], or impregnation[44]. Figure 1-2 shows a schematic overview of the sol-gel process. The sol-gel reaction has been most intensely studied in the hydrolysis of alkoxy silanes to yield silica[40,45], although, the reaction of transition metal oxide precursors has also been reported[46,47].

The advantage of the sol-gel process is that it provides the potential for achieving a tailor-made chemistry of the products. The polycondensation reaction can take place in the reaction mixture at much lower temperature[40] than conventional melt processing. Because thin films usually result from a sol-gel reaction, sol-gel processing has become a versatile way of modifying the surface of various bulk materials.

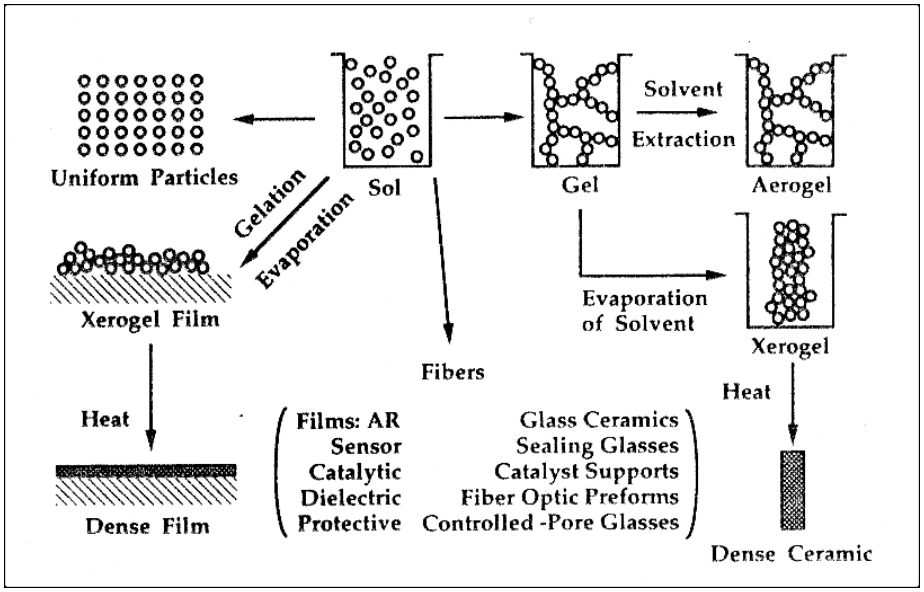

Figure 1-2. A schematic overview of the sol-gel process (adapted from reference 40).

1.6.2 Details of Sol-Gel Chemistry

The sol-gel reaction occurs when a metal alkoxide reacts with water to form a metal hydroxide which condenses to form a metal-oxygen-metal bond. Water and alcohol are liberated as byproducts. The oxides of early transition metals such as Ti, V, Zr, and

Group 13 metals (B and Al) generally exhibit greater chemical reactivity than silicates[48] due to the lower electronegativity of the metal and its ability to exist in several coordination states. Thus coordination expansion occurs spontaneously upon reaction with water or other nucleophilic reagents.

The sol-gel reaction involving silicates can be described in two steps. The first step, the hydrolysis step, is illustrated in Equation 1-1

$$\equiv\text{Si-OR} + \text{H}_2\text{O} \rightarrow \equiv\text{Si-OH} + \text{ROH} \qquad \textbf{Equation 1-1}$$

where "≡Si-" represents a Si atom with a tetrahedral bond geometry, R is an alkyl group, C_xH_{2x+1}, and the nature of the R group plays a role in the rate of the hydrolysis reaction (i.e., bulkiness, steric factors). Generally, the smaller the size of the R group, the faster the hydrolysis rate. For example, tetramethoxylsilane undergoes hydrolysis faster than tetraethoxysilane, under the same reaction conditions.

The second step in the sol-gel process is the polycondensation step, which can take place through either of the two reaction schemes shown below

$$\equiv\text{Si-OR} + \text{HO-Si}\equiv \rightarrow \equiv\text{Si-O-Si}\equiv + \text{ROH} \qquad \textbf{Equation 1-2}$$

$$\equiv\text{Si-OH} + \text{HO-Si}\equiv \rightarrow \equiv\text{Si-O-Si}\equiv + \text{H}_2\text{O} \qquad \textbf{Equation 1-3}$$

Note that both reactions produce siloxane bonds (Si-O-Si) and the by-products, alcohol (ROH) or water. Under most conditions, condensation commences (Equation 1-2 and Equation 1-3) before the hydrolysis (Equation 1-1) is complete. Because water and alkoxysilanes are immiscible, a mutual solvent such as alcohol is normally added as a homogenizing agent. Three (or two) other reactive sites on silicon (not shown in the above schemes) may also undergo a hydrolysis reaction yielding species that eventually participate in network formation.

1.6.3 Silane Coupling Agents

Silane coupling agents were developed as materials that promote adhesion between minerals and organic phases. Specifically, Plueddemann[4] defined them as "materials that improve the chemical resistance (especially to water) of the bond across an interface." He further stated that although any polar group on the polymer will help to promote adhesion, the use of organofunctional silane coupling agents appears to induce optimal adhesion. Today, large quantities of silane coupling agents are available commercially as interfacial adhesion promoters. The silane coupling agent typically possesses the general structure X_3-Si-$(CH_2)_n$-Y, where X is a hydrolyzable group such as methoxy or ethoxy, Y is an functional group (e.g., NH_2 or epoxide) and most commonly n = 0-3. Silane coupling agents generate a water-resistant interface between the organic polymer and the inorganic substrate, as they are able to react or interact with both the substrate and the polymer[49,50]. Most often, silane coupling agents are applied as a dilute aqueous solution or an alcohol solution. Typically using a 0.25 to 5 weight percent silane solution to modify a surface results in monolayer to several multilayers of coverage[51]. The alkoxy groups in the silane molecule undergo hydrolysis and oligomerization in the solution and interact with substrates through hydrogen bonding to surface hydroxy groups, and subsequently condense to form a siloxane network (as noted in Figure 1-3, for the reaction on glass)[9].

1.6.4 Surface Modification by Sol-Gel Reactions of Organosilanes

One of the most technologically important aspects of sol-gel processing is that, sol-gel processing is superior to conventional coating methods in its ability to control precisely the surface chemistry and microstructure of the deposited film[40]. This feature makes sol-gel processing a potentially attractive method for surface modification of bulk material surfaces to achieve targeted surface properties. Sol-gel processing finds extensive use in oxide coatings on glass on siliceous substrates as antireflective (AR) surfaces in solar related applications to improve device efficiency[52-54] and as laser-damage-resistant AR coatings for laser optics,[55,56] ferroelectric films based transition

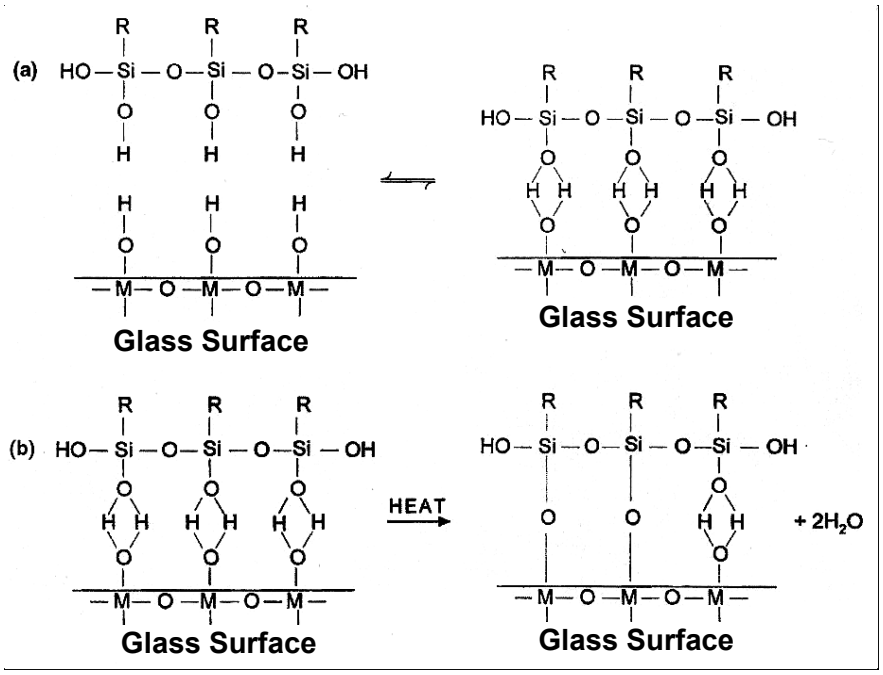

Figure 1-3. Alkoxysilane coupling agents on a glass surface: (a) hydrogen bonding with silanol groups; (b) surface hydrogen bonding and covalent bond formation (adapted from reference 9).

metal oxide gels,[57,58] abrasion and corrosion resistant coatings,[59,60] and adhesion promoting applications[4]. Only the topic of adhesion promotion by sol-gel processing will be reviewed in detail due to its relevance to the goal of this research.

One of the major methods of adhesion promotion for siliceous surfaces is by a silylation reaction. It is commonly carried out *via* sol-gel processing. Silylation is the displacement of an active hydrogen (usually in a hydroxy group) by an organosilyl group[4]. A major application for silylated surfaces has been in modifying glass fibers and fillers for preparation of organic polymer composites. The silylation reaction is also used to impart hydrophobicity or organic functional groups on inorganic surfaces. The silylating materials may act as a means of bonding organic materials (i.e., polymer) to oxide surfaces to obtain the advantages of reactive groups on a stable, insoluble substrate. The silylating material is commonly an organosilane molecule. Once silylated, it is

designed to be resistant to removal from the surface by organic solvents or water. The resistance to water is normally realized when oligomerization or polymerization starts to form the siloxane network. The deleterious effects of water on the adhesion properties of the polymer-metal (untreated) bond have been extensively studied[61]. Diffusion and subsequent reaction of water at the polymer-metal oxide interface are responsible for interfacial delamination.

The silyalation reaction of a generic trialkoxy silane molecule on a glass surface proceeds through interaction of oligermized silanes with surface hydroxy groups *via* hydrogen bonding. Subsequent condensation reactions generate the siloxane bond to the surface (see Figure 1-3). Tripp et al.[62] have demonstrated that for some silane systems, lateral polymerization also occurs to form a network. The siloxane film formed on the glass substrate commonly consists of multiple layers[63,64].

Although the above scheme of silane adsorption/reaction on a glass surface appears straightforward, the application of silane coupling agents is still viewed as a "black art", largely because the nature of bonding between silanes and metal oxide surfaces is not completely understood. Ondrus et al.[65] monitored thin film formation by γ-aminopropyltrialkoxysilane (APS) on iron, titanium, aluminum (1100) and aluminum (2024) substrates by FTIR spectroscopy. The substrate was immersed in the aqueous solution of APS for 1 min. When dried at 110 ^{o}C, the films formed on iron, titanium, and aluminum (1100) substrates exhibited an increased extent of polymerization. However, films formed on aluminum (2024) substrates were oxidized to an imine as evidence by the shift of an IR band from 1600 cm^{-1}(NH_2) to 1660 cm^{-1}(CN). The results showed that the type of oxide layer on the metallic substrate significantly influenced silane adsorption. Esumi et al.[66] showed that the orientation of γ-aminopropyltriethoxy silane was controlled by solution pH. The thin film formed was stable as long as the pH was between the isoelectronic point of the oxide surface and the pK_a of the ionizable silane group. In alkaline solution, adsorption occurs through the amino groups, generating a less stable interface, whereas in an acid solution γ-aminopropyltriethoxysilane deposited on

the surface by forming siloxane linkages. Surface sensitive analytical techniques, such as X-ray photoelectron spectroscopy were used to study γ-aminopropyltriethoxysilane adsorbed onto a silica surface[112]. Two components in the N 1s XPS spectra were observed and could be attributed to free and protonated amino groups[67]. Treating the surface with acidic or basic solution converts some of the amino groups from protonated to unprotonated forms; however, some amino groups remain irreversibly protonated, whereas others remain irreversibly free (unprotonated)[68].

Plueddemann[4] concluded that in practice, monolayer coverage of silanes on substrates is rarely observed. Multilayers with thicknesses <100 Å are more commonly achieved and are sufficient to provide marked improvements in interfacial adhesion in a polymer-metal bond. An example is provided by Belton and Joshi[69], where they demonstrated on a polyimide coated silicon wafer with APS employed as the adhesion promoter, that the time required for removal of the polyimide film increased fourfold as the silane thickness increased from a monolayer to about 10 monolayer equivalents. The thickness of a silane film on a metal surface depends on the nature of the organofuctional groups on silicon, the availability of water, pH and the age of the silane solution, topology of the surface, and the presence or absence of specific catalysts[69].

Infrared and Raman spectroscopy have been extensively used to study the nature of silane absorption on various siliceous surfaces[6,70-73]. Koenig and Shih[70] used argon-ion-laser excited Raman spectroscopy to study the reaction of vinyltriethoxysilane (VTES) on glass fibers and micro beads. Siloxane bond formation (Si-O-Si) on the glass surface was detected at 788 cm^{-1}, the frequency shifted to 783 cm^{-1} after boiling the treated glass for 2 hours in water. The absorption at 783 cm^{-1} corresponded to siloxane homopolymer. The absorption frequency shifted to 788 cm^{-1} again after redrying the glass at 100 ^{o}C. These results indicated that covalent bond formation of VTES to glass is reversible in the presence of water. Koenig et al.[71,72] using FT-IR spectroscopy, demonstrated the reversible nature of silanol condensation and rehydrolysis of silanes deposited on glass fibers. The response of vinylsilanols and cyclohexylsilanols was

compared. The FT-IR investigation[6] also verified the existence of the free NH_2 group and the H^+ bonded NH_2 group from the APS film formed in aqueous solution on glass fibers. This result shows again that the APS molecule can either bond with the surface hydroxy groups *via* Si-OH or *via* the amino group. The hydrolytic stability of silane films was studied by desorption from glass surfaces in water at elevated temperature. Silanol formation in water was monitored using FT-IR[73]. Figure 1-4 shows that there is generally a threshold period during which no silane desorption takes place. Rosen and Goddard[74] observed that the desorbing behavior of silane is due to differences in the structure of the siloxane film. Siloxanes have small alkyl substituents (methyl, vinyl, propyl) that condense into highly cross-linked insoluble siloxane films. Siloxanes having larger organic groups on silicon are more highly cyclized and less highly cross-linked, and are therefore more susceptible to desorption in water. Silanes substituted with higher hydrocarbon (hexyl, phenyl, cyclohexyl, octyl) siloxanes are insoluble in water and are not desorbed in water during the first few hours; however, long term desorption experiments were not carried out by Rosen and Goddard[74].

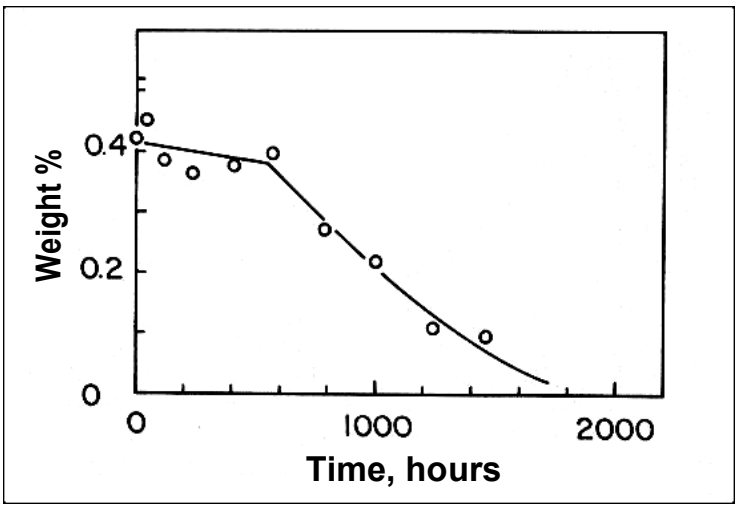

Figure 1-4. The desorption curve of vinyltriethoxysilane adsorbed on glass fibers from 0.4% by weight aqueous solution, at 80 ^oC in water (adapted from reference 73).

Organosilanes are also capable of improving adhesion to polymer resins through the interaction of the organofucntional group with the reactive resin functionalities. In some cases, bonding of polymer resins to a silane was also improved where no chemical reactions could be expected[75-78]. Adhesion improvement *via* a chemical reaction was demonstrated for bonding between polyimide coatings and inorganic substrates (i.e., silicon wafers) using γ-aminopropyltriethoxysilane as the adhesion promoter. The amino group of APS is expected to participate in the thermal imidization of the polyamic acid. The schematic representation of the aminosilane-polyimide adhesion reaction is shown in Figure 1-5. Linde and Gleason[75] observed imide bond formation at the APS/PAA interface (APS thickness <100Å) upon thermal exposure to elevated temperatures. Greenblatt et al.[76] studied adhesion improvement in the PMDA-ODA acid/SiO_2 system using aminosilane adhesion promoters such as $NH_2(CH_2)_3Si(OMe)_3$, $MeNH(CH_2)_3Si(OMe)_3$, $Me_2N(CH_2)_3Si(OMe)_3$, and $Me(CH_2)_3Si(OMe)_3$. They noticed a decrease in peel strength as they systematically removed the active hydrogen from the nitrogen going from a primary amine to a tertiary amine. When nitrogen is totally removed, the silane no longer works as an adhesion promoter for this system. Adhesion studies on similar systems[77] found that the locus of failure is about 20-50Å into the polyimide film. Chiang and Koenig[78] studied the polymerization of an anhydride cured epoxy resin in contact with fiberglass that was treated with N-methylaminopropylsilane. The silane caused an acceleration in the appearance of ester linkages as well as amide linkages, with accelerated loss of unreacted anhydride. They estimated that the silane-polymer interface region had 5-10% greater crosslink density than the bulk of the epoxy polymer. Chaudhury et al.[79] also demonstrated the importance of interdiffusion and crosslinking in the polyvinylchloride-aminosilane-gemanium bond system. XPS depth profile analysis showed that silicon diffused into the PVC polymer.

Kaul et al.[80] showed that interdiffusion is an important mechanism for adhesion improvement in systems where no chemical bonding with the silane coupling agent is expected. It was observed that the low molecular weight silicone polymer diffused

through the silane layer to reach the high density polyethylene substrate. The peel strength increased to a maximum when the APS silane layer reached a thickness of about

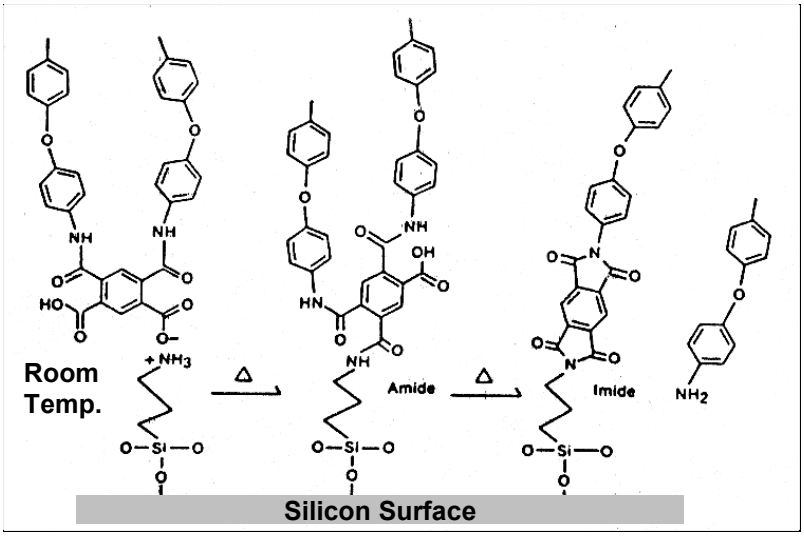

Figure 1-5. A proposed pathway of the aminosilane-polyimide adhesion reaction (adapted from reference 75).

1000Å. Drying the silane layer prior to bond preparation resulted in a decrease in joint strength, indicating that the glassy network of cured silane tends to inhibit silicone interdiffusion. A similar study was performed by Sung et al.[81], where a sapphire surface derivatized with APS was bonded using molten polyethylene. Energy-dispersive X-ray analysis results indicated that APS diffused into the polyethylene, and the peel strength increased with the thickness of the APS layer up to that obtained from a 2% APS aqueous solution[81]. This finding suggested that adhesion strength is directly related to the amount/thickness of silane deposited on a substrate. More recently, Kent et al.[82] used the neutron reflectivity technique and angle resolved X-ray photoelectron spectroscopy to examine the adsorption of water on a molybdenum-polyurethane interface. The silane, 3-glycidoxypropylmethoxysilane (GPS), was pre-dissolved in the polyurethane before bonding. Neutron reflectivity data showed that the silane had diffused from the bulk of the polyurethane to the molybdenum/polyurethane interface after curing. The penetration

of water into the molybdenum oxide/polyurethane interface could be slowed with as little as ~2% (w/w) GPS in polymer. The silane that migrated from the bulk polymer to the interface likely plays a role in water adsorption. Moon and Jang[83] found that the presence of γ-methylmethacryloxypropyltrimethoxysilane (γ-MPS) at the vinyl ester and ultra-high modulus polyethylene (UHMPE) fiber interface enhanced wetting and chemical interaction of the vinyl ester, thereby improving interfacial adhesion.

1.7 Characterization of the Surfaces

Many techniques have been developed for the characterization of solid or liquid surfaces or interfaces to obtain different types of information. Some techniques provide elemental and chemical information, while others give topographical and spatial elemental information.

Electron spectroscopy for chemical analysis (ESCA) or x-ray photoelectron spectroscopy (XPS) is a powerful technique for the analysis of surfaces[84]. XPS yields essential information on surfaces such as semiquantitative elemental analysis, functional group identification, and depth profiling. XPS is ideally suited for surface characterization of thin films deposited by the plasma technique or silane modification reactions. XPS is also useful for examining the surface chemistry of failed bond surfaces in the determination of the failure mechanism.

In XPS a surface is bombarded with mono-energetic radiation ($h\nu$) of sufficient energy so that photons are absorbed by surface atoms and adsorption results in the expulsion of an electron from energy levels of atoms[84]. The kinetic energy of the emitted electrons can be measured with an electron spectrometer. With a known x-ray energy, the binding energy of the electron can be obtained from the following relationship:

$$E_b = h\nu - KE + \Phi \qquad \textbf{Equation 1-1}$$

where E_b is the binding energy of the emitted electron, $h\nu$ is the x-ray energy, KE is the kinetic energy of the ejected electron, and Φ is the work function of the spectrometer[84].

The photoelectrons emitted for the sample surface are separated in energy by an electron energy analyzer and captured by the detector. A plot of the number of electrons detected as a function of binding energy provides the necessary XPS analytical information[84]. The area under each photopeak is proportional to the number of photoelectrons captured for each element. With appropriate correction factors, the elemental percent composition at the surface can be obtained. Each element has a unique electronic structure, thus binding energies for electrons are distinct and readily identified by XPS. Because the energy observed for an electron of a given atom will be influenced by the electron withdrawing power of the nearest neighbor atoms, XPS can also be used to identify functional groups. For example, carbon in a very electronegative environment (i.e., a carboxyl group) will eject a 1s electron that appears at a higher binding energy than that for an electron from carbon in a less electronegative environment (i.e., an aliphatic group). In addition, angular resolved XPS allows the determination of the vertical distribution of an element or a functional group over a depth of about 50 Å from the surface for a given subsrate[85].

Auger electron spectroscopy (AES) is widely used surface sensitive analytical technique. The process by which Auger electrons are generated is called the Auger effect. In AES, incident electrons can remove core state electrons from surface atoms. This core state can be filled by an outer shell electron from the same atom, in which case the electron moves to a lower energy state, and the energy associated with the transition is the difference in orbital energies. This energy must be released in some fashion. In some cases this energy is imparted to a second outer shell electron, which is then ejected from the atom as an Auger electron. The kinetic energy of the ejected electron involved in this process is measured. The Auger transition is designated by indicating the energy levels involved, For oxygen, the Auger transition is KLL.

AES discerns the elemental composition of a solid surface, because the magnitude of the core electron energy for a give atom is a function of the types of chemical bonding with other atoms. Chemical changes in bonding will produce energy shifts in Auger transitions[86]. The chemical environment of a given atom can also be detected by

variations in the shape and fine structure of an Auger peak. A spatial resolution of 5 nm can be reached by AES analysis. Moreover, AES is often used in conjunction with inert gas ion sputtering to obtain information on the composition of a sample as a function of depth[87]. AES coupled with the reactive ion etching (RIE) technique is particularly suited for studying the change in chemical composition as a function of film depth. For example, Cain et. al.[88] used AES with RIE to study an aminofunctional silane deposited on a silicon wafer. The depth profiles for carbon and nitrogen in the aminosilane film showed almost an inverse relationship. The nitrogen content was the highest at the outer edge of the aminosilane layer, while the carbon content was lowest in these regions. Because nitrogen and carbon are in the same molecule, such a profile indicates that the orientation of amino groups is away from the silane/silicon wafer interface.

Contact angles of liquids on solid surfaces are widely used to predict wetting of these solids by calculating their solid-vapor surface tension. The wettability of a solid surface is essential for adhesion, because intimate contact is required between a substrate and an adhesive to achieve good adhesion. Liquids will wet solids of higher surface energy because the overall surface energy of the system is minimized when the solid is covered by the lower surface energy liquid[89]. Although surface energy cannot be measured directly, it can be obtained from the measurement of contact angles of various liquids (at least 2) on a smooth solid surface[90]. While the contact angle will not identify the functional group at the surface, the measurement obtained is sensitive to the chemistry of the surface, as well as surface roughness and other structural imperfections. In the case of a water droplet on a polymer surface, the contact angle increases with increasing hydrophobicity of the surface. The contact angle measurement is different than XPS in that it is more sensitive to the immediate surface with which the liquid is in contact[91].

1.8 Adhesion Testing Methods

Reliable methods for testing adhesion between a brittle polymeric thin film and a rigid semiconductor substrate are much needed in the microelectronics industry[1-3].

Knowing the interfacial strength and durability between a photoresist and a silicon substrate in various environments is crucial for determining the lifetime of a microelectronics device. The measurement of G_c, or the critical strain energy release rate, is desired because of its implications in the design and application of thin-film coatings. Many mechanical testing methodologies have been developed to measure thin film adhesion[92-95], but many of these methods have distinct limitations. Various peel tests[92,93] are widely used for pressure sensitive adhesives; however, they are often not suitable for brittle thin films. Lawn et al.[96] have applied indentation mechanics to characterize and quantify surfaces and interfaces. The indentation test can be performed conveniently on a specimen with simple thin-film geometry; however, it suffers from the drawback that as thin films become thinner, the introduction of a point load or pulling force becomes more problematic since stresses increase dramatically with reduced cross-section. In addition to the brittle nature of the film itself, applied loads can easily fracture the substrate.

Many forms of the blister tests have also been developed[94,95,97-100]; however, these suffer from the general problem that they require a specific testing geometry that often involves elaborate specimen preparation. O'Brien et al.[101] adopted the shaft-loaded blister test (SLBT) to measure the applied strain energy release rate of Kapton® pressure sensitive adhesive (PSA) tape to a rigid substrate. The test can be conducted in an in-situ fashion so that the environmental stress (i.e., thermal cycles) and chemical environment (i.e., fluids) can both be studied during interfacial degradation.

This dissertation describes the use of a novel probe test to quantify the interfacial adhesion energy between a model epoxy and a silicon wafer modified with silane coupling agents. In particular, the probe test will be used to assess the change in adhesion and durability of the model epoxy/SCA/SiO_2/Si bonded system as a function surface preparation (i.e., duration of oxygen plasma pre-treatment and choice of different silanes), properties of chemical media (i.e., pH) and thermal conditions (i.e., static and cyclic temperatures).

1.9 Thesis Statement

The literature review showed that surface modification *via* silane coupling agents is effective in promoting adhesion between polymers and inorganic substrates. The main objective of this study is to examine the effect of surface modification combining both oxygen plasma and silane treatments of silicon substrates on adhesion enhancement for a model epoxy/SCA/Si bonded system. Further, the study explores whether the probe test is feasible and sufficiently sensitive to distinguish changes in durability and adhesion in bonded systems as affected by their exposure to severe environments (i.e., chemical, thermal, and mechanical).

1.10 References

[1] J. H. Lai, *Polymer for Electronic Applications*, CRC Press: Boca Raton, 1989, Chap 1.

[2] H. Lee and K. Neville, *Handbook of Epoxy Resins*, MaGraw-Hill: New York, 1967, Chap 2.

[3] B. Ellis, *Chemistry and Technology of Epoxy Resins*, Blackie Academic & Professional: London, 1993, Chap 4.

[4] E. P. Plueddemann, "*Silane Coupling Agents*", Plenum Press, New York, 1991, Chap 1.

[5] E. P. Plueddemann, H. A. Clark, L. F. Nelson, and K. R. Hoffman, *Mod. Plast*., **39**, 1962, 136.

[6] C. H. Chiang and J. L. Koenig, in "*SPI, 35th Ann*. *Tech*. *Conf*. *Reinf*. *Plast.*", 1980, p. 23-D.

[7] E. Lotz, D. Wood, and R. Barnes, in "*SPI, 26th Ann. Tech. Conf. Reinf. Plast*.", 1971, p. 14-D.

[8] D. J. Vaughan and E. L. McPherson, in "*SPI, 27th Ann. Tech. Conf. Reinf. Plast*.", 1972, p. 21C.

[9] E. K. Drown, H. Al-Moussawi, and L. T. Drzal, *J. Adhes. Sci. Technol*., **5**, 1991, 865.

[10] E. Sacher, in "*Symposium on Silylated Surfaces*," Eds., D. E. Leyden and W. Colloins, Gordon & Breach, London, 1980, p. 347.

[11] H. K. Yasuda, A. K. Sharma, E. B. Hale, and W. J. James, *J. Adhesion*, **13**, 1982, 269.

[12] K. S. Chen, N. Inagaki, and K. Katsuura, *J. Appl*. *Polym. Sci*., **27**, 1982, 4655.

[13] G. Constantino, D. B. Zeik, and S. J. Clarson, *J. Inorg*. *Organo*. *Polym*., **4**, 1994, 425.

[14] J. B. Hudson, "*Surface Science An Introduction*", Butterworth-Heinemann, Stoneham, MA, 1992, Chap. 1.

[15] W. K. Burton, N. Cabrera, and F. C. Frank, *Phil. Trans. Roy. Soc.*, **A243**, 1951, 299.

[16] L. Leidheiser Jr. and P. D. Deck, *Science*, **241**, 1988, 1176.

[17] L. H. Sharpe, *J. Adhesion*, **4**, 1972, 5.

[18] J. Comyn, "*Adhesion Science*", The Royal Society of Chemistry, Cambridge, 1997, Chap. 1.

[19] A. J. Kinloch, "*Adhesion and Adhesives, Science and Technology*", Chapman and Hall, New York, 1987, Chap. 1.

[20] A. J. Kinloch, *J. Mater. Sci.*, **15**, 1980, 2141.

[21] S. S. Voyutski and V. L. Vakula, *J. Appl. Polym. Sci.*, **7**, 1963, 475.

[22] H. Dodiuk and S.Kenig, *Int. J. Adhes. Adhes.*, **83**, 1988, 159.

[23] D. M. Mattox, *Vacuum Tech. Coating*, **1**, 2000, 28.

[24] J. Kikuchi, Brit. UK Patent 2287826, 1995.

[25] J. A. Shields and B. Rangarajan, US Patent 6207582, 2001.

[26] C. -N. Wu and C. -L. Yang, US Patent 6303482, 2001.

[27] J. W. Butterbaugh and D. C. Gray, Eur. Patent 688045, 1995.

[28] R. Divan, N. Moldovan, and H. Camon, *Sensors and Actuators A: Physical*, **74**, 1999, 18.

[29] J. Kikuchi, M. Iga, H. Ogawa, S. Fujimura, and H. Yano, *Jpn. J. Appl. Phys., Part 1*, **33**, 1994, 2207.

[30] A. L. Bogdanov and S. S. Peredkov, *Microelectron. Eng.*, **53**, 2000, 493.

[31] H. K. Yusuda, "*Plasma Polymerization*", Academic Press, Orlando, FL, Chap 4.

[32] H. Suhr, in "*Techniques and Applications of Plasma Chemistry of Polymers*", Eds. J. R. Hollahan and A. T. Bell, Wiley and Sons, New York, 1974.

[33] L. D. Nielsen, Ph.D. Thesis, University of Wisconsin-Madison, December 1995, Chap 2.

[34] N. Inagaki, "*Plasma Surface Modification and Plasma Polymerization*," Technomic Publishing Company, Lancaster, PA, 1996, Chap 3.

[35] P. H. Townsend, R. H. Heistand, D. Castillo, T. M. Stokich, B. Allen, M. Radler, T. Tarnowski, J. Blackson, and H. Klassen, *MRS Symp. Proc.*, **338**, 1994, 589.

[36] G. Phillip and H. Schmidt, *J. Non-Cryst. Solids*. **63**, 1984, 283.

[37] H. H. Huang, B. Orler, and G. Wilkes, *Polym. Bull.*, **14**, 1985, 557.

[38] H. H. Huang, R. H. Glasser, and G. Wilkes, "*Inorganic and Orangometallic Polymers"*, ACS Symp. Ser., **360**, 1988, Chap 29.

[39] J. D. Mackenzie, in "*Ultrastructure Processing of Glass, Ceramics, and Composites*," eds L. L. Hench and D. R. Ulrich, Wiley, New York, 1984, Chap.1.

[40] C. J. Brinker and G. W. Scherer, "*Sol-Gel Science, The Physics and Chemistry of Sol-Gel Science*", Academic Press, New York, 1990, p. xi.

[41] P. J. Flory, "*Principles of Polymer Chemistry*", Cornell University Press, 1953, p. 347.

[42] S. Sakka and K. Kamiya, *J. Non-Cryst. Solids*, **48**, 1982, 31.

[43] H. Dislich and P. Hinz, *J. Non-Cryst. Solids*, **48**, 1982, 11.

[44] D. E. Clark, "*Science of Ceramic Chemical Processing*", Wiley, New York, 1986, p. 237.

[45] R. K. Iler, "*The Chemistry of Silica*", Wiley, New York, 1979, Chap 2.

[46] E. A. Barringer and H. K. Brown, *Langmuir*, **1**, 1985, 414.

[47] D. C. Bradley, R. C. Mehrotra and D. P. Gaur, "*Metal Alkoxides*", Academic Press, London, 1978, Chap 3.

[48] C. Sanchez and F. Ribot, *New J. Chem.*, **18**, 1994, 1007.

[49] D. L. Angst and G. W. Simmons, *Langmuir*, **7**, 1991, 2236.

[50] J. M. Park and R. V. Subramanian, *J. Adhesion Sci. Technol.*, **5**, 1991, 459.

[51] H. Ishida and J. L. Koenig, *Polym. Eng. Sci.*, **18**, 1978, 128.

[52] R. B. Pettit, C. S. Ashley, and C. J. Brinker, in "*Sol-Gel Technology for Thin Films, Fibers, Preforms, Electronics, and Specialty Shapes*", ed. L. C. Klein, Noyes, Park Ridge, NJ, 1988, p. 80-109.

[53] R. B. Pettit and C. J. Brinker, *Solar Energy Materials*, **14**, 1986, 269.

[54] R. Badheka, N. J. Bazin, P. A. Sermon, M. S. W. Vong and J. G. Leadley, in "*Sol-Gel Processing of Advanced Materials*", eds. L. C. Klein, E. J. A. Pope, S. Sakka, and J. L. Woolfrey, The American Ceramic Society, Westerville, OH, 1998, p. 235.

[55] B. E. Yoldas, *Applied Optics*, **23**, 1984, 1418.

[56] S. P. Mukherjee and W. H. Lowdermilk, *Applied Optics*, **21**, 1984, 293.

[57] J. Livage, in "*Better Ceramics Through Chemistry II*", eds. C. J. Brinker, D. E. Clark, and D. R. Ulrich, Materials Research Society, Pittsburgh, PA, 1986, p. 717.

[58] Y-J. Oh, S-H. Kim, H-J. Jung and C-E. Kim, in "*Sol-Gel Processing of Advanced Materials*", eds. L. C. Klein, E. J. A. Pope, S. Sakka, and J. L. Woolfrey, The

American Ceramic Society, Westerville, OH, 1998, p. 161.

[59] H. Schmidt, B. Seiferling, G. Phillipp, and K. Deichmann, in "*Ultrastructure Processing of Advanced Ceramics*", eds. J. D. Mackenzie and D. R. Ulrich, Wiley, New York, 1988, p. 651.

[60] H. Schmidt, G. Rinn, R. Nab, and D. Sporn, in "*Better Ceramics through Chemistry III*", eds. C. J. Brinker, D. E. Clark, and D. R. Ulrich, Materials Research Society, Pittsburgh, PA, 1988, p. 743.

[61] M. R. Rosen and E. D. Goddard, in "*SPI, 34th Ann. Tech. Conf. Reinf. Plast*.", 1979, p.19-E.

[62] C. P. Tripp and M. L. Hair, *Langmuir*, **8**, 1991, 1120.

[63] K. W. Allen, *J. Adhesion Sci. Technol*., **6**, 1992, 23.

[64] E. K. Drown, H. Al Moussawi, and L. T. Drzal, *J. Adhesion. Sci. Technol*., **5**, 1991, 865.

[65] D. J. Ondrus, F. J. Boerio, *J. Colloid Interface Sci*., **124**, 1988, 349.

[66] K. Esumi and K. Meguro, *Bull. Chem. Soc. Jpn*., **56**, 1983, 331.

[67] D. J. Hook, T. G. Vargo, J. A. Gardella, K. S. Litwiler and F. V. Bright, *Langmuir*, **7**, 1991, 142.

[68] P. R. Moses, L. M. Weir, J. C. Lennox, H. O. Finklea, J. R. Lenhard and R. W. Murray, *Anal. Chem.*, **50**, 1978, 576.

[69] D. J. Belton and A. Joshi, in "*Molecular Characterization of Composite Interfaces*", Eds. H. Ishida and G. Kumer, Plenum, New York, 1985, P. 187.

[70] J. Koenig and P. T. K. Shih, *J. Colloid Interface Sci*., **64**, 1978, 565.

[71] H. Ishida and J. L. Koenig, *J. Colloid Interface Sci*., **64**, 1978, 555.

[72] H. Ishida and J. L. Koenig, *J. Polym. Sci., Polym. Phys. Ed.*, **17**, 1979, 615.

[73] H. Ishida and J. L. Koenig, *J. Polym. Sci., Polym. Phys. Ed*., **18**, 1980, 1931.

[74] M. R. Rosen and E. D. Goddard, *Polym. Sci. Eng. Sci*., **20**, 1980, 413.

[75] H. Linde and R. T. Gleason, *J. Polym. Sci., Polym. Chem. Ed*., **22**, 1984, 2183.

[76] J. Greenblatt, C. J. Araps, and H. R. Anderson, Jr., in "*Polyimides: Synthesis, Characterization, and Applications*, Ed. K. L. Mittal, Vol.1, Plenum Press, New York, 1984, p. 573.

[77] H. R. Anderson, Jr., M. M. Khojasteh, T. P. McAndrew, and K. G. Sachdev, *IEEE Trans. CHMT*., **9**, 1986, 364.

[78] C. H. Chiang and J. L. Koenig, *J. Polym. Sci., Polym. Phys. Ed*., **20**, 1982, 2135.

[79] M. K. Chaudhury, T. M. Gentle, and E. P. Plueddemann, *J. Adhesion Sci. Technol.*, **1**, 1987, 29.

[80] A. Kaul, N. H. Sung, I. J. Chin, and C. S. P. Sung, *Polym. Eng. Sci.*, **26**, 1986, 768.

[81] N. H. Sung, A. Kaul, I. J. Chin, and C. S. P. Sung, *Polym. Eng. Sci.*, **22**, 1982, 637.

[82] M. S. Kent, G. S. Smith, S. M. Baker, A. Nyitray, J. Browning, G. Moore, and D. W. Hua, *J. Mater. Sci.*, **31**, 1996, 927.

[83] S. I. Moon and J. Jang, *J. Adhesion Sci. Technol.*, **14**, 2000, 493.

[84] W. M. Riggs and M. J. Parker, in "*Methods of Surface Analysis*", Ed. A. W. Czanderna, Elsevier, New York, 1989, Chap 4.

[85] D. T. Clark and A. Dilks, *J. Polym. Sci., Polym. Chem. Ed.*, **16**, 1978, 911.

[86] A. Joshi and P. W. Davis, in "*Methods of Surface Analysis*", Ed. A. W. Czanderna, Elsevier, New York, 1989, Chap 5.

[87] J. A. Filbey and J. P. Wightman, in "*Adhesive Bonding*", Ed. L. Lee, Plenum Press, New York, 1991, Chap 7.

[88] J. F. Cain and R. W. Murray, *J. Colloid Interface Sci.*, **67**, 1978, 538.

[89] D. J. Shaw, "*Introduction to Colloid and Surfaces Chemistry*", Butterworth-Heinemann, Oxford, 1992, Chap 6.

[90] P. J. Dynes and D. H. Kaeble, *J. Macromol. Sci., Chem.*, **A10**, 1976, 535.

[91] M. Anand, R. E. Cohen, and R. F. Baddour, *Polymer*, **22**, 361, 1981.

[92] K. Kendall, *J. Phys. D.*, **8**, 1975, 1449.

[93] A. N. Gent and S. Kaing, *J. Appl., Polym. Sci.*, **32**, 1986, 4689.

[94] H. Dannenberg, *J. Appl. Polym. Sci.*, **5**, 1961, 125.

[95] K. T. Wan, *J. Adhesion*, **70**, 1999, 209.

[96] B. R. Lawn, in "*Fracture of Brittle Solids*", 2nd Ed., Cambridge Press: New York, NY, 1993, Chap 2 and 3.

[97] M. L. Williams, *J. Adhesion*, **4**, 1972, 307.

[98] M. G. Allen and S. D. Senturia, *J. Adhesion*, **25**, 1988, 303.

[99] D. A. Dillard, Y. S. Chang, and Y. H. Lai, *J. Adhesion*, **27**, 1989, 197.

[100] D. A. Dillard and Y. Bao, *J. Adhesion*, **33**, 1991, 253.

[101] E. P. O'Brien, T. C. Ward, S. Guo, and D. A. Dillard, *J. Adhesion*, **79**, 2003, 69.

2. Experimental

2.1 Materials and Experimental Procedure

The following sections describe the materials and the experimental procedures used in this research.

2.1.1 Silicon Wafers

Si (100) wafers 200mm (8") in diameter with polished front surfaces and non-polished back surfaces were obtained from the Sumitomo Mitsubishi Silicon Group. Si (100) wafers 200 mm (8") in diameter with a thermally oxidized (TOX) surface were obtained from the Sumitomo Mitsubishi Silicon Group. The TOX wafer was subject to surface modification without further surface cleaning. These wafers were cut into small pieces (approximately 15 mm^2 size) for surface and bond specimen preparations.

2.1.2 Silane Coupling Agents

All silane coupling agents were purchased from commercial suppliers and were used without further purification. The silane coupling agents used for the surface modification of the Si wafers included SCA-1 (a trialkoxy silane with primary amine functionality), SCA-2 (a trialkoxy silane with secondary amine functionality), SCA-3 (a trialkoxy silane with two secondary amine functionalities), and SCA-4, SCA-5, SCA-6 (trialkoxy silanes with hydrocarbon functionalities).

2.1.3 Plasma Reactor

A custom made PF plasma reactor, shown in Figure 2-1, was used to modify the wafer surfaces[1]. The apparatus is a Pyrex glass tube joined in sections that is evacuated using a turbo and a rotary pump. The system has three inlets for the introduction of different gases to generate different gaseous plasmas. Internal reactor pressure was monitored using a Hastings-Raydist thermocouple gauge. The gas flow was monitored by

a Brooks Instruments 50 sccm mass flow controller (model 5850). High purity oxygen was obtained from Airgas Inc. and was used as the plasma pre-treatment, treatment, and post-treatment gas.

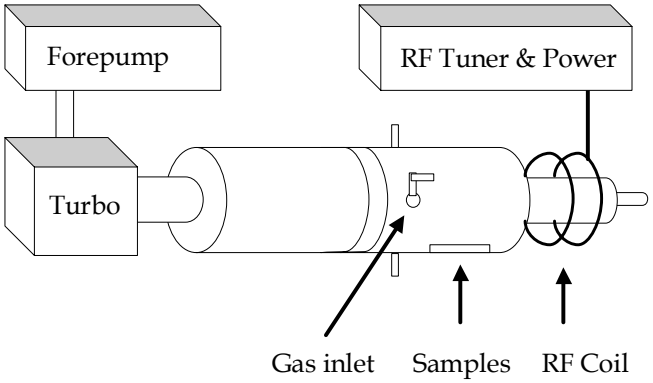

Figure 2-1. Schematic diagram of the plasma reactor[1].

2.1.4 Model Epoxy

An epoxy formulation consisting of bis-phenol F diglycidyl ether (Epon 862), 1,4-butanediol (10 phr), and 4-methyl-2-phenylimidazole (3 phr) was used as a model adhesive/coating. The bis-phenol F epoxy has an epoxide equivalent weight of 171 g/mole[2].

2.1.5 pH Buffer Solutions

Buffer solutions were used as fluids in some of the bond durability immersion studies. The buffer solutions were pH 4 (potassium biphthalate, 0.05M), pH 7 (potassium phosphate-monobasic sodium hydroxide, 0.05M), and pH 9 (boric acid-potassium chloride-sodium hydroxide 0.1M). The buffer solutions were purchased from VWR Scientific Inc. Additional pH solutions used were: deionized water (pH ≈ 6.0) and 0.1M H_2SO_4 (pH = 1)

2.1.6 Aqueous Solutions with Different pH

Aqueous solutions with compositions similar to those for solutions to which the electronic component(s) could be exposed in practice were prepared. The solutions typically included water, a surfactant, organic and inorganic solutes, and organic solvents. The six formulated solutions were Solution-1 (pH 4.15), Solution-2 (pH 6.65), Solution-3 (pH 7.71), Solution-4 (pH 8.24), Solution-5 (pH 4.30), and Solution-6 (pH 8.50). Additional aqueous solutions were prepared using diols with different carbon chain lengths and a surfactant. These materials were purchased from commercial suppliers. The components were used without additional purification.

2.2 Surface Cleaning

2.2.1 Oxygen Plasma Cleaning

An oxygen plasma was used to clean and modify the silicon wafer surface. The effect of an oxygen plasma surface treatment is two fold: 1) the oxygen plasma cleans the surface by removal of residual organic contaminants; and 2) it augments the oxide layer on the silicon surface, which facilitates the subsequent sol-gel surface modification. The plasma treatment time, plasma power, and gas pressure were varied to achieve different oxide thicknesses on the silicon wafer surface. A typical oxygen plasma treatment consisted of a 2 to 30 minute plasma treatment (20 sccm (standard cubic centimeters per minute), 50 to 200 W (watt), O_2), and a post treatment purge of 10 minutes (20 sccm, O_2; no RF power).

2.3 Surface Modification

2.3.1 Treatment with Silane Coupling Agents

Silane coupling agents were used to modify as-received and plasma-treated Si wafers *via* a sol-gel reaction. First, a 100 mL solution of 5% (v/v) silane in 100% ethanol was prepared. To this solution was added 5 mL of 0.1 M HCl. The addition of acid catalyzes the hydrolysis reaction of the silane. This hydrolysis reaction was carried out

for 30 minutes. Separately, the Si wafers were immersed in an acidified ethanol solution (5 mL of 0.1 M HCl added to 100 mL ethanol). The acidified silane solution was then added to the acidified ethanol solution which contained the wafers. The reaction was carried out for 30min at room temperature. After the silane treatment, the wafers were rinsed with pure ethanol and dried in air at room temperature. The modified wafers were subsequently heated in an oven at 110 ^{o}C for about 30 min.

2.4 Sample Preparation

2.4.1 Model Epoxy Adhesive: Composition/Preparation/Curing

The model epoxy adhesive consists of bis-phenol F diglycidyl ether (Epon 862) (**1**), 1,4-butanediol (10 phr, i.e., parts per hundred resin) (**2**), and 4-methyl-2-phenylimidazole (3 phr) (**3**). To prepare the epoxy, a relatively low viscosity clear liquid was obtained by stirring Epon 862 and 1,4-butanediol together at about 80 ^{o}C for several minutes. Subsequently, 4-methyl-2-phenylimidazole catalyst was dissolved in this mixture with stirring for about 15 minutes to obtain a homogenous mixture. This homogeneous epoxy mixture was used for casting the epoxy films. The bulk epoxy mixture or the epoxy mixture cast on Si substrates was cured at 130 ^{o}C for 1 hour. Differential Scanning Calorimetry (DSC) measurements showed that a fully cured model epoxy polymer had a glass transition temperature of 110 ^{o}C[3].

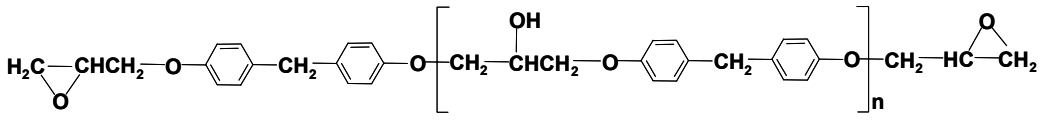

1

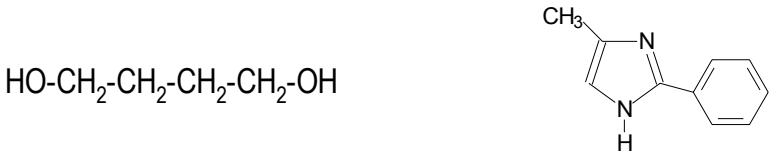

2

3

2.4.2 Immersion Test Specimen Preparation

The model epoxy was cast onto a silicon wafer approximately 15x15 mm in size and was then sandwiched between two Teflon plates, as shown in Scheme 2.1. Teflon shims were added between the two Teflon plates to control the epoxy film thickness to about 75 μm. Another thin Teflon film was placed on top of the coating area to ensure a smooth coating surface. The assembly was held together with two medium size binder clips and cured at 130 ^{o}C for 1 hour in air.

Two types of model epoxy coated specimens were used for immersion studies in various media. One is the "non-cut" specimen and the other is the "cut" specimen (see Scheme 2.2). The "cut" specimens are generated by breaking an as-cured "non-cut" specimen in to smaller pieces. One of the disadvantages of the "cut" specimen is that the stress from breaking the specimen might induce a crack at the film/substrate interface in the vicinity of the cut line. To remedy this problem, each "cut" specimen was subjected to an edge treatment (the process involves immersing freshly cut specimens in a SCA-1 solution (0.1M SCA-1 in ethanol, acid catalyzed with 5% v/v 0.1M aqueous HCl) for 30min, and then heating the specimen at 120 ^{o}C for 30min). This procedure deposits a thin layer of silane film across the freshly exposed epoxy/Si interface, thereby "re-sealing" the interface. The intent of the edge treatment was to inhibit the migration of water/solutions into the interface. In contrast, the "non-cut" specimen was immersed in various media for testing without the edge treatment.

Scheme 2.1

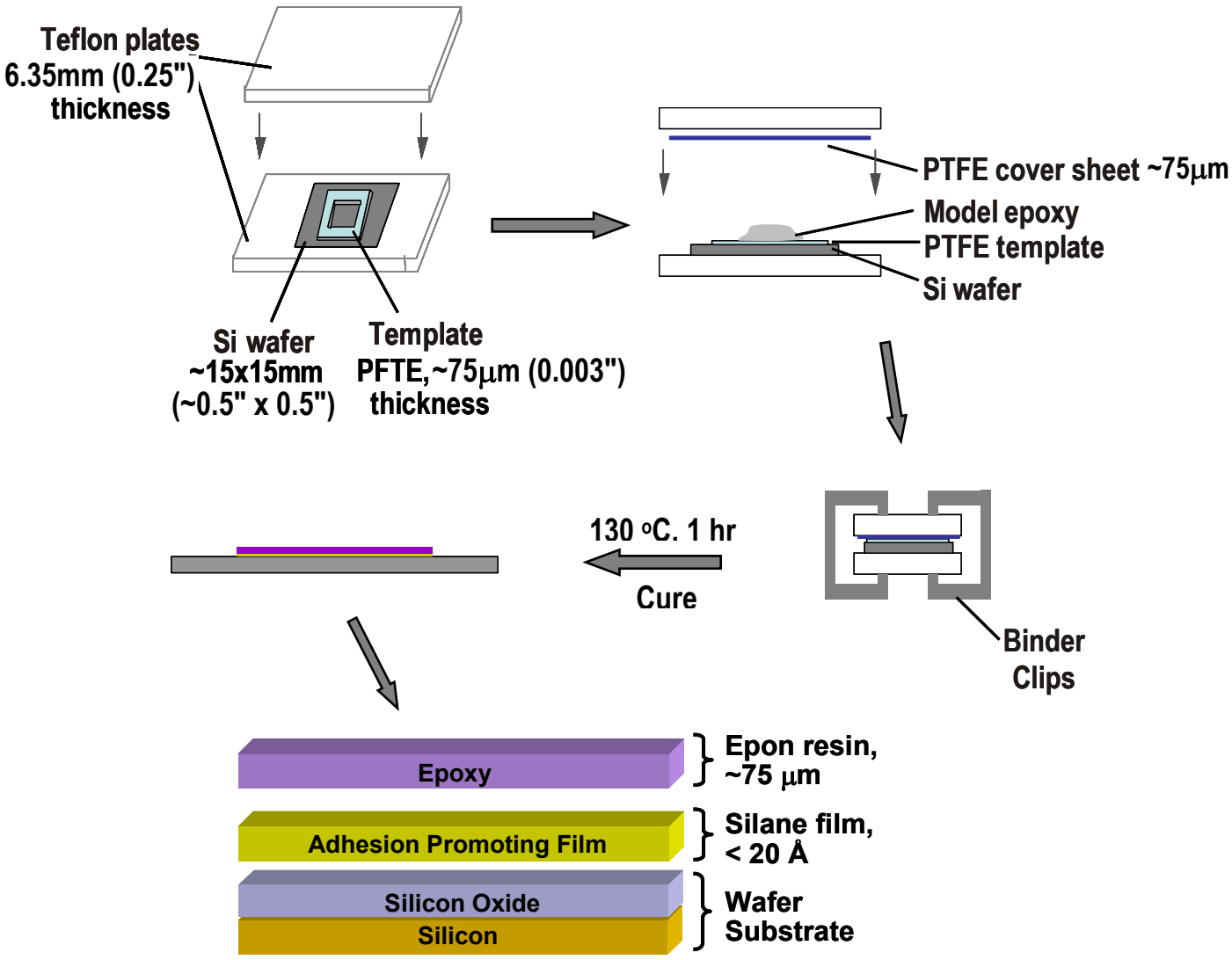

Final Bonded Structure (not to scale)

Scheme 2.2

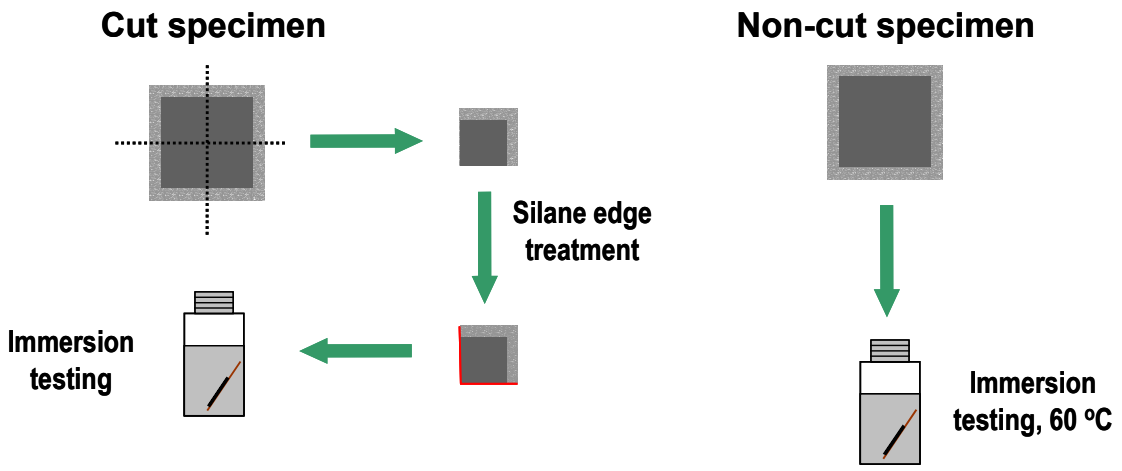

2.4.3 Probe Test Specimen Fabrication

The specimen geometry for the probe test is essentially the same as that used for the immersion studies. To ensure the possibility for a precise probe penetration at the film/substrate interface, excess polymer spew around the square coating area was removed using a razor blade. This process was carried out in a delicate fashion so that the vertical coating edge that is perpendicular to the Si substrate was exposed, while preserving straightness and bond integrity along the coating edge (see Scheme 2.3).

Scheme 2.3

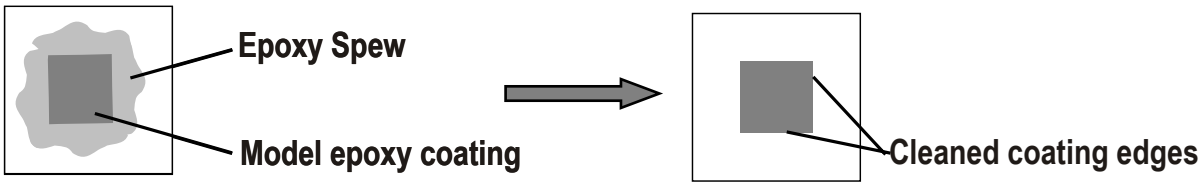

2.4.4 Wedge (DCB) Specimen Fabrication

The Si wafer was cut into 70 x 6 mm strips and used as the adherend (Scheme 2.4a). The model epoxy was used as the adhesive. The bonded specimen has a bond area of approximately 56 x 3 mm and a bond line thickness of 0.25 mm. This bond area was outlined on the Si beam using a Teflon shim with a pre-cut area (56 x 3 mm) placed between the two shim holders on the bottom part of the aluminum fixture (see Scheme 2.4b). Before bond preparation, the Si strips were painted with a Teflon release agent 25 mm (the rest of the Si beam was covered by a plastic sheet during spraying) from the end edge on one side of the Si beam. The release agent induces a weak bonding region at the start of the bond line, and this allows the initial crack to propagate when the wedge is inserted. The surface prepared Si beam was then placed in a custom-made aluminum mold fixture, which when closed, accurately aligned the top and bottom pieces of the Si beams (see Scheme 2.4b) with the Teflon shim and adhesive mixture in the middle. Please the note that the size/length of the top and bottom part of the aluminum fixtures looked different in the picture presented in Scheme 2.4 due to the camera angle, but in fact length of the aluminum fixtures and Si beam are the same. The Teflon shim along with the restraining force provided by the binder clips (which held the entire bond assembly together) restricts the movement and dimension of the adhesive mixture within the bonded area during curing. The assembled wedge specimen was cured in an oven at 130 ^{o}C for 1 hour in air. The final specimen geometry is shown in Scheme 2.4c. The bond line thickness is 0.25 mm.

Scheme 2.4

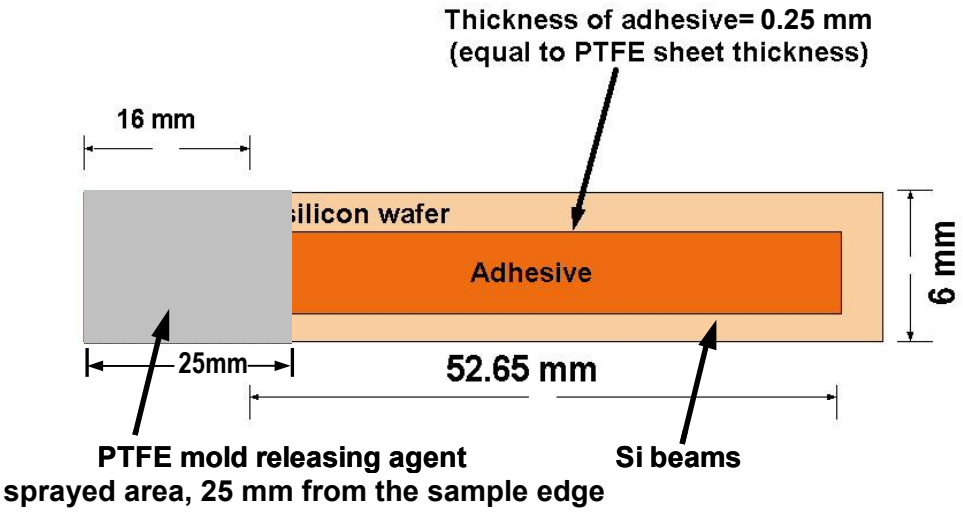

(a)

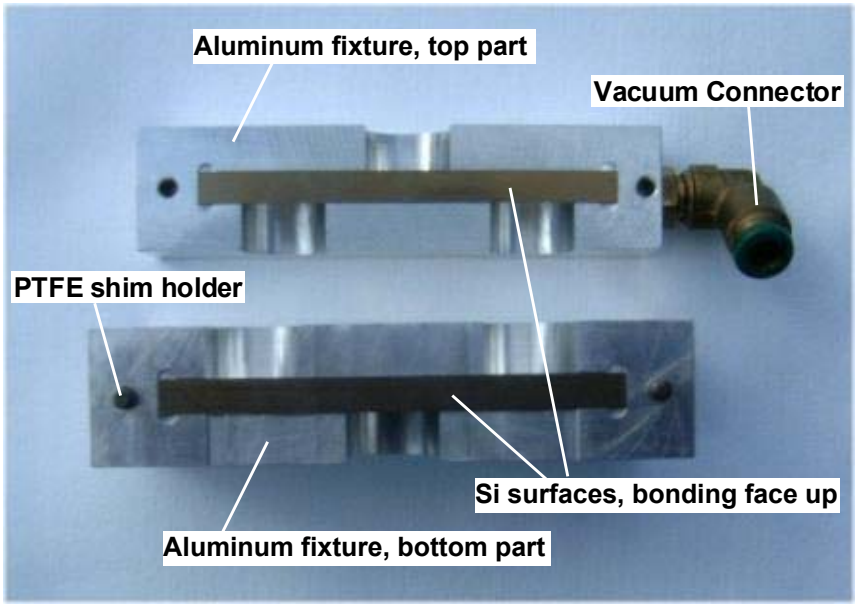

(b)

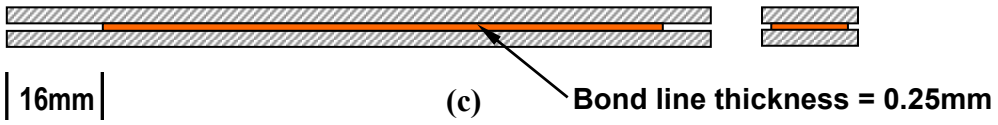

(c)

2.5 Surface Analysis

2.5.1 Contact Angle Measurements

Advancing contact angles of water on polished Si wafer surfaces were measured using a First Ten Angstroms (FTA) 125 Contact Angle Analyzer (Portsmouth, VA). An average of 10 to 12 water droplets was recorded in the measurement for each modified surface. All measurements were taken at room temperature, and the angles from both sides of the drop were measured and averaged. The volume of water used for the measurements was 10 μL.

2.5.2 Ellipsometry Measurements

Ellipsometry measurements were performed on a phase modulation ellipsometer (Beaglehole Instruments, Wellington, New Zealand) at λ= 632.8 nm (HeNe laser). The size of the laser beam was approximately 1 mm^2. Measurements in air were performed at at least eight different positions on the sample to check the quality of the films. The thickness of the SiO_2 layer on the bare Si wafer (polished side) was estimated by performing measurements in different ambient media (MIM)[4]. The MIM technique assumes that the film thickness, *t*, and the refractive index, *n* are known. An ellipsometer determines the state of polarization of light reflected from an interface. The reflectivity ratio, *r*, is the ratio of the reflectivity for *p*- and *s*-polarized light, r_s and r_p, and is a complex number[5].

$$r = r_p/r_s = \mathrm{Re}(r) + i\ \mathrm{Im}(r) \qquad \textbf{Equation 2-1}$$

At Brewster's angle, θ_B, $\mathrm{Re}(r, \theta_B) = 0$ and the imaginary part of *r* at Brewster's angle, $\mathrm{Im}(r, \theta_B)$, is called the ellipticity, ρ [6]. The ellipticity is related to film thickness as follows[4]:

$$\bar{\rho} = \mathrm{Im}(r, \theta_B) = \frac{\pi(\varepsilon_1 + \varepsilon_2)^{1/2}}{\lambda(\varepsilon_1 - \varepsilon_2)} \frac{(\varepsilon - \varepsilon_1)(\varepsilon - \varepsilon_2)}{\varepsilon} t \qquad \textbf{Equation 2-2}$$

where ε, ε_1 and ε_2 are the dielectric constants of the thin film, the incident medium and the substrate, respectively, and λ is the wavelength of light (638 nm). Note that $\varepsilon \sim n^2$. It has been determined that for transparent, thin, homogeneous films, the thickness is directly proportional to $\mathrm{Im}(r, \theta_B)^4$. This proportionality simplifies the determination of n and t. The silane layer thickness on the SiO_2 layer was determined by subtracting the total (silane + oxide) thickness from the native oxide thickness. This assumption is true based on the fact that the refractive indexes for the SiO_2 (~1.45) and organosilanes (~1.40) are very close, thus the ellipticity measured can be additive.

2.5.3 Wyko Surface Profile Measurements

A Veeco profilometer (Model Wyko) was used to examine the surface topography of the epoxy coated wafer specimens. Accurate displacement profiles (± 1nm), in the form of Z height data were obtained. The profilometer operates based on the theory of phase-shifting interferometry (PSI). In phase-shifting interferometry, a white-light beam is filtered and passed through the interferometer objective lens to reach the specimen surface. Half of the incident beam was reflected through the interferometer beamsplitter to a reference within the interferometer. The beams reflected from the specimen surface and the reference surface were recombined to form interference fringes. During the measurement, a small known amount of phase shift was introduced between the test and reference beams resulting in interference patterns at many different relative phase shifts, which were converted to phase data by integrating the intensity data. The relative surface height, $h(x, y)$ was calculated from the wavelength of the source beam and the phase data as follows:

$$h(x, y) = \frac{\lambda}{4\pi}\phi(x, y) \qquad \textbf{Equation 2-3}$$

where λ is the wavelength of the source beam, and $\phi(x, y)$ is the wavefront (phase) data.

2.5.4 X-Ray Photoelectron Spectroscopy (XPS)

The surfaces of samples were characterized using a Perkin-Elmer PHI Model 5400 XPS spectrometer equipped with a Mg K_α X-ray source (1253.6 eV), operated at 300 W. The spot size analyzed was a 1.0 x 3.0 mm area. Photoelectrons were analyzed in a hemispherical analyzer and were detected using a position-sensitive detector. The C-C/C-H carbon 1s peak was calibrated to a binding energy of 285.0 eV[7]. The atomic percentages were calculated by measuring the peak area of the respective photopeaks and correcting the measurement to account for ionization probability, analyzer transmission characteristics, and detector sensitivity. The results are given in atomic percent. Additionally, curve-fit analyses were performed for C 1s, Si 2p, and N 1s photopeaks using Gaussian functions in the effort to identify the functionalities associated with each element. Table 2-1 summarizes the peak assignments (binding energy values) used for individual functionalities. The full width at half maximum (FWHM) values used for the curve fits were: C 1s ≈1.7 eV; N ≈1.8 eV; and Si 2p varied from 1.2 eV to 1.7 eV. In some cases, the FWHM values were varied by ± 0.15eV to obtain the best curve-fit. The consistency of XPS data was verified by scanning two different spots on the same specimen or the measurement was repeated with a specimen obtained using the same experimental conditions.

Table 2-1. XPS peak assignments for C 1s, Si 2p, and N 1s photopeaks.[7-10]

Peak Assignments	Peak Position, eV
C-H/C-C	285.0
C-O	286.3 - 286.7
C=O	287.8 - 288.2
O=C-O	289.2
Si^o	99.0 - 99.3
$Si\text{-}(OR)_x$	100.5 -101.0
Si-O-Si	102.2 - 102.7
SiO_2	103.2 - 103.9
$-NH_2$	399.7 - 400.0
$-NH_3^+$	401.4 - 401.6

2.5.5 Auger Electron Spectroscopy (AES)

Auger electron spectroscopic (AES) measurements were performed using a Perkin Elmer PHI 610 Scanning Auger Microprobe. The electron gun beam voltage was 3000 V, the current was 0.05 μA, and the raster size varied from 2 mm^2 to no raster. The argon ion gun beam voltage was 4 kV, with a current of 5 μA. The sputter rate was typically 5 Å/min. The sputter rate was calibrated using a Ta_2O_5 wafer of known oxide thickness. The thickness of the oxide layer or silane film was determined by estimating the depth where the atomic concentration profile line for either silicon approached 100% or oxygen approached 0%.

2.6 Adhesion and Durability Measurements

2.6.1 Immersion Test

The debonding studies were carried out by immersing specimens of model epoxy-coated Si wafers in different aqueous solutions and pH buffer solutions at 60 ^oC and 70 ^oC. Specimens were placed in 20mL capped vials that contained about 5mL of liquid. Samples were inspected periodically to discern debonding events (i.e., fluid ingression at the coating edge and/or blister formation at the film/substrate interface). General observations were performed visually and closer inspection was performed using an optical microscope. The patterns and rates of debonding of the epoxy coatings were examined as a function of immersion time. Cyclic thermal testing of model epoxy coated Si substrates was carried out using a custom assembled apparatus (Figure 2-2). The specimens were immersed in solutions (~30 ml) in capped vials and the vials were subsequently placed in baskets. The baskets were alternatively placed in water baths at 25 ^oC and 70 ^oC for 30 min each. This process was accomplished automatically using a digital event controller. About 10 seconds was required to transfer the baskets from one bath to the other. Specimens were always withdrawn from the 25 ^oC water bath after a pre-determined immersion time (or number of cycles) for probe test adhesion measurements.

(a) **(b)**

Figure 2-2. Photographs of the cyclic thermal testing apparatus. (a) Rotating assembly and water baths, (b) basket holding glass vials that contain bonded specimens immersed in solutions.

2.6.2 Probe Test

All probe test measurements were performed on a Nikon UM-2 Measurescope microscope with a digital measuring stage. A schematic of the experimental apparatus is shown in Figure 2-3. A Sony digital camera was attached to the viewing lens to photograph debonding events. The debonds were created using a tungsten probe with a probe tip radius of 5 μm attached to an articulating arm of a KarlSUSS micromanipulator probe head. The micromanipulator was operated in XYZ directions by manually turning the geared thumbscrews. The articulating arm facilitated the use of different probe angles in the experiment. A probing angle of $25.0^{o} \pm 0.5$ was used to obtain results described in this dissertation. The coated silicon sample was secured to the microscope stage with an aluminum clamping plate.

2.6.3 Wedge (DCB) Test

Double cantilever beam[11,12] type bonded specimens consisting of Si and epoxy components were prepared for subcritical wedge tests. A Sonic Incorporated HS1000 model scanning acoustic microscope was used to measure the crack length of the

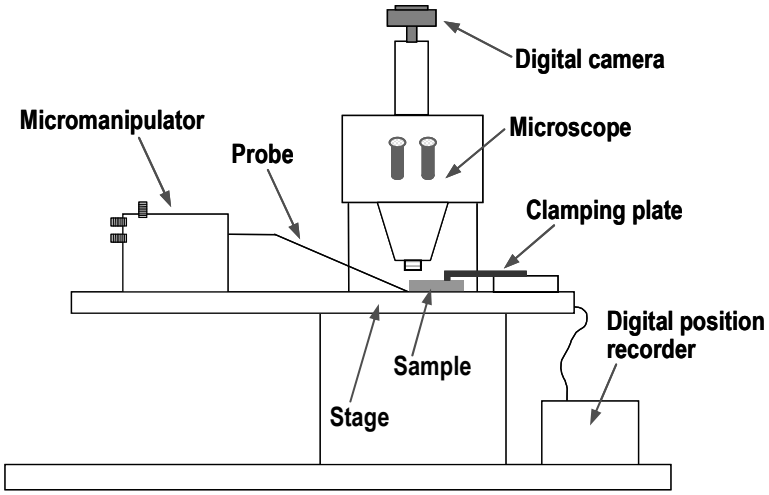

Figure 2-3. A schematic of the experimental probe test apparatus.

specimens in water. The crack was initiated in air at room temperature by inserting a stainless steel wedge of 0.5 mm thickness at the end of the specimen. The initial crack length for the wedge specimen was recorded and subsequent crack length measurements were taken as a function of immersion time in different fluids. Based on simple beam theory, the strain energy release rate, G, is given as[13]:

$$G = \frac{1}{a^4}\frac{9\Delta^2 E_1 E_2 I_1 I_2}{2B(E_1 I_1 + E_2 I_2)} \qquad \textbf{Equation 2-4}$$

where a is the crack length, Δ is the wedge thickness, B is the bean width, E_1 and E_2 are the Young's modulus of the adherend, I_1 and I_2 are the thicknesses of the adherends. In this case, E_1 equals to E_2 and I_1 equals to I_2.

2.7 Bond Failure Mode Analysis

XPS measurements were carried out to determine the failure mode for specimens tested in the various fluids (i.e., formulated solutions and pH buffer solutions). To carry out such analyses, the elemental composition and XPS spectral features of the failed epoxy side and failed wafer side of the specimens were examined, and compared to the spectral features for the as-prepared surfaces. Based on the XPS evidence, the location of failure in the model epoxy/SCA/Si bonded specimen was determined. Generally, interfacial failure could occur at the epoxy-silane interface or at the silane-Si substrate interfacial region.

2.8 Summary of Experiments

Table 2-2 lists all essential experimental parameters used in the various experiments in this research. Results of different experimental combinations along with factors such as type of silane surfaces, pH, temperature, etc. will be discussed in the following chapters.

Table 2-2. Summary of experiments conducted in this research.

Surface Chemistry			Durability and Adhesion	Failure Mode Determination
Type of surface	**Surface preparation**	**Surface characterization**		
Si, as received Si, O_2 plasma treated Si, TOX	SCA-1 SCA-2 SCA-3 SCA-4 SCA-5 SCA-6	XPS Angle-resolved XPS AES Ellipsometry Contact angle Surface profilometer	Immersion test (stress free) Immersion test (with cyclic thermal stress) Probe test (critical G) In-situ probe test (critical G + environment) DCB wedge test (subcritical G + environment)	Stress-free failure (immersion test) Stressed + no environment failure Stressed + environment failure 1) Probe test specimen 2) DCB test specimen

2.9 References

[1] R. A. DiFelice, Ph.D. Dissertation, Virginia Tech, May 2001, p 51.

[2] M. Sankarapandian and J.E. McGrath, unpublished report.

[3] S. L. Case, Ph.D. Dissertation, Virginia Tech, 2003, Chap 4.

[4] M. Mao, J. Zhang, R.-H. Yoon, and W. A. Ducker, *Langmuir*, **20**, 2004, 1843.

[5] J. L. Keddie, *Curr. Opin. Colloid Interface Sci*. **2**, 2001, 102.

[6] D.Beaglehole and H. K. Christenson, *J. Phys. Chem*., **96**, 1992, 2295.

[7] G. Beamson and D. Briggs, High *Resolution XPA of Organic Polymers*, John Wiley & Sons, West Sussex, England, 1992, p 277.

[8] C. D. Wagner, W. M. Riggs, L. E. Davis, J.F. Moulder, and G.E. Muilenburg, *Handbook of X-Ray Photoelectron Spectroscopy*; Perkin-Elmer: Eden Prairie, MN, 1979; Appendix 3.

[9] E. T. Vandenberg, L. B. Bertilsson, B. L. Kasjsa Uvdal, R. Erlandsson, H. Elwing, and I. Lungstrom, *J. Colloid Interface Sci*., **147**, 1991, 103.

[10] M. R. Alexander, R. D. Short, F. R. Jones, M. Stollenwerk, and W. Michaeli, *J. Mater. Sci*., **31**, 1996, 1879.

[11] S. W. Freiman, *J. Am. Cer. Soc.*, 1974, **57**, 350.

[12] S. M. Wiederhorn, S. W. Freiman, E. R. Fuller, and C. J. Simmons, *J. Mat. Sci.*, **17**, 1982, 3460.

[13] H. K. Singh, K., K-T. Wan, Z. Sun, and D. A. Dillard, Proceedings of the Annual Meeting of the Adhesion Society, **26**, 2003, 225.

3. Surface Characterization of Silicon Substrates

3.1 Introduction

Understanding the surface chemistry of modified silicon substrates is critically important because any variation of surface composition on the silicon surface could have a direct influence on performance (i.e., adhesion, durability) for the bonded system. Two major types of silicon surfaces were studied, the as-received (unmodified) surface and the modified surface. Detailed characterization of the as-received surfaces serves as a reference and a basis of comparison for modified surfaces. Several surface sensitive analytical techniques were used to characterize the substrate surface. X-ray Photoelectron Spectroscopy (including angle resolved XPS) and Auger Electron Spectroscopy depth profiling were employed to obtain surface compositional information as a function of substrate depth. Ellipsometry measurements compliment the XPS and AES techniques in that ellipsometry results reveal the thickness of a particular material layer by optical means. Contact angle measurements provide information related to the wettability of the silicon substrate. The modified substrates consist of oxygen plasma-treated surfaces and various silane-treated surfaces. The oxygen plasma treatment "cleans" the surface by removing any residual carbon-containing contaminants. In a controlled fashion, the oxygen plasma also creates silicon oxide functionalities that promote interaction with the silane coupling agents. A comparison of surface composition for the as-received Si substrate and a thermally oxidized (TOX) Si substrate is presented.

3.2 As-Received Si Substrates

Two different types of as-received Si wafers were used in this study; the as-received (untreated) Si wafer and the thermally oxidized (TOX) Si wafer. Carbon, oxygen, and silicon were detected on both substrate surfaces. Table 3-1 lists the elemental surface composition for the as-received- and TOX-Si wafers. Figure 3-1a shows the curve-fit C 1s spectrum for carbon on the as-received Si surface. The C 1s photopeak

Table 3-1. Elemental composition of as-received Si wafer surfaces at a 45^o take-off angle (atomic percent).

Sample	C	O	Si	O/Si$_{total}$
Si, as-received (untreated)	10.0	44.2	45.8	0.97
Si, TOX	3.3	65.2	31.5	2.1

was resolved into three individual Gaussian peaks. Peak C_I at a binding energy of 258.0 eV was assigned to carbon associated with C-H/C-C; peak C_{II} at 286.7 eV corresponds to carbon singly bonded to oxygen, C-O; and peak C_{III} at 288.6 eV represents carbon in the form of C=O, carbon doubly bonded to oxygen. The three types of carbon arise either from residues remaining after wafer polishing and cleaning processes or are organic species adsorbed on the wafer surface from the atmosphere. Figure 3-1b shows a well-defined O 1s peak at 532.4 eV, which was associated with oxygen in SiO_2. The Si 2p spectrum in Figure 3-1c shows a Si photopeak at 103.1 eV, which represents oxidized Si (SiO_2) and the peak at 99.2 eV which corresponds to elemental Si (Si^o). The ratio of SiO_2 to Si^o is 0.38. That elemental Si was detected (at an electron take-off angle of 45^o) suggests that the SiO_2 layer on top of elemental Si is very thin.

The carbon content on the thermally oxidized Si surface was significantly less than that on the as-received Si wafer (see Table 3-1). The TOX wafer surface was cleaner due to the extensive thermal treatment in an oxidizing environment. The same three types of C 1s peaks noted for the as-received wafer (Figure 3-1a) were also detected on the TOX wafer (Figure 3-2a). However, the C_I (C-H/C-C) contribution was dominant on the TOX wafer. The peak width for the O 1s peak at 533.3 eV was approximately 1.8 eV (Figure 3-2b). The binding energy was almost 1 eV higher than the O 1s peak for the as-received Si wafer (Figure 3-1b). Figure 3-2c shows only a single Si 2p photopeak at 103.8 eV; no peak for elemental silicon was observed. The higher binding energy O 1s peak and the Si 2p peak for the TOX surface are due to more extensive SiO_2 formation during the thermal treatment process. This finding indicates that the SiO_2 layer is much thicker than the escape depth of the electron from elemental silicon at a 45^o take-off

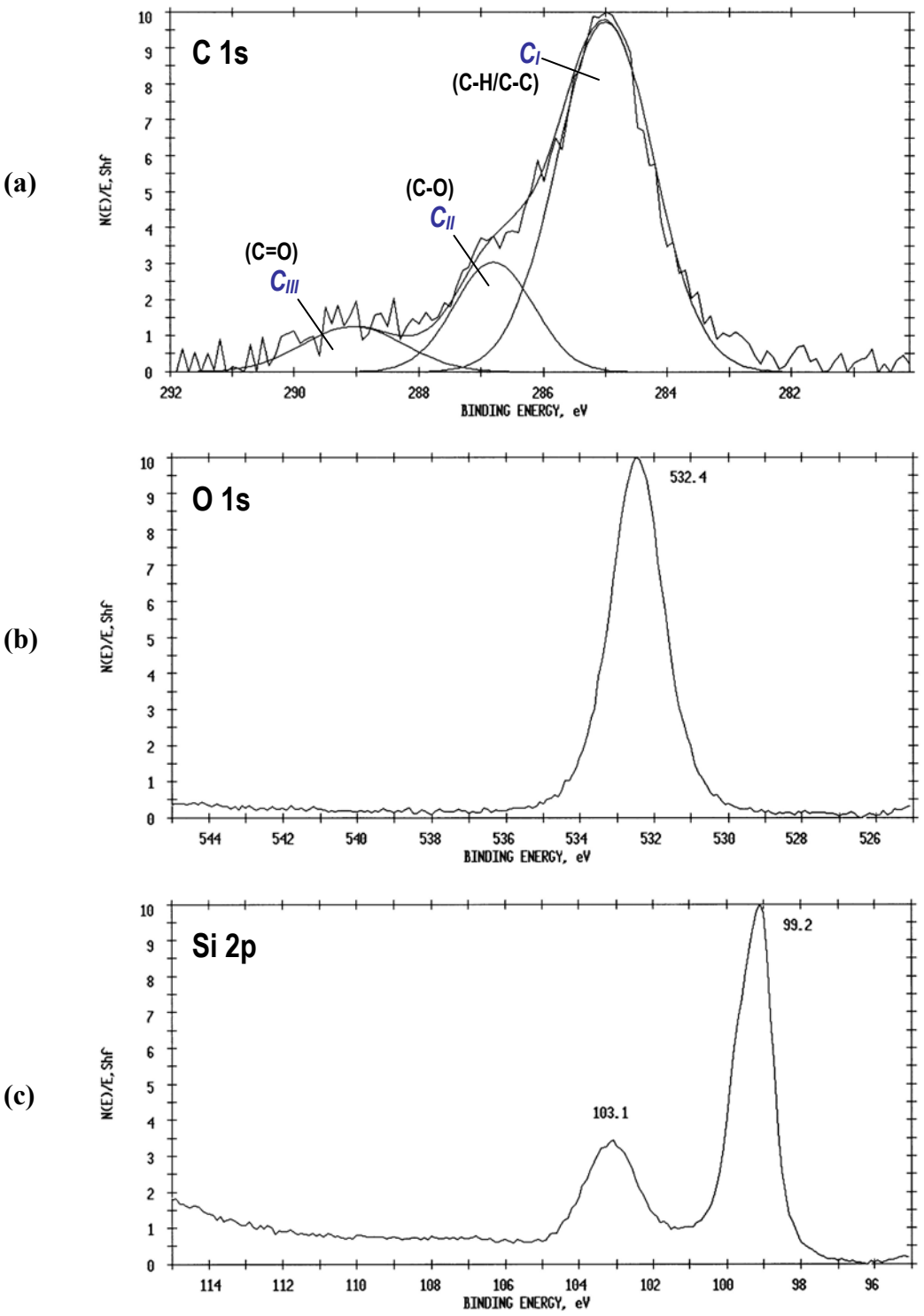

Figure 3-1. XPS spectra of an as-received (untreated) Si wafer surface. (a) C 1s, (b) O 1s, and (c) Si 2p.

(a)

(b)

(c)

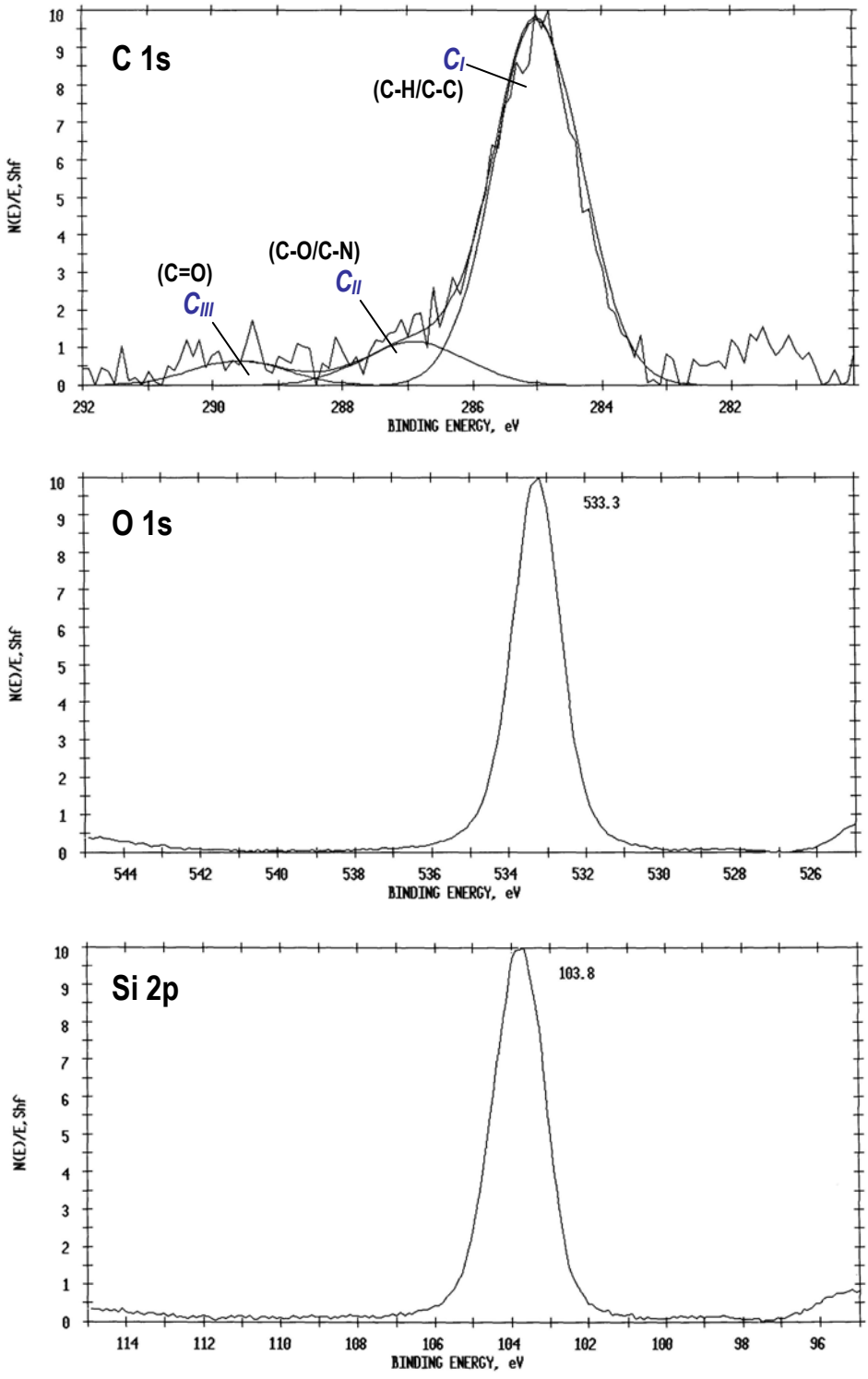

Figure 3-2. XPS spectra of a thermally oxidized (TOX) Si wafer surface. (a) C 1s, (b) O 1s, and (c) Si 2p.

angle. The O to Si ratio shown in Table 3-1 is consistent with SiO_2 on the surface.

3.3 Silane Modified Si Substrates

The Si wafers were treated with silane coupling agents according to the procedures outlined in the experimental section. The SCA-1 modified as-received and TOX wafers showed carbon, oxygen, silicon, and nitrogen. Table 3-2 summarizes the elemental surface composition for the two wafer surfaces. The percent composition for each element varied by less than 5% of the measured value when comparing the results for two equivalent samples prepared using identical experimental conditions. The oxygen content for the SCA-1 modified TOX Si surface was higher than that for the as-received Si surface because of a thicker SiO_2 layer underneath the silane layer. For the same reason, the Si content on the SCA-1 modified TOX Si surface was lower than that for the as-received Si surface because SiO_2 and elemental silicon were both detected on the as-received wafer. It should be noted that the percent silicon values shown in Table 3-2 represent the total Si content (SiO_2 + Si^o) within the XPS sampling depth at a 45^o electron take-off angle.

Table 3-2. Elemental composition of SCA-1 modified as-received Si wafer surfaces.

Sample	C	O	Si	N
Si, as received	32.7	31.3	33.4	2.6
Si, TOX	33.6	39.4	23.9	3.1

Figures 3-3 and 3-4 show the curve-fit spectra for the SCA-1-modified as-received Si surface and the SCA-1-modified TOX Si surface. The binding energies for the resolved carbon peaks were essentially the same for the two silicon surfaces (see Table 3-3); however, the percentages for individual carbon species were slightly different. This difference was due to the different distribution of carbon species for the as-received Si and TOX Si surfaces, as well as errors associated with the curve-fitting. For curve-fit Si spectra for the as-received/SCA-1 surface, four Si peaks were resolved. Peak Si_{III} at 102.2 eV was attributed to Si-O-Si functionality from the hydrolyzed SCA-1

(a)

(b)

(c)

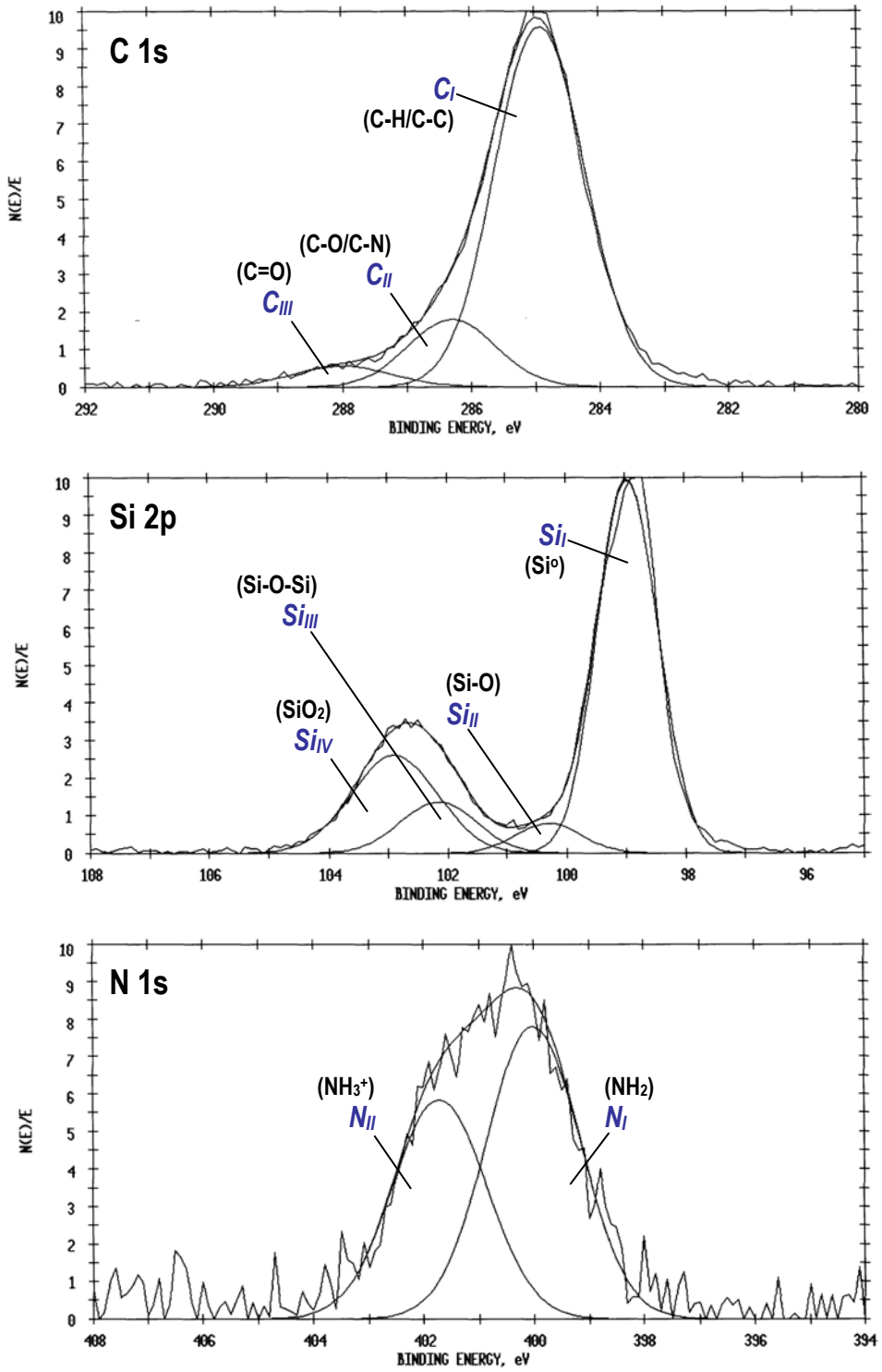

Figure 3-3. Curve-fit XPS spectra for a SCA-1 treated as-received Si wafer surface. (a) C 1s, (b) Si 2p and (c) N 1s.

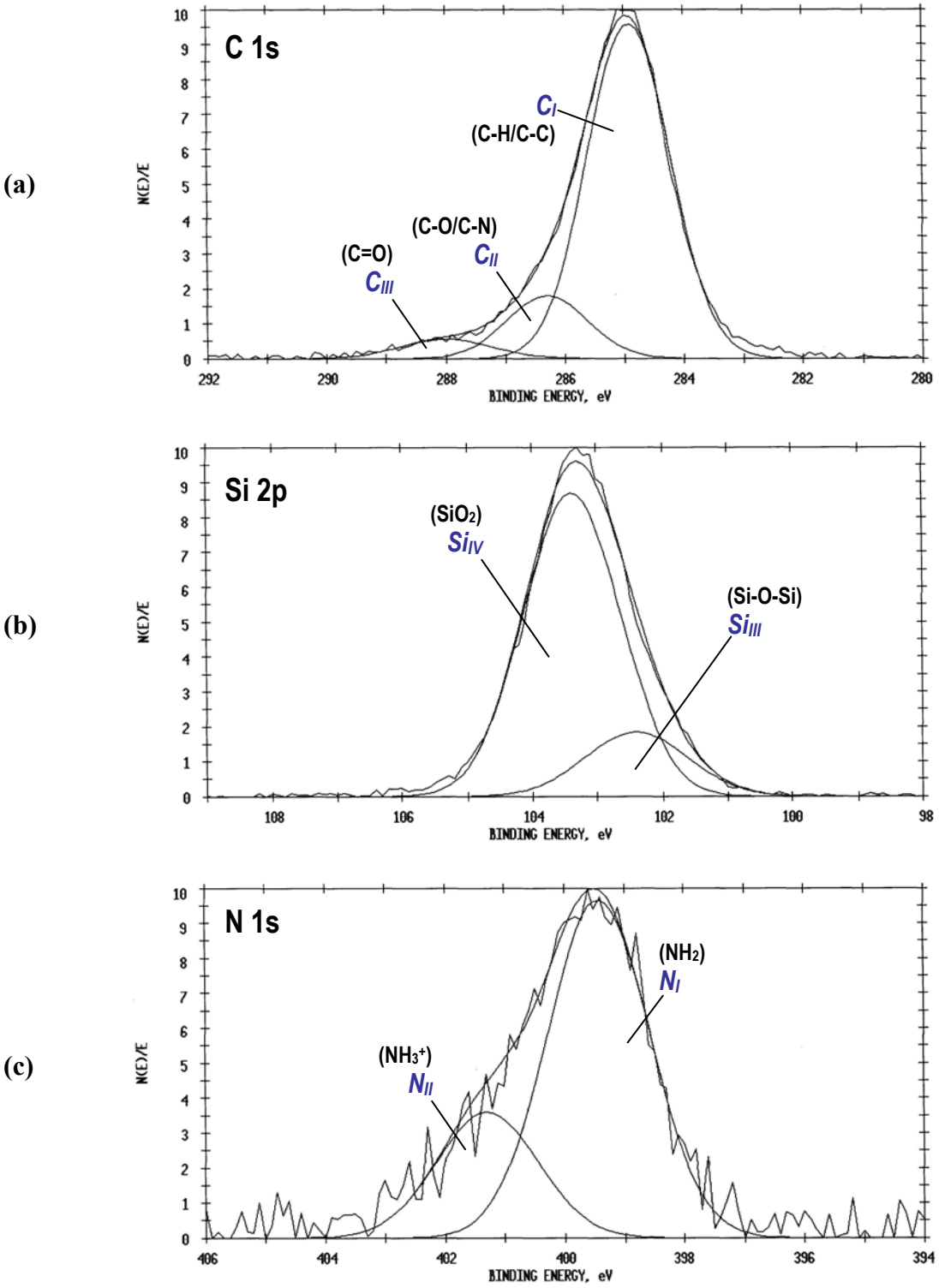

Figure 3-4. Curve-fit XPS spectra for SCA-1 treated as-received TOX Si wafer surface. (a) C 1s, (b) Si 2p and (c) N 1s.

at the SiO_2 surface, and peak Si_{IV} at 103.0 eV was attributed to the existing SiO_2 layer.

Table 3-3. Peak assignments for the curve-fit C 1s spectra for SCA-1 modified as-received Si wafer surfaces.

Sample/Peak No.	Peak Position, eV	%	Assignment
Si, as received, C_I	285.0	73.1	C-H/C-C
Si, as received, C_{II}	286.5	17.6	C-O/C-N
Si, as received, C_{III}	288.4	9.3	$C=O_x$
Si, TOX, C_I	285.0	80.2	C-H/C-C
Si, TOX, C_{II}	286.4	14.7	C-O/C-N
Si, TOX, C_{III}	288.1	5.1	$C=O_x$

Table 3-4. Peak assignments for the curve-fit Si 2p spectra for SCA-1 modified as-received Si wafer surfaces.

Sample/Peak No.	Peak Position, eV	%	Assignment
Si, as received, Si_I	99.0	61.1	Si^o
Si, as received, Si_{II}	100.3	5.3	$Si-(OR)_x$
Si, as received, Si_{III}	102.2	10.6	Si-O-Si (siloxane)
Si, as received, Si_{IV}	103.0	23.0	SiO_2
Si, TOX, Si_{III}	102.2	18.3	Si-O-Si (siloxane)
Si, TOX, Si_{IV}	103.4	81.7	SiO_2

Table 3-5. Peak assignments for the curve-fit N 1s spectra for SCA-1 modified as-received Si wafer surfaces.

Sample/Peak No.	Peak Position, eV	%	Assignment
Si, as received, N_I	400.0	57.3	$-NH_2$
Si, as received, N_{II}	401.7	42.7	$-NH_3^+$
Si, TOX, N_I	399.4	72.9	$-NH_2$
Si, TOX, N_{II}	401.3	27.1	$-NH_3^+$

The elemental Si (peak Si_I) at 99.0 eV was the dominant peak. Peak Si_{II} at a low intensity may be attributed to Si with unknown structure/composition. That the Si-O-Si species could be curve-fit from the SiO_x Si 2p peak suggests that the silane layer on the SiO_2

layer was very thin. For the SCA-1 modified TOX Si surface, the composite SiO_2 peak (Figure 3-4b) shifted slightly to a lower binding energy compared to that for the pure TOX surface (Figure 3-2c). The peak width of the composite SiO_2 peak was also wider due to the contribution from Si-O-Si (peak Si_{III} at 102.2 eV).

Figure 3-3c and Figure 3-4c show the curve-fit N 1s spectra for SCA-1 modified Si surfaces. The co-existence of free amine $-NH_2$ at ~399.4 ± 0.3 eV and the protonated amine $-NH_3^+$ at ~401.3 ± 0.2 eV was in agreement with findings by a number of other researchers[1,2]. The orientation and nature of the SCA-1 molecule on silicon surfaces depends strongly on the pH of the solution[3,4]. However, it is interesting to note that under that same reaction conditions (i.e., pH, silane concentration, treatment time, and curing conditions), the percentages of $-NH_2$ and $-NH_3^+$ are different for Si substrates with different extents of surface oxidation (see Table 3-5). As Chiang *et al*.[5] suggested the presence of $-NH_3^+$ was indicative of a cyclic structure of the SCA-1 molecule (i.e., 5 or 6-memebered ring[6]) and NH_2 was representative of a free amine on the oxide surface. Thus, one could argue that for the more oxidized TOX Si surface, a higher silanol group density would facilitate a greater level of coupling with the hydrolyzed SCA-1 molecule in forming the stable siloxane linkage. Subsequently, the percent occurrence of cyclic SCA-1 formation is lower. Further, it should be noted that adsorption of the SCA-1 molecule in the cyclic form would inhibit its effectiveness as a coupling agent with a polymeric adhesive.

In addition to SCA-1, studies with SCA-2 and SCA-3 were also carried out to modify Si wafer surfaces. These silanes differ in the number of the tri-alkoxy groups and in the nature and number of reactive functional groups. The XPS data in Table 3-6 present the elemental compositions of the silane-treated Si surfaces. The carbon content was higher for SCA-2 and SCA-3 modified surfaces than for a SCA-1 modified surface. This finding is consistent with relative carbon content of the silanes. Also, the total nitrogen percent on the SCA-3 modified surface is approximately twice that on the SCA-1 modified surface. In addition, the ratio of unprotonated (free) amine to the protonated

amine decreases in the manner: SCA-1 > SCA-2 > SCA-3. From the curve-fit results a higher Si-O-Si/Si^o ratio was observed for SCA-2 or SCA-3 modified surfaces than for the SCA-1 modified surface. This result suggests that more Si-O-Si moieties existed on the Si surface following reactions with SCA-2 and SCA-3.

Table 3-6. Elemental composition for various silane-treated as-received Si wafer surfaces.

Sample	C	O	Si	N	Si-O-Si/Si^o	Unprotonated amine/ protonated amine
SCA-1	32.7	31.2	33.0	3.1	1.00	1.33
SCA-2	44.6	28.6	22.8	4.0	1.55	2.77
SCA-3	42.8	27.3	24.1	5.8	1.71	4.16

3.4 Oxygen Plasma Treated Si Substrates

XPS surface analyses were carried out to determine the elemental composition for a SCA-1/O_2 plasma/Si specimen. To study the relationship between Si surface oxidation and silane derivitization, Si wafer backside surfaces were treated for 2 min, 15 min, and 30 min in an O_2 plasma. These oxidized surfaces and the as-received wafer surface were treated in a 0.1M SCA-1 solution (with 5% v/v 0.1M HCl aqueous solution) for 30 minutes. Table 3-7 summarizes the XPS surface composition for O_2 plasma treated Si wafers. The carbon content decreased from about 11% to ~6%, as the plasma treatment time increased; the oxygen content increased consistently from about 40% to 60%, the total Si content decreased from about 48% to 36%, and the SiO_2 to Si^o ratio increased from 0.38 to 1.81. These findings are consistent with the fact that the O_2 plasma cleans the surface by removing some of the organic contamination and oxidizes the wafer to generate more silicon dioxide. The increases in SiO_2/Si^o and Si-O-Si/Si^o ratios (both from curve-fit data) as a function of plasma treatment time are shown in Figure 3-5. It should be noted that the SiO_x content is the sum of the SiO_2 (oxide generated from the plasma treatment) and Si-O-Si (silane reaction).

Table 3-7. Elemental composition for O_2 plasma treated Si wafer surfaces.

Sample	C	O	Si	SiO_2/Si^o
As received	11.2	40.9	47.9	0.38
2min O_2, 50W, 20 sccm	6.2	54.8	39.0	1.00
15min O_2, 50W, 20 sccm	5.9	58.1	36.0	1.55
30min O_2, 50W, 20 sccm	4.2	59.6	36.2	1.81

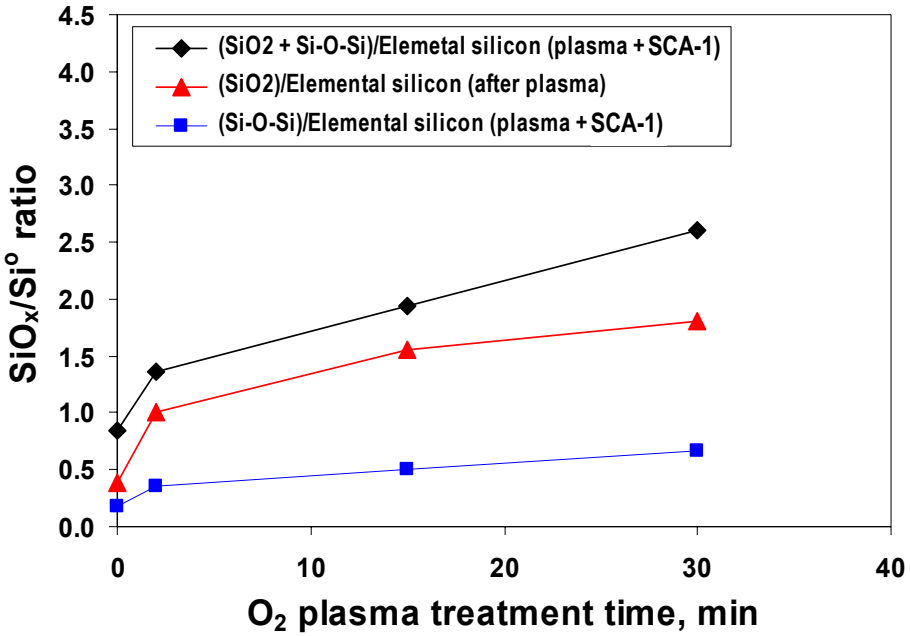

Figure 3-5. Silicon oxide (SiO_x)/elemental silicon ratio as a function of O_2 plasma and SCA-1 treatments on Si backside surfaces. The SiO_x content includes SiO_2 (O_2 plasma generated) and Si-O-Si (silane modification).

The surface composition for SCA-1 treated Si wafers that were first O_2 plasma treated is summarized Table 3-8. The SiO_x/Si^o ratio represents the ratio of total silicon-oxygen species (SiO_2 and Si-O-Si) to elemental silicon. The SiO_2 and Si-O-Si contributions were obtained from the curve fit of the SiO_x peak. The surface analysis results show that the carbon and silicon contents decreased slightly (~3-5 %), the surface oxygen content increased slightly, while the nitrogen content remained essentially unchanged (<2 %), as the time of the oxygen plasma treatment increased. In addition, the SiO_x/Si^o, Si-O-Si/Si^o, and Si-O-Si/N ratios increased as the oxygen plasma treatment time

increased. The Si-O-Si/N ratio is evaluated by dividing the Si concentration attributed to Si-O-Si based on curve-fit results by the total N concentration. Also, the $-NH_2/-NH_3^+$ ratio did not vary significantly as the time of the oxygen plasma treatment increased. These findings suggest that the amount of SCA-1 deposited on the Si surface did not vary significantly as the O_2 plasma pretreatment time increased.

Table 3-8. Elemental composition for O_2 plasma (50W, 20 sccm) treated, SCA-1-modified Si wafer backside surfaces.

Sample	C	O	Si	N	$-NH_2/-NH_3^+$	SiO_x/Si^o	(Si-O-Si)/SiO_2	(Si-O-Si)/N
As received	33.2	31.2	32.1	3.5	1.79	0.85	0.40	0.83
2min O_2	28.2	39.3	29.4	2.6	2.01	1.36	0.26	1.32
15min O_2	31.7	39.3	26.9	2.1	1.89	1.94	0.26	1.78
30min O_2	27.0	43.3	26.8	2.9	2.23	2.61	0.26	2.68

Figure 3-6 shows the curve-fit Si 2p spectra for the Si wafer backside surfaces after a 15 min O_2 plasma treatment and after a 30 min SCA-1 treatment. For the oxygen plasma treated (only) surface, the Si 2p XPS spectrum showed silicon features characteristic of SiO_2 (at 103.2 eV) and elemental silicon, Si^o (at 98.7 eV). This observation indicates that a thin layer of SiO_2 is present on the as-received Si wafer substrate (see small insert in Figure 3-6a). For the SCA-1 modified surfaces, the Si 2p XPS spectrum showed silicon features characteristic of SiO_x (at 102.9 eV) and Si^o (at 98.7 eV). This silicon oxide (SiO_x) peak was curve fit to yield a SiO_2 peak (at 103.2 eV) and a Si-O-Si peak (at 102.4 eV). The Si-O-Si peak is identified as the siloxane functionality resulting from the silane treatment. As shown in the small insert in Figure 3-6b, Si-O-Si represents silane chemically bonded to the SiO_2 surface. However, it is noted that the SiO_2 to Si^o ratio (based on curve fit results) for the SCA-1 modified surface (Table 3-8 and Figure 3-6b) is about the same as that for the just oxidized surface (Table 3-7 and Figure 3-6a). The half width of the Si 2p (SiO_x) peak in Figure 3b was slightly broadened compared to the Si 2p peak for just oxidized SiO_2 in Figure 3-6a. The increase in peak width indicates a change in surface composition.

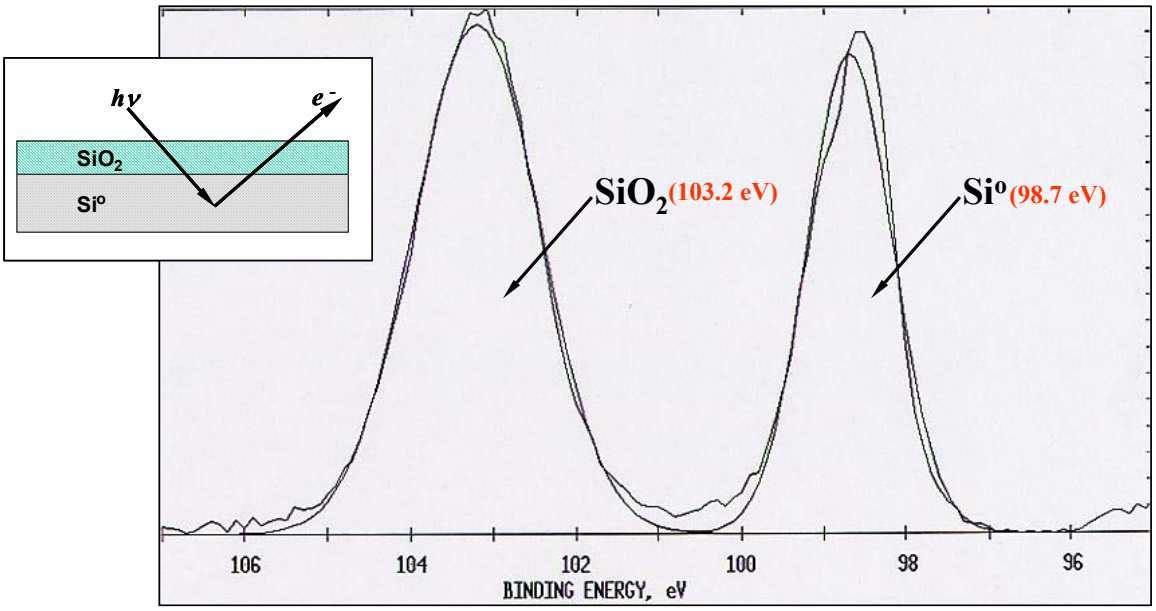

(a)

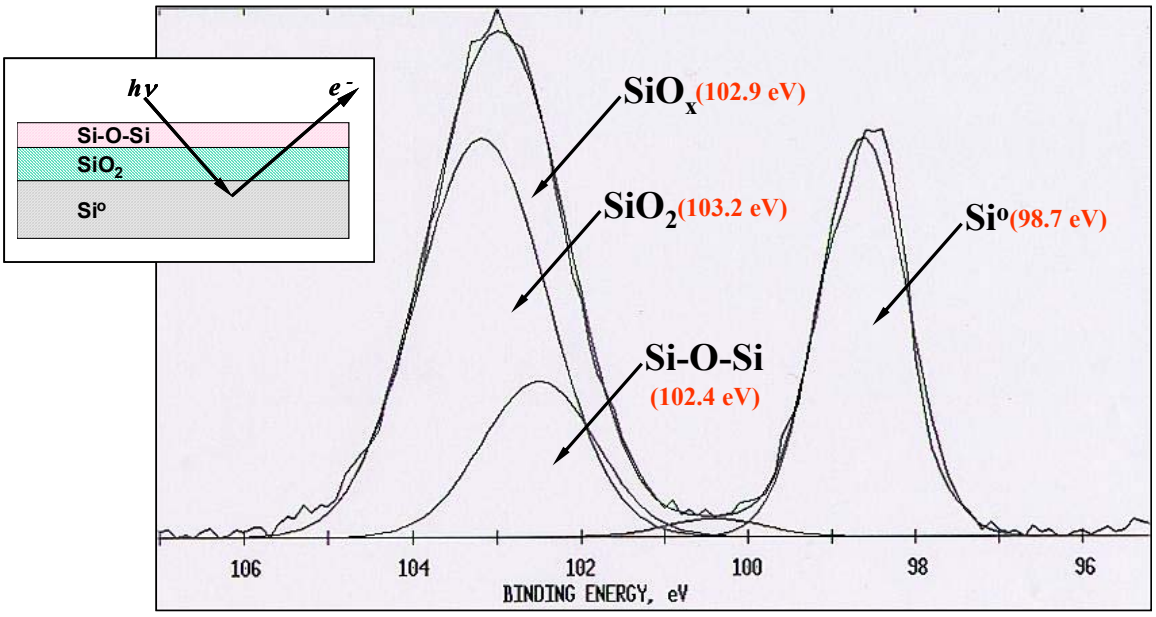

(b)

Figure 3-6. Curve fit Si 2p spectra (take-off angle = 45°) of the Si wafer backside surfaces: (a) 15min O_2 plasma treatment, 50W, 20sccm; (b) 15min O_2 plasma treatment, 50W, 20sccm, followed by 30min SCA-1 treatment.

Tables 3-8 and 3-9 summarize the surface composition for SCA-2 and SCA-3 treated Si wafers that were first treated in an O_2 plasma, respectively. The XPS results show that the respective carbon, oxygen, silicon, and nitrogen contents did not change significantly as the time of the oxygen plasma treatment increased for both silane-modified Si surfaces. The SiO_x/Si^o, Si-O-Si/Si^o, and Si-O-Si/N ratios increased as the time of the oxygen plasma treatment increased, while the -NH/-NH_2^+ ratios showed no particular trend. The slight increasing trend in Si-O-Si/N ratios was associated with the Si-O-Si content based on the curve-fit results as oxygen plasma treatment time increased. The values for the Si-O-Si/N ratio for SCA-2-modified surface range from 1.41 to 1.75. For the SCA-3-modified surface, the observed ratio is close to one. Thus, the amounts of SCA-2 or SCA-3 deposited on the Si surface do not increase with the oxygen plasma pre-treatment time.

Table 3-9. Elemental composition for O_2 plasma (50W, 20 sccm) treated, SCA-2-modified Si wafer backside surfaces.

Sample	C	O	Si	N	-NH/-NH_2^+	SiO_x/Si^o	(Si-O-Si)/SiO_2	(Si-O-Si)/N
As received	34.8	31.5	30.6	3.1	2.75	0.83	0.50	1.41
2min O_2	33.8	35.6	27.4	3.1	2.97	1.30	0.69	1.56
15min O_2	33.4	37.4	25.2	4.0	2.28	2.20	0.63	1.64
30min O_2	42.8	32.1	21.5	3.7	3.01	4.50	0.55	1.75

Table 3-10. Elemental composition for O_2 plasma (50W, 20 sccm) treated, SCA-3-modified Si wafer backside surfaces.

Sample	C	O	Si	N	-NH/-NH_2^+	SiO_x/Si^o	(Si-O-Si)/SiO_2	(Si-O-Si)/N
As received	42.8	27.7	24.1	5.4	3.97	1.46	0.40	0.74
2min O_2	39.2	31.5	23.6	5.8	2.92	1.51	0.46	0.73
15min O_2	38.3	32.3	23.9	5.5	2.74	1.94	0.47	0.80
30min O_2	42.2	30.9	21.1	5.8	3.18	2.45	0.57	0.91

For an atomically smooth elemental Si surface coated with an overlayer of SiO_2, it is possible to estimate the SiO_2 layer thickness using the following equation:[7]

$$t_{OX} = \lambda_{SiO_2} \sin\theta \ln\left[\left(\frac{I^{\infty}_{Si}}{I^{\infty}_{SiO_2}}\frac{I^{\exp}_{SiO_2}}{I^{\exp}_{Si}}\right)+1\right] \qquad \textbf{Equation 3-1}$$

where λ_{SiO2} is the attenuation length of the Si 2*p* photoelectrons in SiO_2, θ is the electron take-off angle, $I^{\infty}_{Si}/I^{\infty}_{SiO2}$ is the ratio of Si 2*p* intensities for substrate Si^o and SiO_2, and $I^{exp}_{SiO2}/I^{exp}_{Si}$ is the ratio of intensities for SiO_2 and Si^o for the wafer, respectively. In this case, θ was 45°. A reported λ_{SiO2} value of 2.6 nm, and a reported $I^{\infty}_{Si}/I^{\infty}_{SiO2}$ value of 1.46 were used[8,9].

Table 3-11 shows the calculated SiO_2 layer thickness as a function of oxygen plasma treatment time. It is clear that as the plasma treatment time increased, the thickness of the SiO_2 layer on Si^o increased.

Table 3-11. Calculated SiO_2 layer thickness on Si^o for as-received plasma-treated Si wafer substrates (backside).

Sample	SiO_2/Si^o	SiO_2 layer thickness, nm
As received	0.38	0.81
2min O_2, 50W, 20 sccm	1.00	1.65
15min O_2, 50W, 20 sccm	1.55	2.17
30min O_2, 50W, 20 sccm	1.81	2.37

3.5 Angle Resolved-XPS Characterization of Treated Si Substrates

In the previous section, XPS characterization of silicon modified with various silane coupling agents was presented. The oxygen RF plasma was used to pretreat the as-received Si wafer to increase the surface oxide content. Increased oxygen plasma pretreatment time resulted in an increase in silicon oxide content on the wafer surface.

The XPS characterization also showed that the silane films on the Si wafer were very thin.

Angle resolved XPS was used as an aid in determining the molecular orientation of the silane molecule on the Si surface by comparing relative intensities at low and high take-off angles. The results indicate whether a species is enriched or depleted in the surface region. Knowing the molecular orientation on the surface is important because silane adsorption on the Si surface can either take place *via* interaction between the silane silanol groups and the surface silanol groups, or between the silane amine functionality and the surface silanol groups. The later case results in an undesirable molecular orientation for adhesion promotion because the amine functionalities are no longer available for 'coupling' with the polymer. However, it is known that both orientations coexist on the Si surface if the deposition of silane takes place in a polar solvent (i.e., alcohol)[3,4].

Figure 3-7 shows the atomic composition of the three different SCAs on the SiO_2 surface as a function of XPS electron take-off angle. The Si wafer was exposed to an O_2 RF plasma for 30min prior to the 30min silane treatment. In general, the elemental distributions for SCA-1, SCA-2 and SCA-3 films on the Si surface are very similar. The nitrogen content is the highest for all three films at the lowest take-off angle, which indicates that nitrogen bearing functionalities extend principally from the surface.

Figure 3-8 shows the silane layer thickness on the SiO_2 surface as a function of O_2 plasma treatment time. The thickness was calculated using XPS data taken at a 45^o take-off angle by taking the difference between total film thickness ($SCA/SiO_2/Si$) and the oxide film thickness (SiO_2/Si). The film thickness was about 6 ± 1 Å for all three silanes. The film thickness increased initially and quickly leveled off as the oxygen plasma pre-treatment time increased. This finding suggests that the duration of the oxygen plasma pre-treatment, which resulted in an increase in the thickness of the SiO_2 layer (Table 3-9), has a minimum effect on the thickness of the silane layer on the SiO_2 surface.

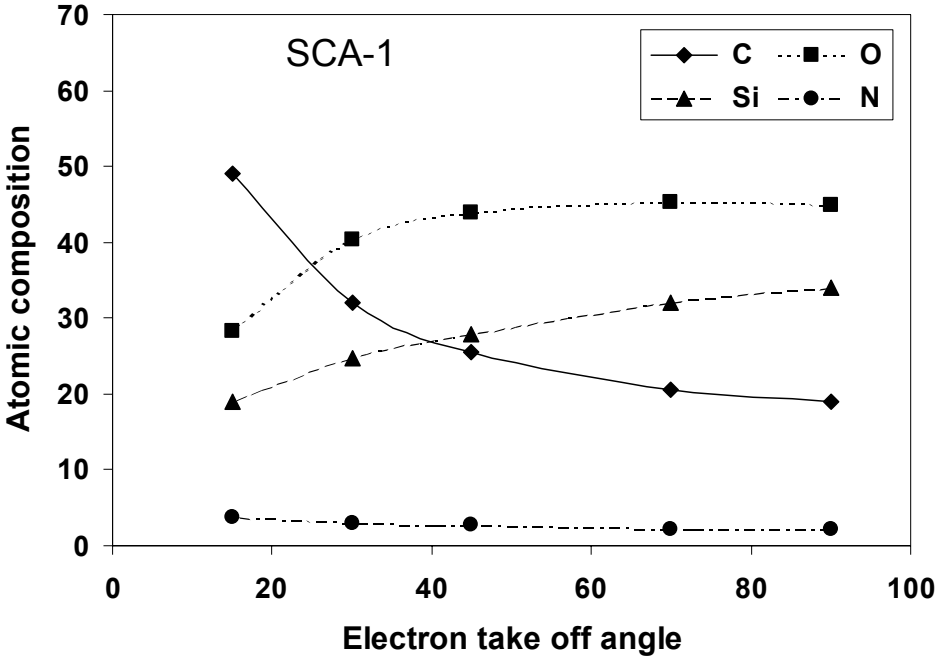

(a)

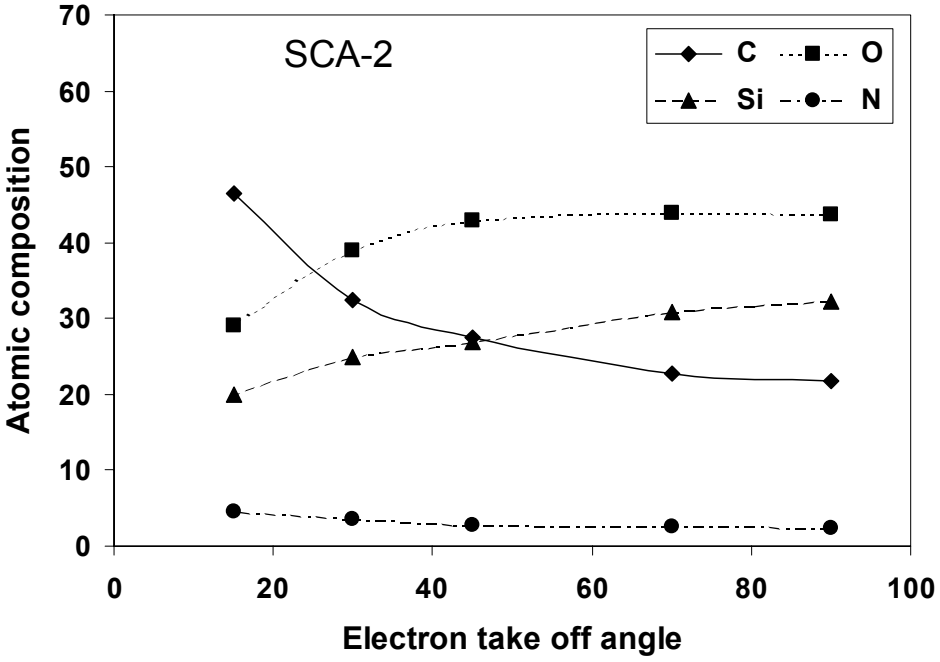

(b)

Figure 3-7a, b. Atomic composition of silane on the SiO_2 surface as a function of XPS electron take-off angle. The Si wafer was exposed to a 30min O_2 RF plasma, prior to a 30min silane treatment (0.1M) in ethanol. (a) SCA-1 and (b) SCA-2.

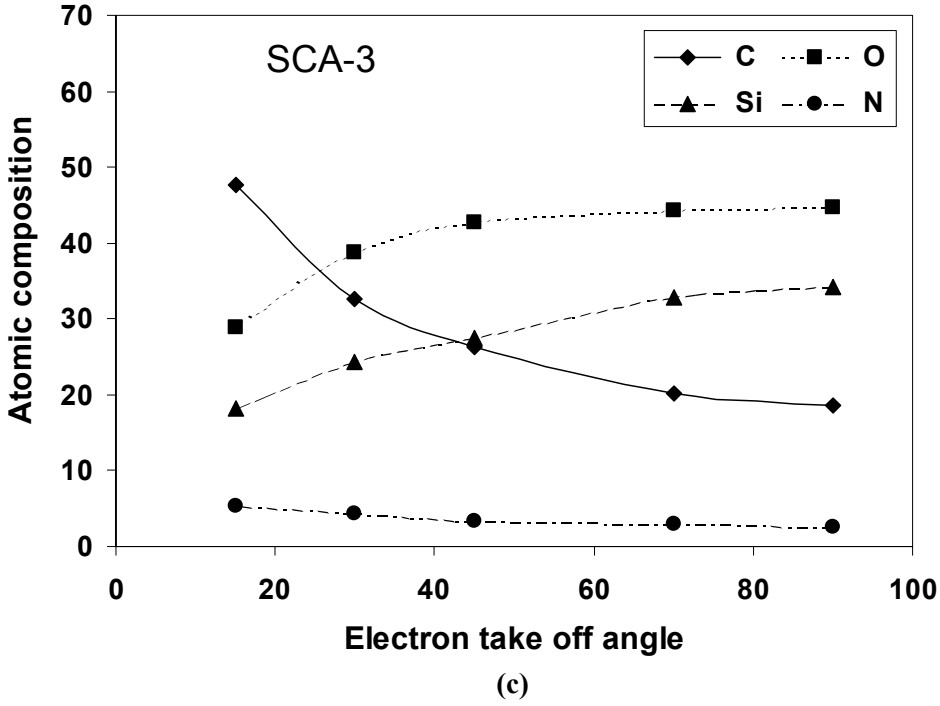

(c)

Figure 3-7c. Atomic composition of silane on the SiO_2 surface as a function of XPS electron take-off angle. The Si wafer was exposed to a 30min O_2 RF plasma, prior to a 30min silane treatment (0.1M) in ethanol. (c) SCA-3.

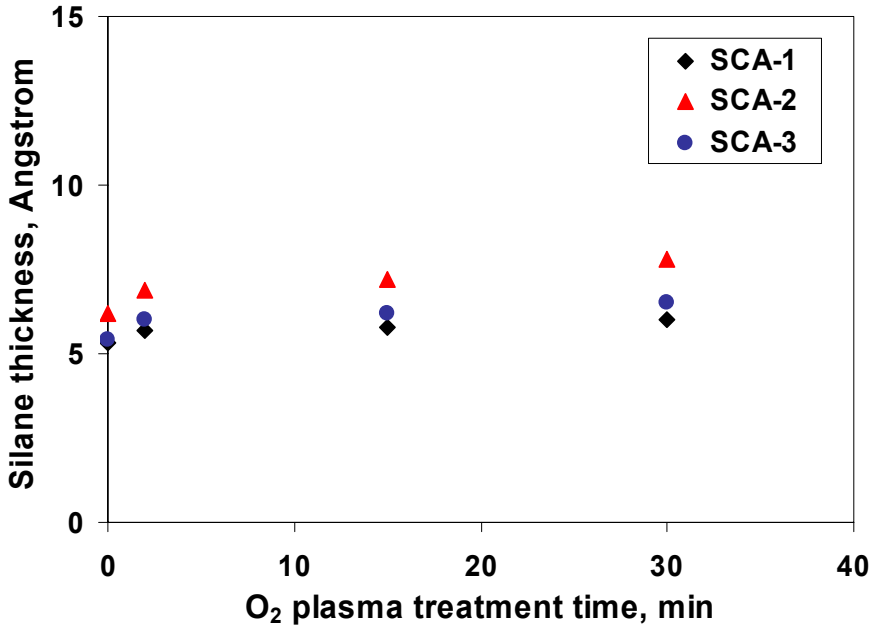

Figure 3-8. Silane layer thickness on the SiO_2 surface as a function of O_2 plasma treatment time; calculated based on XPS data at a 45° take-off angle. The oxygen plasma treated Si wafer was immersed in a 0.1M SCA solution for 30 min.

3.6 Auger Electron Spectroscopy Characterization of Silane Treated Si Substrates

Depth profiling by Auger electron spectroscopy (AES) using noble gas ion sputtering can sample the substrate composition to a much greater depth. As shown from the XPS data, the total film thickness of the SiO_2 layer and silane layer on the elemental silicon substrate is less than 50 Å. Thus, to obtain detailed compositional information, AES depth profiling was conducted at a low sputtering rate of about 1 Å/min.

Figure 3-9a shows the AES depth profile for an as-received Si wafer surface without an oxygen plasma treatment. The plot shows about 60 at %Si, 35 at %O and low C and N contents at the starting depth. The Si content increases to nearly 100% at approximately 25 Å, and the carbon content diminishes to 0% at about the same depth. After treating the as-received Si wafer in the oxygen plasma for 30min, the depth profile changed in that the rate of increase of the %Si and the rate of decrease in %C were slower compared to the profile for an as-received substrate (see Figure 3-9b). The depth at which the Si content approaches 100% and the carbon content approaches 0% was also greater, indicating that the thickness of the SiO_2 layer increased as a result of exposure to the oxygen plasma.

Figure 3-10 shows the AES depth profiles for an as-received Si wafer surface treated with various silane coupling agents. The presence of carbon in a significant amount was due to silane modification. The depth profiles for SCA-1, SCA-2 and SCA-3 modified surfaces were generally similar. However, the depth at which Si approached 100% and C decreased to 0% was less for the SCA-1 derivatized surface than for the SCA-2 and SCA-3 modified surfaces.

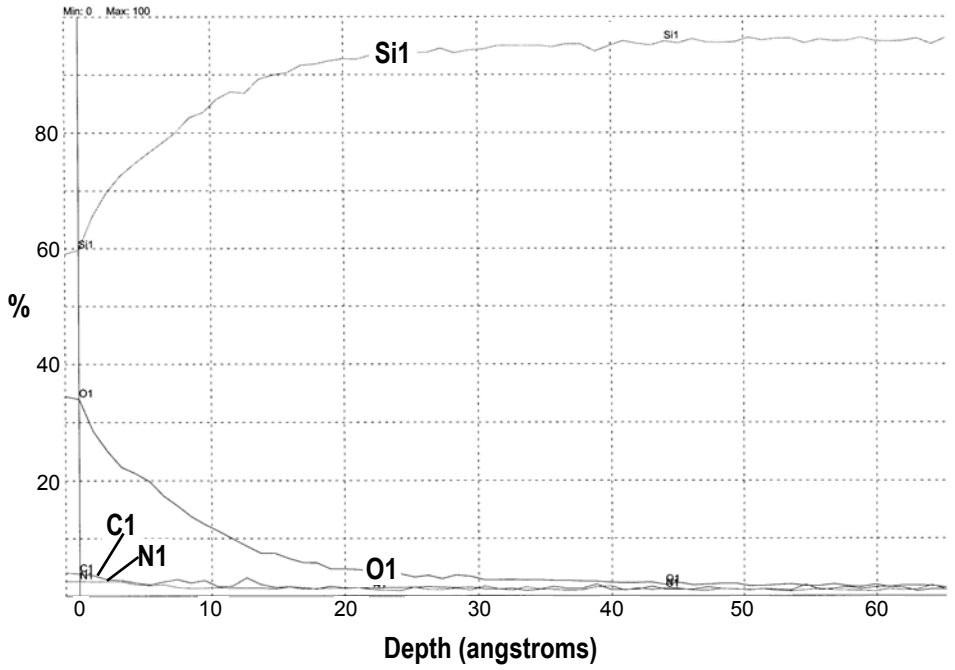

(a)

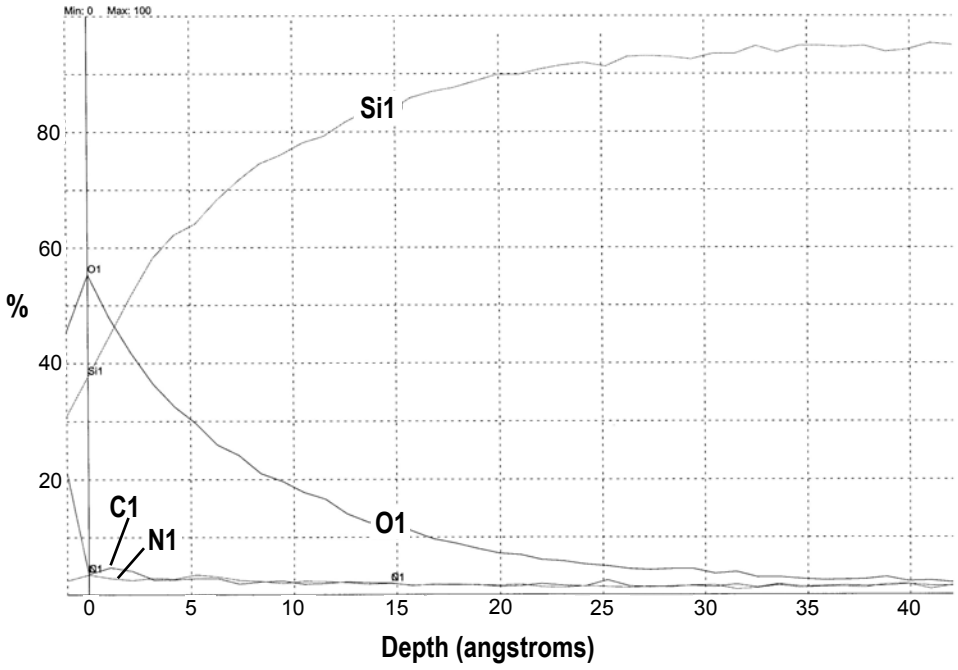

(b)

Figure 3-9. AES depth profile for oxygen plasma treated as-received Si wafer. Data collected at a sputtering rate of 1Å/min. (a) after 0min (without plasma treatment) and (b) after 30min oxygen plasma.

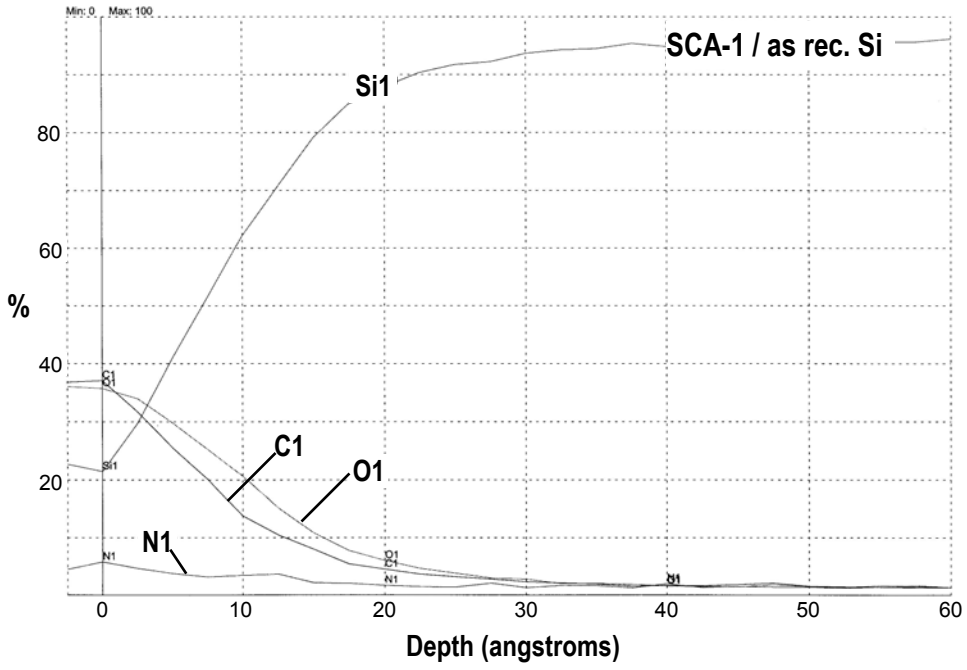

(a)

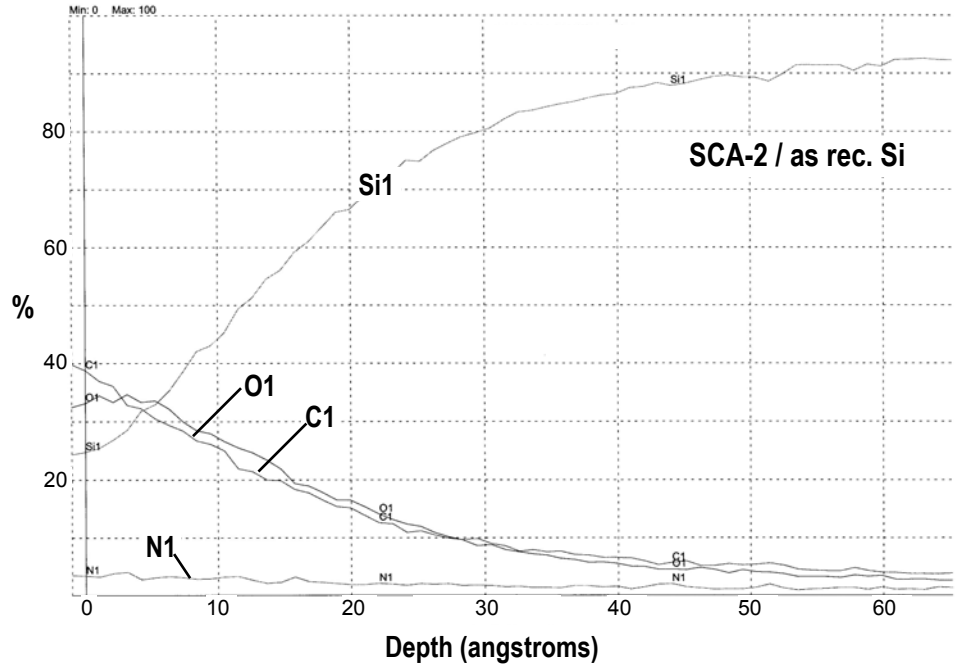

(b)

Figure 3-10a,b. AES depth profile of silane treated as-received Si wafer. Data collected at a sputtering rate of 1Å/min. (a) SCA-1, 0.1M, 30min and (b) SCA-2, 0.1M 30min. (both SCA solutions in EtOH with 5% v/v 0.1 HCl aqueous solution).

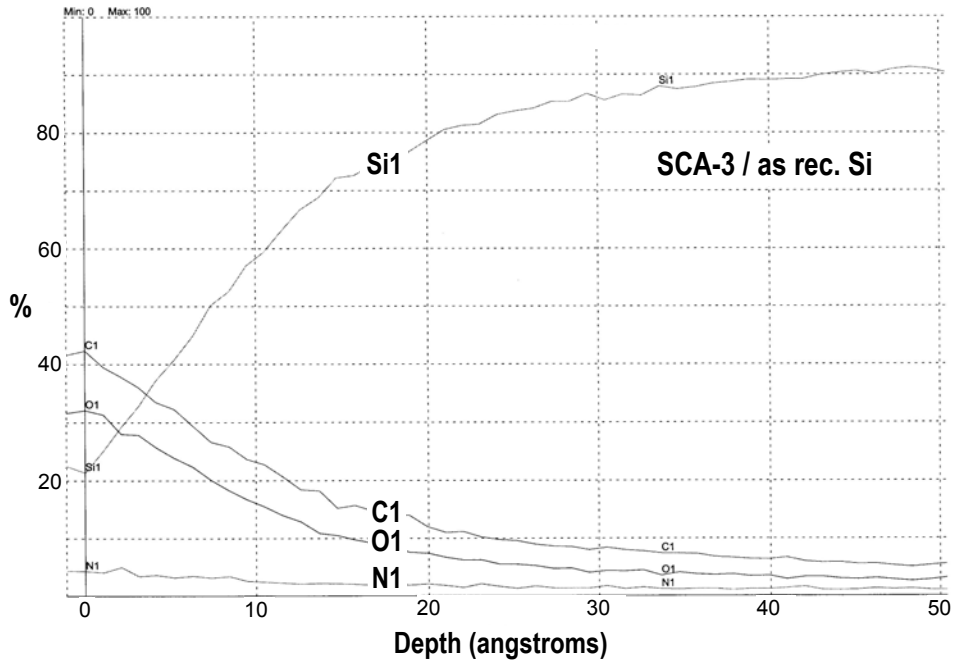

(c)

Figure 3-10c. AES depth profile of silane treated as-received Si wafer. Data collected at a sputtering rate of 1Å/min. (c) SCA-3, 0.1M (in EtOH with 5% v/v 0.1 HCl aqueous solution), 30min.

3.7 Ellipsometry Characterization of Silane Treated Si Substrates

Ellipsometry can also be used to determine the thickness of multilayer structures with thicknesses from sub-monolayer to millimeters, provided optical constants are approximately known. In this case the silane film thickness and the SiO_2 thickness can be determined knowing the index of refraction of the Si substrate. As shown in Figure 3-11, the SiO_2 layer thickness increases with longer oxygen plasma treatment time. However, the increase in SiO_2 layer thickness did not correlate with the silane thickness as a function of the oxygen plasma pre-treatment time, as evident in Figure 3-12. The silane layer thickness reaches a constant value of about 12-13Å after only a very short exposure of the Si substrate in the oxygen plasma. This finding suggests that it is the number of bonding sites (i.e., surface silanol groups) on the oxide surface, not the thickness of the

oxide layer that controls the amount of silane adsorption. The film thickness ranges from 10-12 Å for all three silanes, which corresponds to a mono to bi layer coverage on the surface. It was reported in the literature that SCA-1 forms a mutilayer in polar solutions, primarily due to its crosslinking ability, while a monoalkoxy analog of SCA-1 forms a monolayer on silica[10]. A SCA-1 monolayer formed *via* vapor phase adsorption has a thickness of 7 ± 1 Å as determined by ellipsometry[11].

To examine the silane film thickness as a function of silane derivatization conditions on the SiO_2 surface, the concentration of the SCA-1 solution was varied from 0.2M to 0.004M in ethanol for varying reaction times. Note that these ethanol solutions all contain 5% v/v aqueous 0.1M HCl solution. The results shown in Figure 3-13 indicate that the silane layer thickness (as measured by ellipsometry) depends strongly on the concentration of the SCA-1 solution. It was found that 0.02M SCA-1 with a 5-minute treatment time, resulted in a film thickness of approximately 7 Å. In this case, the Si wafer surface used for silane modification had no O_2 plasma treatment. XPS analysis of the Si surface treated with various SCA-1 concentrations and exposure times showed varying surface compositions (Table 3-12). The amount of SCA-1 deposited was increased either by increasing the silane concentration in the solution or by increasing the treatment time, as reflected by the nitrogen content on the Si surface.

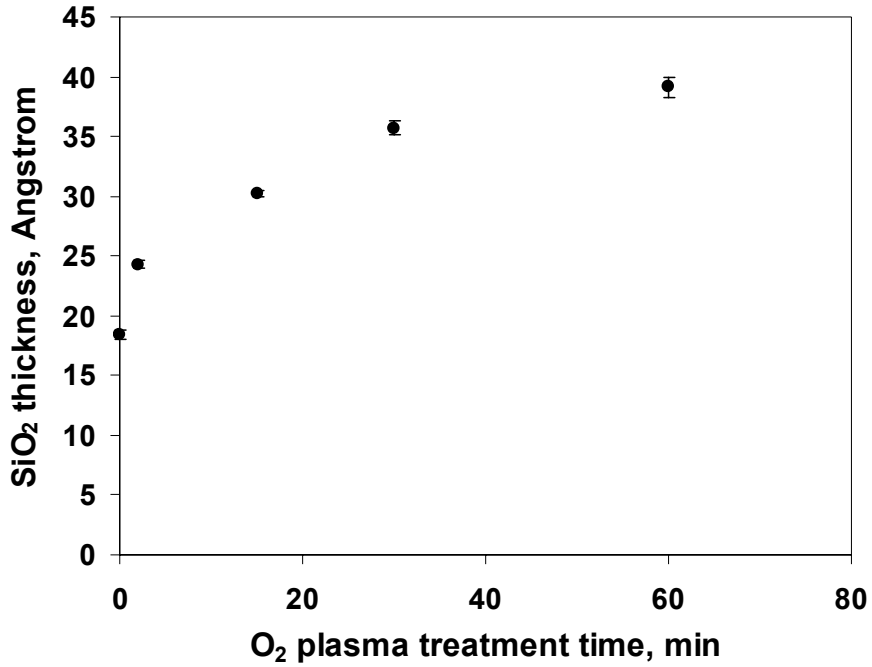

Figure 3-11. SiO_2 layer on Si as a function of O_2 plasma treatment time. The Si wafer was exposed to an O_2 RF plasma maintained at 50W, 20sccm O_2 flow rate.

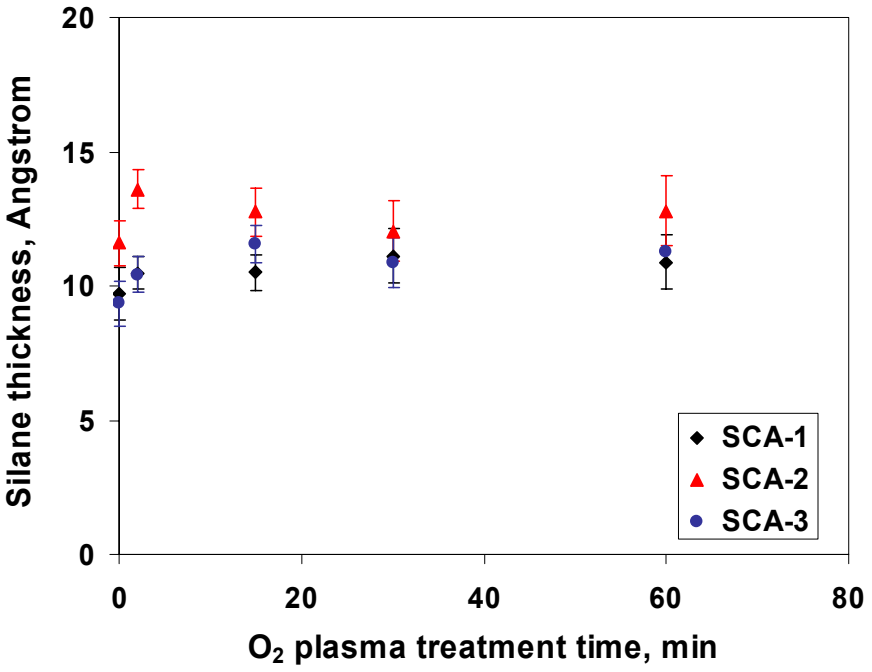

Figure 3-12. Silane layer thickness on the SiO_2 surface as a function of O_2 plasma treatment time. Oxygen plasma oxidized Si wafer was immersed in 0.1M acidified silane solutions.

Table 3-12. Elemental composition (atomic %) for as-received Si wafers treated with SCA-1 solutions at various concentrations.

Sample No.	Surface Treatment	C	O	Si	N
1	As received, no silane	6.9	47.0	46.1	< 0.1
2	0.004M*, SCA-1, 5 min	13.2	36.1	50.0	0.7
3	0.01M, SCA-1, 5 min	22.7	33.7	42.1	1.5
4	0.02M, SCA-1, 5 min	23.0	31.3	44.1	1.6
5	0.02M, SCA-1, 15 min	23.6	32.7	41.8	1.9
6	0.1M, SCA-1, 1 min	25.4	43.9	28.3	2.4
7	**0.1M, SCA-1, 30 min****	**33.2**	**31.2**	**32.1**	**3.5**
8	0.1M, SCA-1, 5 min	32.0	40.3	24.8	2.9
9	0.2M, SCA-1, 5 min	31.2	34.8	30.1	3.9

* Standard SCA-1 concentration and treatment time used previously.
** Note that these ethanol solutions all contain 5% v/v aqueous 0.1M HCl solution.

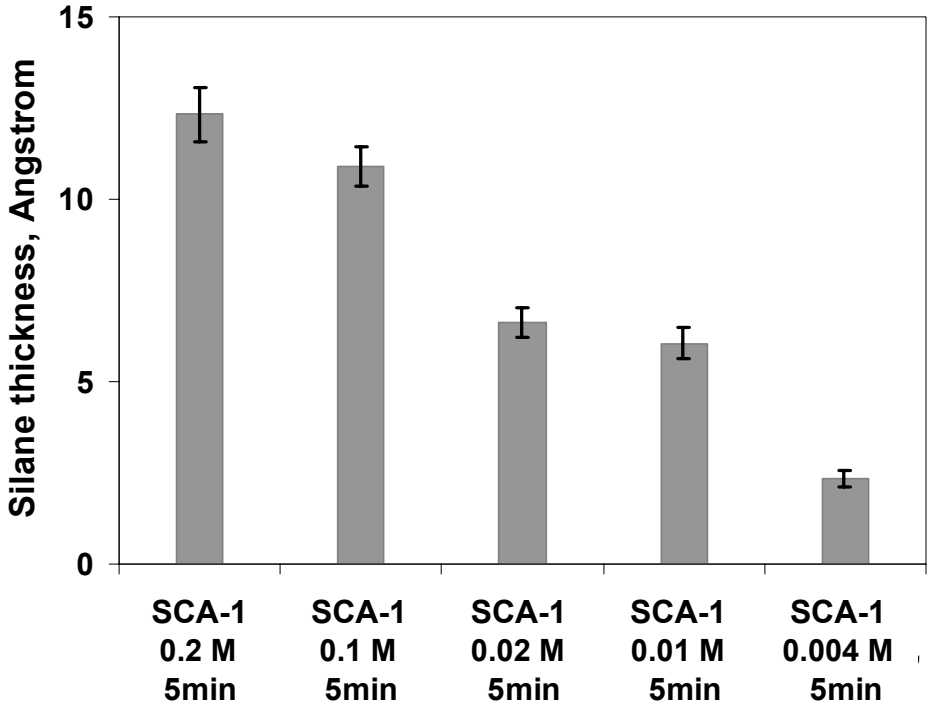

Figure 3-13. Silane layer thickness (ellipsometry) on the SiO_2 surface as a function of the concentration of the SCA-1 solution. The Si wafer surface was used for silane modification without O_2 plasma oxidation treatment. Error bars are determined from at least 9 measurements at different sample spots. Note that these ethanol solutions all contain 5% v/v aqueous 0.1M HCl solution.

3.8 Contact Angle Study of Silane Treated Si Substrates

For O_2 plasma treatment of as-received Si wafers, the advancing water contact angle was measured as a function of oxygen plasma treatment time. A contact angle for water of 10^o was observed for an as-received Si surface. The non-zero contact angle can be attributed to the presence of residual organic contamination on the wafer surface as verified by XPS data (Table 3-13). The water contact angle approached 0^o after approximately 10 minutes of exposure in an oxygen plasma (see Figure 3-14a). The attainment of a zero contact angle was primarily due to the removal of the trace organics and exposure of the polar SiO_2 surface.

Table 3-13. Advancing water contact angle on Si surfaces for different durations of the oxygen plasma treatment.

	Si, as received	Si, 2min O_2	Si, 15min O_2	Si, 30min O_2
Contact angle	9.6 ± 0.8	2.0 ± 0.3	0	0

The water contact angles for a silane treated Si surfaces that had received an oxygen plasma pre-treatment are shown in Figure 3-14b. For all three silanes studied, different oxygen plasma treatment times had no effect on the contact angle, respectively. This suggests that the silane layer density and silane surface chemistry (i.e., outer most functional groups) were not altered as the plasma treatment time increased. The value for the water contact angle of ~70^o for a SCA-1 modified surface is close to values reported in a number of studies with similar systems[12-15]. Apparently, in spite of the presence of polar (NH_2) and ionic groups (NH_3^+), molecular orientation and packing expose non-polar functionalities at the surface resulting in a reduction of wettability. The water contact angle for SCA-2 and SCA-3 modified surfaces was 15-20^o lower than that for the SCA-1 modified surface. This result is possibly due to the fact that some non-surface bound silanol groups and/or more amine groups were exposed at the top of the silane surface in the SCA-2 or SCA-3 surfaces contributed to surface properties.

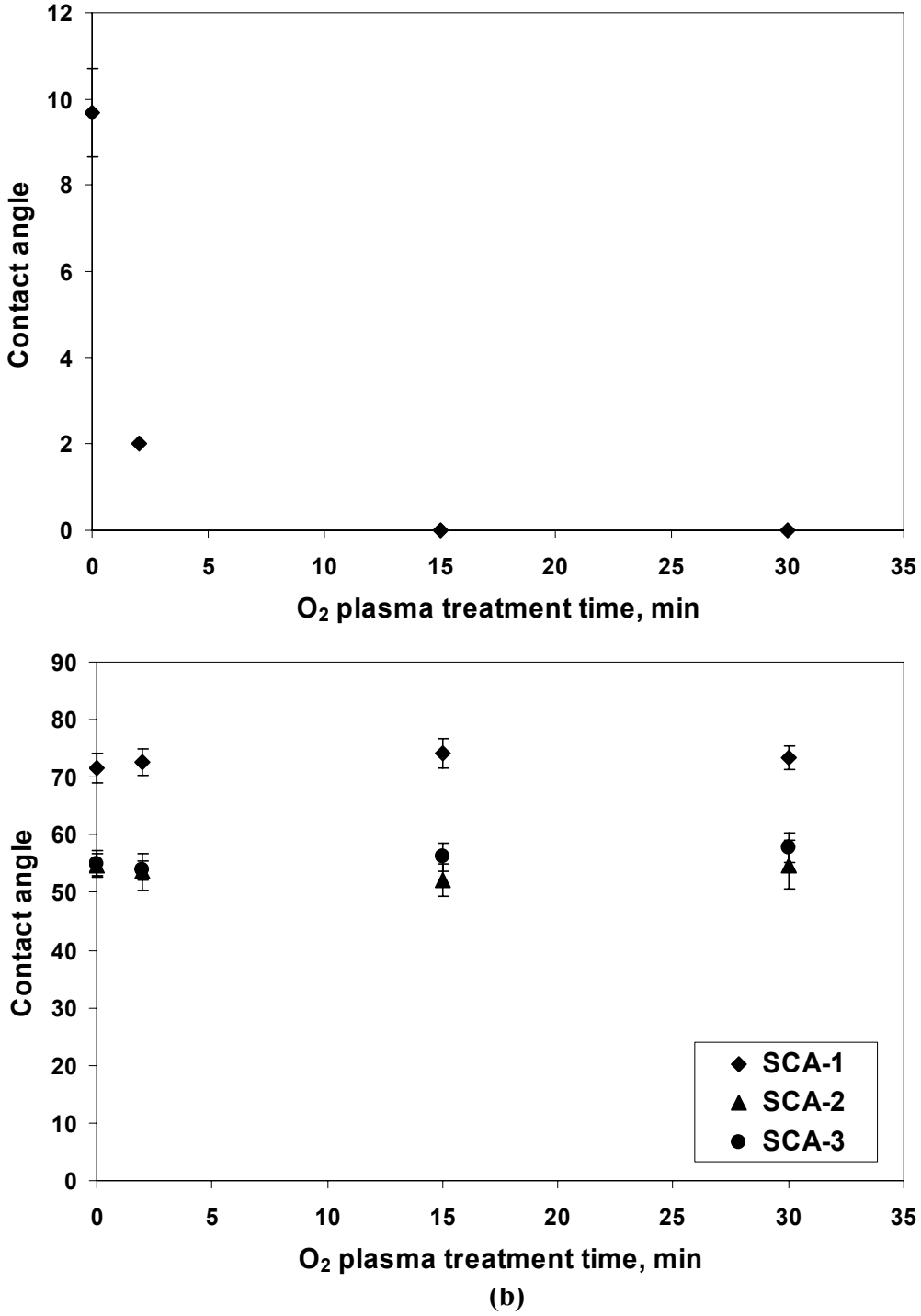

Figure 3-14. Advancing contact angle for water on (a) oxygen plasma treated Si surfaces, and (b) silane treated Si surface with prior oxygen plasma treatment.

3.9 Conclusions

The SiO_2 layer thickness on a silicon wafer can be controlled by varying the oxygen plasma treatment time. Longer treatment times resulted in a thicker oxide layer as confirmed by XPS, AES depth profiling, and ellipsometry data. Although the trend of oxide increase as a function of plasma treatment time was consistent among these studies, minor discrepancies existed between results from ellipsometry and XPS measurements (Table 3-14). Please note that the thickness values calculated from XPS were the average values based on two sets of surface characterization results obtained for Si surface treated under identical conditions. The two sets of values differ within 10%.

Table 3-14. Summary of SiO_2 thickness on Si by different techniques (in Å).

Technique	As received	2min O_2	15min O_2	30min O_2
XPS	8.1	17	22	24
Ellipsometry	18 ± 0.4	24 ± 0.3	30 ± 0.3	35 ± 0.6
AES	~15	~20	~25	~25

The SiO_2 layer thickness measured from ellipsometry was consistently higher than the results from XPS. This feature is likely due to the fact that an amorphous silicon layer was formed by the oxygen plasma treatment rather than a crystalline silicon layer, which has a higher refractive index[16]. Consequently, the oxide thickness was over-estimated by ellipsometric parameters. AES measurements showed oxide thickness values similar to the calculated XPS results, with the exception of the value for the as- received sample. For the silane modified Si surfaces, the Si-O-Si/Si^o ratio increased as the oxygen plasma treatment time increased. It is reasonable that the longer oxygen plasma treatment resulted in a more uniformly oxidized SiO_2 surface, which would afford more silanol groups for reaction with silanes. The silane thickness, however, was unaffected by the thickness of the SiO_2 layer (see Table 3-15). The NH_2/NH_3^+ ratio based on XPS data showed that the percentage of NH_2 content was significantly higher for the SCA-2 and SCA-3 modified surfaces than for the SCA-1 modified surface, suggesting that the SCA-2 and SCA-3 modified surfaces would be more reactive toward an epoxide.

Table 3-15. Summary of silane thickness by different techniques (in Å).

Technique	Surface	As received	2min O_2	15min O_2	30min O_2
XPS	**SCA-1**	5.3	5.7	5.8	6.0
	SCA-2	6.2	6.9	7.2	7.8
	SCA-3	5.4	6.0	6.2	6.5
Ellipsometry	**SCA-1**	9.7 ± 0.9	10.4 ± 0.6	10.5 ± 0.7	11.1 ± 1.0
	SCA-2	11.6 ± 0.8	13.6 ± 0.7	12.7 ± 0.9	12.2 ± 1.1
	SCA-3	9.4 ± 0.8	10.4 ± 0.7	11.5 ± 0.7	11.3 ± 0.9

3.10 References

[1] F. J. Boerio, L. H. Schoelein, and J. E. Grievenkamp, *J. Appl. Polym. Sci.*, 1978, **22**, 203.

[2] J. N. Kinkel and K. K. Unger, *J. Chromatogr.*, 1984, **316**, 193.

[3] H. Okabayashi, I. Shimizu, E. Shimizu, E. Nishio, and C. J. O'Connor, *Colloid Polym. Sci.*, 1997, **275**, 744.

[4] K. Esumi and K. Meguro, *Bull. Chem. Soc. Jpn.*, 1983, **56**, 331.

[5] C. H. Chiang, H. Ishida, and J. L. Koenig, *J. Colloid Interface Sci.*, 1980, **74**, 396.

[6] E. P. Plueddemann, *Silane Coupling Agents*, Plenum Press: New York, 1991, Chap1.

[7] J. M. Hill, D. G. Royce, C. S. Fadley, L. F. Wagner, and F. J. Grunthaner, *Chem. Phys. Lett.*, 1976, **44**, 225.

[8] Z. H. Lu, J. P. McCafferey, B. Brar, G. D. Wilk, R. M. Wallace, L. C. Feldman, and S. P. Tay, *Appl. Phys. Lett.*, 1997, **71**, 2764.

[9] D. F. Mitchell, K. B. Clark, J. A. Bardwell, W. N. Leonard, G. R. Massoumi, and I. V. Mitchell, *Surf. Interface Anal.*, 1994, **21**, 44.

[10] K. M. R. Kallury, P. M. Macdonald, and M. Thompson, *Langmuir*, **10**, 1994, 492.

[11] D. G. Kurth and T. Bein, *Langmuir*, **9**, 1993, 2965.

[12] X. Q. Zhang, W. Y. Yang, X. Z. You, and Y. Wei, *Appl. Surf. Sci.*, 1995, **84**, 267.

[13] Y. C. Araujo, P. G. Toledo, V. Leon, and H. Y. Gonzales, *J. Colloid Interface Sci.*, 1995, **176**, 485.

[14] D. Kowalczyk, S. Slomkowski, M. M. Chehimi, and M.Delamar, *Int. J. Adhe. Adhesives*, 1996, **16**, 227.

[15] K. Emoto, Y. Nagasaki, and K. Kataoka, *Langmuir*, 1999, **15**, 5212.

[16] B. Yous, J. M. Berger, J. P. Ferraton, and A. Donnadieu, *Thin Solid Films*, 1981, **82**, 279.

4. Adhesion and Durability Study of Model Epoxy/SCA/Si Specimens

4.1 Introduction

The adhesion of thin films on rigid substrates is of significant interest in many technical applications, yet the existing methods for the quantitative determination of adhesion are often not applicable to specific systems. In this chapter, the adhesion and durability results for model epoxy coated Si substrates with various means of surface modification are presented. Three different tests were used to determine adhesion and durability of the bonded specimens. A simple immersion test that involves placing an epoxy coated Si substrate in various chemical environments (i.e., water, solutions) at 60 ^{o}C and 70 ^{o}C was adopted to determine the durability in the absence of an applied mechanical stress. The general purpose of the immersion test was to obtain trends in bond durability for samples exposed to various environments and to evaluate the effectiveness of different surface preparation methods. The information gathered from the immersion tests is qualitative in nature. It should be noted that no external stress is applied to the bonded specimen during the immersion. However, residual stresses may be present in the system originating from bond curing and from cyclic thermal conditions.

The second part of this chapter describes adhesion and durability results obtained using a novel probe test, which is a promising alternative for testing thin film adhesion[1-3]. This test involves lifting a free coating edge from the substrate. The lifting is initiated by the precise penetration of a sharp needle-like probe at the film/substrate interface. The semicircular debond envelope that results from probe penetration allows a precise measurement of the debond radius. The advantage of this test over other thin film adhesion test methods is that it requires a simple specimen geometry, which permits the test to be conducted with a high throughput with repeated measurements. Thus the test is ideally suited for adhesion research, material selection, or quality control purposes. A mathematical model allows a quantitative estimation of the strain energy release rate. It should be noted that the strain energy release rate obtained from the probe test is the

critical value (i.e., energy needed to cause fracture). Further, an in-situ probe test technique was developed to study the behavior of interfacial adhesion, in a situation where stress and a fluid environment were coexistent at the crack tip.

The third part of this chapter describes results from wedge DCB (double cantilever beam) tests for the study of environment-assisted crack growth at the epoxy/SCA/Si interface as a function of applied strain energy release rate. The findings presented compliment the immersion and probe test results at a similar testing temperature, chemical exposure/immersion environment, and surface preparation. The subcritical strain energy release rate was obtained using the wedge (DCB) test geometry.

4.2 Silicon Surfaces

Most of the durability results to be discussed in Section 4.3 were obtained using the backside surface of a silicon wafer (as received, as received/SCA, O_2 plasma treated, or O_2 plasma treated/SCA) unless otherwise indicated. The Si backside surface has a rougher, non-polished surface. The silane modified-Si frontside surface (i.e., polished surface) was used to compare results for bond durability of modified quartz and glass surfaces (Section 4.3.2.5). The durability and adhesion results were obtained using the modified-Si backside surfaces *via* the probe test for dry and immersion bonded specimens. The in-situ probe test results discussed in Section 4.4.5 were all obtained using Si frontside surfaces. This approach was required because the Si frontside surface is more reflective and affords more accurate viewing of the crack front in the presence of fluids. The TOX Si backside surfaces were used in the DCB studies (Section 4.5).

4.3 Immersion Test Results

To evaluate the durability of the model epoxy/SCA/Si bonded systems, a simple immersion experiment was conducted in selected media (i.e., formulated solutions, pH buffer solutions, deionized water, and acid/base solutions). All immersion experiments were conducted at 60 ^{o}C.

4.3.1 Durability Results for "Cut" Specimens

4.3.1.1 Debond Observations--Blister Formation vs. Edge Diffusion

The “cut” and “non-cut” specimens were used for the immersion tests. Two major types of debond events were observed for these specimens. For the "non-cut" specimens, the primary debond event was blister formation in the bonded area (Scheme 4-1). As immersion time increased, the blisters either appeared at more locations and/or grew in size. The rate and location of blister formation were different in the various media. Evidence from both visual examination and a 3-dimensional surface profile (obtained using a laser profilometer) indicated a localized bulging of the film surface in the blistered area. It is likely that these localized blisters were formed in the presence of fluid at the epoxy/Si interface. Also, the absence of any debond event at the coating edge and the random location of blisters, suggest that the major diffusion path for the fluid is through the bulk polymer coating for the "non-cut" specimen. However, after prolonged immersion, debonding in the form of fluid ingression at the coating edges also occurred, but it took place much later (i.e., several months) than the initial blister formation.

For "cut" specimens, the initial and primary debond event was fluid ingression at the epoxy/Si interface along the edges of the specimen (Scheme 4-1). In most cases, fluid ingression occurred first along the two cut edges (edges created after cutting the bonded specimen) of the specimen, and took place later at the two regular (non-cut) coating edges (film on substrate). This observation indicates that the two cut edges are more susceptible to attack by fluid, and it is believed that failure/debonding is due to weakening of the interfacial bond caused by mechanically breaking the bonded specimen. Recall, each "cut" specimen was subjected to an edge treatment in an attempt to re-seal the interface and to maintain the interfacial integrity along the coating edges. However, a

Scheme 4-1

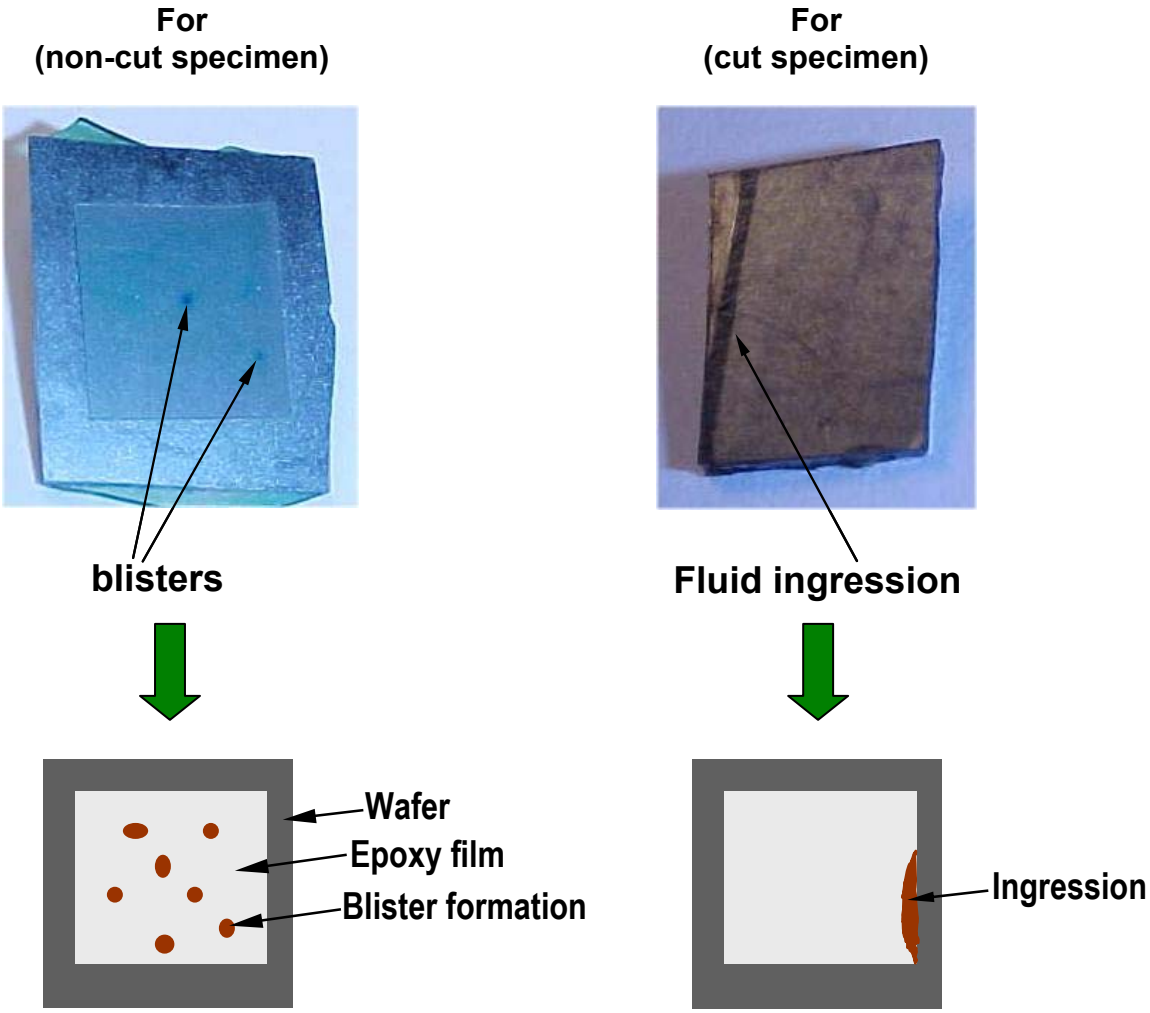

comparison of durability results for "non-cut" and "cut" specimens with the same silane surface treatment, indicated that the performance of the "cut" sample was much poorer, which was independent of the type of silane treatment and the properties of the immersion medium. The ineffectiveness of the silane edge treatment may be due to two factors. One, the stress input on the specimen *via* cutting/fracturing was not immediately alleviated and was able to cause crack propagation which facilitated the diffusion of water into the interface. Secondly, although re-dipping the specimen in the silane solution deposits silane molecules across the epoxy/SCA/Si interface along the cut edge, the small

surface area might not allow an extensive siloxane network to form among the SCA moieties. Thus, if "cutting" stress is dominant (cause 1), the sealing approach is not likely an effective way to provide enough "sealing" to prevent diffusion of water/solution into to the interface. That debonding on the edge rather than blister formation is the initial and the primary mode of failure indicates that edge diffusion is the dominant mechanism for fluid migration in this system.

4.3.2 Durability Results for "Non-Cut" Specimens

The durability results presented hereafter were all collected using the "non-cut" specimens. No additional edge treatment was performed prior to durability testing.

4.3.2.1 Effect of Silane Treatment

Table 4-1 illustrates the difference in bond performance upon immersion in 60 ^{o}C deionized water for various model epoxy/SCA/Si specimens. For all bonded specimens without silane modification, the bond failed after about 1 day of immersion in deionized water at 60 ^{o}C. In most cases, the model epoxy was lifted from the Si substrate without applying any external force. The bond failure was due to the rapid ingression of water into the epoxy/Si interface. In contrast, the Si surface that received a silane modification showed extraordinary durability. This finding is no doubt due to the formation of a water resistant interface that consists of a siloxane network that inhibits the diffusion of water along the interface.

Table 4-1. Bond performance for various Si surfaces upon immersion in DI water at 60 ^{o}C.

Sample	Time to Debond
Si, as received	< 1 day
Si, base/acid cleaned	< 1 day
Si, oxygen plasma treated	1-2 days
Si, TOX	1-2 days
Si, as received, SCA-1 treated	**~ 100 days**

4.3.2.2 Effect of Oxygen Plasma Pretreatment

To explore the effect of pH on the durability of the model epoxy/SCA/Si bond, specimens were immersed in different pH buffer solutions at 60 ^{o}C. Figure 4-1 shows the type of blister debond noted for specimens immersed in pH 9 buffer solution. As shown in Figure 4-1, the extent of blister formation is clearly the highest for the specimen receiving no O_2 plasma treatment prior to the SCA-1 deposition. For the sample prepared using a 30 min O_2 plasma, no blisters were noted after about 120 days of immersion in pH 9 buffer solution. It is likely that the longer oxygen plasma treatment generated a higher surface oxide density and thus a higher number of surface silanol groups. These silanol groups may form a greater number of siloxane bonds and improve the overall hydrolytic stability of the silane layer.

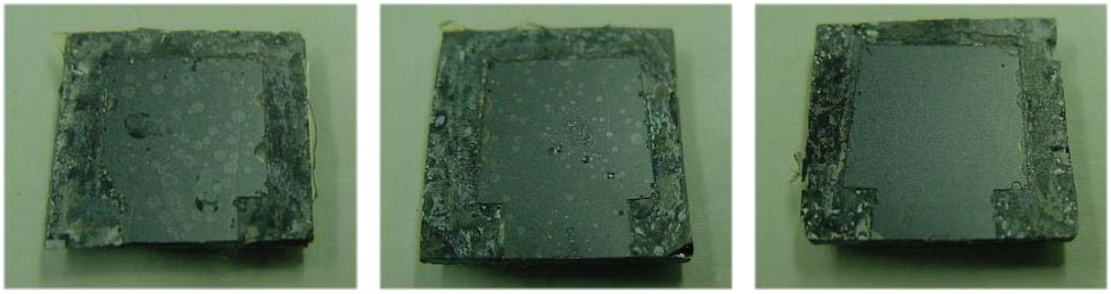

Figure 4-1. Photographs of bonded specimens (model epoxy/SCA-1/Si, **"non cut"**) showing blister formation in the bond area after immersion in pH 9 buffer solution at 60 ^{o}C for 4 months. The Si substrate was treated with an O_2 plasma for different times prior to SCA-1 deposition.

As argued above, blister formation for the "non-cut" specimen involves the diffusion of water (or other molecules) through the bulk polymer film and the congregation of water at the epoxy/Si interface. Water at the interface hydrolyzes the siloxane bond. Thus, surfaces with a higher siloxane bond density slow the hydrolysis reaction and improve durability. Blister formation is not observed for the specimens with

the same oxygen plasma/SCA-1 treatment immersed in the pH 4 buffer solution for the same time of immersion (same as shown in Figure 4-1). This result indicates that debonding is also a pH dependent process for the model epoxy/SCA-1/Si system.

4.3.2.3 Effect of the pH of Immersion Fluids

Figure 4-2 shows the adhesion performance from the immersion test for the model epoxy/SCA/Si bonded system at 60 °C in different formulated solutions and in different pH buffer solutions. For specimens immersed in different formulated solutions, the best durability was observed for the SCA-2-modified Si backside surface. Secondly, the durability is much better for specimens immersed in the basic solutions (Solution-3, pH 7.7 and Solution-4, pH 8.2) than in the acidic solutions (Solution-1, pH 4.2 and Solution-2, pH 6.6). The difference in durability between the acidic and basic solutions is also dependent on the silane used for surface preparation.

To elucidate the effect of pH on bond durability, specimens were immersed in aqueous pH buffer solutions with pHs ranging from 4 to 9. As shown in Figure 4-2, the best durability was observed for the SCA-2 and SCA-3 modified Si backside surfaces. Secondly, there is a clear dependence of bond durability on the pH of the buffer solutions. The durability is the best in pH 4 buffer and the poorest in pH 9 buffer. This dependence on buffer pH is directly opposite to that observed for tests in the formulated solutions. This difference may be related to specific solution components (i.e., surfactant, solvents, salts), which may influence bond durability to a greater extent than the effect of solution pH, either singularly or synergistically. However, previous studies showed that the equilibrium moisture uptake for bulk model epoxy specimen established after 700 hours of immersion at 60 ^{o}C in water-solvent mixtures was about 2.25 wt% and was not dependent on solution pH[4]. Thus, the bond durability dependence on pH observed here must be associated with the disruption of epoxy-silane or silane-Si linkages as the solution pH varies.

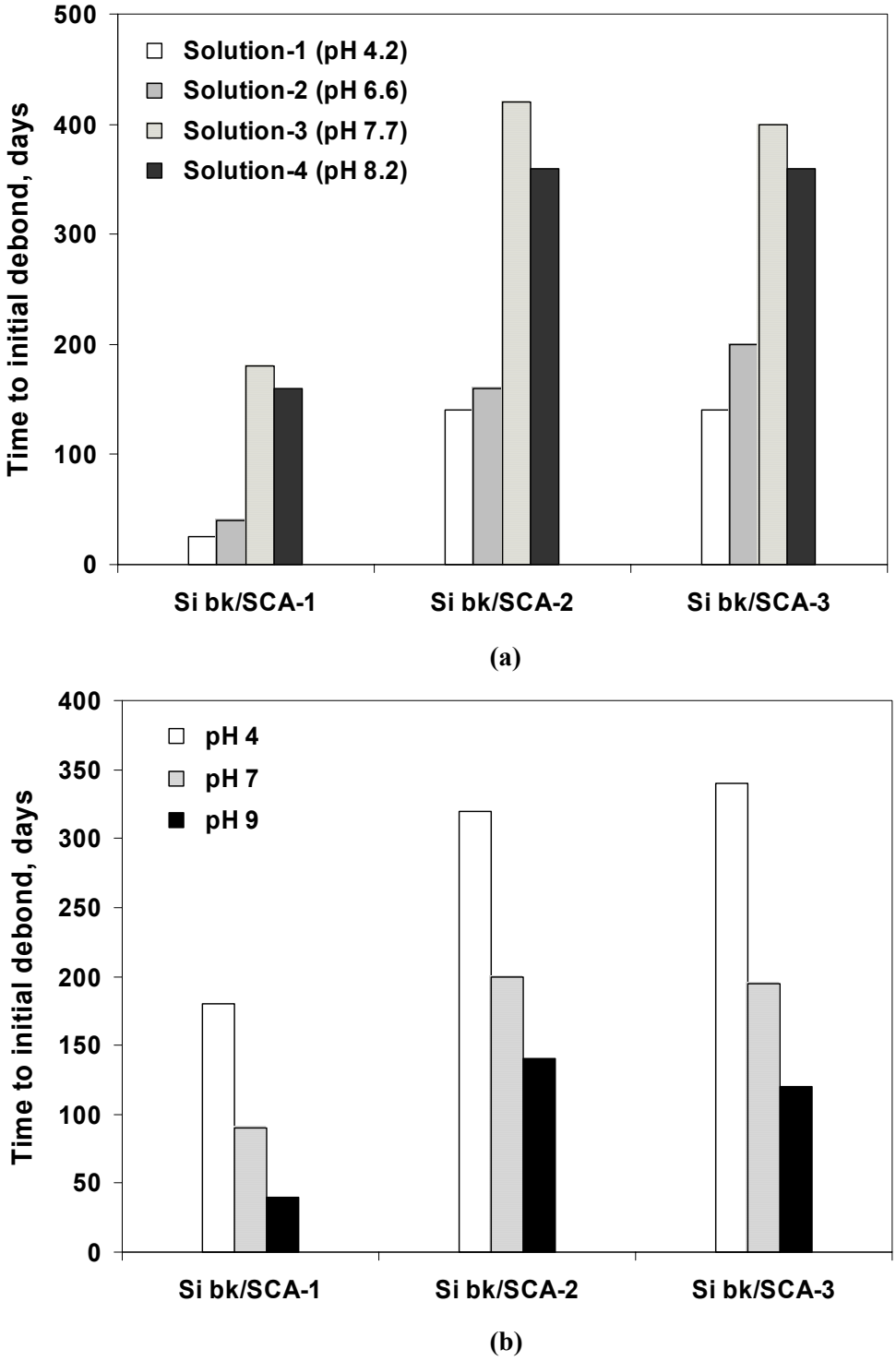

Figure 4-2. Durability of model epoxy/SCA/Si with different silane treated samples immersed at 60 °C in a) formulated solutions, and b) pH buffer solutions.

Figure 4-3 shows typical debonding specimens with blister formation as a result of immersion in formulated solutions and pH buffer solutions. The specimens containing SCA-2 or SCA-3 modified surfaces were twice as durable as the SCA-1 treated sample.

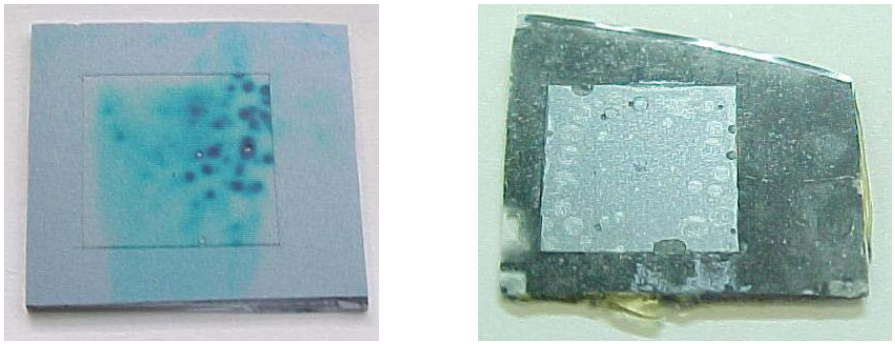

(a) **(b)**

Figure 4-3. Photographs of typical debonding specimens with blister formations in (a) Solution-2, pH 6.6 (Si, as received/SCA-3/model epoxy), and (b) pH 9 buffer solution (model epoxy/SCA-2/Si, as received).

4.3.2.4 Effect of Immersion Temperature, 60 ^{o}C versus 70 ^{o}C

To investigate the effect of temperature on bond durability, model epoxy/SCA/Si specimens were also immersed in different pH solutions at 70 ^{o}C. With higher temperature, diffusion should occur more rapidly as dictated by the Arrhenius relationship. As shown in Figure 4-4 and Figure 4-5, the bond durability was roughly two times better at 60 ^{o}C than at 70 ^{o}C. The trend of the effect of pH on durability remained consistent at the two temperatures. For an as-received Si surface or TOX Si surface treated with silane coupling agent, durability varied in the manner SCA-2 ≈ SCA-3 > SCA-1. This durability trend is likely due to the fact that the secondary amine functionality in SCA-2 and SCA-3 is more nucleophilic in the reaction with the epoxide than the primary amine in SCA-1. In addition, the SCA-2 or SCA-3 surfaces exhibited a significantly higher unprotonated/protonated amine ratio compared to that for the SCA-1 surface. As a result, more free amine is available to react with epoxide.

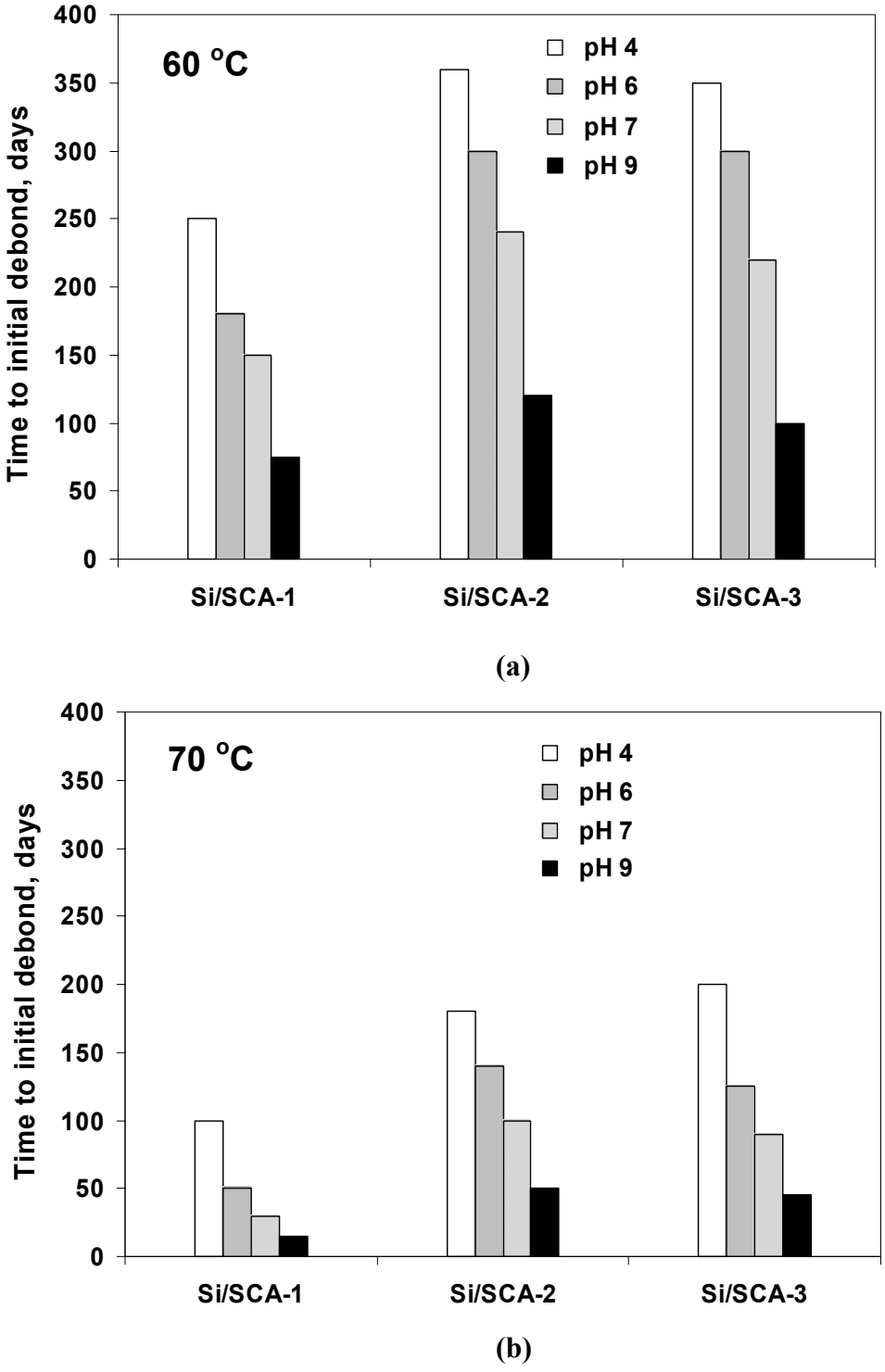

Figure 4-4. Durability of model epoxy/SCA/Si with different silane treated samples immersed in different pH buffer solutions. (a) Immersion at 60 °C and (b) immersion at 70 °C.

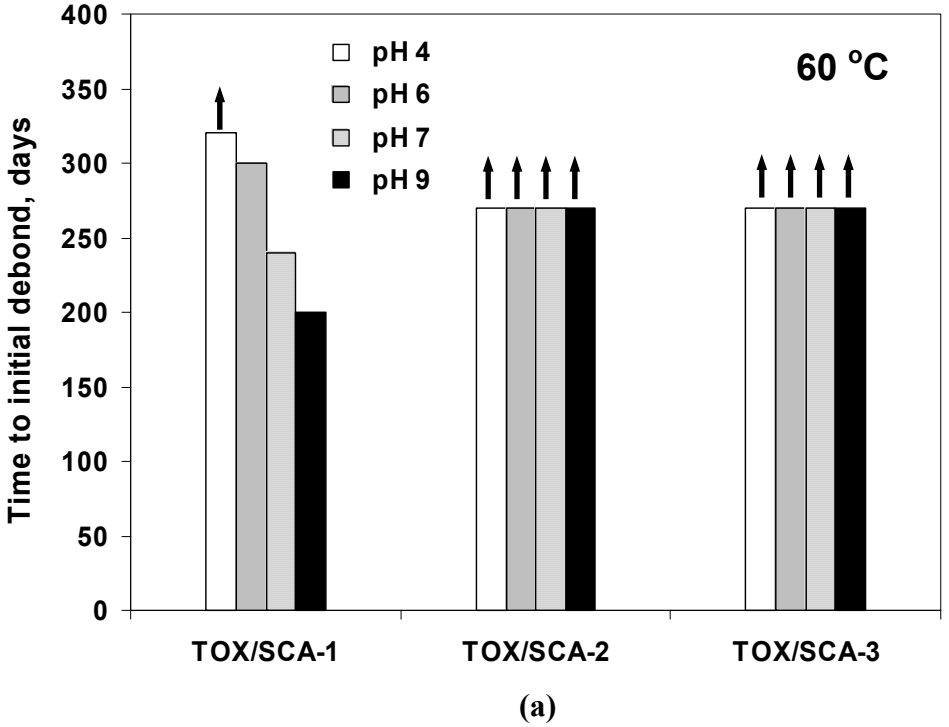

(a)

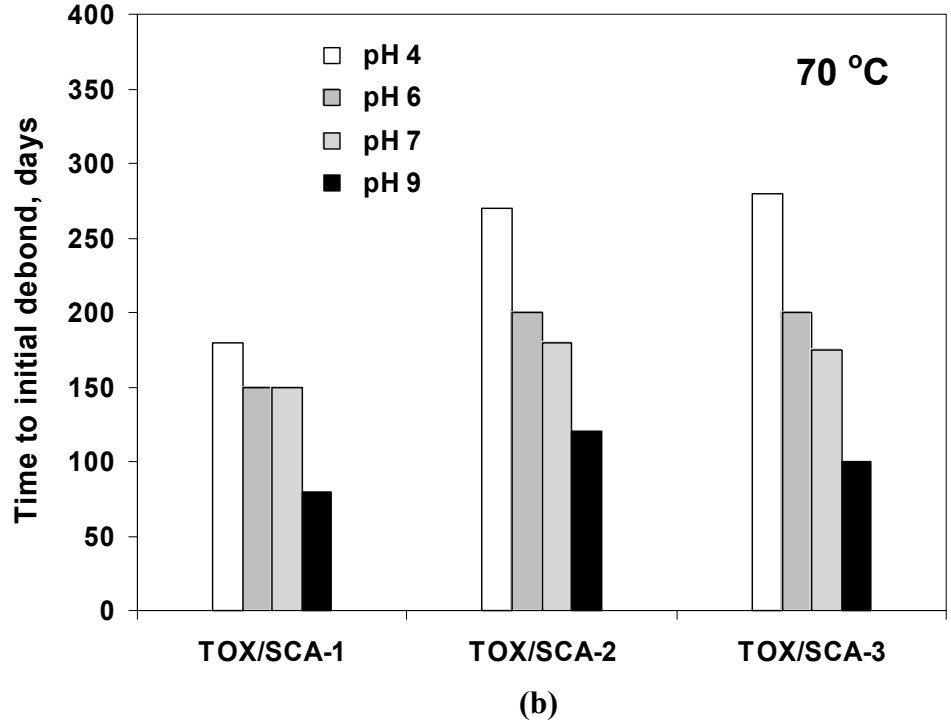

(b)

Figure 4-5. Durability of model epoxy/SCA/Si with different silane treated samples immersed in different pH buffer solutions. (a) Immersion at 60 ^{o}C and (b) immersion at 70 ^{o}C. The arrows indicate that the sample had not yet reached an initial debond stage under the conditions tested.

Though SCA-3 contains two secondary amine units, the bond durability for SCA-3 and SCA-2 modified surfaces is similar. This observation may arise from spacial constraints existing during the amine-epoxide interaction, in that once the first amine group reacted with the epoxy chain end, the spacial availability becomes limited for another epoxy chain to approach the second free amine group on the same SCA-3 molecule.

The silane modified TOX Si surface yielded better durability than that for the corresponding as-received Si surface. This finding is consistent with the XPS surface analysis results in that the unprotonated to protonated amine ratio for all three silane modified TOX Si surfaces is much higher than the corresponding values for the silane modified as-received Si surfaces. A higher percentage of free amine in either NH_2 or -NH- form attached to the adsorbed silane molecule could lead to more interactions with the epoxy chain ends during curing. The protonated amine in either NH_3^+ or $-NH_2^+-$ form does not effectively catalyze the curing reaction[5].

4.3.2.5 Effect of Substrates, Silicon versus Glass or Quartz

Figure 4-6 summarizes the adhesion performance for the immersion tests for different substrates treated with SCA-1 and coated with the model epoxy. The purpose of this experiment was to examine whether the type of SiO_2 surface plays a role in bond durability. It is known that the common Si wafer and glass (borosilicate) have an amorphous type of SiO_2 surface, whereas quartz has a crystalline SiO_2 surface. As the results shown in Figure 4-6 indicate, a quartz surface modified with SCA-1 yielded much better durability both in formulated solutions and in buffer solutions compared to the performance for the Si front side surface and the glass surface. The elemental composition for the SCA-1 treated Si wafer front side, glass, and quartz surfaces are nearly identical (Table 4-2). The ratios for the unprotonated to protonated amine functionality are essentially the same for all three surfaces, suggesting similar surface reactivity with the epoxide. The Si-O-Si to SiO_2 ratio was higher for the SCA-1/as-

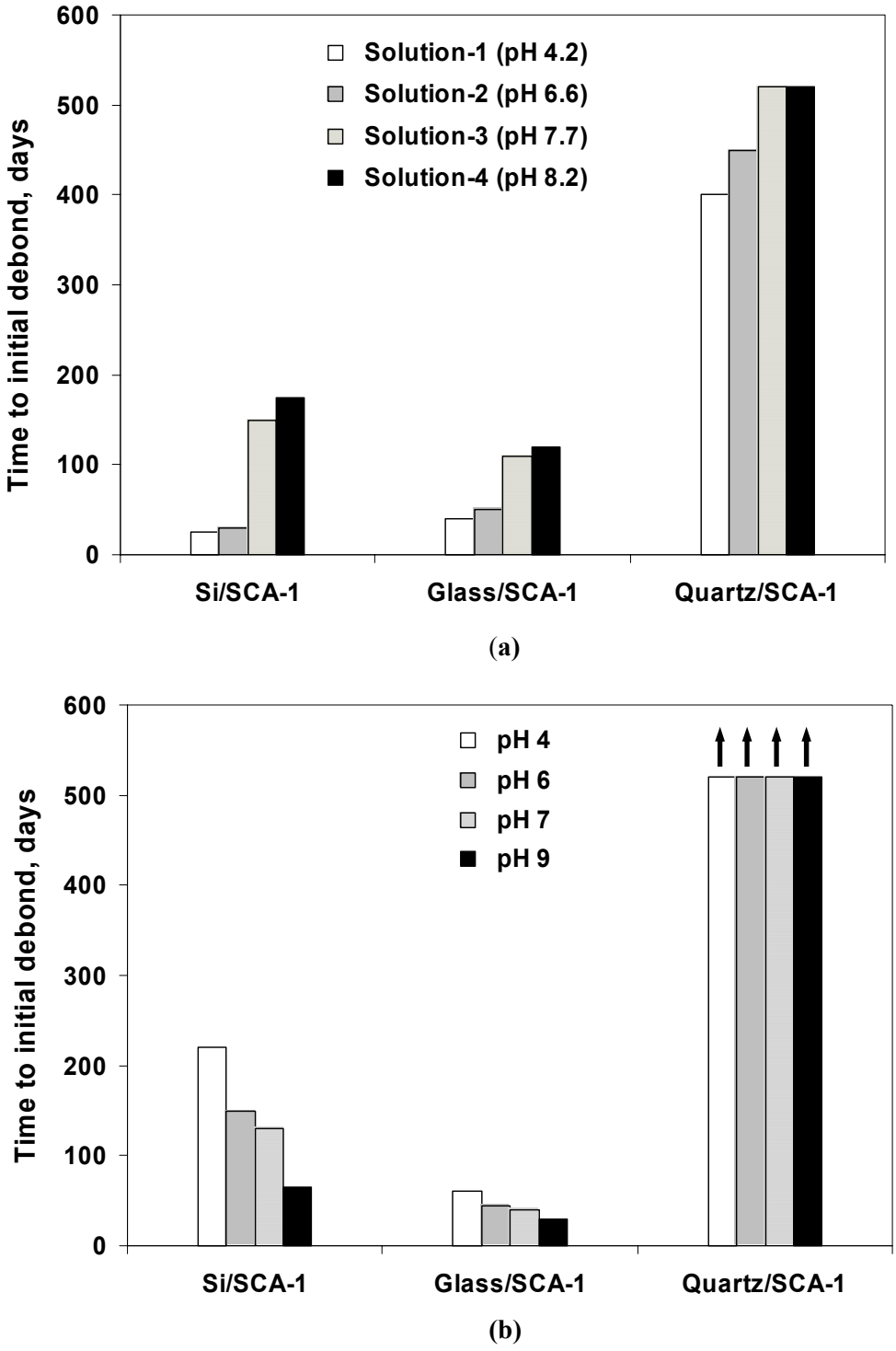

Figure 4-6. Bond durability of model epoxy and different silicon substrates treated with SCA-1 immersed at 60 °C in, a) formulated solutions, and b) pH buffer solutions. The arrows indicate that the sample had not yet reached the initial debond stage under the conditions tested.

received Si frontside surface than for the corresponding glass and quartz surfaces, because the SiO_2 content was less on the Si wafer surface.

Table 4-2. **Elemental composition of SCA-1-treated substrates.**

Sample	C	O	Si	N	$-NH_2/-NH_3^+$	$Si-O-Si/SiO_2$
Si frontside/SCA-1	33.5	33.3	29.7	3.5	2.7	0.39
Glass/SCA-1	31.1	42.8	22.2	3.9	2.2	0.25
Quartz/SCA-1	29.3	43.0	24.2	3.4	2.5	0.25

4.3.2.6 Effect of Silanes without Reactive Functionality

Non-reactive silane coupling agents were also used to modify the Si backside surface. "Non-reactive" is defined as a surface modified with a functional group that is non-reactive with the epoxide group (i.e., a hydrocarbon moiety). The purpose of this study was two fold: 1) to establish a reference point in bond durability and adhesion performance compared to the reactive silane systems, and 2) to investigate the bond failure mode for both non-reactive and reactive silane derivatized systems. The silane solutions, 0.1M SCA-4, SCA-5, and SCA-6 were used to modify the as-received Si wafer substrate. Subsequently, the modified Si surfaces were coated with model epoxy. Immersion studies for cured bonded specimens were carried out at 60 ^oC in deionized water. The results shown in Table 4-3 demonstrate that the bond durability for the Si front side surfaces modified with non-reactive silanes is essentially the same as that for the Si front side surface without silane modification. The XPS analysis data for the treated wafer (unbonded) showed that the carbon content on the modified silane surfaces was less than that on the SCA-1 surface under the identical reaction conditions. The smaller amount of non-reactive silane deposited is due to the slower hydrolysis rate in a polar solvent. The non-reactive silane coating behaves as a weak boundary layer. This finding indicates that the interface constituted with a silane network is not in itself sufficient to enhance durability, the presence of chemical interactions between the

reactive functional groups and epoxy polymer are critical for enhancing bond strength and durability.

Table 4-3. **Bond performance of various Si front-side surfaces treated with different silanes (0.1 M) upon immersion in deionized water at 60 ^{o}C. XPS data for treated Si surfaces (before bonding).**

Sample	Time to Debond	C	O	Si	N
Si, as received	< 1 day	10.0	44.2	45.8	< 0.1
Si, SCA-4	< 1 day	19.7	36.8	43.5	< 0.1
Si, SCA-5	< 1 day	16.3	39.4	44.3	< 0.1
Si, SCA-6	< 1 day	25.9	32.7	41.4	< 0.1
Si, as received, SCA-1	**~ 100 days**	33.2	31.2	32.1	3.5

4.4 Probe Test Results

4.4.1 Basic Experimental Observations

A probe test was used to measure thin film adhesion. To initiate a debond, a conical micro-probe tip of 5 μm radius was introduced into the polymer film/substrate interface. The applied force from the probe tip causes an initial deformation at the interface which in turn becomes a shearing stress as the debond propagates. The propagating debonding produces a characteristic semi-circular debond radiating outward from the point of intrusion. As the probe tip advances along the film/substrate interface, the debond propagates forward, and the profile and dimensions of the debonded area change accordingly. From the debond features, interfacial adhesion can be evaluated as a function of surface modification of the bonding substrates. Also, exposure of the interface to various chemical environments (i.e., pH solutions) reduces interfacial adhesion leading to an increase in delamination dimensions, and allows a determination of strain energy release rate.

In these probe tests, the debonding area and debond aspect ratio were examined as a function of the surface modification, immersion in buffer solutions at different pHs, and the duration of exposure. The as-received Si wafer backside and front side (polished) surfaces were used as substrates. These surfaces were either directly coated with the

model epoxy or treated *via* silane reactions and then coated with the model epoxy. The model epoxy coating thickness was about 75 μm.

Figure 4-7a shows the probe at the epoxy-Si interface prior to the penetration of the probe tip. The crack front was recorded and used to calculate the debond area and debond aspect ratio (Figure 4-7b). The debond area was calculated by assuming an elliptical shape for the debond area(Figure 4-7c). Furthermore, the critical strain energy release rate, G_c, is inversely proportional to the debond radius, a, to the fourth power[6].

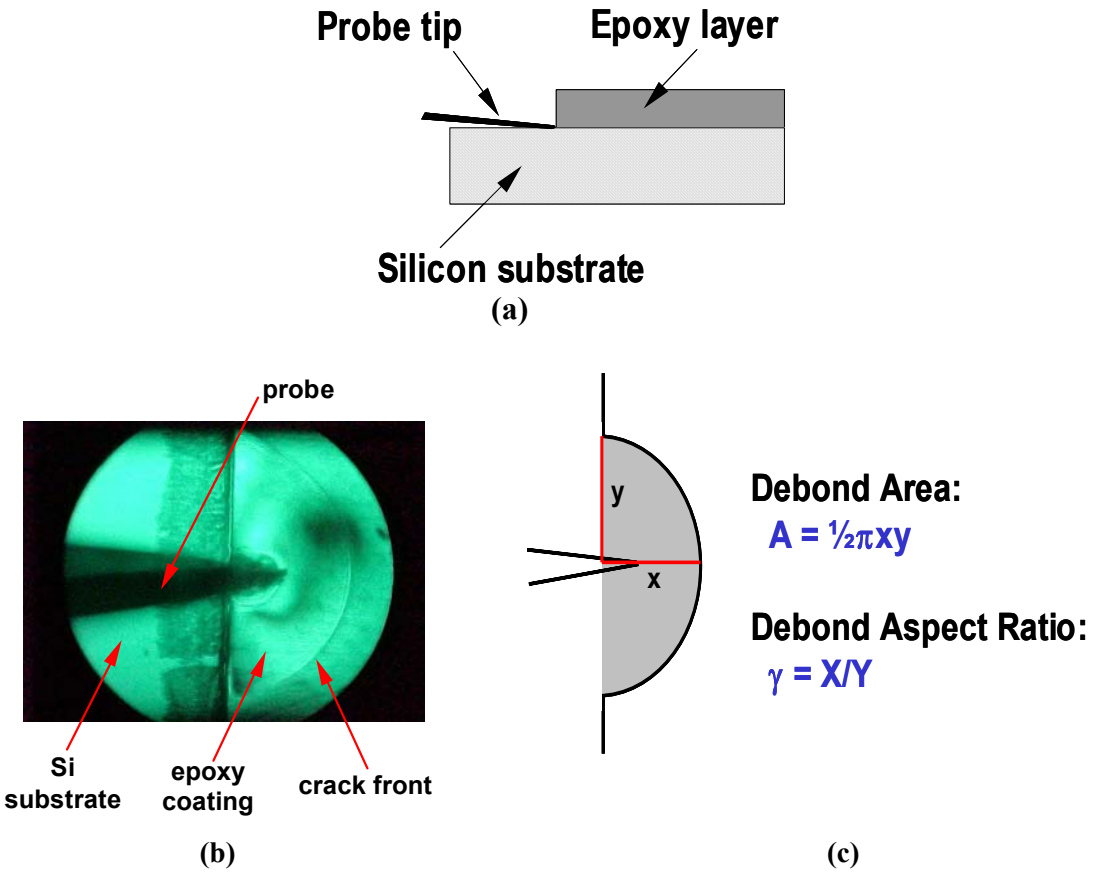

Figure 4-7. (a) A schematic showing the location of probe penetration; (b) A picture showing the probe tip penetrating along the epoxy/Si interface causing a semicircular debond; (c) calculation of the debond area and debond aspect ratio.

Figure 4-8 shows the debonding progress at different probe penetration distances for the specimen; Si frontside, as-received/model epoxy. At a probe penetration distance of 0.05 mm, the initial debond appeared to be small and circular. At 0.10 mm, the immediate debond area grew slightly in the X and Y circular profile. As the probe penetration distance increased, the semi-circular crack front became more pronounced and the debond radius in the X and Y directions increased.

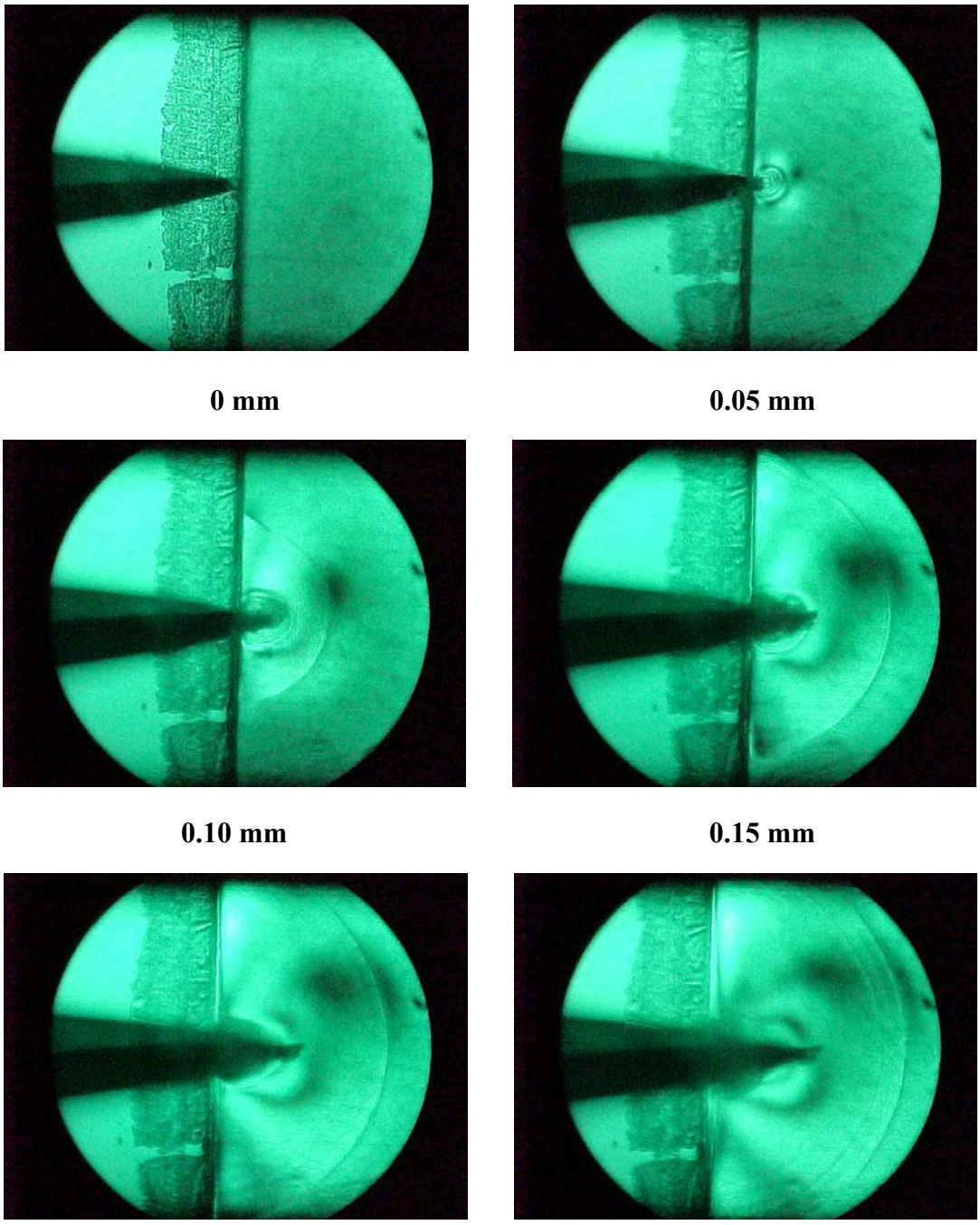

Figure 4-8. Debond profiles of model epoxy films at different probe penetration distances for the Si frontside as-received/model epoxy surface under dry conditions.

The debond area was calculated assuming a semi-elliptical shape and the results are shown in Figure 4-9 for "dry condition" tests (i.e., as-prepared bonded specimen not exposed to moisture or fluids). The Si backside surface yielded much better adhesion than the Si frontside surface when tested under dry conditions. The debond area was 7 times greater for debond tests on the frontside (polished) of the wafer. This large difference in film adhesion under dry conditions is likely due to the fact that the roughness of the backside surface results in a higher surface area, thereby offering more contact with the model epoxy. The curves in Figure 4-9 have about a 5% error in debond area value. A minimum of six runs was conducted among several identical specimens for each surface, respectively.

Three types of the probe test experiments were conducted in this work. The first type was performed to evaluate adhesion. In this, the bonded specimen was probed under "dry conditions" (i.e., an as-prepared sample was tested not having been immersed in any solution). Results from this test established a baseline or reference standard of adhesion. The second type was performed to evaluate bond durability. A bonded specimen was probed after exposing the specimen to selected environments; immersion in water, formulated solutions, and pH buffers for a given time. The information obtained from this test reveals degradation in adhesion as a result of long-term exposure to the environment. The rate of degradation and the failure mode were used to evaluate bond durability. The third type, the in-situ test, was performed to reveal information on the dynamic response on adhesion when the interfacial region was subjected to a simultaneous mechanical stress and a chemical/fluid environment. The specimens used for the in-situ test included both the as-prepared (i.e., no-pre-soak, dry interface) bonded specimens and the pre-soaked (i.e., immersed in various liquids for a pre-determined time) bonded specimens.

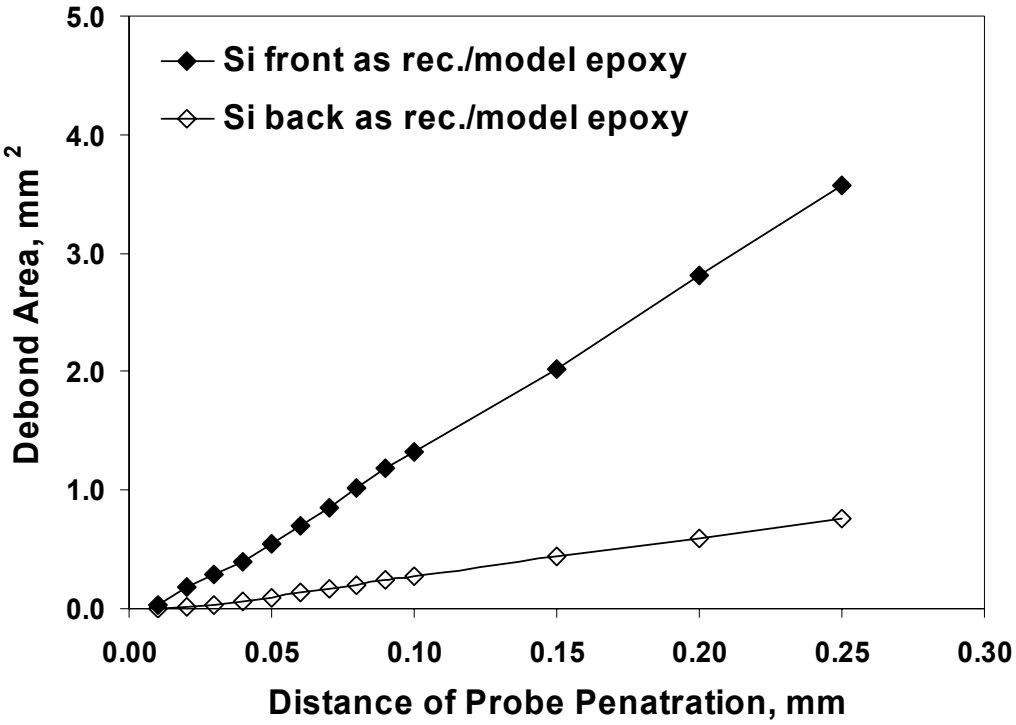

Figure 4-9. Debond area as a function of probe penetration distance for a model epoxy coated as-received Si front side and back side specimens tested under dry conditions.

4.4.2 The Mechanical Model

The data shown in Figure 4-9 present a qualitative comparison of adhesion for two different bonded specimens based on debond area. To compare quantitatively the adhesion energy for both specimens, the strain energy release rate may be deduced from the debond measurement. A preliminary model is presented to estimate the value of G_c from the debond radius obtained in the probe test.

The most striking feature of the probe test is that the debond profile appears to be semicircular. The evaluation of G_c can be approximated *via* the semicircular debond profile using the equation given by Timoshenko[6] for the case of a symmetrical bending of circular plates with applied load at the center. For the debond geometry of the probe test, only half the mechanical model shown in Figure 4-10a is considered. The maximum deflection at the center is

$$w_0 = \frac{3Fa^2(1-\nu^2)}{2\pi Eh^3} \qquad \textbf{Equation 4-1}$$

where F is the external force, a is the crack radius, ν is Poisson's ratio, E is the elastic modulus of the film, and h is the film thickness. w_0 is measured as the maximum vertical separation distance of the film from the substrate at the point of intrusion. It is also known that the elastic energy stored in an elastic medium is given as

$$U_E = \int F \cdot dw_0 \qquad \textbf{Equation 4-2a}$$

The critical strain energy release rate, G_c, is related to U_E as

$$G_c = -\frac{dU_E}{dA}\Big|_{w_0} = -\frac{d}{dA}\int F \cdot dw_0 \qquad \textbf{Equation 4-2b}$$

where A is the debond area. Rearranging Equation 4-1 in term of F, and substituting F into Equation 4-2b, for half of the circular area (for $A = \pi a^2/2$), G_c can be derived as

$$G_c = \left(\frac{F}{2}\right)\frac{dw_0}{d\left(\pi a^2/2\right)} = \left(\frac{F}{2\pi a}\right)\frac{dw_0}{da} \qquad \textbf{Equation 4-3}$$

By evaluating dw_0/da for Equation 4-1 and substituting the results into Equation 4-3, G_c can be written as

$$G_c = \frac{3F^2\left(1-\nu^2\right)}{2\pi^2 Eh^3} \qquad \textbf{Equation 4-4}$$

Note that the above equation is force dependent; however, F is difficult to measure in the probe test experiment (The force applied to advance the probe along the film/substrate interface is achieved by manually turning the micrometer connected to a spring). Thus, an alternative form of G_c is obtained by substituting the F in the crack profile equation (Equation 4-1) into the expression for G_c as given in Equation 4-4. Thus G_c for the probe test can be derived as

$$G_c = \frac{3\left(1-\nu^2\right)}{2\pi^2 Eh^3}\left(\frac{2\pi Eh^3 w_0}{3a^2\left(1-\nu^2\right)}\right)^2 = \frac{2Eh^3}{3\left(1-\nu^2\right)}\left(\frac{{w_0}^2}{a^4}\right) \qquad \textbf{Equation 4-5}$$

where w_0 is the film debond height at the edge, and a is the debond radius (see Figure 4-10b). Experimentally, the debond radius can be accurately measured with the microscope and recorded *via* the digital position recorder, and knowing the probing angle θ, and the probe penetration distance l, the debond height can be calculated. For a semi-elliptical-shaped debond, the debond radius, a, is determined as the square root of the product of the a_{max} and a_{min}, where a_{max} and a_{min} are the radii of the major and minor debond axes, respectively. Equation 4-5 accounts for the total strain energy release rate involved for both mode I and mode II fracture.

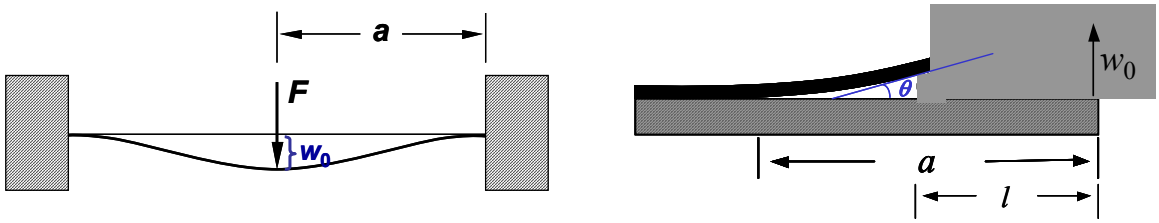

(a) (b)

Figure 4-10. (a) Symmetrical bending of circular plates with applied load at the center; (b) debond geometry of the probe test.

Several concerns exist regarding the accuracy of the debond radius measurement as well as debond height, w_0, at the free edge. For the debond radius measurement two problematic phenomena existed. One is that localized crushing of the coating due to high bearing stress resulted from the initial probe penetration (usually at short distance). Measurement of the debond radius was avoided at this point as a regular-shaped semicircular debond envelope was not developed. The extent of crushing depended largely on the interfacial strength. Second is the change in the profile of the debond aspect ratio for the debond envelope. As shown in Figure 4-11, the X-axis debond radius and Y-axis average debond radius are identical up to 0.15mm probe penetration distance or approximately 100μm debond height. At a probe penetration distance beyond 0.15mm, the values deviate substantially from one another, in that the profile of the aspect ratio (X-axis debond radius/Y-axis debond radius) of the debond envelope is decreasing. This finding is due to the different boundary conditions that exist in the X and Y directions.

The aspect ratio of the debond envelope is also a function of interfacial adhesion. For aged specimens exposed to thermal and chemical environments, the aspect ratio was lower. The debond radius in the Y direction is affected by the stretching of the epoxy coating, which deviates from the true opening mode (basis for Equation 4-5) substantially. Thus, for the calculation of the strain energy release rate using Equation 4-5, the X-axis radius or, a, is expected to give a more accurate estimate.

Another concern that could exist is related to the accuracy of the measurement of the debond height, at the free coating edge, as the flexing of the probe shaft could result in an opening height less than estimated for the probe angle and probe penetration distance if the coating modulus were high. This problem could be remedied by using a stiffer probe shaft (i.e., tungsten carbide instead of tungsten tip), or by lowering the probe angle with respect to the substrate (i.e., less resistance for bending the probe shaft). For the model epoxy/SCA/Si boned specimens studied, flexing of the probe shaft during probe penetration was not observed. Additionally, regular semi-circular debond profiles can be obtained for a range of film thicknesses (10 to ~200 μm) by varying probes with different shaft gauges and probe tip diameters.

Furthermore, because Equation 4-5 is derived based on a linear plate bending solution, it assumes that both the debond height (or central deflection) and the film thickness (~75 μm) are small compared to the debond radius. However, at small probe penetration distances, the latter assumption is not valid. Calculations using Equation 4-5, resulted in an exaggeration of the fracture energy at small probe penetration distances (as shown in Figure 4-12). At longer probe penetration distances, and greater debond radii, the fracture energy tends to plateau to a limiting value. To obtain G_c values to compare fracture energy for various silane treated surfaces, debond radius results at 0.25 mm probe penetration distance were used.

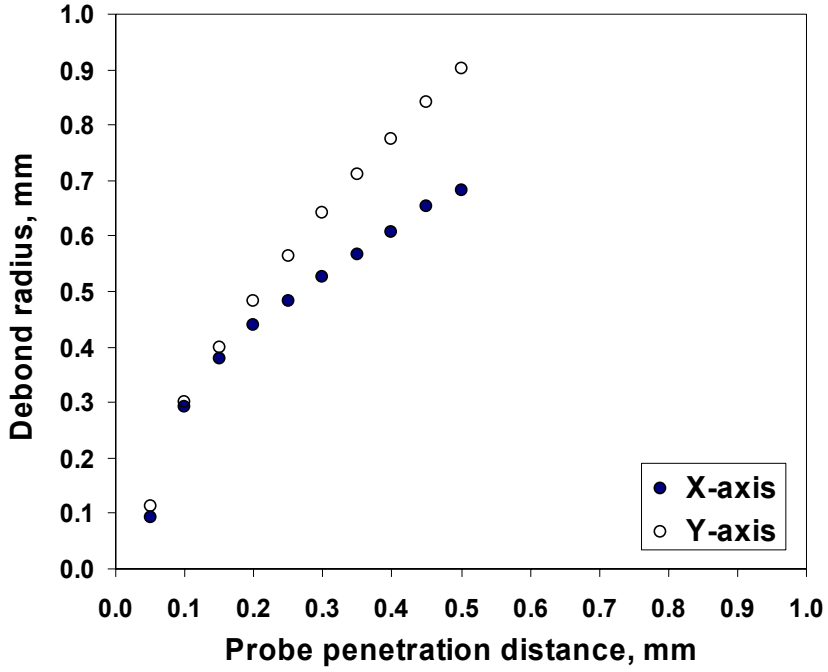

(a)

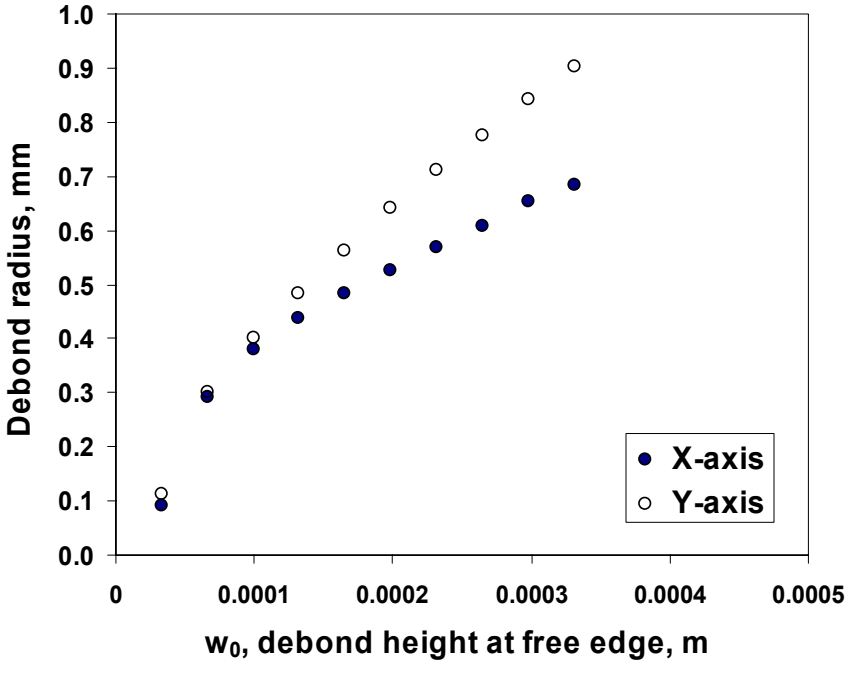

(b)

Figure 4-11. X-axis and y-axis debond radius versus (a) probe penetration distance and (b) w_0, the debond height at the free edge of the coating for a debond measured for model epoxy/SCA-1/Si bonded specimen under dry conditions. Film thickness is 75 μm.

Additionally, for probe tests performed on specimens immersed in various fluids at elevated temperature, the change in film modulus due to liquid sorption and change in residual stress in the specimen were ignored when estimating the critical strain energy release rate using Equation 4-5.

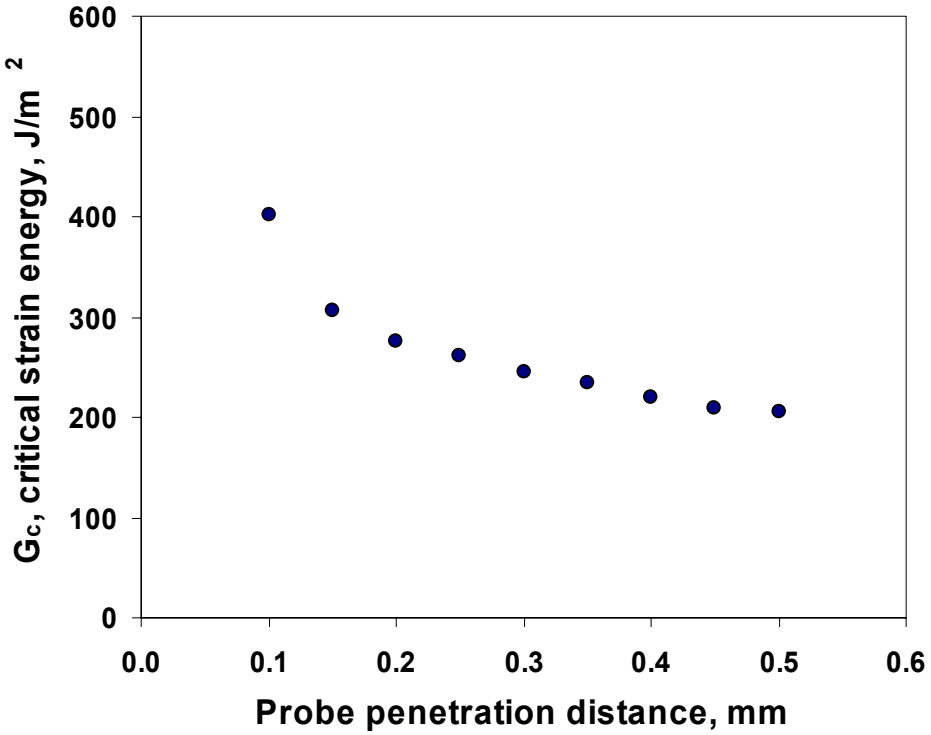

Figure 4-12. G_c, critical strain energy release rate versus probe penetration distance for the debond measured for the specimen model epoxy/SCA-1/Si under dry conditions. Film thickness is 80 μm.

4.4.3 Probe Test Performed on Dry Specimens

4.4.3.1 Effect of Different Silanes

The results for debond areas examined as a function of the surface modification, immersion in buffer solutions at different pHs, and the duration of exposure are described in this section. Using the mechanical model derived above, it is possible to quantify thin film adhesion in terms of strain energy release rate. Figure 4-13 shows G_c, the critical

strain energy release rate, as a function of probe penetration distance for an as-received Si frontside surface with different surface modifications. Recall that as the probe penetrates further into the interface, a larger debond radius results. The model predicts a typical a^{-4} decay for G_c as a function of probe penetration distance. It should be noted, at a small probe penetration (< 0.05mm), the model estimates an exceptionally high value of G_c, which is not a true measure of thin film adhesion. To compare film adhesion with the same specimen geometry but with different surface preparations, a fixed probe penetration distance (i.e., same debond height) at 0.25 mm was chosen as the point where the debond radius was measured. In most cases, the G_c values at 0.25 mm penetration distance have reached or are approaching limiting values.

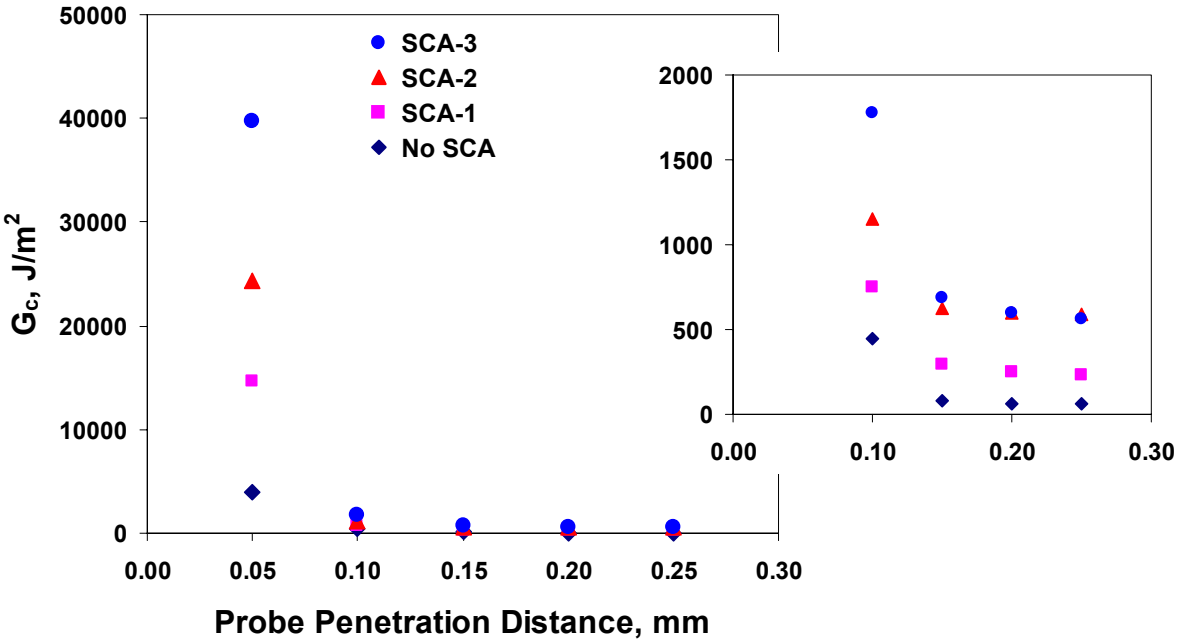

Figure 4-13. Critical strain energy release rate as a function of probe penetration distance for four different surface treatments. The small insert on the right shows an expanded G_c axis scale.

The first type of probe experiment was performed to evaluate adhesion quality under "dry conditions". Results from this test establish a baseline or reference standard of adhesion. Figure 4-14 shows G_c calculated from the debond radius at 0.25 mm probe

penetration distance for as-received Si samples derivatized using four different surface preparations. Specimens with surfaces treated with SCA-2 and SCA-3 exhibited a strain energy release rate twice that for a SCA-1 modified surface. The adhesion strength for the no-silane treated Si surface was about 10-fold less than that for the SCA-2-treated surface. The error bars in Figure 4-14 were determined from at least six measurements among at least two identical specimens for each silane surface treatment.

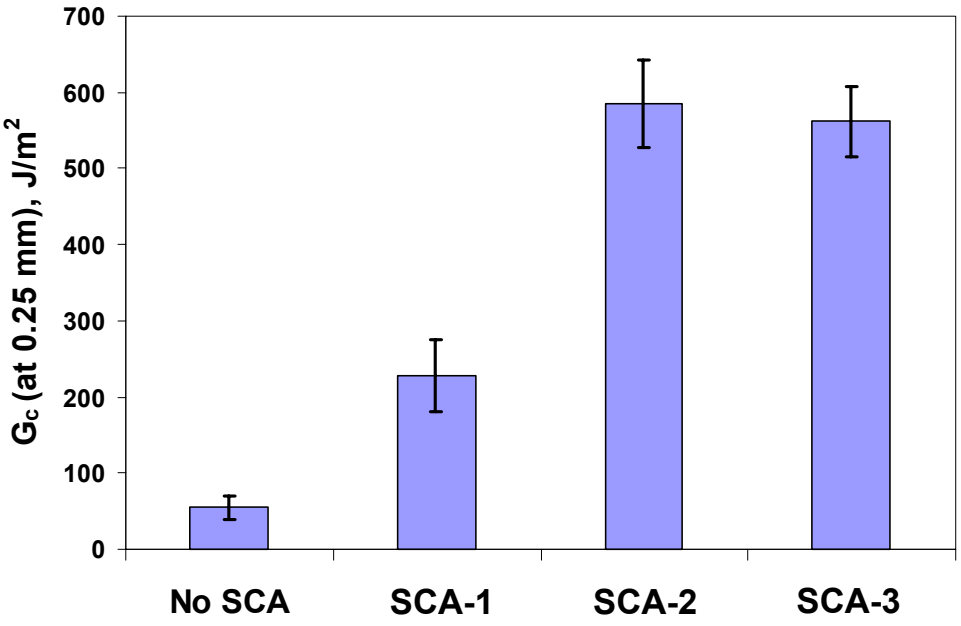

Figure 4-14. Comparison of G_c obtained at 0.25 mm probe penetration distance for Si samples with four different surface treatments. Probe tests were conducted under dry conditions.

4.4.3.2 Effect of the Nature of the Silicon Oxide on the Si Surface: O_2 Plasma Treatment

Specimens that had been modified *via* an oxygen plasma treatment and derivatized with different silanes were probed under dry conditions, and the results are summarized in Figure 4-15. Specimens with SCA-2- and SCA-3-treated surfaces exhibited a strain energy release rate twice that for a SCA-1 modified surface. Additionally, adhesion increased for the model epoxy/SCA/O_2 plasma treated/Si sample

as the oxygen plasma pre-treatment time increased (Figure 4-15). This increase in adhesion is likely due to the formation of a higher number of Si-O-Si bonds between the silane molecules and the Si substrate.

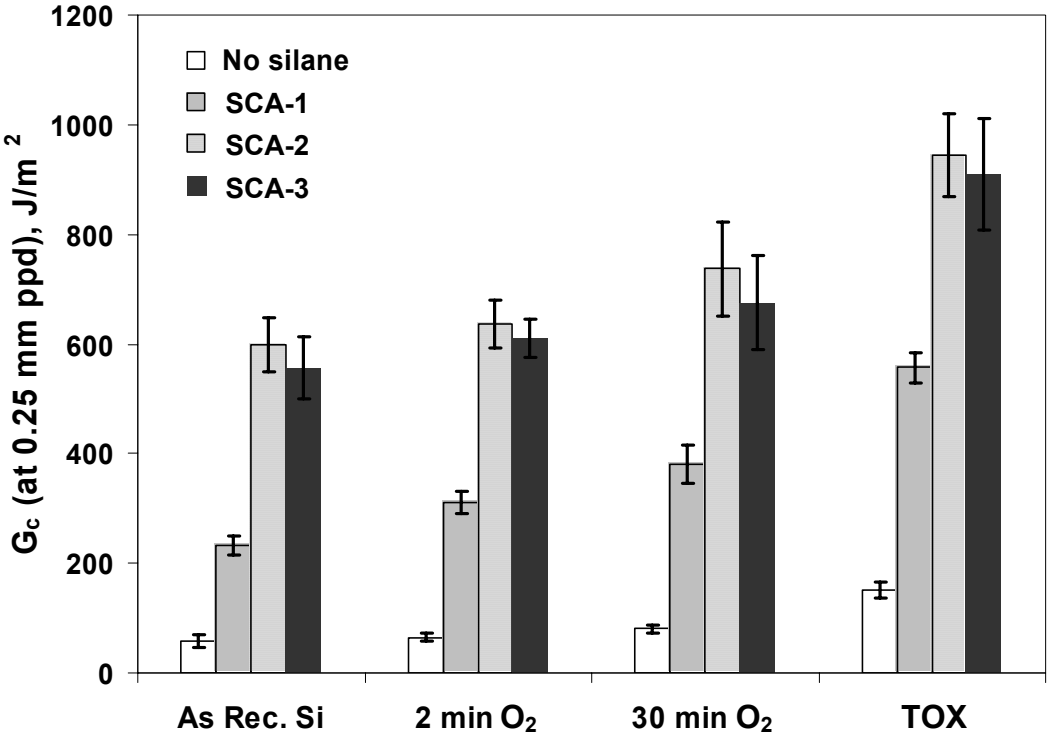

Figure 4-15. Comparison of G_c obtained at 0.25 mm probe penetration distance for four different surfaces. Probe test results were collected under dry conditions.

The results in Table 4-4 indicate that as the oxygen plasma treatment time increased, the Si-O-Si)/Si^o ratio increased. Figure 4-15 shows a comparison of G_c values obtained at 0.25 mm probe penetration distance for four different surfaces, three of which were modified with different silane coupling agents. It is apparent that as the oxygen plasma treatment time increases, G_c increased for the no silane, SCA-1, SCA-2 and SCA-3 modified surfaces. The SCA-2 modified surface offered slightly higher adhesion strength. The TOX Si surface yielded a higher G_c value than that for the oxygen plasma treated as-received Si surfaces. This result is likely due to a more extensive oxide layer on the TOX wafer surface.

Table 4-4. Change in the (Si-O-Si)/Si^0 ratio for O_2 plasma-treated Si surfaces modified with silane.

Sample	(Si-O-Si)/Si^0		
	SCA-1	SCA-2	SCA-3
As received	0.18	0.40	0.32
2min O_2, 50W, 20 sccm	0.35	0.53	0.47
15min O_2, 50W, 20 sccm	0.50	0.69	0.59
30min O_2, 50W, 20 sccm	0.67	0.86	0.75

4.4.3.3 Effect of the Quantity of Silane on the Si Surface

It is know that the amount of silane deposited on the Si wafer surface can be controlled by altering the preparation parameters such as the concentration of the silane solution and the treatment time. Some literature reports[7-10] indicate that a well-ordered monolayer coverage of silane molecules on the Si surface provides a higher adhesion strength than multilayer coverage. A coverage corresponding to less than a monolayer would provide lower adhesion strength in a bonded system.

Figure 4-16 shows the debond area profiles for the model epoxy/SCA-1/Si (front side) bonded specimens prepared with different reaction concentrations of SCA-1 in the modification process. The average data (~5% error) of at least six runs conducted among several identical specimens for each surface were plotted. The data were collected using the probe test under dry conditions. The debond area increased (Figure 4-16) with decreasing treatment concentration of SCA-1 (see Table 4-5). The curve presented in Figure 4-16 shows a small non-linear curvature. This result deviates slightly from the mathematical model (Equation 4-5) for the probe test, which predicts a linear relationship between debond area and the probe penetration distance (or debond radius, *a*).

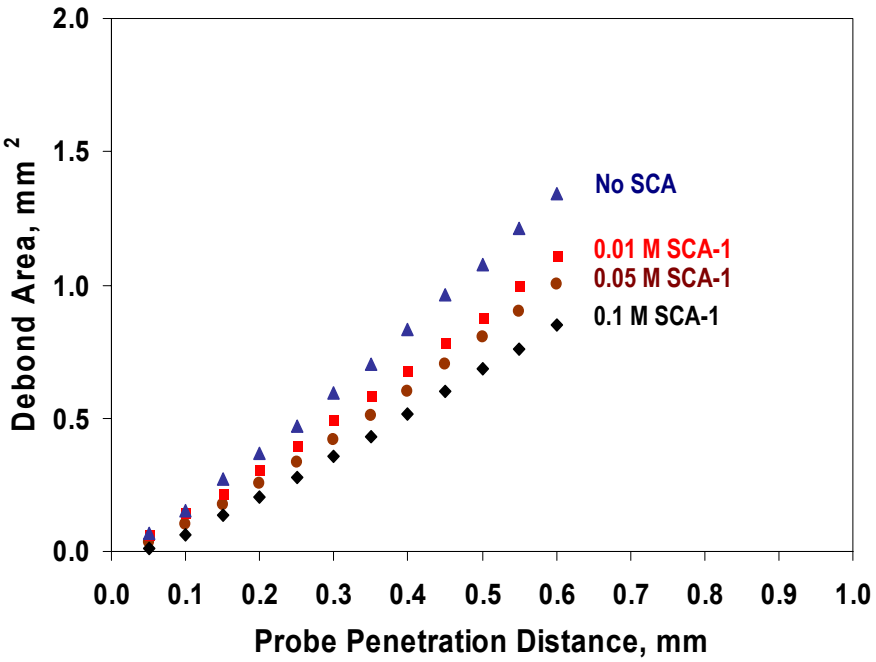

Figure 4-16. Debond area profiles for model epoxy/SCA-1/Si bonded specimens determined using the probe test under dry conditions (experiment **Type I**).

Table 4-5. **Elemental composition (atomic %) for as-received Si wafers treated with SCA-1 solutions at various concentrations.**

Surface Treatment	C	O	Si	N
As received, no SCA	6.9	47.0	46.1	< 0.1
0.004M, SCA-1, 5 min	13.2	36.1	50.0	0.7
0.01M, SCA-1, 5 min	22.7	33.7	42.1	1.5
0.05M, SCA-1, 5 min	23.0	31.3	44.1	1.6
0.1M, SCA-1, 5 min	32.0	40.3	24.8	3.0

It is also possible to quantify thin film adhesion in terms of strain energy release rate. It was shown previously that the point of the appearance of a true semicircular debond is a function of debond height, w_0, and the nature of the surface preparation. In this case, to compare film adhesion with the same specimen geometry but with different concentrations of silane (i.e., amounts of silane modification), a fixed probe penetration distance was chosen. Figure 4-17 shows the critical strain energy release rates for model epoxy/SCA-1/Si bonded specimens that were determined using the probe test at 0.25mm

probe penetration distance. G_c increased as the concentration of SCA-1 used in the modification increased. As shown in Figure 4-17, a noticeable increase in adhesion occurred when comparing surfaces prepared with 0.004 M and 0.1 M SCA-1 solutions. The low G_c value is consistent with findings shown in Figure 3-13, where the silane layer thickness on the surface treated with 0.004M SCA-1 was much lower than that for the surface prepared with 0.1M SCA-1.

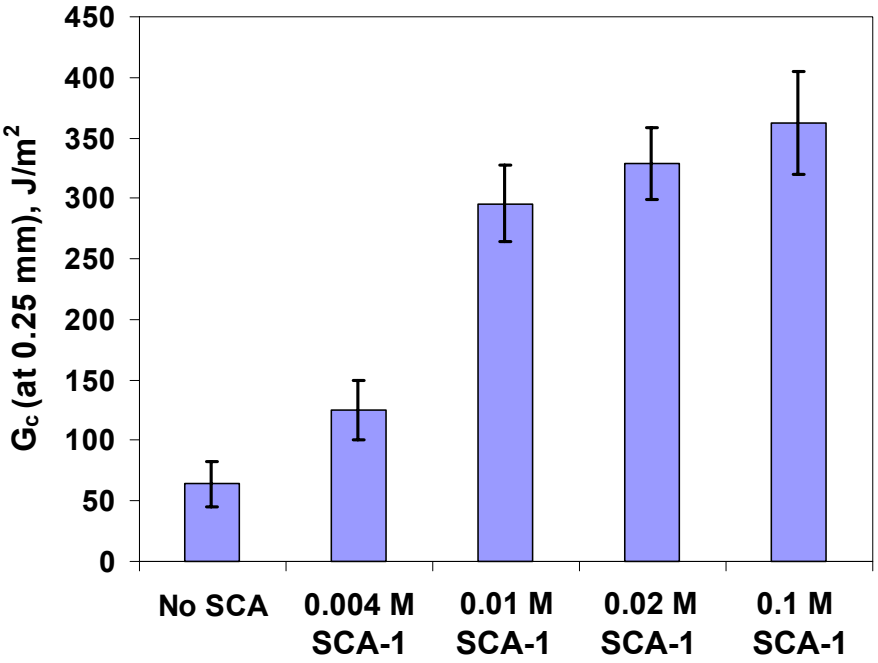

Figure 4-17. G_c values for model epoxy/SCA-1/Si bonded specimens determined using the probe test at 0.25mm probe penetration distance. The SCA-1 treatment time was 5min.

4.4.3.4 Effect of Silanes without Reactive Functionality

Figure 4-18 provides a comparison of the debond area profiles for model epoxy coated specimens with an as-received SCA-1 treated Si surface and a SCA-4 modified Si surface. The probe test was carried out under dry conditions. As shown in Figure 4-18, Si surfaces treated with SCA-4 yielded essentially the same debond area as that for the unmodified Si surface. SCA-4 did not promote adhesion to the epoxy polymer compared

to SCA-1 due to the lack of a reactive functional group for the epoxide. Further, adhesion promotion *via* interpenetration or chain entanglement is unlikely because of the monolayer thickness (5Å ± 0.5, ellipsometry) of the SCA-4 film on the Si surface.

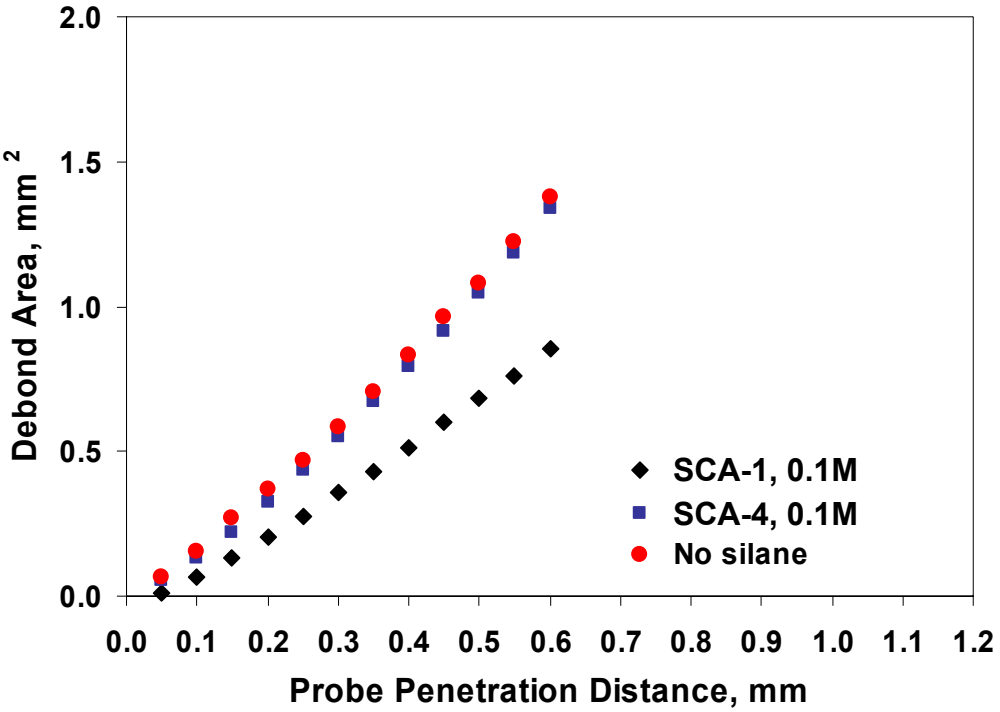

Figure 4-18. Debond area profiles for model epoxy/SCA/Si bonded specimens determined using the probe test under dry conditions. The silane treatment was 30 min.

4.4.4 Probe Test Performed on Immersed Specimens

4.4.4.1 Effect of Silane Treatment

In the second type of probe experiment, a bonded specimen was probed after immersing the specimen in fluid environments (i.e., immersion in solutions, water, etc.) for a given period. The information obtained from this test should reveal degradation in adhesion as a result of long-term exposure to a fluid medium. The rate of degradation was used as a measure of bond durability. Since the probe only penetrates less than one millimeter from the edge of the coating, the result obtained in this test is based on the

assumption that degradation at the coating edge is the same as that in the middle part of the coating (i.e., the diffusion of water or solvents occurs uniformly through the bulk thin film over the entire coated area). The probe test was conducted prior to the time that any visible debonding had occurred (i.e., fluid ingression or blister formation).

Figure 4-19 compares the bond durability for SCA-1 and SCA-2 modified surfaces for tests using different pH buffers at 60 ^{o}C. The error bars on each data point were calculated from several probe measurements along different coating edges for a specimen immersed at particular condition. The results indicated that the SCA-2 modified surface yielded a higher initial G_c (600 ± 50 J/m^2) compared to that for the SCA-1 (270 ± 30 J/m^2). The initial rate of decrease in G_c is actually higher for the SCA-2 modified surface, but the rate slowed considerably after about 35 days of immersion. Similarly, treated specimens immersed in pH 1, 4, and 6 buffer solutions showed essentially the same rate of degradation (within experimental error). The rate of degradation was noticeably higher for specimens immersed in the pH 9 buffer solution. The G_c values after 35 days of immersion in pH 9 buffer solution are 40 ± 10 J/m^2 and 250 ± 40 J/m^2 for SCA-1 and SCA-2 treated specimens, respectively. It should be noted again, that previous studies showed that the equilibrium moisture uptake for a bulk model epoxy specimen immersed at 60 ^{o}C in water-solvent mixtures was not dependent on solution pH[4]. Thus, the rate of bond degradation is likely associated with the rate of hydrolysis of the siloxane bond at the SCA/Si interface and these findings are similar to durability results discussed earlier for the immersion test, However, pH conditions would also affect the hydrolysis of bonds at the epoxy/SCA interface.

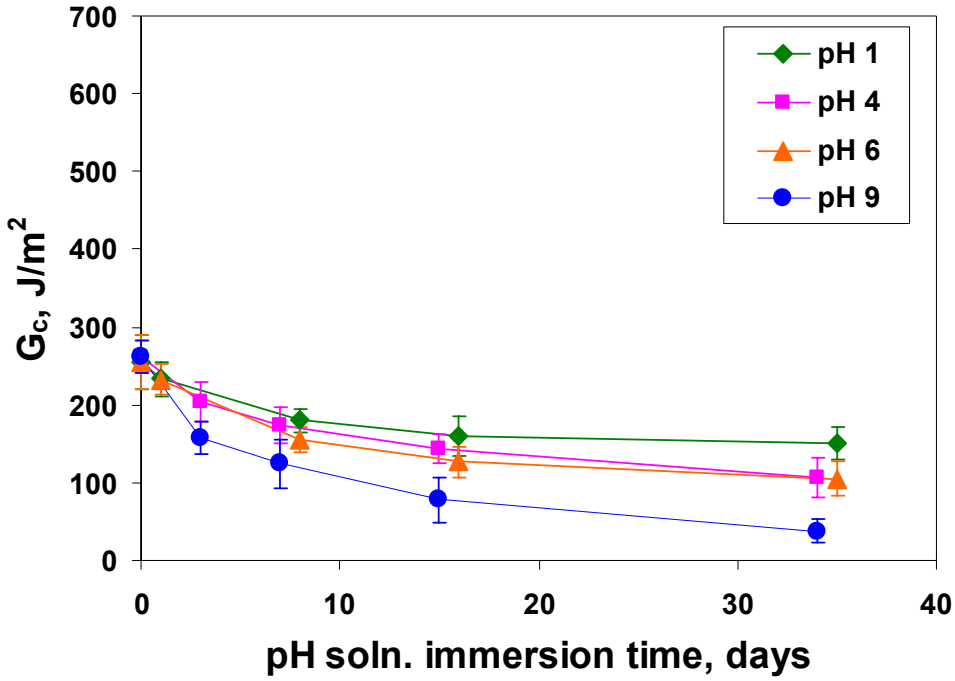

(a)

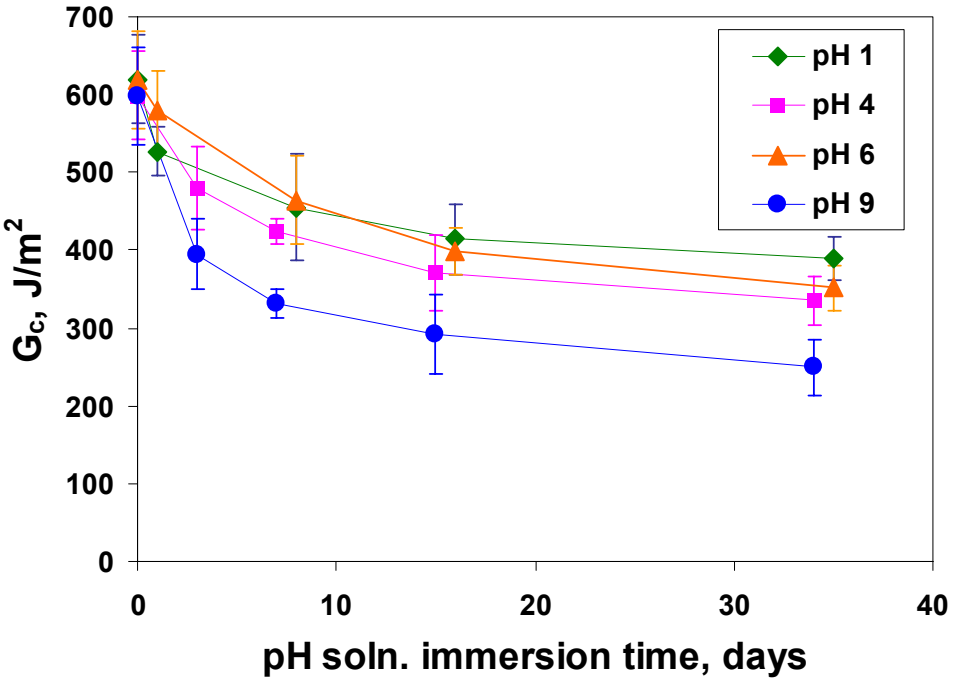

(b)

Figure 4-19. Critical strain energy release rate, G_c, (at 0.25 mm probe penetration distance) as a function of the immersion time at 60 ^{o}C in buffer solutions for Si surfaces treated with different silanes; (a) SCA-1/Si and (b) SCA-2/Si.

4.4.4.2 Effect of Oxygen Plasma Pretreatment

The durability of oxygen plasma-treated bonded specimens was determined by measuring adhesion strength after immersing the specimens in pH buffers or water for a given time. The information obtained from this test should reveal degradation in adhesion as a result of long-term exposure to aqueous media.

Figure 4-20 shows a comparison of experimentally determined G_c values plotted as a function of immersion time for various SCA-1 and SCA-2 modified as-received Si and TOX Si samples immersed in two different pH buffer solutions. The initial rate of decrease in G_c is higher for specimens modified with SCA-2; however, after 100 days of immersion at 60 ^oC, the rate of decrease in G_c values had slowed and leveled off. At this point, the G_c value for the SCA-2 modified sample was greater than that for the SCA-1 modified surface. This behavior occurs because the SCA-2 modified sample had a much higher initial G_c value. The reason for faster rate of decrease in G_c for the SCA-2 surface treated specimen upon immersion in the pH buffer solutions is not known. As previously discussed, the higher initial adhesion strength for the SCA-2 modified surface is probably related to the greater nucleophilic character of the secondary amine functionality leading to the formation of a stronger interface.

The durability for the as-received TOX Si surface modified with both silanes was better than that for the oxygen plasma treated Si surfaces. The overall rate of decrease in G_c (durability) is slightly higher for specimens immersed in pH 9 buffer (Figure 4-20b) than for those immersed in pH 4 buffer solution (Figure 4-20a). These results are consistent with the fact the Si-O-Si bond tends to hydrolyze faster under basic conditions[11] than in acidic solutions. This assertion assumes that a possible failure location is at the silane/Si interface. However, it should also be realized that the pH conditions could also affect the bonds formed between the epoxide and amine groups.

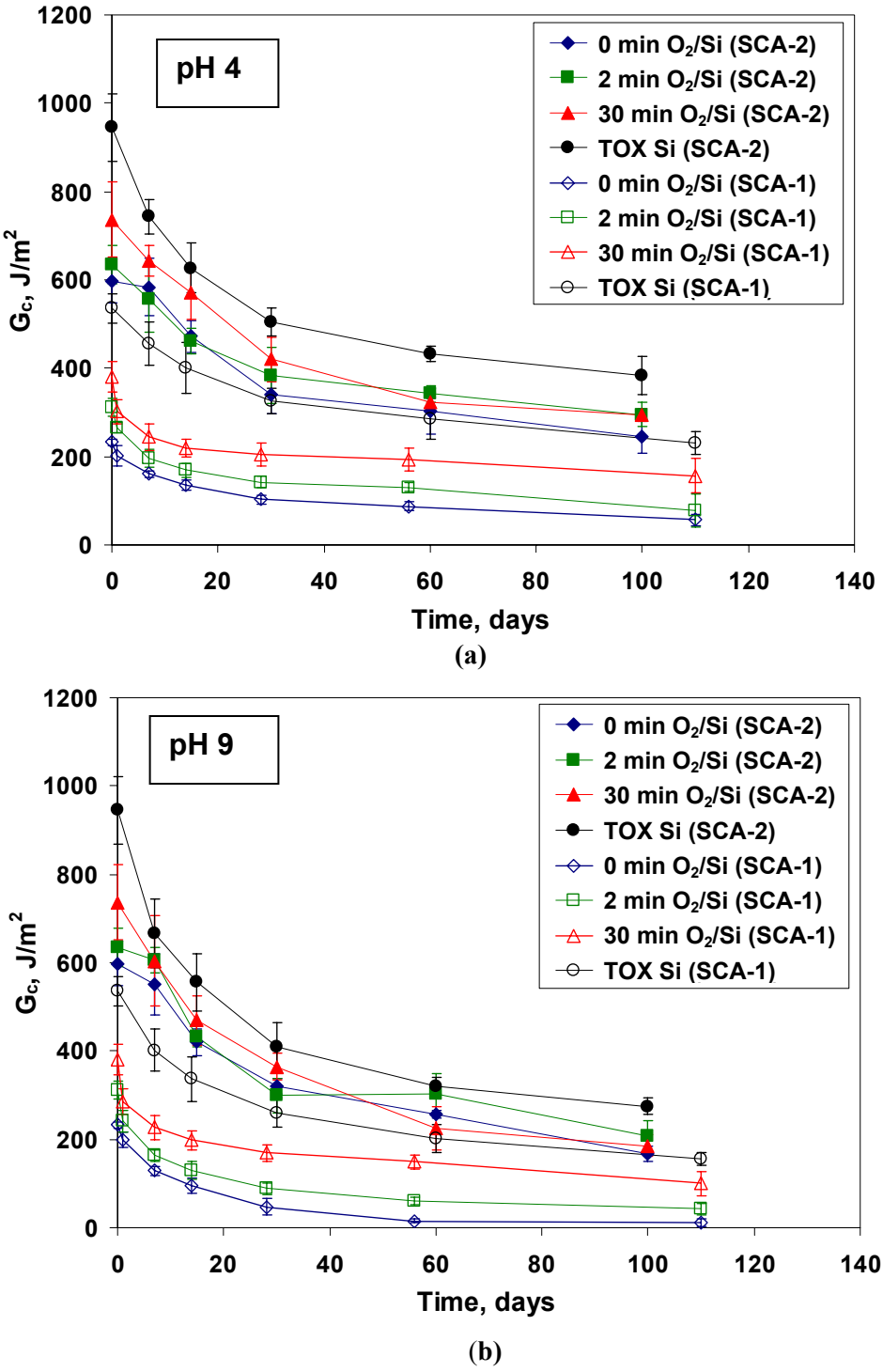

Figure 4-20. Critical strain energy release rate, G_c, (at 0.25 mm probe penetration distance) for SCA-Si samples as a function of the immersion time at 60 ^{o}C. (a) in pH 4 buffer solution and (b) in pH 9 buffer solution.

4.4.5 In-Situ Probe Test

By exposing the bonded system to water or a high humidity environment, water molecules penetrate either through the bulk polymer coating or along the interface at the coating/substrate edge. As water penetrates, it first binds to sites in the polymer[12,13], and at higher concentration forms aggregates[14]. Water may eventually diffuse to the interfacial region if the chemical component of the interface is more polar than that of the bulk adhesive. Some researchers have established a critical concentration of water or a humidity threshold level at which adhesive bond weakening takes place in selected systems[15,16]. In these cases, it is difficult to elucidate the effect of a fluid of choice (water) on the chemical bonds formed between the silane coupling agent and organic and inorganic phases across the interface. In the in-situ test approach, water, liquid, or solution can be delivered to the crack front in the bonded specimen, so that the fluid migrates only along the polymer/substrate interface (assuming that the diffusion of water/fluid into the polymer matrix is insignificant on a short time scale). Thus, the in-situ probe experiment is particularly suited to reveal the dynamics of adhesive debonding when the interfacial region was subjected to a simultaneous mechanical stress and a chemical environment. The procedure for the "in-situ" experiment is shown in Scheme 4-2. First, a routine initial probe penetration is commenced to a predetermined distance, and a semicircular debond is formed. The liquid (fluid) of interest is then delivered to the vicinity of the crack opening with the probe maintained in position. The liquid spreads quickly over the entire debond area at the film/substrate interface. A time delay of about 10 min is allowed for the liquid to migrate into the interfacial area ahead of the crack front thereby degrading local adhesion such that the stress on the system causes additional crack growth. After the time delay, further probe penetration is carried out for a pre-determined distance or in incremental steps (0.05mm). The debond area is evaluated to determine the extent of adhesive bond weakening.

Scheme 4-2

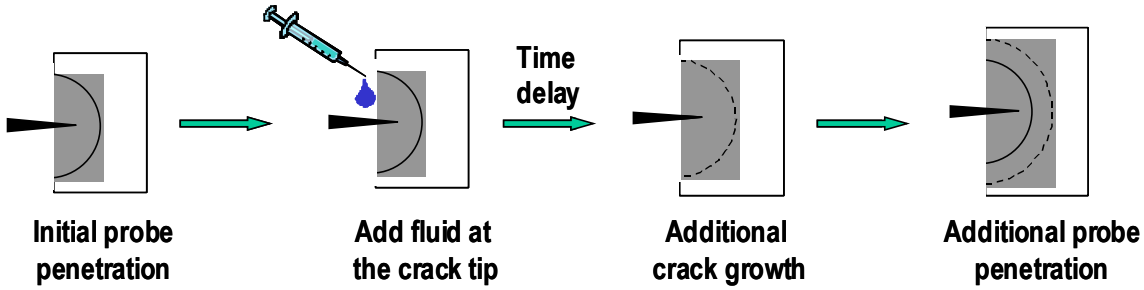

A schematic illustration showing the debond characteristics obtained in the in-situ probe experiment are shown in Figure 4-21. Three major features of Figure 4-21 are: 1) the debond area data collected under the dry conditions may or may not exhibit a different slope compared to data collected after the addition of fluid. The slope of the line after water/fluid addition gives an indication of the extent that the interface is affected by the presence of the water/fluid. 2) the debond area increase after fluid introduction causes a discontinuity in the plot, which is due to crack growth during the time delay following the delivery of the fluid to the crack front. During the time delay, the position of the probe was held stationary. 3) imaginary data points can be located by extending the data line collected under dry conditions to correspond to the next incremental probe penetration distance along the x-axis. The area increase above this imaginary data line is the area increased due to the introduction of fluid for the particular incremental probe advance.

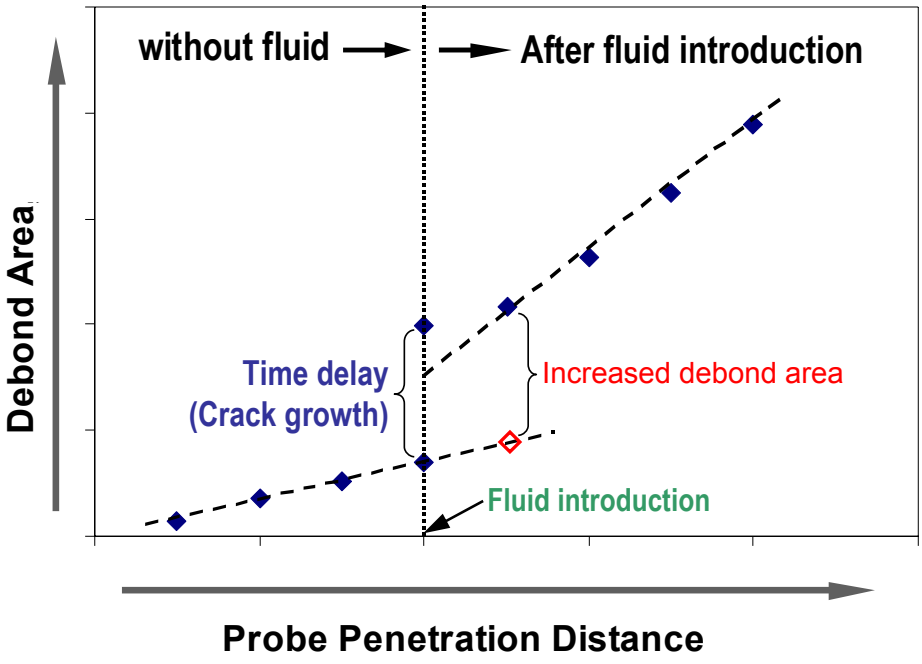

Figure 4-21. Debond area as a function of probe penetration distance for a typical in-situ experiment at room temperature.

4.4.5.1 Effect of Silane Treatment

Figure 4-22 shows the effect on the debond profile as a function of the introduction of deionized water starting at different probe penetration distances for model epoxy/as-received/Si and the model epoxy/SCA-1/Si specimens. The respective data collected under dry conditions exhibited slightly different slope for as-received and SCA-1 modified specimens indicating the difference in adhesion performance in the bonded specimens. However, under in-situ (fluid introduction) conditions the slope for the data collected increased substantially upon introduction of deionized water. A greater slope is noted for fluid introduction at greater probe penetration distances, and suggests that for a larger debond area (i.e., 0.4 mm in Figure 4-22a) more crack front is exposed to the fluid, resulting in a greater increase in the debond area for each incremental probe advancement. Further, note that the slope for data points representing the debond area at

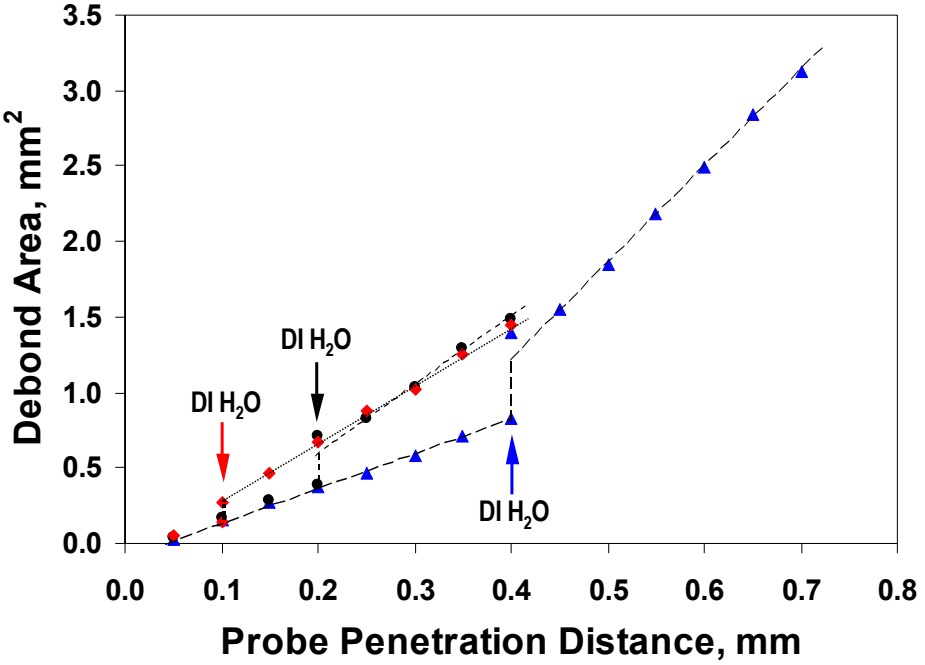

(a)

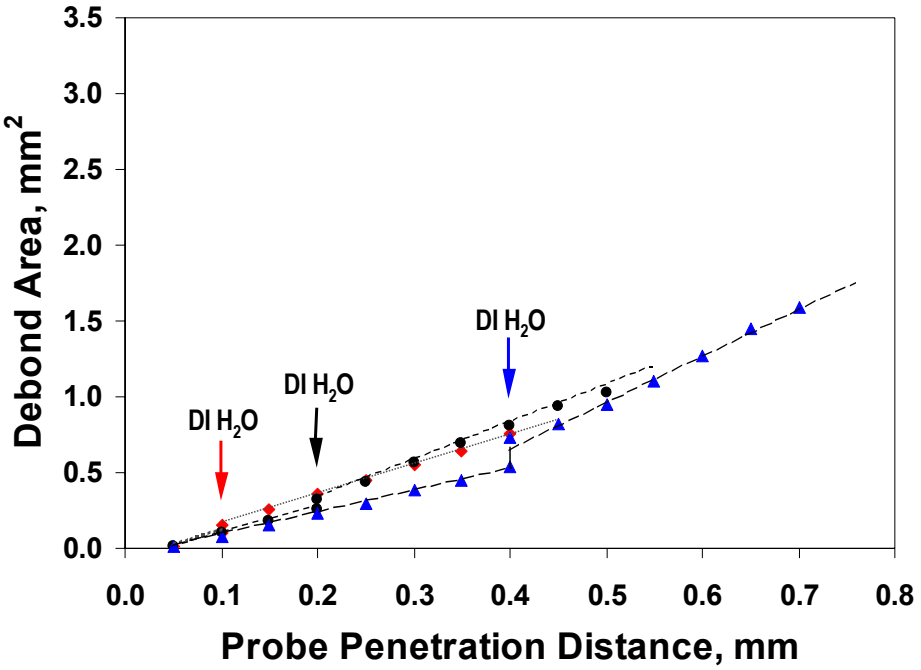

(b)

Figure 4-22. Debond profiles as a function of the fluid introduction at different probe penetration distances; (a) as-received Si frontside surface without silane coupling agent, and (b) Si frontside surface modified with SCA-1.

the end of a 10 min delay was higher than the slope for data points collected with incremental probe advances in the presence of the fluid. Such results signify a decreased adhesion bond strength.

4.4.5.2 Effect of Applied External Stress

Figure 4-23 shows the percent debond area increase after the introduction of deionized water at 0.1, 0.2, and 0.4 mm probe penetration for Si frontside surfaces without silane coupling agent and with a SCA-1 treatment. The percent debond increase (equal to [ΔA/A] x 100) is greater for the Si surface with no SCA-1 treatment at each position at which the in-situ experiment was initiated. The percent debond increase values are much lower for the SCA-1/Si samples. These results are summarized in Table 4-6. For the as-received/Si samples, the highest % debond increase occurred during the advancement of the probe from 0.10 mm to 0.15 mm in the presence of water. The percent area increase is less for the probe advance increment from 0.20-0.25 mm and 0.40-0.45 mm. This behavior occurs because the stress per unit debond area (dry) is the greatest for the debond caused by probe penetration at 0.10 mm prior to the addition of water. The presence of water in the vicinity of the crack front weakens the interfacial adhesion and resulted in an immediate crack growth. By contrast, this large difference in percent debond area increase is not observed for the epoxy/SCA-1/Si sample at each probe advance increment. This result occurs because the interfacial adhesion energy is high due to the function of the silane coupling agent, The effect is that the stress per unit debond area applied from the probe penetration is reduced. Ritter *et. al.*[17] indicated that the flexibility of the silane molecule helps to relieve strained Si-O-Si bonds near the Si surface, and thereby decreases the susceptibility of the interfacial siloxane bond to attack by water.

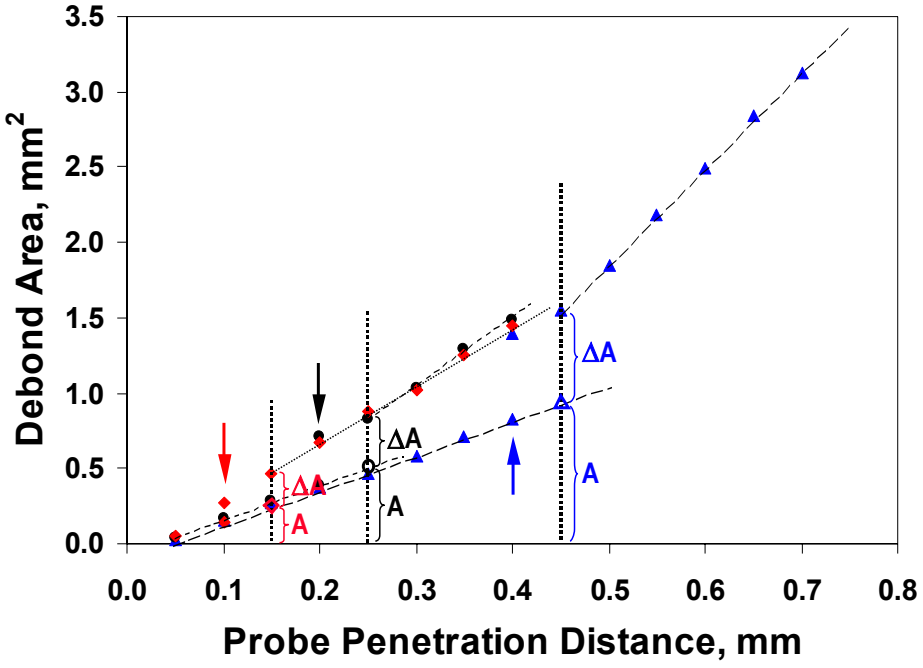

(a)

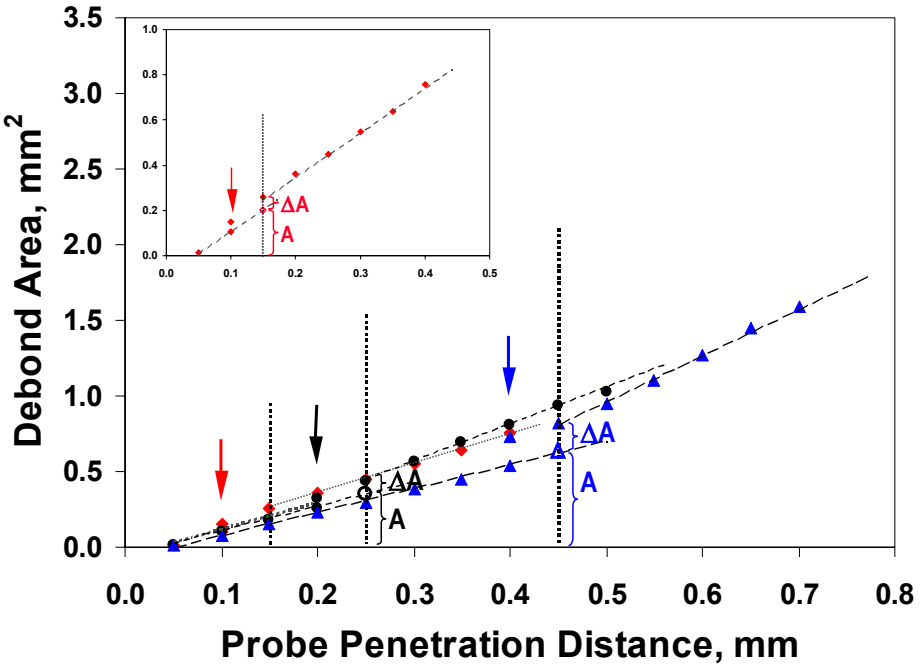

(b)

Figure 4-23. Calculation of percent debond area increase as a function of the fluid introduction at different probe penetration distances; (a) model epoxy/as-received Si (frontside), and (b) model epoxy/SCA-1/Si (frontside).

Table 4-6. Percent debond area increase after fluid introduction at the crack front at different probe penetration distances for in-situ experiments conducted at room temperature.

Probe Advancement Increment	Type of Surface	% Debond Area Increase
0.10-0.15 mm	Si/no silane	92
0.20-0.25 mm	Si/no silane	70
0.40-0.45 mm	Si/no silane	63
0.10-0.15 mm	Si/SCA-1	29.4
0.20-0.25 mm	Si/SCA-1	28.8
0.40-0.45 mm	Si/SCA-1	28.2

4.4.5.3 Effect of Pre-soak Time in Water

It can be assumed that the only substantial amount of water at the film/substrate interface in the dry specimen is from the addition of the liquid once the thin epoxy film was cracked from the substrate. It is reasoned that the water added migrates into the interfacial area of the crack front, and thereby degrades interfacial adhesion. The outcome is demonstrated by the fact that the slopes of plots of the debond area versus probe penetration distance are clearly different for the dry test (no fluid at the interface) and the in-situ test where water is present at the interfacial area; the in-situ condition yields the higher slope.

In a bonded system, bond durability depends on how soon water can diffuse through the polymer film and cause degradation in the interfacial area (assuming diffusion from the coating edge is not predominant). If this assumption is true, the gradual degradation of interfacial strength can be verified by pre-soaking (immersing) the dry specimens in a fluid for different times. The in-situ test can then be used to study the effect of water (or fluid) in the interfacial region on adhesion in pre-soaked specimens.

Figure 4-24 shows the change in debond profile as a function of soaking time for the in-situ experiment. Deionized water was introduced with the probe penetration distance at 0.2 mm. (Note: for 0.2 mm PPD, the debond radius is larger than 0.2 mm). As the soaking time increases, the debond area for the in-situ test also increases in the

presence of water. This result is possibly due to the fact that as immersion time increases, water that saturated the epoxy film has the tendency to migrate to the epoxy/Si interface, because the silane layer (SCA-1 or SCA-2) is more hydrophilic than that the epoxy film. Though the amount of water within the silane layer may be much lower than that in the bulk film, if uniformly distributed, the interfacial strength would be reduced. In Figure 4-24, it is noted that a trend of increasing debond area was observed as a function of soaking time for those data points collected prior to the addition of water to the crack front. Thus, the debond area increased (or G_c decreased) as immersion time increased.

To better illustrate the change in the debond profile as a function of the in-situ experiment starting location, the slope of the curves for data points collected in the presence of water (i.e., data points after water was introduced) was calculated and plotted in Figure 4-25. Introduction of water at 0.1, 0.2 and 0.4mm yielded essentially the same trend, in that the rate of increase in slope is higher initially and approaches a limiting value after about 30 days of immersion in water at 60 ^{o}C. The higher slope of the debond data curve resulted for specimens in the presence of water with longer pre-soak can be explained by the possibility of capillary pressure at the wet interface, which adds energy to produce a larger debond. Introduction of water at greater probe penetration distances (PPD = 0.4 mm) produces the higher slope. This is due to the fact that a large area crack front was exposed. Slopes on the average are lower for the SCA-2-modified Si surface indicating that it is more resistant to debonding when water is added at the crack front. This trend is consistent with findings observed in immersion studies and durability probe studies.

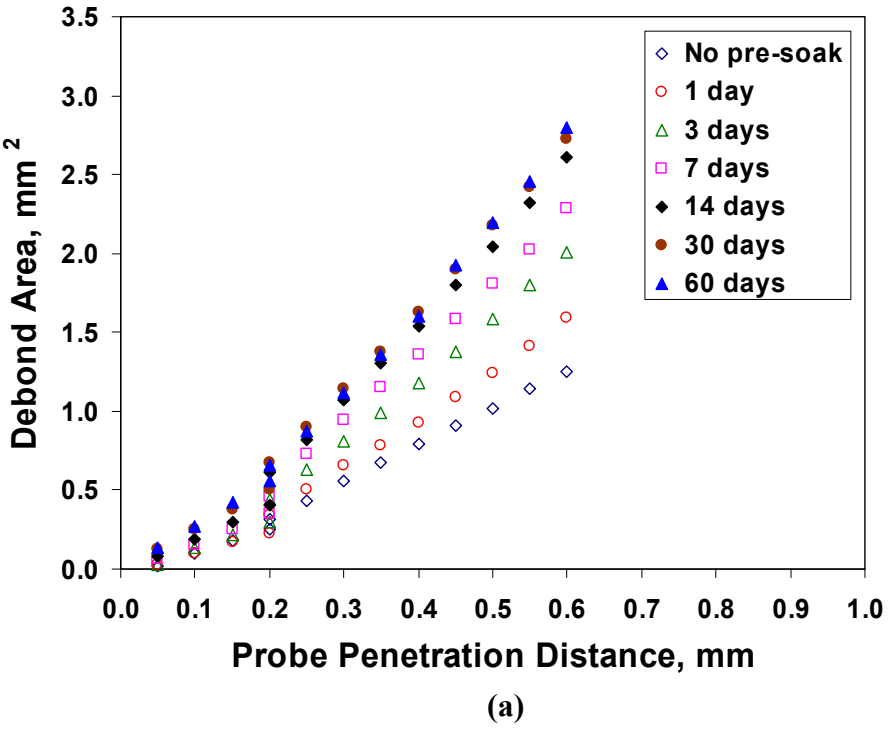

(a)

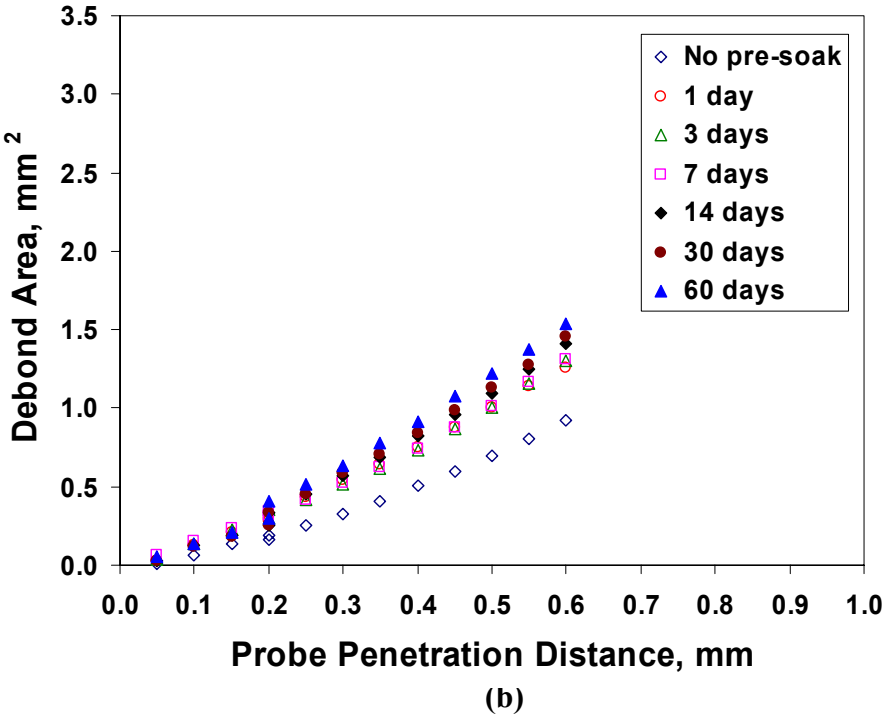

(b)

Figure 4-24. Debond profiles for a model epoxy/SCA/Si bonded specimens as a function of pre-soaking time. (a) SCA-1/Si and (b) SCA-2/Si. Fluid (DI H_2O) introduction occurs at a probe penetration distances of 0.2 mm. The specimens were pre-soaked in DI H_2O at 60 ^oC.

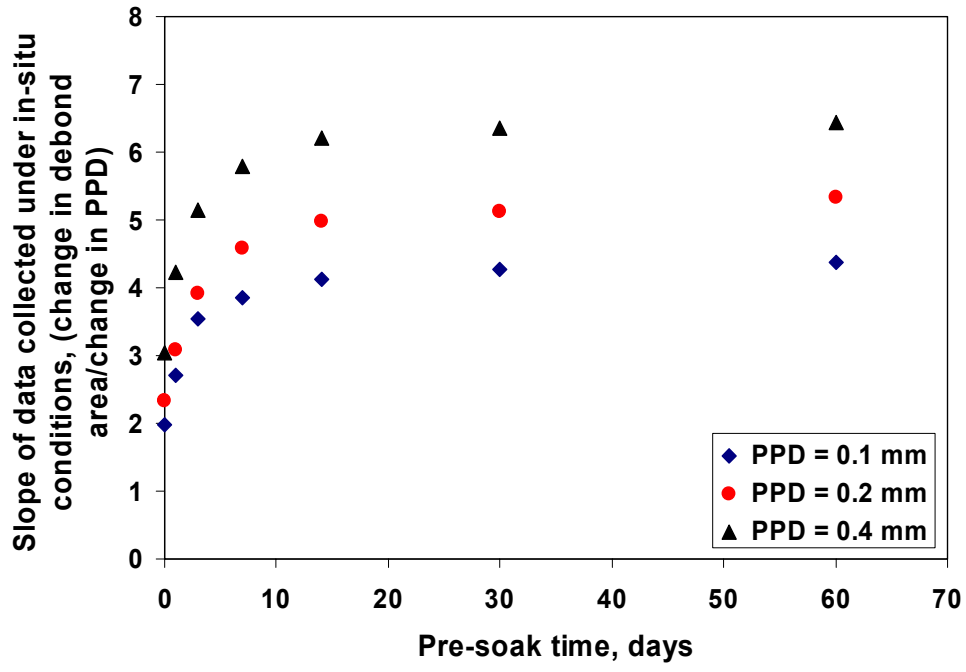

(a)

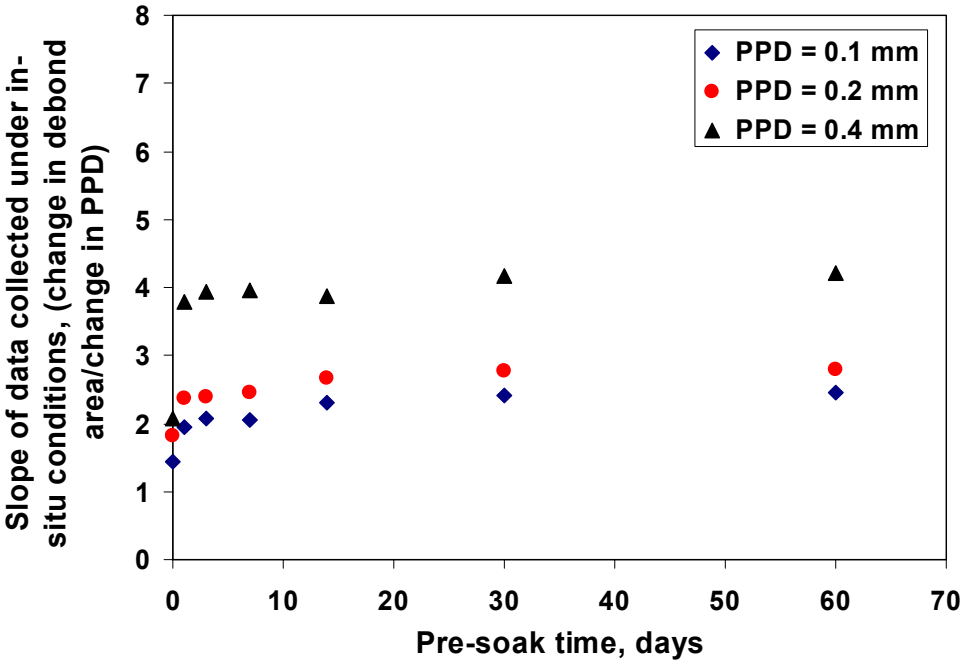

(b)

Figure 4-25. Change in debond profile (evaluated as the slope of the data in the debond area vs. probe penetration plot in the presence of fluid) as a function of pre-soaking time: in-situ test conditions. (a) Model epoxy/SCA-1/Si and (b) model epoxy/SCA-2/Si.

4.4.5.4 Effect of Solution pH

To establish a baseline response for the effect of pH on interfacial adhesion in the model epoxy/SCA-1/Si bonded system, extreme pH conditions were examined. Figure 4-26a shows the debond profile for the in-situ probe experiment when strong acid and base solutions were used as the in-situ fluid. The bonded specimen was not subjected to pre-soaking. The debond curve contains the specific features for the in-situ probe test in that the slope of the curve collected with liquid at the crack front deviates significantly from the slope of the curve if no fluid were added. The amount of debond area increase (at 0.2 mm PPD) at the point where the fluid was added is a function of the property of the fluid and the strength of the interface. As shown in Figure 4-26a, the debond profile is essentially the same regardless of the pH of the in-situ fluid. The amount of debond increase at 0.2mm probe penetration distance is also about the same after a 10 minute delay time. These observations suggest that for short exposure times, the Si surface treated with 2.5% v/v SCA-1 solution was durable enough to withstand the interfacial degradation in the presence of strong acid or base.

To further examine interfacial degradation in the model epoxy/SCA-1/Si bonded system, another as-received Si surface was treated with 0.25% v/v SCA-1 solution and subsequently coated with the model epoxy. The in-situ test using strong acid and base yields the debond profile shown in Figure 4-25b. It is apparent that the strong base solution caused more interfacial degradation for this specimen in that the slope of the curve after fluid addition is much higher than that for the strong acid or deionized water. Also, crack growth did not approach a limiting value during the 10 min delay time for tests in the strong base environment (Figure 4-27). These results suggest that the in-situ probe experiment is sensitive enough to distinguish the effect of various chemical environments if the bond interface is sufficiently weak (so that less time is needed to cause interfacial bond disruption by the chemical environment) for the current probe test geometries.

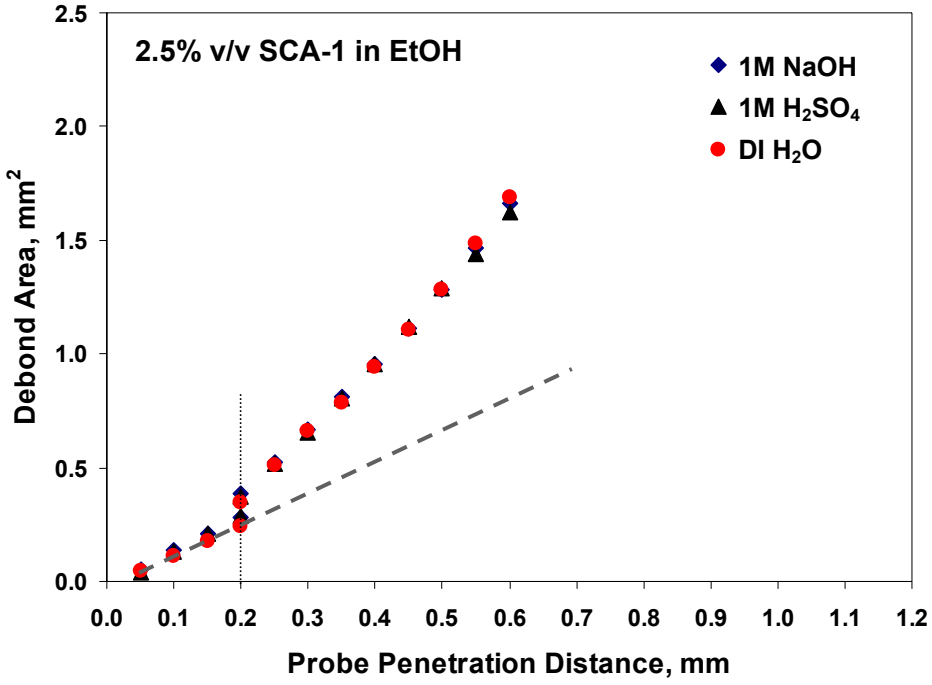

(a)

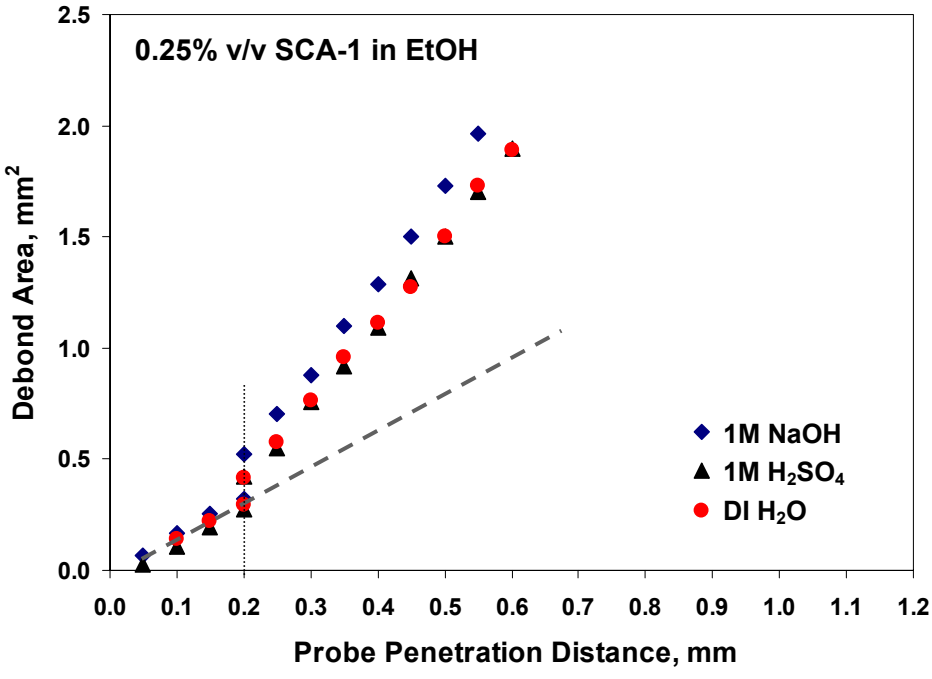

(b)

Figure 4-26. Effect on debond profiles for a model epoxy/SCA-1/Si bonded specimen as a function of pH; (a) for Si surface treated with 2.5% v/v SCA-1 in acidified ethanol, and (b) with 0.25% v/v SCA-1 in acidified ethanol. The dashed line indicates the debond profile if no fluid were added.

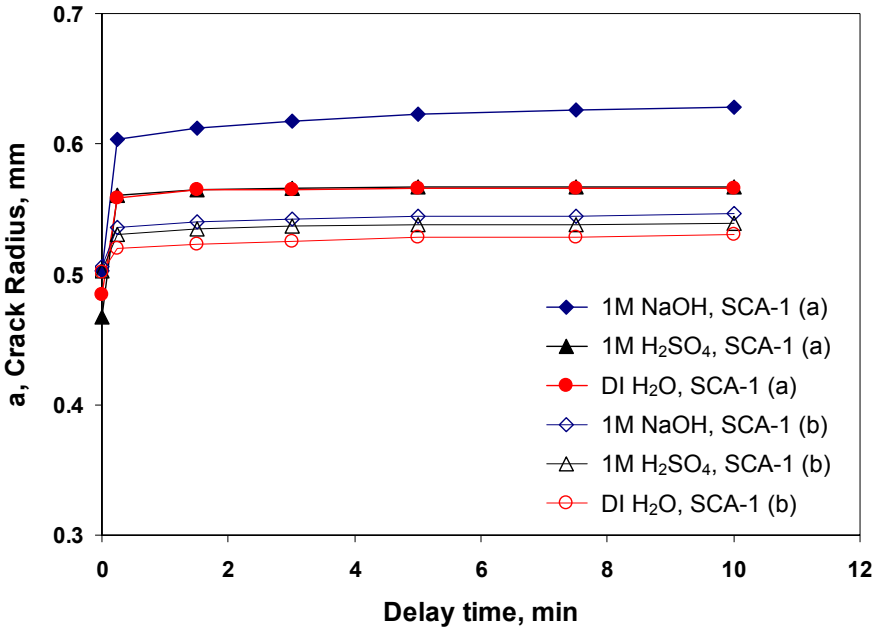

Figure 4-27. Crack growth at 0.2 mm probe penetration distance upon the introduction of fluid to the crack front. (a) Si surfaces treated with 0.25% v/v SCA-1 and (b) surfaces treated with 2.5% v/v SCA-1 concentrations in acidic ethanol, respectively.

4.4.5.5 Effect of Solution Surface Energy

To study the effect of surface energy of the solutions on interfacial adhesion in the Si/epoxy system, deionized water (γ = 72.2 mJ/m^2) and Triton X-100 solution (0.277 mM in DI H_2O, γ = 33.4 mJ/m^2) were chosen as the fluids for the in-situ probe experiment. The surface tension of the solutions was measured using the Wilhelmy plate method at room temperature. The concentration of the Triton X-100 solution is in the vicinity of its critical micelle concentration (CMC) in water. Figure 4-28 shows the results of the in-situ probe experiment when using liquids of two surface tensions as the in-situ liquid. The addition of the solution occurs at 0.20 mm of probe penetration. It is clear that altering the surface tension of the fluid does not affect the debond profile under the in-situ environment for fluids in the range of the surface energies tested.

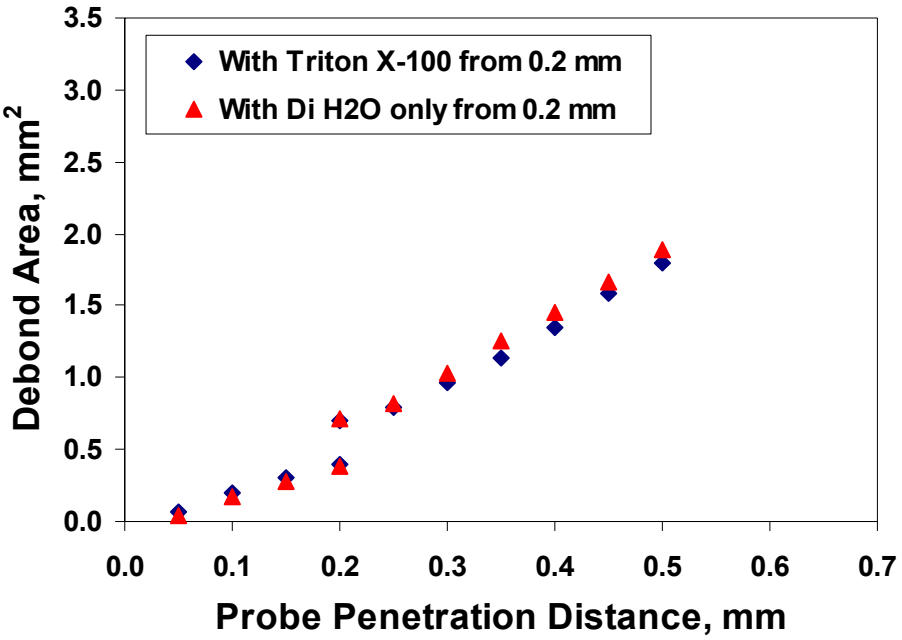

Figure 4-28. Debond profile using in-situ fluids with different surface energies; model epoxy/as-received Si surface; no silane treatment. In-situ experiment at room temperature. The concentration of the Triton X-100 is 0.277 mM in DI H_2O. γ_{H2O} = 72.2 mJ/m^2 and $\gamma_{\text{Triton X-100}}$ = 33.4 mJ/m^2 at room temperature.

4.4.5.6 Effect of Pre-soak Time in Various Solution Components

Figure 4-29 shows the effect on debond profiles for a model epoxy/SCA-1/Si bonded specimen (not pre-soaked) when using six different solution component mixtures (with compositions listed in the Figure's caption) as the in-situ fluids. The debond profile is essentially the same regardless of the composition of the solution component mixture. The amount of crack growth as a function of delay time was essentially the same when each of the six solution component mixtures was added in the in-situ test (see Figure 4-30).

The same bonded specimens were pre-soaked in individual solution component mixtures for 1 week and 2 weeks at 60 ^{o}C. Figure 4-31a, shows in-situ test results and the effect on adhesion where the in-situ fluid was an aqueous solution of 10% w/w diol-1 and 2% w/w surfactant and an aqueous solution of 10% w/w diol-2 and 2% w/w surfactant.

Immersion in and in-situ testing using the mixture containing diol-2 resulted in a greater debond area. It is argued that diol-1 tends to penetrate epoxy networks and swells the polymer network to a greater extent than diol-2, because of its ability to act as a surfactant[17]. This feature for diol-1 may lead to a lower modulus for the polymer coating on the Si substrate, thus yielding a smaller debond for the same amount of applied external stress from the probe tip.

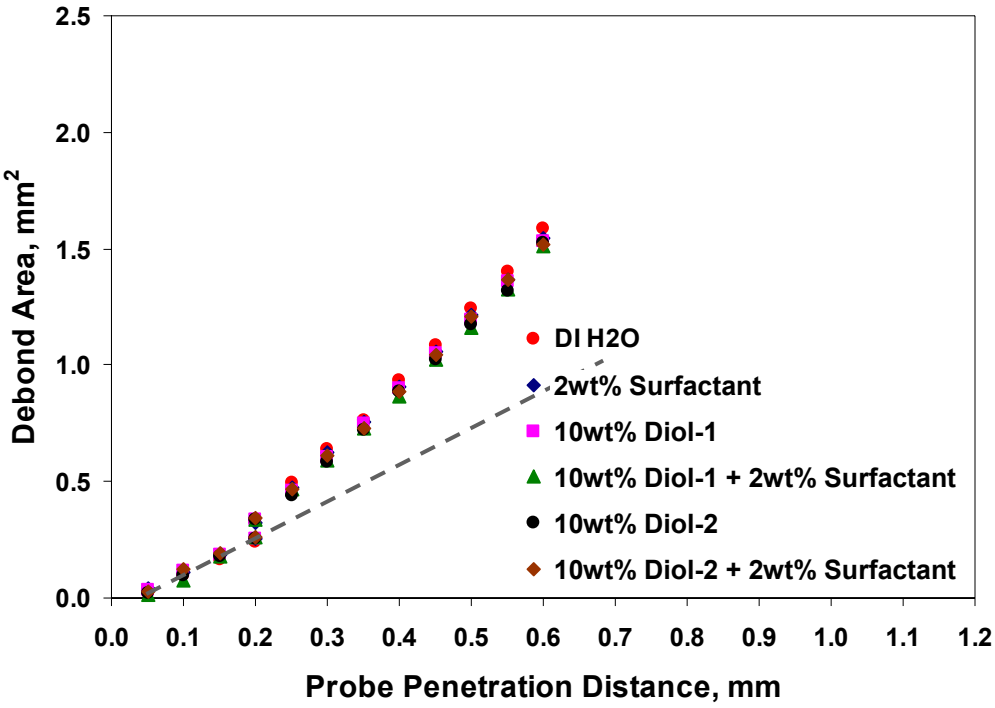

Figure 4-29. Debond profiles for a model epoxy/SCA-1/Si bonded specimen as a function of various solution components. The fluid introduction occurs at a probe penetration distance of 0.2 mm. Bonded specimens were not subjected to pre-soaking. Si surfaces were treated with 2.5% v/v SCA-1 in acidic ethanol.

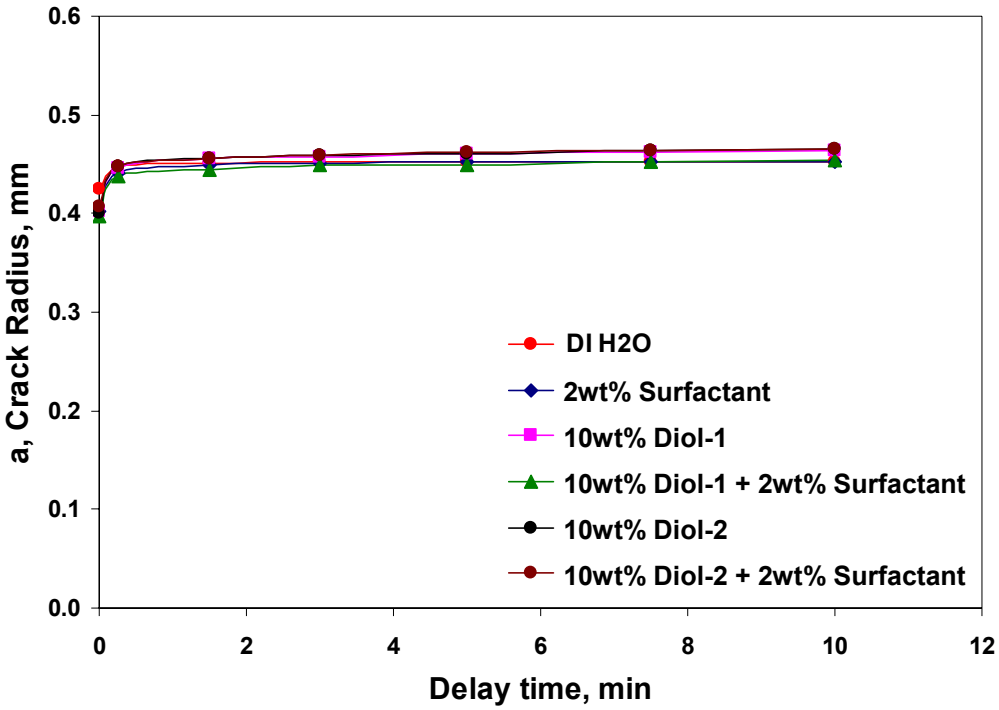

Figure 4-30. Crack growth at 0.2 mm probe penetration distance upon the introduction of various solution components at the crack front. Bonded specimens were not subjected to pre-soaking. Si surfaces treated with 2.5% v/v SCA-1 in acidic ethanol.

Figure 4-31b shows the effect on adhesion when comparing an aqueous solution of 10% w/w diol-1 and an aqueous solution of 10% w/w diol-2. Immersion in the mixture containing diol-2 produced a more extensive debond area. However, the overall debond area was lower (at 0.6mm probe penetration distance) than that for mixtures containing the surfactant component. This finding suggests that the surfactant component has a limited 'add-on' effect rather than a synergistic effect in terms of promoting interfacial degradation. When a solution containing only surfactant was studied, the effect on debond behavior was insignificant (Figure 4-31c). The slope of the curve after fluid introduction was essentially the same for specimens pre-soaked in deionized water and in a 2% w/w surfactant solution.

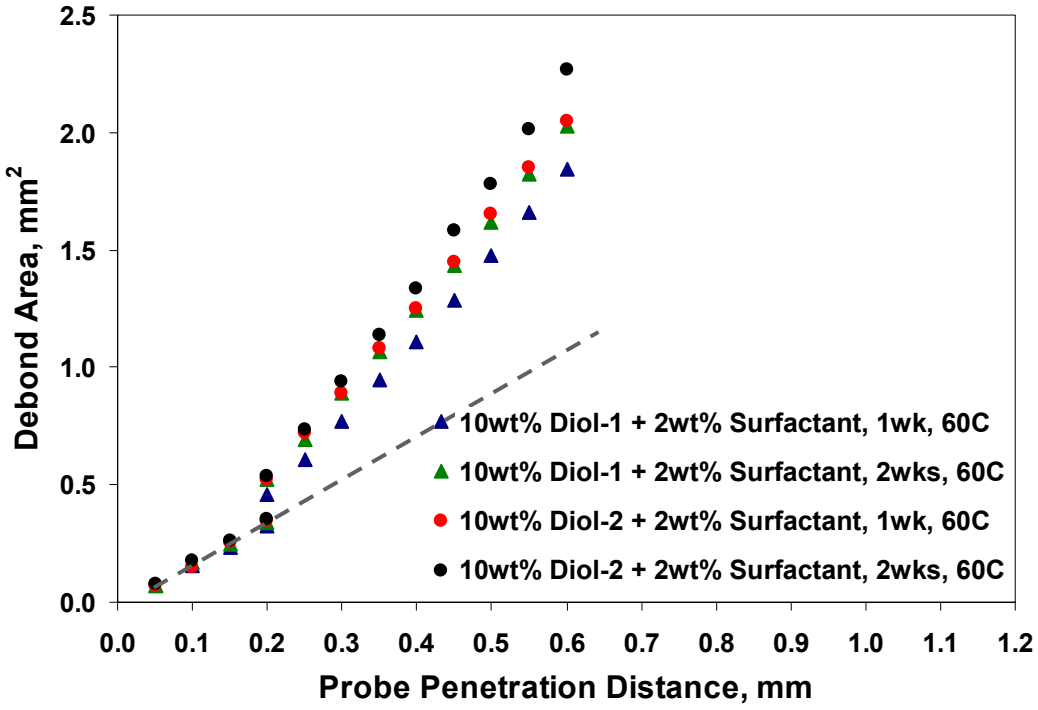
Debond Area, mm2
Probe Penetration Distance, mm
10wt% Diol-1 + 2wt% Surfactant, 1wk, 60C
10wt% Diol-1 + 2wt% Surfactant, 2wks, 60C
10wt% Diol-2 + 2wt% Surfactant, 1wk, 60C
10wt% Diol-2 + 2wt% Surfactant, 2wks, 60C

(a)

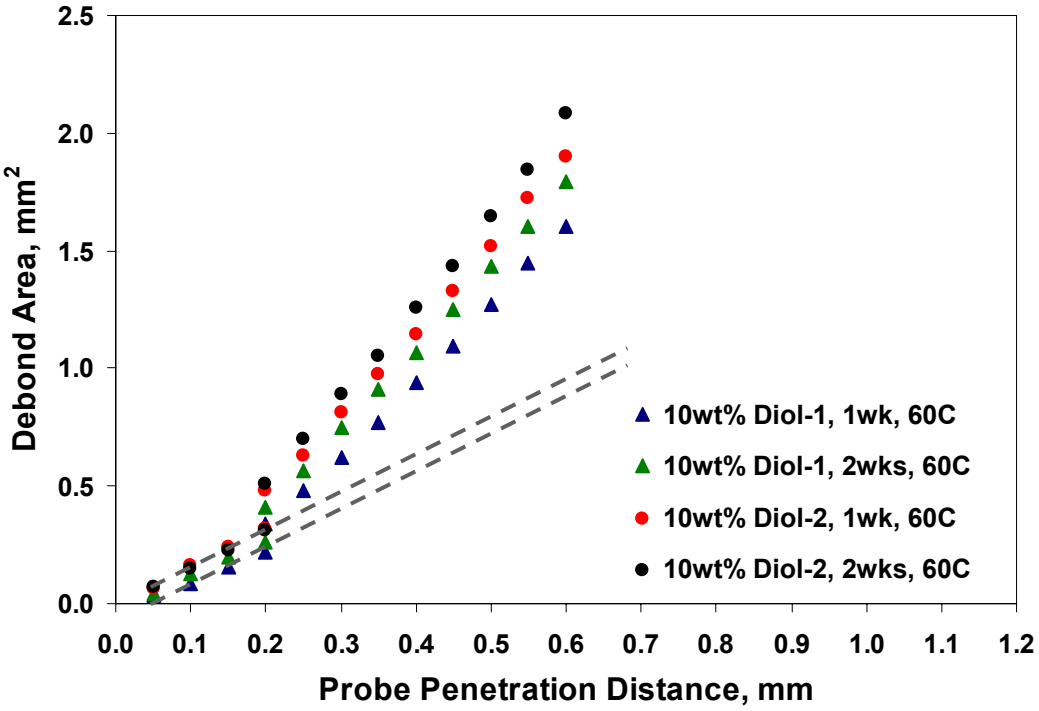
Debond Area, mm2
Probe Penetration Distance, mm
10wt% Diol-1, 1wk, 60C
10wt% Diol-1, 2wks, 60C
10wt% Diol-2, 1wk, 60C
10wt% Diol-2, 2wks, 60C

(b)

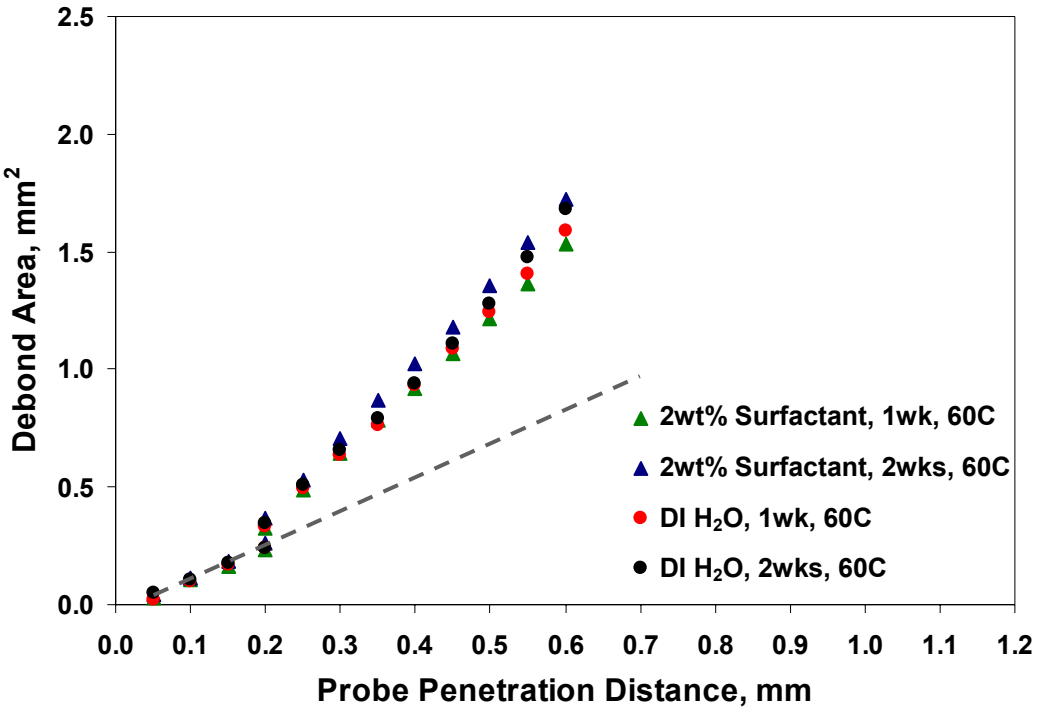

(c)

Figure 4-31. Effect on debond profiles for a model epoxy/SCA-1/Si bonded specimen as a function of various solution components. Bonded specimens were subjected to pre-soaking in individual mixtures at 60 °C. Si surfaces were treated with 2.5% v/v SCA-1 in acidic ethanol; (a) an aqueous solution of 10% w/w diol-1 and 2% w/w surfactant, and an aqueous solution of 10% w/w diol-2 and 2% w/w surfactant; (b) an aqueous solution of 10% w/w diol-1, and an aqueous solution of 10% w/w diol-2; (c) an aqueous solution of 2% w/w surfactant, and DI water.

However, data shown in Figure 4-31 do not truly reveal the liquid-interfacial chemical bond interaction for a system under stress. This is because in a bonded system, such as a thin epoxy film bonded to a Si substrate, water or solvent molecules can diffuse through the polymer film and bind or accumulate around the polar sites in the interfacial region. Previous studies[16-19] indicated that water at the interface promotes crack propagation for a system under stress when additional water was added in the in-situ fashion. Thus, to study the 'true' liquid-interface interaction, the crack front for a system under stress must be moisture free, so that the only liquid present at the crack front is the fluid/solution of choice.

To examine the debonding characteristics of a weaker SCA interface, a Si wafer was treated with 0.25% v/v SCA-1 in acidic ethanol. Figure 4-32 shows the effect on debond profiles for a model epoxy/SCA-1/Si bonded specimen as a function of various solution components in the in-situ fluid for bonded specimens that were not pre-soaked. In-situ test using an aqueous solution containing diol-2 yielded a greater debond area than that for an aqueous solution containing diol-1. The data presented in each curve represent an average of at least four runs and have about a 5% error for the calculated debond areas at each data point.

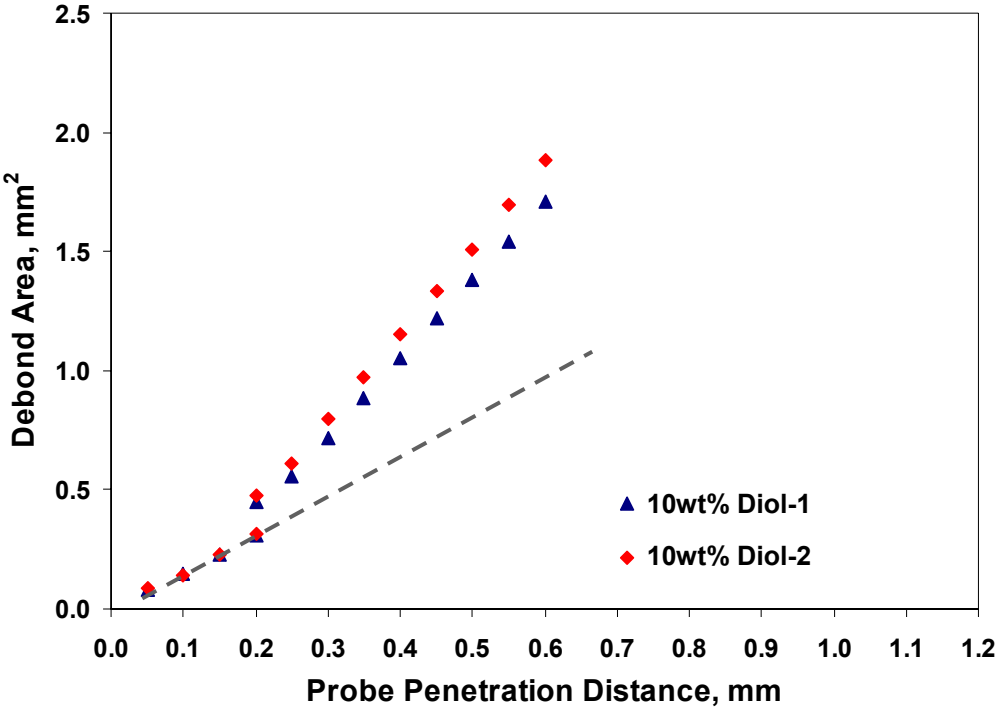

Figure 4-32. Debond profiles for a model epoxy/SCA-1/Si bonded specimen as a function of various solution components. Bonded specimens were not subjected to pre-soaking. Si surfaces were treated with 0.25% v/v SCA-1 in acidic ethanol.

4.4.5.7 Effect of Silanes with No Amine Functionality

Figure 4-33 illustrates the debond area profiles for model epoxy coated Si specimens modified with SCAs and tested *via* in-situ conditions using deionized water as the in-situ liquid. The slope of debond area versus probe penetration distance curve is essentially the same for the SCA-4 silane- and unmodified-Si surfaces. This observation is consistent with the results for dry adhesion behavior as discussed in Section 4.3.3.4. in that no improvement in adhesion resulted for SCA-4 modified Si surfaces. The data presented in each curve represent an average of at least four runs and have about a 5% error for the calculated debond areas at each data point.

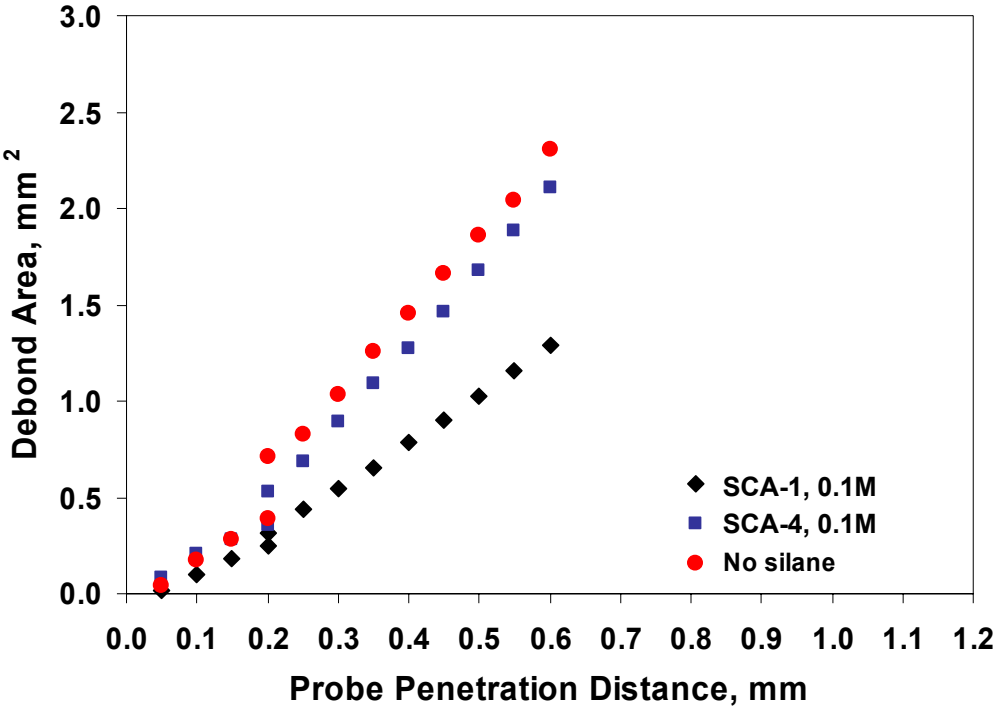

Figure 4-33. Debond area profiles for model epoxy/SCA/Si bonded specimens determined using the probe test under in-situ conditions (DI water).

4.5 Wedge (DCB) Test Results

Wedge testing of double cantilever beam type specimens was conducted to evaluate the durability of the model epoxy/SCA/Si bonded system when exposed to chemical environments of different properties. The purpose of this study was to determine the effectiveness of various silane surface preparations on the durability of the epoxy/Si system in conditions mimicking use conditions of the microelectronic devices. The experimental parameters included in this study are:

Substrate:	HP TOX wafer
Surface preparation:	as received (no SCA), SCA-1, SCA-2
Adhesive:	model epoxy (see composition/curing in Section 2.5.4)
Curing Conditions:	130 ^{o}C for 1 hr
Environment:	Solution-5 (pH 4.30), Solution-6 (pH 8.50)
Temperature:	room temp (25 ^{o}C), 40 ^{o}C, 60 ^{o}C, 70 ^{o}C

A full test matrix consisting of the entire parameter group yielded 24 sample conditions. Three DCB specimens were prepared for wedge testing for each sample condition. In this chapter, the measurements of subcritical crack growth velocity for a wedge specimen are presented. Measurements of crack length were conducted *ex situ* (preconditioned specimen). Figure 4-34 shows a schematic of a typical stress corrosion cracking curve[20]. Between $G_{threshold}$ and $G_{critical}$ values, three distinct regions occur. Region III is independent of environmental factors and is dominated by critical fracture events[20,21]. Therefore, the measurements in this region do not provide the subtle effects of chemical reactions occurring at the crack tip. Data in this region were not collected in this study. In region II, the crack velocity strongly depends on the environment and is fairly insensitive to G. A plateau velocity is often observed. In this region, the rate controlling process is believed to be the transport of the environmental agent(s) to the crack tip[22]. There is often, but not always, a threshold value of strain energy release rate (or crack driving energy) $G_{threshold}$, below which a crack does not grow. In this region the crack velocity is

controlled by the stress-activated chemical reaction of the environmental agent with the bond components at the crack tip[23].

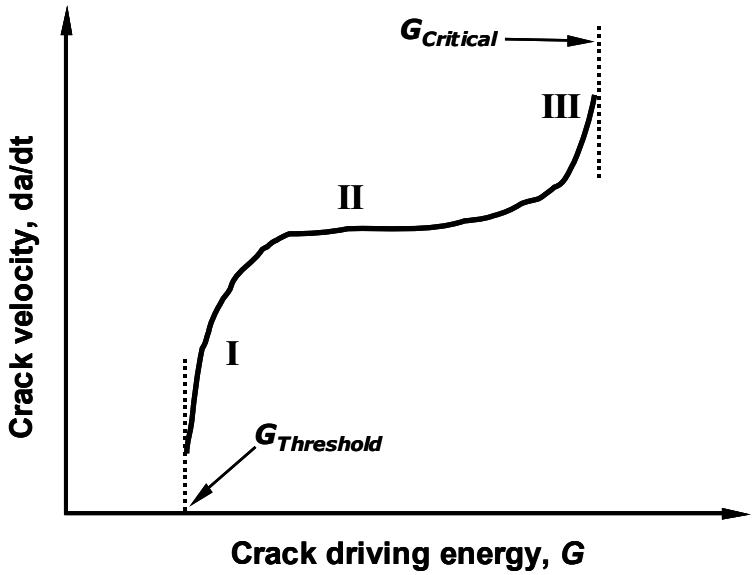

Figure 4-34. Schematic of a typical stress corrosion cracking curve. Regions I, II, and III represent different debond behavior[20].

Crack velocity (V = `*da/dt*) and strain energy release rate (*G*) were calculated and plotted as shown in Figures 4-35 to Figure 4-38. In Figure 4-35a, the crack velocity for samples immersed in both solutions exhibited a strong dependence on testing temperature for substrate surfaces with no silane treatment. At lower temperatures (25 and 40 ^{o}C), the system exhibited a $G_{threshold}$ value, which is estimated when the crack growth has ceased (this is based on the capability of measuring the crack growth). At higher temperatures (60 and 70 ^{o}C), crack growth is very rapid, and no $G_{threshold}$ value can be obtained. Debonding at higher temperatures is diffusion controlled, in which case crack velocity is based on how fast the solvent/or water molecules diffuse into the interfacial area ahead of the crack front. Figure 4-35b shows the debond data for silane-treated surfaces (SCA-1 and SCA-2). In this case, only at 70 ^{o}C is the system under diffusion controlled

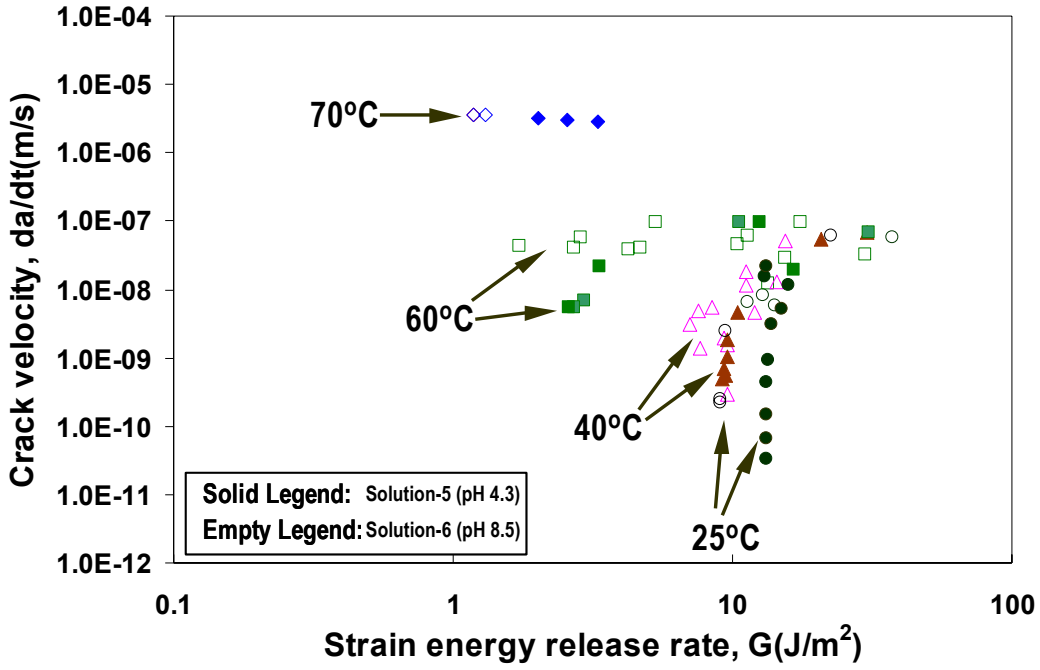

(a)

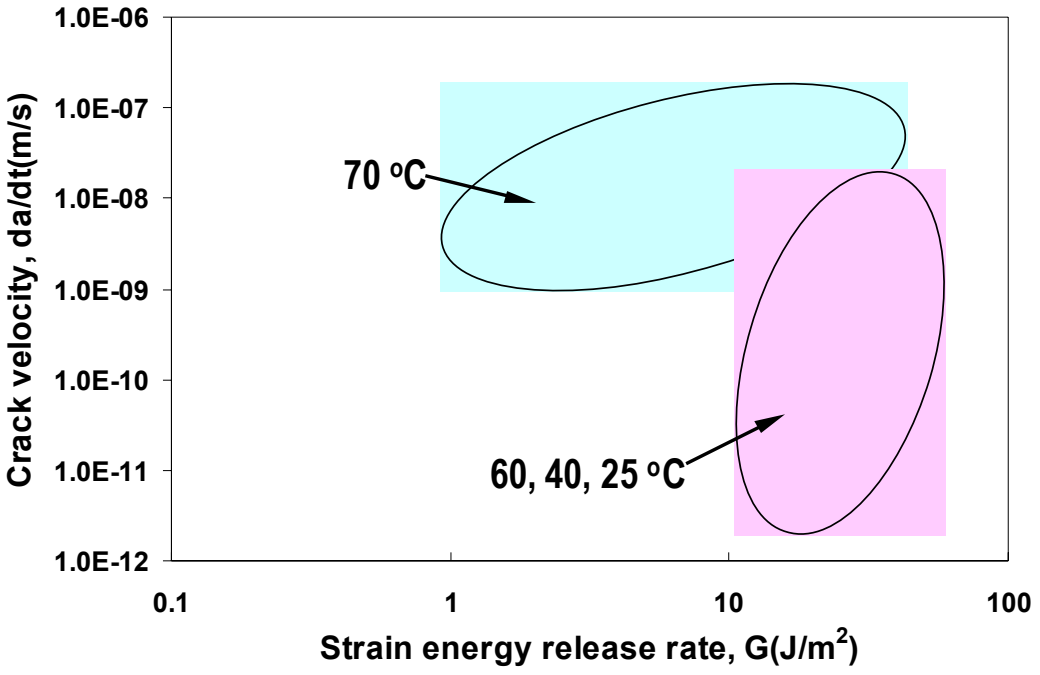

(b)

Figure 4-35. Crack velocity versus strain energy release rate at different temperatures in Solution-5, pH 4.3 and Solution-6, pH 8.5; (a) Si surface without silane, and (b) Si surface with SCA-1 and SCA-2.

debonding, whereas at 60, 40 and 25 ^{o}C, $G_{threshold}$ values can be obtained. The sudden deviation of the debonding trend at 70 ^{o}C, suggests that the debond mechanisms (or bond failure mechanisms) are different at each condition. Comparing data shown in Figure 4-35a to 4-35b, the crack velocity is higher for a substrate surface with no SCA treatment, and this trend is more significant at 70 ^{o}C, indicating overall poor bond durability. Also, for the temperature at which the $G_{threshold}$ was obtained, the $G_{threshold}$ value for a SCA treated surface is between 10-50 J/m^2, whereas the $G_{threshold}$ value for a non silane-treated surface is near 10 J/m^2.

Figures 4-36a and 4-36b compare the effect of solutions with different pH on durability for different surface preparations at 25 and 40 ^{o}C. In all cases, specimens tested in Solution-5, pH 4.3 yielded higher $G_{threshold}$ values than that those tested in Solution-6, pH 8.5. The findings suggest that Solution-5 is a less aggressive environment (yielding higher $G_{threshold}$ values). The $G_{threshold}$ values at room temperature show that the bond strength related to surface preparation varies in the order: SCA-2 > SCA-1 > no silane. Similar data are plotted in Figure 4-37 for specimens tested at 60 and 70 ^{o}C.

For systems tested at 60 ^{o}C, a different debonding behavior was observed. The trend for the effectiveness of various surface preparations is equivalent to that found at RT and 40 ^{o}C . For SCA-1 and SCA-2 modified surfaces, the $G_{threshold}$ values were still obtained, with the SCA-2 surface yielding a higher value. However, for no silane treated surface, no $G_{threshold}$ was obtained and its crack velocity is higher than for the silane modified surfaces. Immersion in different pH solutions yielded nearly identical results in $G_{threshold}$ values and in the crack velocity (Figure 4-37a).

For systems tested at 70 ^{o}C, the difference between Solution-5 and Solution-6 is nearly non-existent, as all systems show diffusion controlled debonding. The samples with no-silane treated surface showed high crack velocity (with only several data points collected prior to failure of the DCB specimen). The specimens with SCA-1-and SCA-

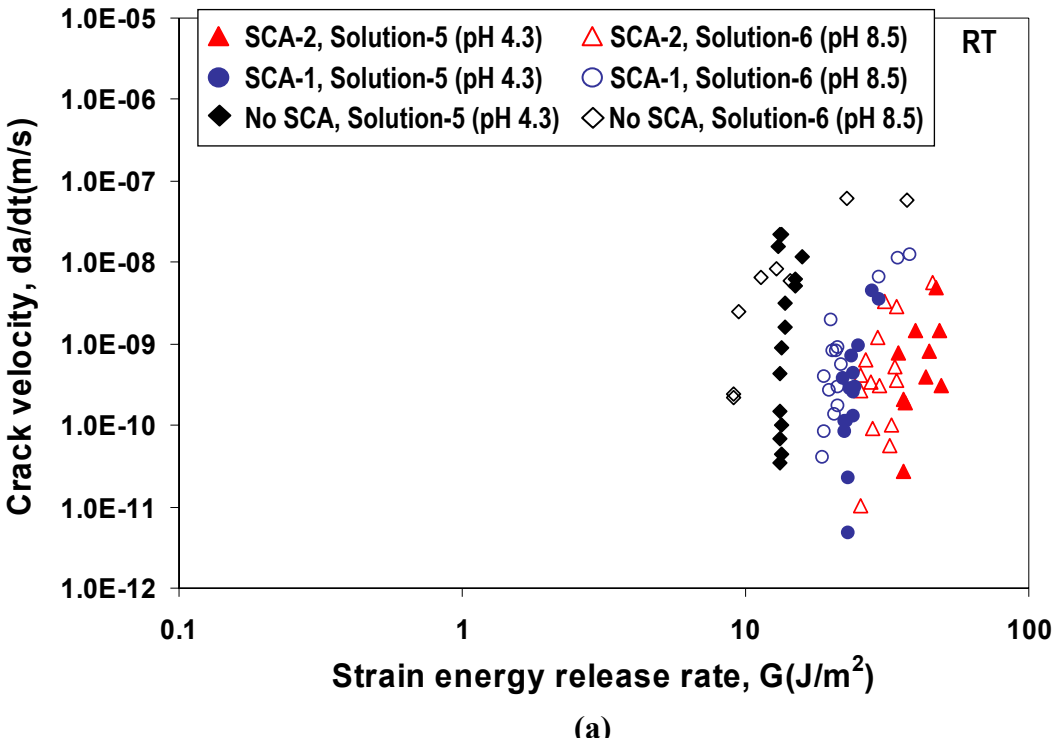

(a)

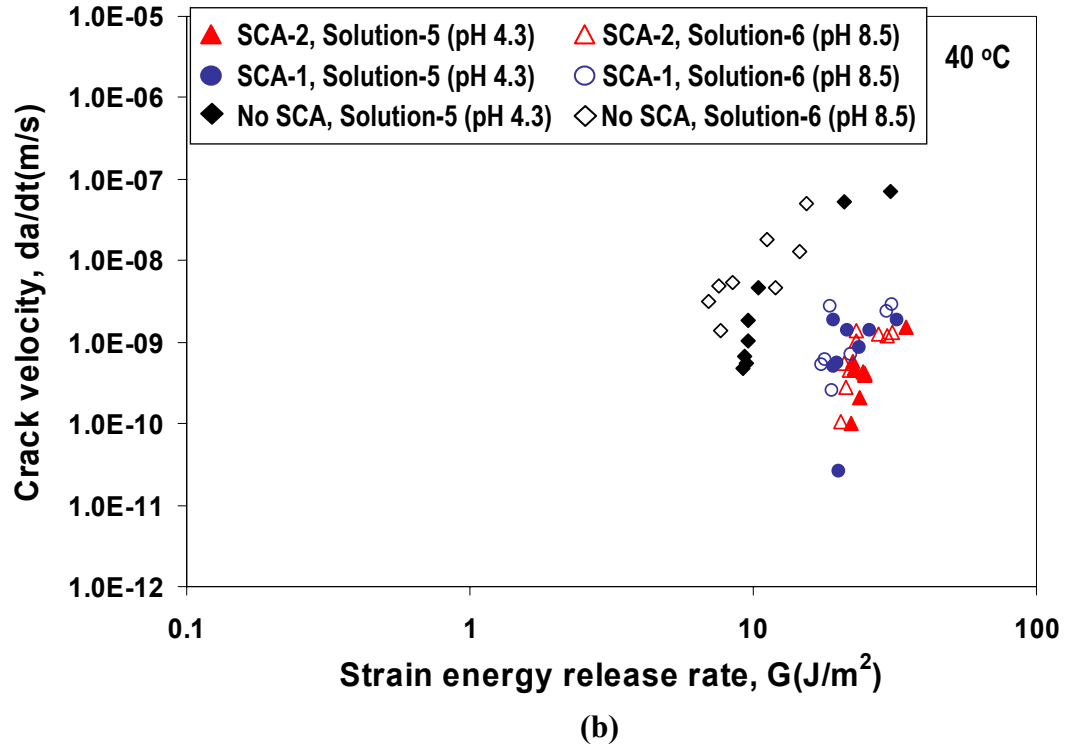

(b)

Figure 4-36. Crack velocity vs. strain energy release rate for Si with different silane treatments in Solution-5, pH 4.3 and Solution-6, pH 8.5; (a) at RT, and (b) at 40 ^{o}C.

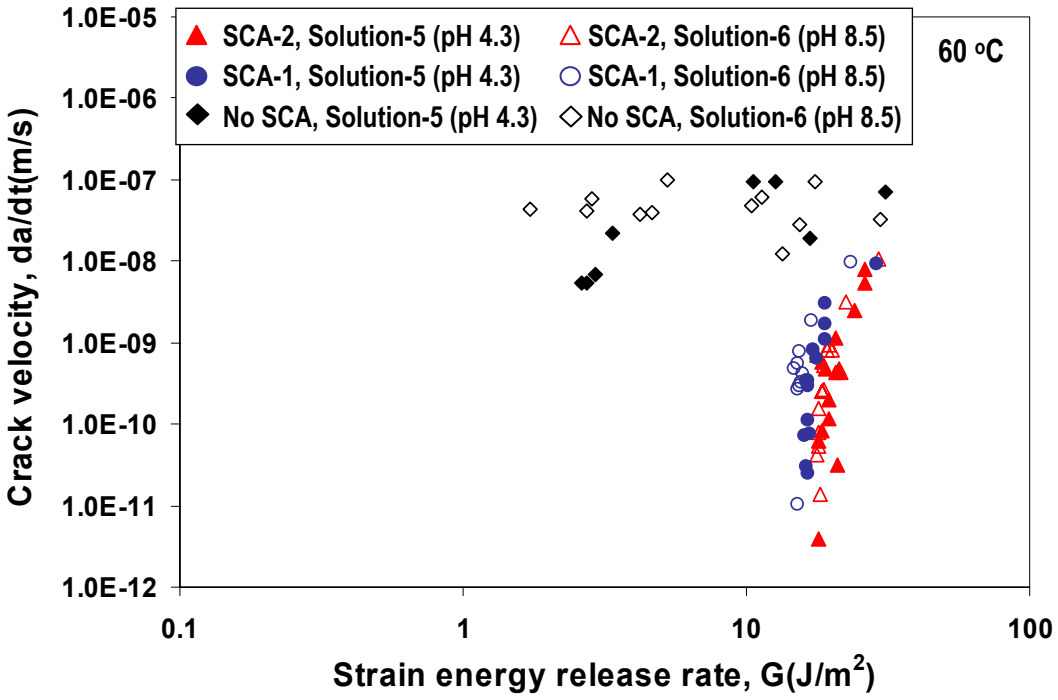

(a)

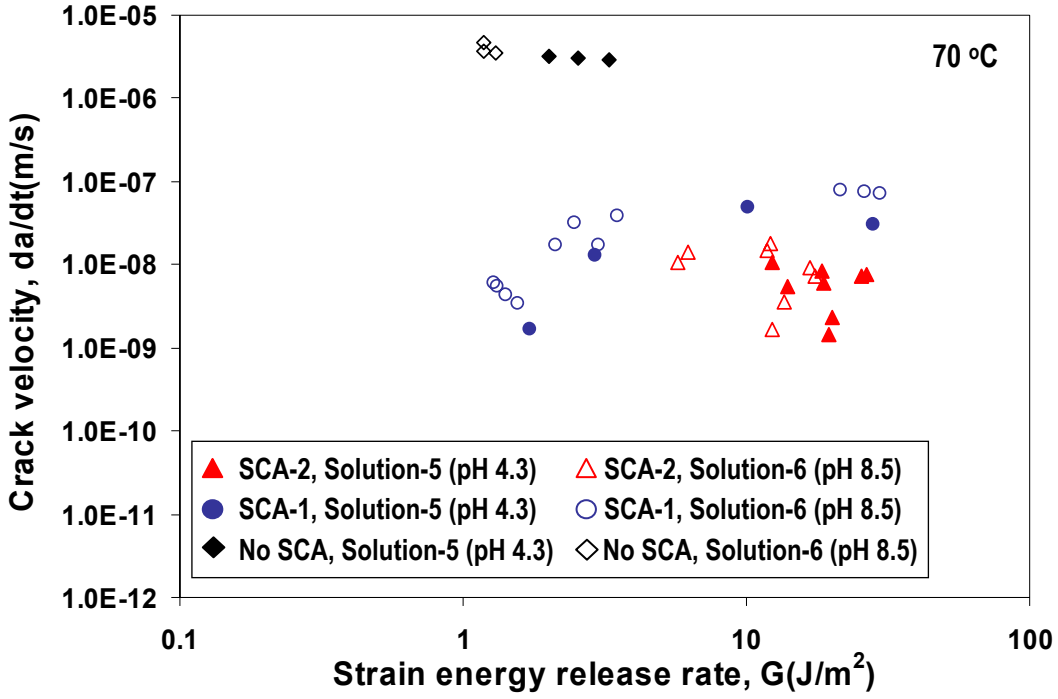

(b)

Figure 4-37. Crack velocity vs. strain energy release rate for Si with different silane treatments in Solution-5, pH 4.3, and Solution-6, pH 8.5; (a) at 60 °C, and (b) at 70 °C.

modified surfaces eventually fail but at a crack velocity of nearly two orders of magnitude lower than that for the no silane-treated sample. The difference in bond durability for SCA-2-and SCA-1-modified surfaces is evident at 70 ^{o}C but not at 60 ^{o}C, as the SCA-2 data were located at higher G values (see Figure 4-37b).

Figure 4-38 summarizes the findings presented in Figures 4-35 to 4-38 in terms of changes in V-G curve profiles as a function of environmental conditions. The diamond symbols represent specimens that undergo diffusion controlled debonding. The square symbols represent specimens that undergo diffusion controlled debonding showing a tendency towards a $G_{threshold}$ (however, $G_{threshold}$ was not established prior to failure of the DCB specimen). The triangle and circular symbols represent specimens undergoing little to no diffusion controlled debonding with established $G_{threshold}$ values. The arrows indicate the shift of the V-G curves as influenced by the changes in temperature, environmental aggressiveness, and bond interfacial strength (i.e., surface preparation).

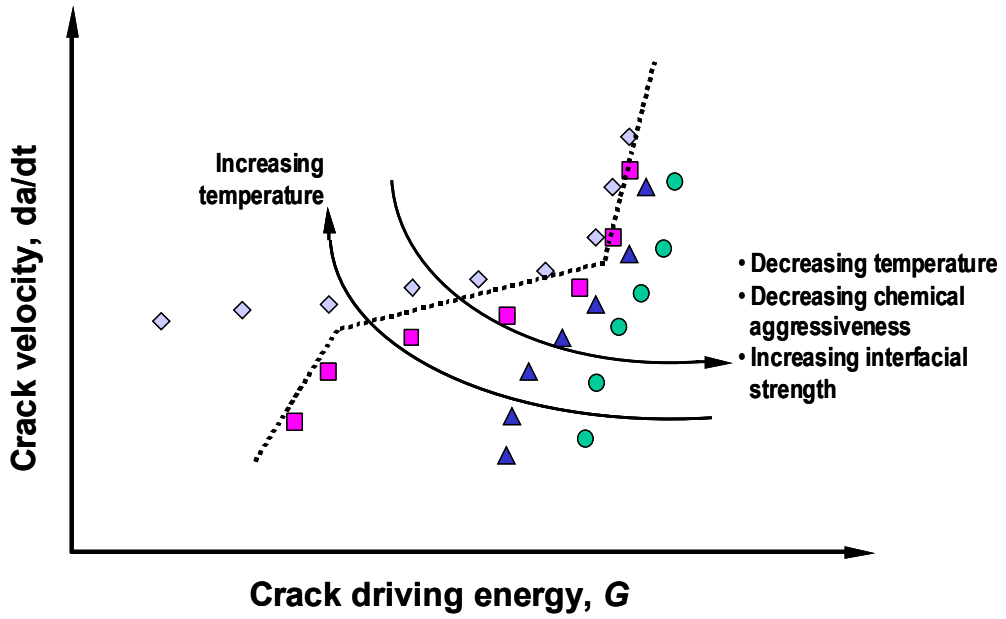

Figure 4-38. A schematic model of trends in changes of V-G curve profiles as a function of environmental conditions[20-22].

4.6 Conclusions

The durability and adhesion of the model epoxy/SCA/Si bonded systems were studied using the immersion test, the probe test, and the wedge DCB test in various thermal and chemical environments. The durability of the model epoxy/SCA/Si bonded system showed a general trend that depended on the silane coupling agent; durability varied in the manner SCA-2 > SCA-3 > SCA-1 > no silane. This result is likely related to the nucleophilic reactivity of the silane with the epoxy. Immersion and probe test results showed that bond durability is also a function of the pH of the aqueous environment, and better durability was observed in weakly acidic conditions, a fact that is associated with the rate of hydrolysis of either amide or siloxane bonds. On the other hand, the bond durability is also dependent on the pH of solutions, but with an opposite trend; better durability was noted at high pH. This latter finding suggests that other solution components (i.e., surfactant, solvents, salts, etc.), influence bond durability to a greater extent than solution pH, either singularly or synergistically. Bond durability increased for the model epoxy/SCA modified/O_2 plasma treated/Si bonded system as the oxygen plasma pre-treatment time increased. The increase in durability is attributed to the increase in SCA density on the Si surface as the duration of oxygen plasma pre-treatment was increased. Bond durability is a function of pH under long-term immersion at 60 ^{o}C (i.e., months). However, for bonded specimens exposed (i.e., minutes) for a short-time to various pH solutions (with the immediate presence of solution at a stress crack front at room temperature), no pH dependence was found. This pH dependence only existed when the silane interface was weak (i.e., less silane deposited). This finding suggests that time is needed for the environment to cause a significant degradation (i.e., bond disruption) in the epoxy/SCA/Si bonds. The in-situ probe test results showed no difference in debond profile for different water-solvent mixtures containing surfactant, diol-1, and diol-2 if the bonded specimens were not pre-soaked in the component mixtures. For pre-soaked specimens, the mixture composition containing the diol-2 component was more aggressive towards interfacial degradation. The addition of a surfactant had a limited 'add-on' effect rather than a synergetic effect. This finding

indicates that the interfacial strength has a direct effect on the adhesion response in the chemical environment. Immersion of the specimens at 70 ^{o}C yielded a different behavior than immersion in solutions at 60 ^{o}C, 40 ^{o}C and 25 ^{o}C in the V-G curve collected using the wedge DCB test in different solutions. Higher crack velocity and the absence of a $G_{threshold}$ value were noted in tests at 70 ^{o}C. The $G_{threshold}$ value increased as the strength of the interface increased and as the chemical aggressiveness of the environment decreased.

4.7 References

[1] C. Scott, K.-T. Wan, D. A. Dillard, and S. Khasawinah, *Proceedings of the 25th Annual Meeting of the Adhesion Society*, Orlando, FL, 2002, 139.

[2] D. Xu, K.-T. Wan, J. G. Dillard, C. V. Scott, and D. A. Dillard, *Proceedings of the 26th Annual Meeting of the Adhesion Society*, 2003, Myrtle Beach, SC, 420.

[3] D. Xu, J. G. Dillard, D. A. Dillard, and K.-T. Wan, *Proceedings of the 27th Annual Meeting of the Adhesion Society*, 2003, Wilmington, NC, 244.

[4] S. L. Case, Ph.D. Dissertation, Virginia Tech, 2003, Chap 5.

[5] C. H. Chiang and J. L. Koenig, in "*SPI, 35th Ann. Tech. Conf. Reinf. Plast.*", 1980, p. 23-D.

[6] S. P. Timoshenko and S. Woinowsky-Krieger, "*Theory of Plates and Shells*", 2nd ed., McGraw-Hill, New York, 1959, Chapter 3.

[7] E. Feresenbet, D. Raghavan, and G. A. Holmes, *J. Adhesion*, **79**, 2003, 643.

[8] A. Franquet, H. Terryn, and J. Vereecken, *Thin Solid Films*, **441**, 2003, 76.

[9] K. G. Sachdev, S. Cheng, H. R. Anderson Jr., and M. M. Khojasteh, *Proc. Elec. Comp. Conf.*, **36**, 1986, 345.

[10] N. G. Cave and A. J. Kinloch, *J. Adhesion*, **34**, 1991, 175.

[11] R. K. Iler, in "The Chemistry of Silica", Wiley: New York, 1979, Chap 2.

[12] J. Comyn, *J. Adhesion*, 1989, **29**, 121.

[13] V. Bellenger, J. Verdu, and E. Morel, *J. Mat. Sci.*, 1989, **24**, 63.

[14] J. Brettle, D. M. Brewis, J. Comyn, B. Cope, M. T. Goosey, and R. D. Hurditch, *Int. J. Adh. and Adh.*, 1983, **3**, 189.

[15] A. J. Kinloch, *J. Adhesion*, 1979, **10**, 193.

[16] J. Cognard, *J. Adhesion,* 1994, **47**, 83.

[17] J. E. Ritter, J. R. Fox, D. I. Hutko, and T. J. Lardner, *J. Mat. Sci.*, **33**, 4581, 1998.

[18] L. C. Uhlic-Tsang and J. R. Moffatt, EP 1391489, A1 20040225, 2004.

[19] M. W. Lane, J. M. Snodgrass, and R. H. Dauskardt, *Microelectonics Reliability*, **41**, 1615, 2001.

[20] S. W. Freiman, *J. Am. Cer. Soc.*, 1974, **57**, 350.

[21] S. M. Wiederhorn, S. W. Freiman, E. R. Fuller, and C. J. Simmons, *J. Mat. Sci.*, 1982, **17**, 3460.

[22] S. M. Wiederhorn, *J. Am. Cer. Soc.*, 1967, **50**, 407.

[23] R. H. Jones, and R. E. Ricker, "*Mechanisms of stress-cross cracking, Stress-Corrosion Cracking*", R. H. Jones, ASM International, Ohio, USA. 1992, Chap 3.

5. Effect of Thermal Cyclic Conditions on Bond Durability

5.1 Introduction

The principal goal of this aspect of the research was to determine the durability of the bond for two different chemically modified silicon surfaces and an epoxy adhesive upon immersion in aqueous solutions at various pH values under both static and cyclic temperature conditions. Static and cyclic environmental exposure may alter durability and/or failure mechanisms. The cyclic thermal testing environment was chosen for a 60-minute cycle between 25 ˚C and 70 ˚C. The upper temperature limit is selected because it is near the T_g of the epoxy polymer. For polymers, the coefficient of thermal expansion (CTE) can be an order of magnitude greater if the polymer is above its glass transition temperature[1]. It was also the purpose of this study to determine the effect of pH of the aqueous medium on the debonding rate for the epoxy/SCA/Si system, because the rate of hydrolysis of the Si-O-Si bond or the epoxy/silane linkage may be different at different pH values and temperatures. Both critical and sub-critical tests were used to determine the durability and adhesion energy.

5.2 Cyclic Thermal Conditions

Cyclic thermal testing of model epoxy coated Si substrates was carried out using a custom apparatus. The probe specimens were prepared according to procedures outlined in Scheme 2.1, and the wedge DCB specimens were prepared according to Scheme 2.4. Si surfaces were treated with SCA-1 and SCA-2.

5.3 Chemical Environments

The bonded specimens were immersed in pH 4 buffer solution and pH 9 buffer solution.

5.4 Probe Test Results

Probe tests were performed to determine the change in critical interfacial bond strength between the thin epoxy film and substrate after the thermal cycle and exposure to different pH environments. Thermal cycles result in tensile stresses that can initiate debonds or reduce the energy needed for debonding[2]. The probe test was employed to evaluate interfacial adhesion. Exposure of the interface to various chemical environments reduces interfacial adhesion and results in an increase in delamination dimensions. The debond dimensions were used to calculate the debonded area and then the strain energy release rate, G_c, using Equation 4-5[3,4].

It is likely that temperature cycling in the region of the metal/polymer interface (where micro circuits are embedded) affects the durability of the epoxy/Si bond in an aqueous solution. Temperature cycling may contribute to poor adhesion in this system in two ways; first, a rapid temperature change in the system could lead to expansion and contraction of the different materials across the interface. Because the epoxy polymer and the wafer substrate all have different coefficients of thermal expansion (CTE), expansion and contraction could lead to stresses at each bonding interface and could eventually contribute to debonding. Secondly, temperature changes in the system can affect the rate of chemical processes (i.e. hydrolysis of Si-O-M bonds or adhesive-coupling agent bonds) at the interface, which will influence bond durability. Additionally, swelling in the polymer can take place from the absorption of water or solvent resulting in polymer volume changes, which could lead to stresses at the bonding interface or changes in the polymer physical properties (modulus, etc.)

Figure 5-1a shows the G_c, critical strain energy release rate as a function of immersion time for silicon surfaces modified with SCA-1 and SCA-2 for immersion in two different pH buffer solutions under static thermal conditions. The SCA-2 modified-Si surface exhibits a greater critical interfacial strength than the SCA-1 modified-Si surface. The critical strain energy release rate decreases as a function of time, which indicates a

weakening of the bond interface. The effect of the pH of the medium is not distinguished due to the fact that most of the error bars overlap.

Comparing the durability results obtained under static thermal conditions with those obtained under cyclic thermal conditions (Figure 5-1b), no significant difference was found in bond durability. The SCA-2 modified-Si surface showed better critical interfacial strength than that for the SCA-1 modified-Si surface. Thermal cycling at between 25 ^{o}C and 70 ^{o}C with a 1.0 hour cycle did not show a significant effect on bond durability compared to that noted for static exposure at 70 ^{o}C. These results suggest that for this particular bonded system (i.e., epoxy/SCA/Si), the rate of debonding may be related to the time needed for water molecules to diffuse through the bulk coating to degrade the interface. Under cyclic thermal conditions, the exposure time for specimens at the elevated temperature is half of that for immersion under static thermal conditions.

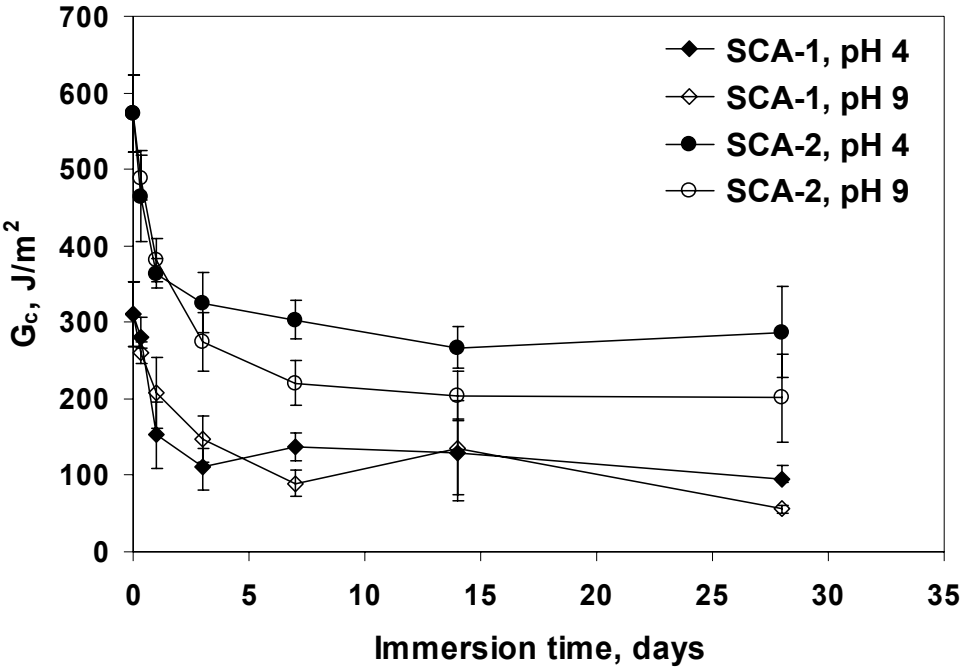

(a)

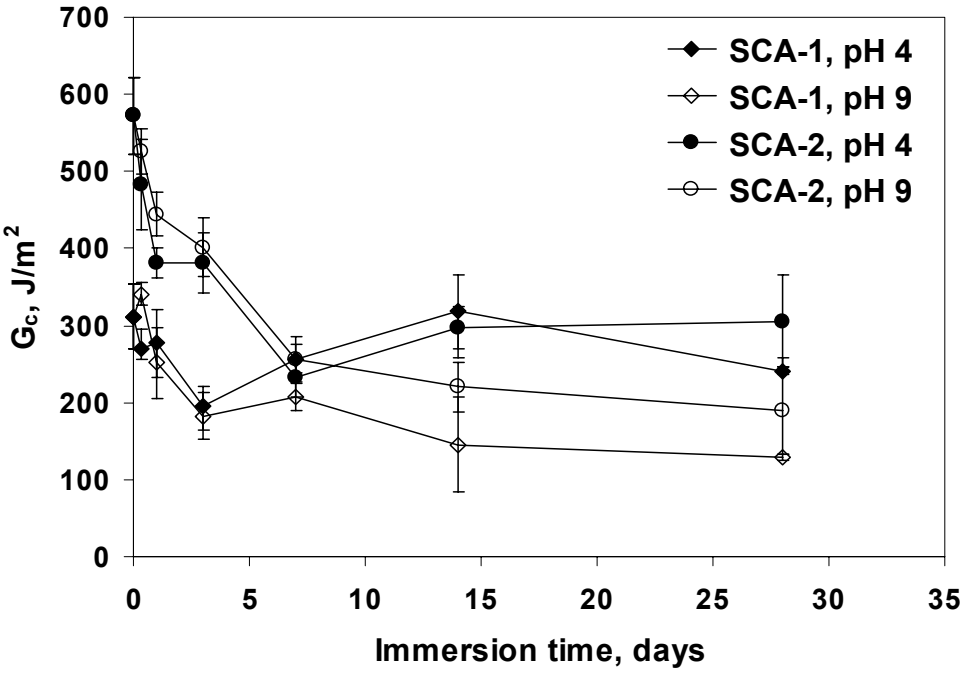

(b)

Figure 5-1. Strain energy release rate for the model epoxy/SCA/Si bonded specimen as a function of immersion time in pH 4 and pH 9 buffer solutions. (a) Under static 70 ^{o}C, and (b) under a 60-minute 25 ^{o}C-70 ^{o}C cycle.

5.5 Wedge (DCB) Test Results

Wedge testing of double cantilever beam type specimens was conducted to evaluate the durability of the model epoxy/SCA/Si bonded system when exposed to chemical environments at different pHs. The purpose of this study was to compare the effect of static and cyclic environmental exposure on durability and/or failure mechanisms.

Figures 5-2 and 5-3 show subcritical debonding curves for wedge specimens of model epoxy/SCA/Si samples under static and cyclic temperature conditions, respectively. For specimens tested at static 70 ^{o}C, the V-G (crack velocity versus strain energy release rate) curves for model epoxy/SCA-1/Si (Figure 5-2a) show diffusion controlled debonding (in the form of a crack velocity plateau) and $G_{threshold}$ values. No significant difference was observed in the crack velocity for the two pH conditions (plateau region). As the crack velocity slows, specimens tested in a pH 9 buffer solution exhibited a lower $G_{threshold}$ value (1.3 J/m^2) than the samples tested in a pH 4 buffer solution (2.2 J/m^2). This result is likely associated with the effect of the pH on the hydrolysis of Si-O-M bonds or the disruption of the epoxy-amine interaction across the epoxy-SCA-Si interface. Specimens with the SCA-2 modified Si surface yielded slightly higher $G_{threshold}$ value (1.9 J/m^2 for pH 9 buffer and 2.8 J/m^2 for pH 4 buffer) under the identical test conditions (Figure 5-2b).

For specimens tested under cyclic thermal conditions, the V-G curves (Figure 5-3) show lower debonding velocity compared to the results given in Figure 5-2. The absence of a crack velocity plateau suggests that the debond process is not diffusion driven, as was the case for static thermal testing. $G_{threshold}$ was not established after 4 months of testing. This result suggests that the stress imparted by the thermal cyclic loading does not contribute significantly to failure at the bonding interface; rather it is the thermal energy (i.e., temperature) and the environmental conditions (i.e., pH) that determine the subcritical debonding and the *G* threshold value. Specimens with the SCA-2 modified Si

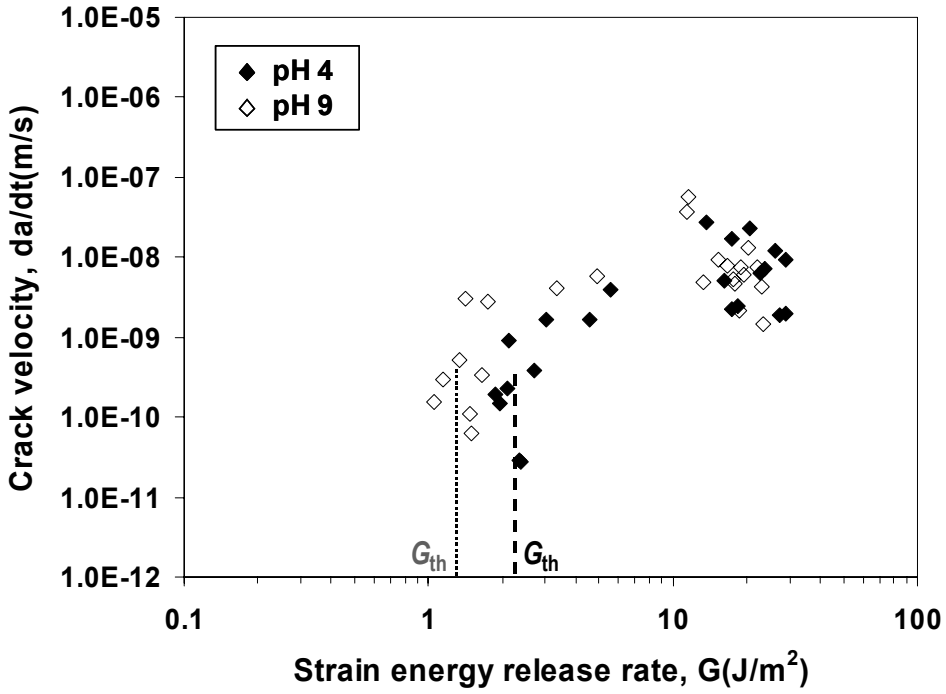

(a)

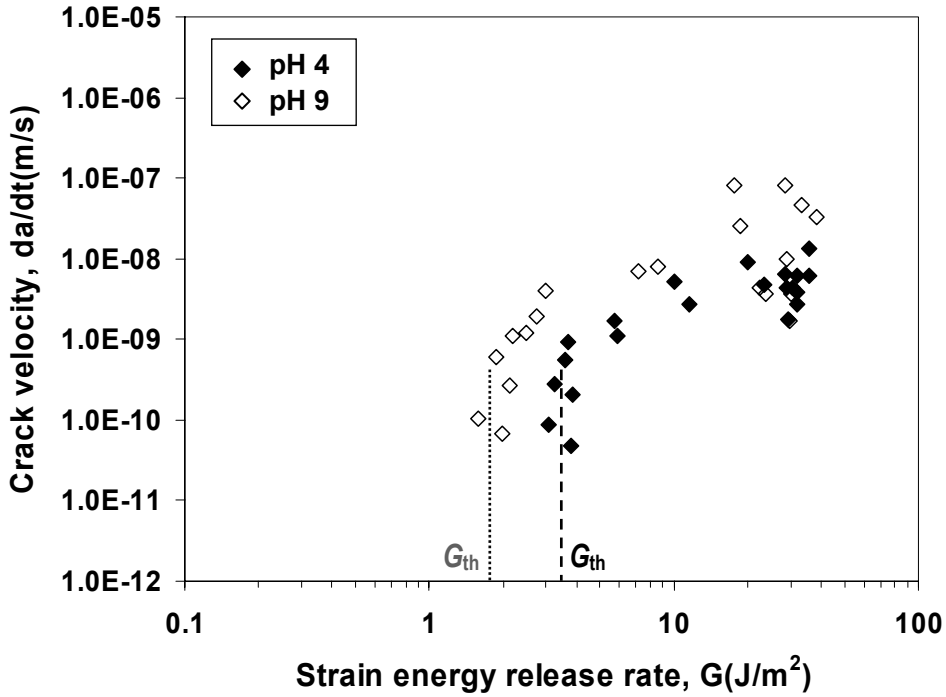

(b)

Figure 5-2. Crack velocity versus strain energy release rate for model epoxy/SCA/Si bonded specimens immersed in pH 4 and pH 9 buffer solutions at a static temperature of 70 ^{o}C. (a) SCA-1 and (b) SCA-2 modified Si surfaces.

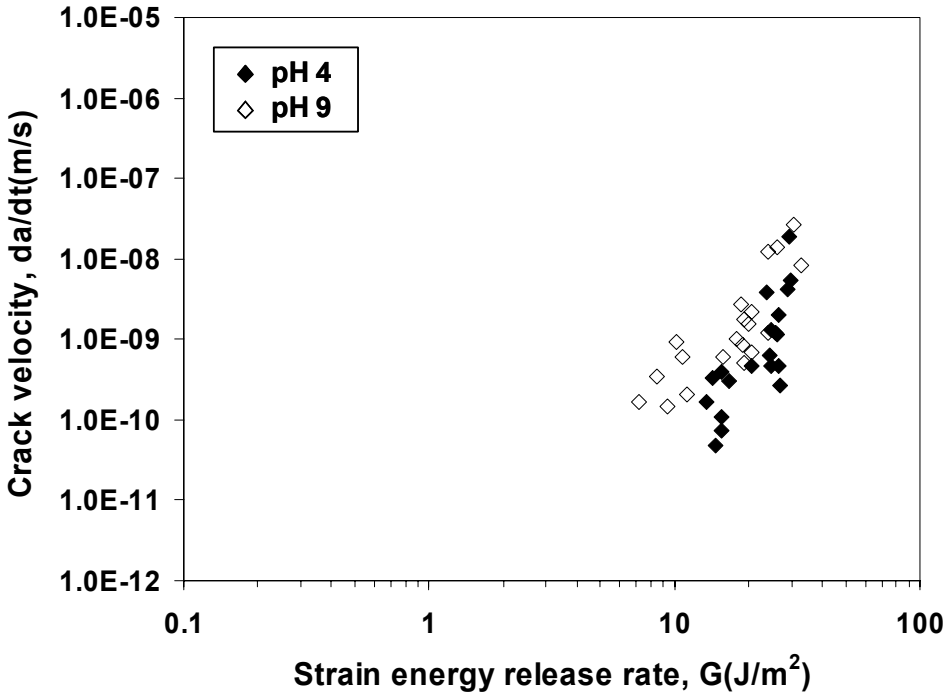

(a)

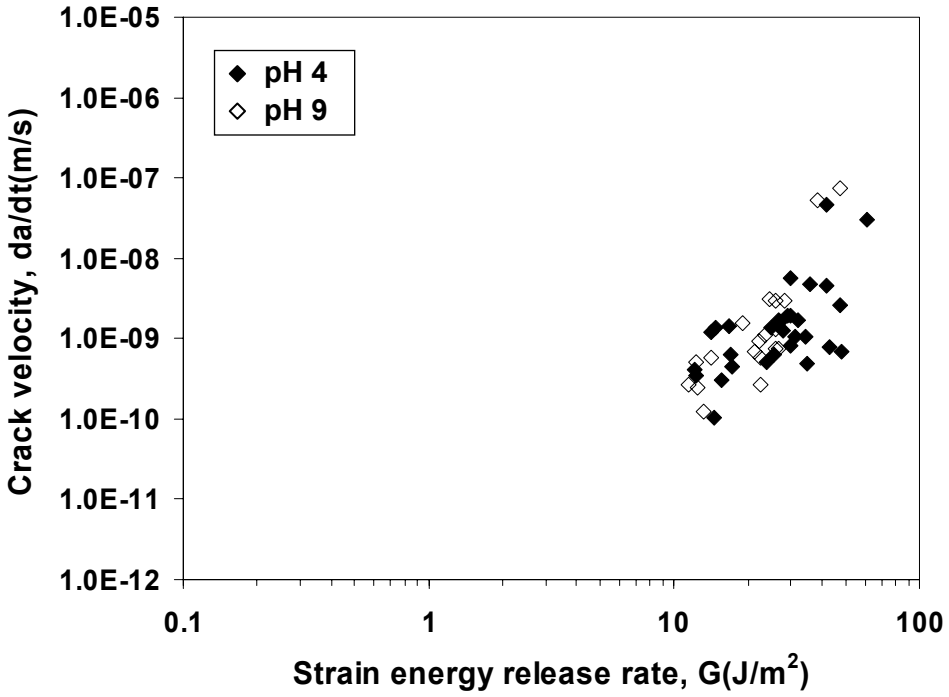

(b)

Figure 5-3. Crack velocity versus strain energy release rate for model epoxy/SCA/Si bonded specimens immersed in pH 4 and pH 9 buffer solutions under a 60-minute 25 ^{o}C-70 ^{o}C temperature cycle. (a) SCA-1 and (b) SCA-2 modified Si surfaces.

surfaces yielded $G_{threshold}$ values slightly higher than those for the SCA-1 modified surfaces.

5.6 Conclusions

The probe test results showed that the critical strain energy release rate for the model epoxy/SCA/Si bonded system was not significantly different at various immersion times when tested under static and cyclic thermal conditions. G_c was higher for a bonded SCA-2 modified silicon surface, which may be due to higher reactivity of the secondary amine functional group with the epoxy polymer. The influence of pH on the debond rate and on the critical G value of the system was not apparent, largely due to scatter in the data.

The subcritical debonding results collected using the double cantilever beam specimen with the same bond system showed diffusion controlled debond behavior and a G threshold when tested under static 70 ^{o}C conditions. Only limited crack growth occurred for samples tested under 25-70 ^{o}C thermal cycling. This difference suggests that thermal energy is an important factor that influences the rate of diffusion of water into the region at the crack tip. Contrary to critical debonding results collected with the probe test, the higher pH yielded lower $G_{threshold}$ values for the wedge specimens under static thermal conditions in the subcritical case.

5.7 References

[1] J. Kuczynski and A. K. Sinha. *IBM J. Res. Dev*., **45**, 783, 2001.

[2] D. A. Dillard, S. Guo, B. Chen, and J. H. Yu, *Mechanics of Time-Dependent Materials*, **7**, 21, 2003.

[3] D. Xu, K. T. Wan, J. G. Dillard, C. V. Scott, and D. A. Dillard, Proceedings of the 26th Annual Meeting of the Adhesion Society, Feb 23-26, 2003, Myrtle Beach, SC.

[4] D. A. Dillard, C. Scott, K. Mount, D. Xu, K. T. Wan, R. West, and J. G. Dillard, Proceedings of ASME International Mechanical Engineering Congress: Washington, DC, 15-21 Nov. 2003.

6. Bond Failure Mode Determination by XPS

6.1 Introduction

Surfaces of failed bonded specimens from the immersion test, the probe test, and the wedge DCB test were characterized *via* XPS to determine the failure mode. It is the intent of this chapter to correlate the results of XPS analysis with the bond durability data. Precise determination of the failure locus across the model epoxy/SCA/Si interface would also assist in engineering stronger interfaces. The first section of this chapter discusses the failure mode for bonded specimens immersed in different pH solutions when no external stress was applied. Bond failure in this case could occur due to the interfacial chemical bond disruption caused by fluids diffusing through the bulk epoxy coating. The bond failure mode for environment-assisted failure was compared to that when samples were not exposed to a degrading environment. In the second part of this chapter, the bond failure mode under external assisted stress (probe test and DCB test) will be discussed. Finally, the bond failure mode for the wedge DCB specimens will be presented, where a different bond geometry (i.e., substrate/epoxy/substrate) could produce a different failure mode as the crack front is exposed to stress and a chemical environment. Scheme 6-1 illustrates all the systems investigated for bond failure. The extent of failure at the epoxy/SCA or SCA/Si interface depends on immersion time, immersion temperature, stresses, and bond geometry. Only one side of the adherend for the DCB specimen was drawn in Scheme 6-1. The possibility of failure within the silane layer was not illustrated in Scheme 6-1.

6.2 Bond Failure under Stress-Free Conditions

The bond failure mode was determined by comparing the surface compositions and spectral features for the as failed epoxy- and Si-side surfaces with spectral features for the as-prepared epoxy and Si surfaces prior to bonding. XPS spectral features indicate the presence or absence of specific elements and chemical functionalities on the failed surfaces.

Scheme 6-1

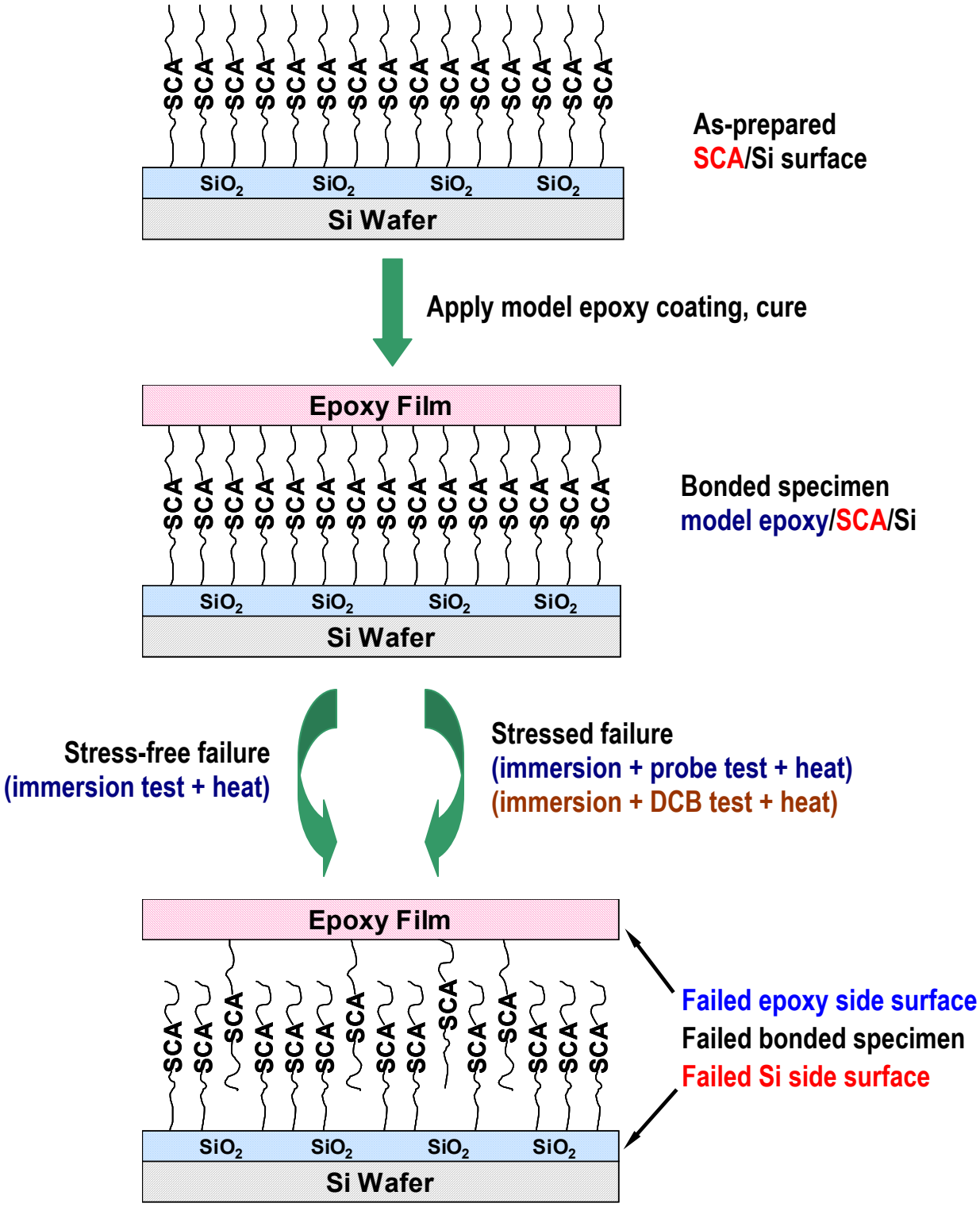
SCA
SiO2
Si Wafer
As-prepared
SCA/Si surface
Apply model epoxy coating, cure
Epoxy Film
Bonded specimen
model epoxy/SCA/Si
Stress-free failure
(immersion test + heat)
Stressed failure
(immersion + probe test + heat)
(immersion + DCB test + heat)
Failed epoxy side surface
Failed bonded specimen
Failed Si side surface

The atomic % results in Table 6-1 show that the compositions for the as-prepared model epoxy surface and the as-prepared SCA-1 treated Si surfaces with different oxygen plasma pre-treatments were vastly different. Nitrogen was absent on the as-prepared model epoxy surface even though nitrogen (at low concentration) was present in the 4-methyl-2-phenylimidazole curing agent. Nitrogen is likely buried in the bulk epoxy matrix at chain ends. The three SCA-1 modified, oxygen plasma pre-treated Si surfaces showed a significant amount of nitrogen. For the as-prepared model epoxy surface, silicon was not detected. For the as-prepared SCA-1 surface, the Si 2p spectrum (see Figure 6-1) showed the SiO_x feature (SiO_2 + silane) at ~103.1 eV and Si^o (elemental silicon) at ~98.7 eV. A detailed comparison of these three as-prepared surfaces was presented in Section 3.2. The C 1s spectra for the as-prepared model epoxy surface showed a significant C-O photopeak at ~286.5 eV, which can be attributed to the epoxy functionality. By comparison, the C-O contribution from the SCA-1 modification on the Si surface is less significant (see Figure 6-1).

6.2.1 Model Epoxy/SCA-1/O_2 plasma/Si specimen: Failure under pH 4 buffered conditions

XPS analysis of the failed model epoxy/SCA-1/Si bonds was carried out after the model epoxy film had completely debonded from the Si substrates which had been immersed in different pH buffered solutions at 60 ^oC. For specimens that failed in pH 4 buffered solutions, the failed Si surface composition (see Table 6-1) was generally similar to that for the as-prepared SCA-1/Si surfaces. A slightly lower percentage of nitrogen was observed; indicating that the amount of silane on the Si surface was less than that on the as-prepared surface. The C 1s spectrum for the failed SCA-1 surface (Figure 6-2) showed a slight broadening in peak width compared to that for the as-prepared SCA-1 Si surface (Figure 6-1), suggesting that additional C-O functionality was present on the failed Si side surface. The C-O functionality can be attributed to a small amount of the epoxy. For specimens that failed in pH 4 buffered solutions, on the failed epoxy side surface, the respective atomic percentages of C and O were similar to those

for the as-prepared model epoxy surface. However, low amounts of Si and N were detected for all three failed epoxy sides for model epoxy/SCA-1/O_2 plasma/Si specimens (Table 6-1), as evidenced by the weak Si 2p and N 1s spectral signals (Figure 6-2). Silicon and nitrogen were not detected on the as-prepared epoxy surface, so the Si and N signals must originate from SCA on the failed Si substrate. Thus, for model epoxy/SCA-1/O_2 plasma/Si bonded samples immersed in pH 4 buffer solutions at 60 ^oC, failure occurred primarily at the epoxy/silane interface with some minor failure in the SCA/Si substrate region (Figure 6-3a).

Table 6-1. Elemental surface compositions (atomic %) for as-prepared and failed bonded surfaces after the immersion test at 60 ^oC in pH 4 and pH 9 buffer solutions.

Type of Surfaces	Surface/Sample/pH	C	O	Si	N
As-prepared surfaces **(prior to bonding)**	Model epoxy, as prepared	81.6	18.4	<0.1	<0.1
	Si, 0min O_2 plasma, SCA-1	33.2	31.2	32.1	3.5
	Si, 2min O_2 plasma, SCA-1	28.2	39.3	29.4	2.6
	Si, 30min O_2 plasma, SCA-1	26.9	43.3	26.8	2.9
Failed surfaces **(after debonding)**	Failed Si side, Si/0min O_2/SCA-1, pH4	35.4	37.1	24.5	3.0
	Failed epoxy side, Si/0min O_2/SCA-1, pH4	80.0	19.5	0.2	0.3
	Failed Si side, Si/2min O_2/SCA-1, pH4	32.2	39.8	25.7	2.3
	Failed epoxy side, Si/2min O_2/SCA-1, pH4	79.8	19.8	0.2	0.2
	Failed Si side, Si/30min O_2/SCA-1, pH4	33.5	42.6	21.3	2.6
	Failed epoxy side, Si/30min O_2/SCA-1, pH4	78.9	20.3	0.4	0.4
	Failed Si side, Si/0min O_2/SCA-1, pH9	25.5	47.4	25.6	1.5
	Failed epoxy side, Si/0min O_2/SCA-1, pH9	76.4	22.3	0.8	0.6
	Failed Si side, Si/2min O_2/SCA-1, pH9	23.8	48.3	26.6	1.4
	Failed epoxy side, Si/2min O_2/SCA-1, pH9	77.0	21.2	1.0	0.8
	Failed Si side, Si/30min O_2/SCA-1, pH9	24.6	47.2	26.6	1.6
	Failed epoxy side, Si/30min O_2/SCA-1, pH9	76.9	20.7	1.5	0.9

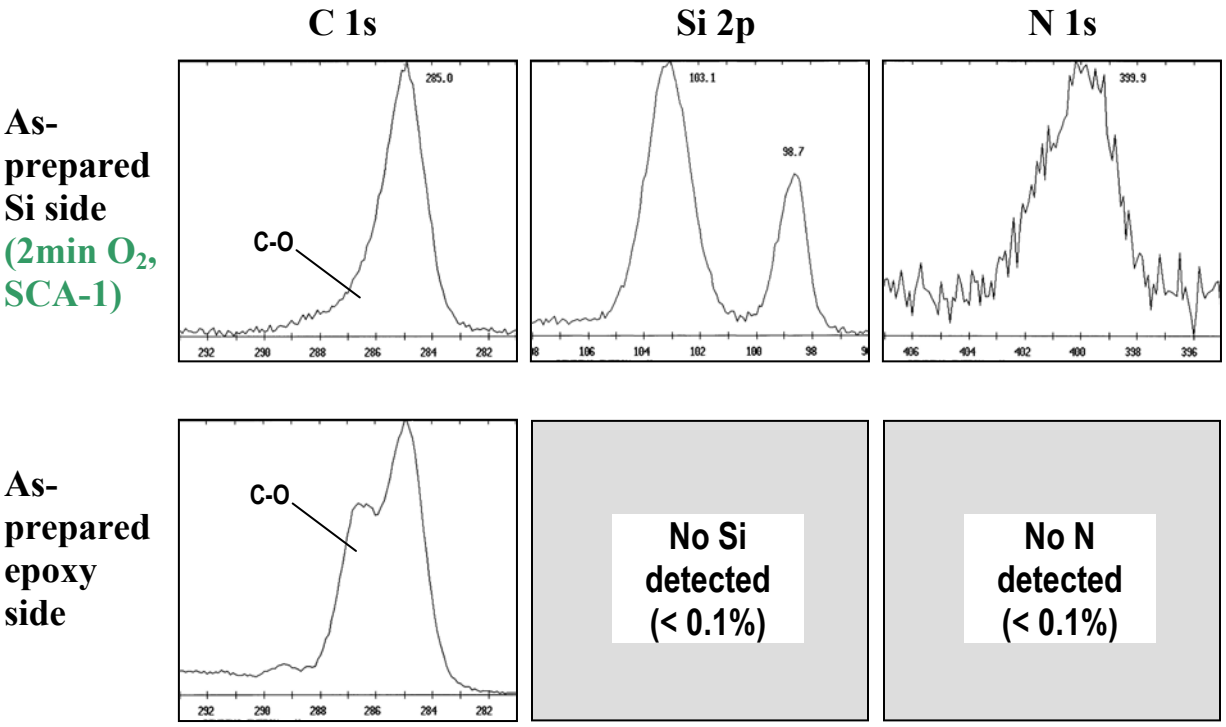

Figure 6-1. C 1s, Si 2p, and N 1s XPS spectral regions for SCA-1/Si surfaces and as-prepared model epoxy.

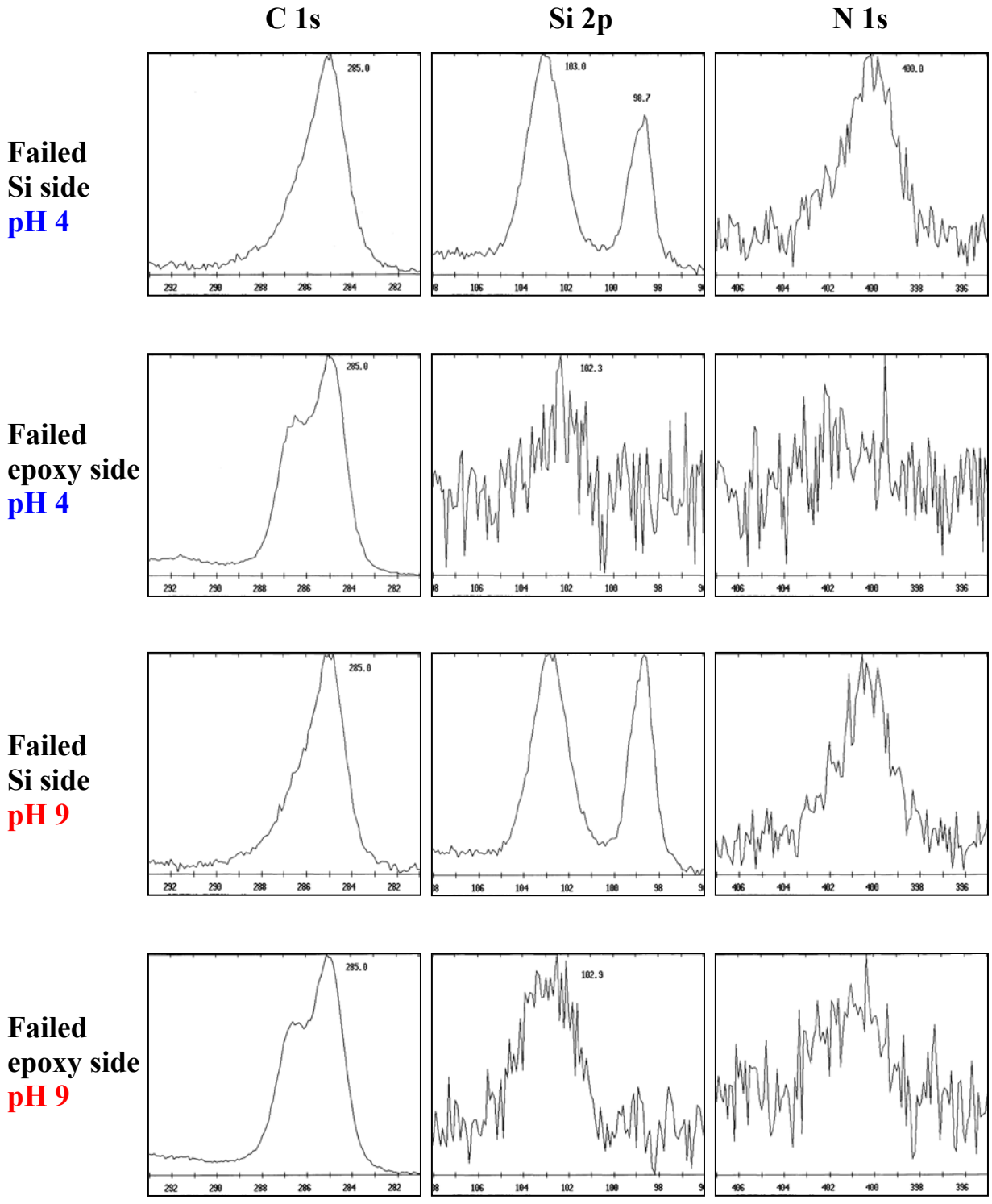

Figure 6-2. C 1s, Si 2p, and N 1s XPS spectral regions for failed model epoxy/SCA-1/O_2 plasma treated/Si bonded surfaces. Bonded specimens were immersed in pH buffer solutions at 60 ^{o}C.

6.2.2 Model Epoxy/SCA-1/O_2 plasma/Si specimen: Failure under pH 9 buffered conditions

For specimens that failed while immersed in a pH 9 buffered solution, a lower percent of N (~1.5%) was detected on the failed Si surfaces (Table 6-1) compared to that on the as-prepared SCA-1/Si surfaces (~3.5%). The reduction in the percent N was much greater than that for samples tested in the pH 4 buffer. The percent C on all three failed Si surfaces (Table 6-1) was generally lower than that on the as-prepared Si surface. The silicon and oxygen contents are higher and the carbon percents are lower on the failed silicon surfaces in pH 9 buffer compared to the findings for studies in pH 4 buffer. These observations suggest that failure occurred to a greater extent at the SCA-1/Si substrate interface for samples exposed to pH 9 buffered solutions compared to results for pH 4 buffered solution tests (see Figure 6-3). On the failed epoxy side surface for specimens that failed in pH 9 buffers, low amounts of Si and N were detected (Table 6-1). The increase in the percent N was consistently higher (0.3%-0.6%) than that for samples tested in pH 4 buffer conditions (see Figure 6-2). These findings suggest that more silane was present on the epoxy side failure surface (i.e., a greater extent of failure occurred at the SCA-1/Si substrate interface) for samples failing in the pH 9 buffer. It was also noted that the failure mode for bonded specimens with the as received, 2min O_2 plasma treated and 30min O_2 plasma treated surfaces were essentially equivalent, even though the durability for the 30min O_2 plasma treated sample was the greatest.

Thus, for model epoxy/SCA-1/O_2 plasma/Si bonded samples immersed in pH 9 buffer solutions at 60 ^oC, failure occurred both at the epoxy/silane interface and in the silane/Si substrate region (Figure 6-3b). The extent of failure occurring at the SCA-1/Si substrate is greater for the specimens immersed in pH 9 buffer than for those tested in pH 4 buffer (see Figure 6-3). This result is consistent with the rate of hydrolysis of Si-O-Si bonds between the silane and the Si substrate under basic conditions[1].

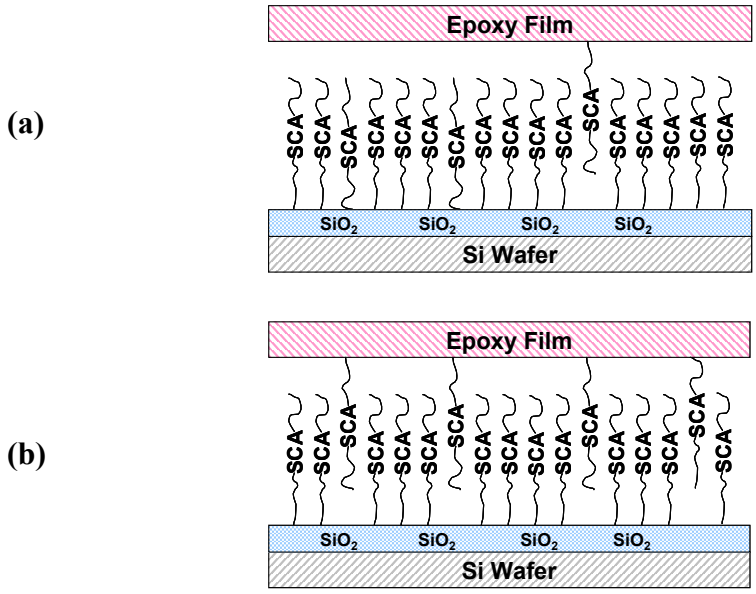

Figure 6-3. Proposed failure mode for model epoxy/SCA-1/O_2 plasma treated/Si bonded samples: tested free of mechanical stress immersed in pH buffer solutions at 60 ^{o}C, (a) pH 4 and (b) pH 9. Note the greater failure at the silane/SiO_2 interface at pH 9. (Not drawn to scale).

6.2.3 Model Epoxy/Silane/as rec./Si specimen: Bond Failure at 60 ^{o}C versus 70 ^{o}C

The failure mode for the model epoxy/SCA/Si samples with as-received Si surfaces treated with SCA-1, SCA-2, and SCA-3 that were immersed in pH 4 and pH 9 buffer solutions at 60 ^{o}C and 70 ^{o}C was also determined. The failed epoxy and Si side surfaces were analyzed by XPS when the epoxy films were fully debonded from the Si substrates. The XPS results are summarized in Table 6-2. Only results for failure for pH 9 conditions are given. Samples immersed in pH 4 buffer solutions have not yet failed (after >450 days at 60 ^{o}C and >250 days at 70 ^{o}C).

Compared to the compositions for the as-prepared silane surfaces, the surface compositions of all three failed Si surfaces (three different silanes) at both temperatures showed a significant decrease in the percent carbon and nitrogen, while the oxygen content increased. For example, the reduction in C is ~33% to ~26% at 60 ^{o}C, and is

~33% to ~22% at 70 °C upon comparing the as-prepared SCA-1/Si surface with the failed SCA-1/Si surface. The reduction in N is 3.5% to 1.5% at both 60 °C and 70 °C. The lowering of the C and N amounts (i.e., silane components) on the SCA-1/Si surface suggests that some failure occurred at the silane/Si interface. The presence of a Si 2p peak (at ~102.2 eV) and the N 1s peak (at ~400.0 eV), both resulting from silane components, also indicate that failure occurred at the SCA/Si interface. Thus, for model epoxy/SCA/as received/Si bonded samples immersed in pH 9 buffer solutions at 60 °C and 70 °C, failure occurred both at the epoxy/SCA interface and in the SCA/Si substrate region (Figure 6-4). The failure mechanism for the model epoxy/SCA-3/Si specimen is similar to that for the SCA-2-modified surface.

Table 6-2. Elemental surface compositions (atomic %) for as prepared and failed bonded surfaces after the immersion test for various silane modified Si surfaces at 60 °C and 70 °C in pH 9 buffer solution.

Type of Surfaces	Sample	C	O	Si	N
As-prepared surfaces **(prior to bonding)**	Model epoxy, as prepared	81.6	18.4	<0.1	<0.1
	Si, as received, SCA-1	33.2	31.2	32.1	3.5
	Si, as received, SCA-2	44.6	28.6	22.8	4.0
	Si, as received, SCA-3	42.8	27.3	24.1	5.8
Failed surfaces **(after debonding)**	**60 °C immersion**				
	Failed Si side, Si/SCA-1, pH9	25.5	47.4	25.6	1.5
	Failed epoxy side, Si/SCA-1, pH9	76.4	22.3	1.0	0.4
	Failed Si side, Si/SCA-2, pH9	30.8	43.7	23.5	1.9
	Failed epoxy side, Si/SCA-2, pH9	74.4	23.1	1.5	1.0
	Failed Si side, Si/SCA-3, pH9	26.6	48.2	27.6	1.6
	Failed epoxy side, Si/SCA-3, pH9	77.1	20.7	1.5	0.7
	70 °C immersion				
	Failed Si side, Si/SCA-1, pH9	21.9	52.2	24.3	1.5
	Failed epoxy side, Si/SCA-1, pH9	73.0	24.0	1.9	1.2
	Failed Si side, Si/SCA-2, pH9	23.8	50.8	24.0	1.5
	Failed epoxy side, Si/SCA-2, pH9	74.5	22.7	2.0	0.8
	Failed Si side, Si/SCA-3, pH9	22.5	52.5	22.9	2.2
	Failed epoxy side, Si/SCA-3, pH9	74.6	23.4	1.4	0.6

Based on the XPS results presented in Table 6-2, no significant difference in the failure mode was found for different silane-treated surfaces. The extent of failure at the SCA/Si interface is perhaps only slightly more at 70 ^{o}C than that at 60 ^{o}C. This finding indicates that the bond durability trends observed, SCA-3 ≈ SCA-2 > SCA-1, and 60 ^{o}C > 70 ^{o}C only depend on the rate at which the interfacial bonds, primarily at the epoxy/SCA interface, were compromised. The basic environment (high pH) was more detrimental to the epoxy/SCA/Si bonds, as the hydrolysis rate at high pH is faster[1].

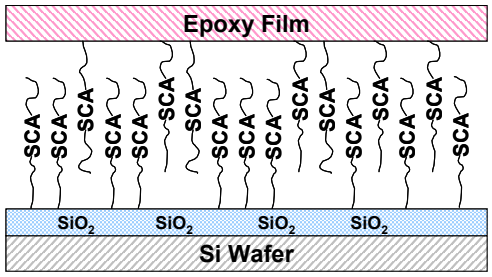

Figure 6-4. Proposed failure mode for model epoxy/SCA/as-received/Si bonded samples: tested free of mechanical stress immersed in pH 9 buffer solutions at either 60 ^{o}C or 70 ^{o}C. (Not drawn to scale).

6.3 Bond Failure Assisted by External Stress

Bonded model epoxy/SCA/Si specimens (probe tests), not exposed to a chemical environment, were failed by inserting a razor blade precisely at the epoxy/Si interface to cause debonding of the epoxy film. For bonded specimens (probe tests) that were exposed to a chemical environment and cyclic thermal conditions, a debond was initiated by probe insertion at the epoxy/Si interface at the coating edge. For bonded Si/model epoxy/Si DCB specimens that were exposed to a chemical environment and cyclic thermal conditions, a debond was initiated by insertion of a wedge at the specimen edge. XPS analysis was then performed on the debonded epoxy and Si surfaces.

6.3.1 No Exposure to Chemical Environment: Failure in Model Epoxy/Silane or No Silane/Various as-Received Si Surfaces Bonded Specimens (Film-on-Substrate)

The elemental surface compositions for the as-prepared Si surfaces and the mechanically failed model epoxy and Si side surfaces are shown in Table 6-3. For Si adherends, without silane modification, the compositions for failed model epoxy surfaces were essentially identical to those for the as-prepared model epoxy surface. The absence of Si or N on the failed epoxy surfaces indicated a clean interfacial failure at the epoxy/Si interface.

Table 6-3. Elemental surface compositions (atomic %) for as-prepared and failed bonded surfaces without exposure to solutions.

Sample	C	O	Si	N
As prepared surfaces				
Model epoxy, as prepared	81.6	18.4	<0.1	<0.1
Si, as received (no O_2 plasma)	10.0	44.2	45.8	<0.1
TOX Si, as received (no O_2 plasma)	3.3	65.2	31.5	<0.1
Si, as received (no O_2 plasma), SCA-1	33.2	31.2	32.1	3.5
Si, as received (no O_2 plasma), SCA-2	44.6	28.6	22.8	4.0
Si, as received (no O_2 plasma), SCA-3	42.8	27.3	24.1	5.8
Si, as received (no O_2 plasma), SCA-4	28.7	36.8	34.5	<0.1
Failed model epoxy surfaces				
Model epoxy/Si, as received (no O_2 plasma)	80.7	19.3	<0.1	<0.1
Model epoxy/TOX Si (no O_2 plasma)	81.3	18.7	<0.1	<0.1
Model epoxy/SCA-1/Si, as received (no O_2 plasma)	79.7	19.6	0.4	0.3
Model epoxy/SCA-2/Si, as received (no O_2 plasma)	77.7	20.6	0.9	0.8
Model epoxy/SCA-3/Si, as received (no O_2 plasma)	79.5	19.7	0.4	0.4
Model epoxy/SCA-4/ Si, as received (no O_2 plasma)	80.0	19.6	0.5	0.2

For Si surfaces with silane modification, low Si and N concentrations were detected on the failed epoxy surfaces that had been modified with both reactive and non-reactive silanes. The Si 2p binding energy was approximately 102.2 eV (Figure 6-5), which was attributed to Si existing in the Si-O-R or Si-O-Si form. These results confirm that the predominant failure location is at the epoxy/SCA interface, and that limited

failure occurred within the silane layer or possibly at the SCA/SiO_2 interface (see Figure 6-6). The origin of minor quantities of Si on the failed epoxy surface could occur in two ways. One is that non-surface bonded excess silanes or silane oligomers could be separated from the silane film (thickness more than monolayer coverage). The silane may or may not involve a bond breaking process. Second, the surface bound silanes could debond by breaking the Si-O-Si bond at the SiO_2 surface. The second scenario is less likely because each silane molecule could be anchored to the Si surface with up to three Si-O-Si bonds. The failure mode for a SCA-4 modified Si surface was also interfacial. Minimal Si and N percentages were also detected on the failed SCA-4/SiO_2 surface, which resulted from the detachment of loose silane chains. This result is the anticipated failure mode, as there are no functional groups in SCA-4 to react with the epoxy.

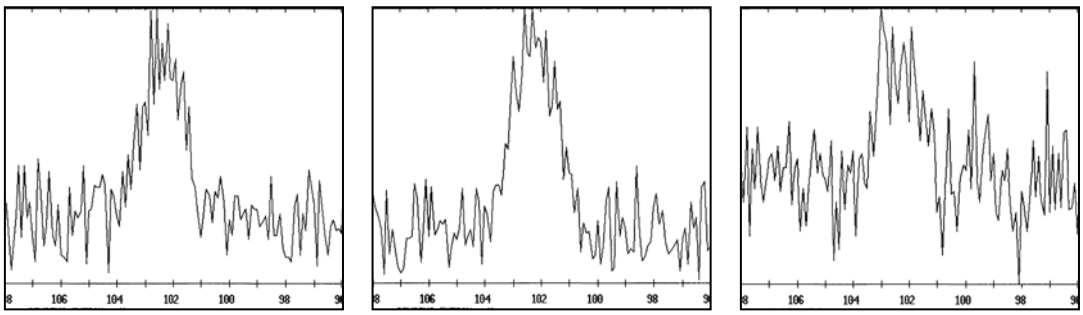

Figure 6-5. Si 2p XPS spectral regions for failed model epoxy/SCA/Si bonded surfaces. Bonded specimens were failed mechanically under as prepared conditions in air. (a) SCA-1, (b) SCA-2, and (c) SCA-4. All Si surface prepared with 0.1M silane solutions in acidified ethanol.

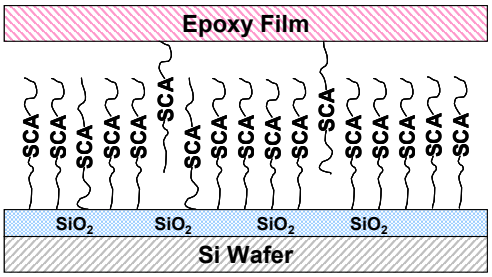

Figure 6-6. Proposed failure mode for model epoxy/SCA-1/Si bonded samples: tested specimens failed with mechanical stress in air at room temperature. (Not drawn to scale).

6.3.2 Exposure to Chemical Environments

6.3.2.1 Failed Probe Test Specimens

After sample immersion (1 month) at different pH conditions, debond areas on both failed surfaces from the probe tests (not in-situ) were analyzed by XPS to determine the failure mode. The specimens were exposed to a static (70 ^{o}C) and cyclic (between 25 ^{o}C and 70 ^{o}C, 1 hr cycle) temperature conditions. The debond caused in these specimens was assisted by both environmental exposure (i.e., pH) and stresses (i.e., applied stress and thermal stress). The thermal stress, originating from the expansion and contraction of the dimensions of the adherends and adhesive layer, may result in added stress on the interfacial bonds. The results of surface analysis are presented in Table 6-4. It was noted that no particular trend existed with respect to surface composition for failed surfaces as the thermal conditions and pH environments were varied. The failed epoxy side surfaces all showed low percentages of Si (BE = 102.2 eV) and N (BE = 400.0 eV) indicating the presence of silane components on the failed epoxy surfaces. However, no significant reduction in C content was observed on the failed Si surfaces compared to that on the as-prepared SCA/Si surfaces. The Si contents on the failed Si surfaces modified with either SCA-1 or SCA-2 were slightly lower those on the as-prepared SCA-1 and SCA-2 surfaces, respectively. This comparison suggests that only minor amounts of silane debonded from the Si surfaces. This finding indicates that failure occurred interfacially and to a large extent at the epoxy/SCA interface, with minor failure at the SCA/Si interface (See Figure 6-7).

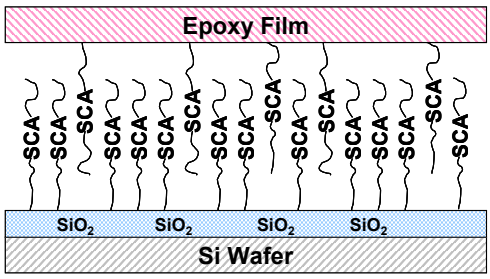

Figure 6-7. Proposed failure mode for model epoxy/SCA/Si bonded samples; failed in the probe test after immersion at either 70 ^{o}C (1 month) or 25-70 ^{o}C (1 month) in either pH 4 or pH 9 buffer solutions. (Not drawn to scale).

Table 6-4. Elemental surface compositions (atomic %) for as-prepared and failed bonded surfaces after the probe test with immersion at 70 °C (static) or 25-70 °C (cyclic) in pH 4 and pH 9 buffer solutions.

Type of Surfaces	Sample	C	O	Si	N
As-prepared surfaces **(prior to bonding)**	Model epoxy, as prepared	81.6	18.4	<0.1	<0.1
	Si, as received, SCA-1	33.2	31.2	32.1	3.5
	Si, as received, SCA-2	44.6	28.6	22.8	4.0
Failed surfaces **(after debonding)**	Failed Si side, SCA-1, **70 °C**, pH4	40.7	32.8	23.3	2.2
	Failed epoxy side, SCA-1, **70 °C**, pH4	76.5	21.8	1.2	0.5
	Failed Si side, SCA-2, **70 °C**, pH4	44.3	33.7	19.9	2.2
	Failed epoxy side, SCA-2, **70 °C**, pH4	77.6	21.6	0.5	0.4
	Failed Si side, SCA-1, **70 °C**, pH9	31.4	40.8	25.7	2.1
	Failed epoxy side, SCA-1, **70 °C**, pH9	77.6	21.3	0.6	0.5
	Failed Si side, SCA-2, **70 °C**, pH9	35.4	40.4	21.4	2.8
	Failed epoxy side, SCA-2, **70 °C**, pH9	77.5	20.7	1.1	0.7
	Failed Si side, SCA-1, **25-70 °C**, pH4	33.5	35.0	29.5	2.0
	Failed epoxy side, SCA-1, **25-70 °C**, pH4	76.5	21.2	1.5	0.8
	Failed Si side, SCA-2, **25-70 °C**, pH4	43.2	30.8	24.1	2.0
	Failed epoxy side, SCA-2, **25-70 °C**, pH4	77.1	21.2	1.3	0.4
	Failed Si side, SCA-1, **25-70 °C**, pH9	29.3	40.6	28.0	2.1
	Failed epoxy side, SCA-1, **25-70 °C**, pH9	77.8	20.9	0.6	0.7
	Failed Si side, SCA-2, **25-70 °C**, pH9	39.8	34.8	22.3	3.1
	Failed epoxy side, SCA-2, **25-70 °C**, pH9	77.8	20.6	1.2	0.5

6.3.2.2 Failed Wedge Test Specimens

Following the durability studies for DCB specimens immersed in pH 4 and pH 9 buffer solutions under either static (70 °C) or cyclic (between 25 °C and 70 °C) temperature conditions, samples were retrieved from solutions after crack propagation had arrested and Si DCB strips were separated by mechanical force. To analyze the failure mode, surfaces near the arrested crack front on the failed epoxy side and failed Si side were analyzed by XPS. The surface compositions for the various sample surfaces are summarized in Table 6-5.

For specimens that failed under static immersion at 60 ^{o}C for both pH conditions, the respective failed epoxy and Si surfaces showed surface compositions that were different to some extent compared to the respective as-prepared surfaces. The C content on the failed Si surface was slightly higher than that for the as-prepared SCA/Si surface, which suggests that minor failure occurred at the surface of the epoxy film. The Si and N contents on the failed silicon surfaces were lower than the corresponding compositions on the as-prepared surface. Minor Si components attributed to silane were also detected on the failed epoxy side surface. These findings support the conclusion that failure occurred primarily at the SCA/epoxy interface (Figure 6-8a). This failure mode is similar to that for the test specimens immersed at 70 ^{o}C. The failure mode was equivalent when comparing tests for different silane surfaces or immersion under different pH conditions.

For specimens that failed under cyclic thermal testing at both pH conditions, a significantly greater SCA silicon content (at ~102.2 eV) was detected on all failed epoxy surfaces. This result, no doubt, indicates that debonding occurred to a greater extent at the SCA/Si interface (Figure 6-8b) under the cyclic thermal conditions than for tests under the static thermal conditions. Since the parameters for surface preparation and exposure to chemical environments were the same, this change of failure mode can only be attributed to the stress build up across the epoxy/SCA/Si interface during the thermal expansion and contraction under the cyclic temperature test conditions. Thus, the SCA/Si interface was more affected by the thermal stress than the epoxy/SCA interface. This finding may be attributed to the possibility that the bond(s) between silane (or oligomeric silanes) and the Si surface has (have) less flexibility than the linkage between the amine and epoxy functionalities. Thus, more failure occurs at the SCA/Si interface under thermal stress.

Table 6-5. Elemental surface compositions (atomic %) for as prepared and failed bonded surfaces after DCB wedge tests with immersion at 70 °C (static) or 25-70 °C (cyclic) in pH 4 and pH 9 buffer solutions.

Type of Surfaces	Sample	C	O	Si	N
As-prepared surfaces **(prior to bonding)**	Model epoxy, as prepared	81.6	18.4	<0.1	<0.1
	Si, as received, SCA-1	38.5	31.2	27.1	3.2
	Si, as received, SCA-2	44.6	28.6	22.8	4.0
Failed surfaces **(after debonding)**	Failed Si side, SCA-1, **70 °C**, pH4	45.3	34.6	18.3	1.9
	Failed epoxy side, SCA-1, **70 °C**, pH4	77.9	21.2	0.5	0.4
	Failed Si side, SCA-2, **70 °C**, pH4	44.7	34.5	18.8	2.0
	Failed epoxy side, SCA-2, **70 °C**, pH4	81.0	17.6	0.9	0.5
	Failed Si side, SCA-1, **70 °C**, pH9	50.3	31.9	16.6	2.3
	Failed epoxy side, SCA-1, **70 °C**, pH9	79.7	19.0	0.7	0.6
	Failed Si side, SCA-2, **70 °C**, pH9	45.7	33.5	18.8	2.0
	Failed epoxy side, SCA-2, **70 °C**, pH9	80.0	18.8	0.7	0.6
	Failed Si side, SCA-1, **25-70 °C**, pH4	48.5	32.7	16.7	2.0
	Failed epoxy side, SCA-1, **25-70 °C**, pH4	73.4	21.3	3.9	1.4
	Failed Si side, SCA-2, **25-70 °C**, pH4	34.2	41.3	23.3	1.3
	Failed epoxy side, SCA-2, **25-70 °C**, pH4	67.8	26.4	4.5	1.3
	Failed Si side, SCA-1, **25-70 °C**, pH9	44.3	34.6	18.4	2.7
	Failed epoxy side, SCA-1, **25-70 °C**, pH9	74.1	20.8	3.8	1.3
	Failed Si side, SCA-2, **25-70 °C**, pH9	35.3	38.8	24.2	1.7
	Failed epoxy side, SCA-2, **25-70 °C**, pH9	68.8	22.4	6.5	2.3

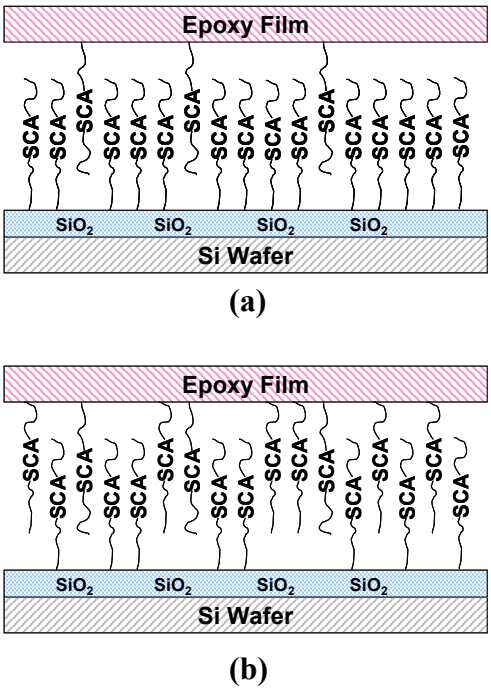

Figure 6-8. Proposed failure mode for model epoxy/SCA/Si bonded sample; failed in the DCB test after immersion at either (a) 70 ^{o}C (1 month) or (b) 25-70 ^{o}C (1 month) in either pH 4 or pH 9 buffer solutions. Note the greater extent of failure at the silane/SiO_2 interface for the 25-70 ^{o}C cyclic test. (Not drawn to scale).

6.4 Conclusions

The failure mode of the model epoxy/SCA/Si bonded specimens with different bond geometries that were exposed to various pH and thermal conditions has been determined using XPS. For the film-on-substrate bond geometry, the failure mode was affected by the duration of exposure of the bond interface to chemical environments. Long-term immersion (several months) led to a greater extent of debonding at the SCA/Si interface which was likely caused by hydrolysis of the Si-O-Si bonds under basic conditions. Under short-term immersion (30 days), the effect of the chemical environment on the failure mode was not substantial. It should be noted for either long or short-time immersion, the greater percentage of failure occurred at the epoxy/SCA interface.

The location of the bond failure was largely influenced by mechanical stresses applied to the epoxy/SCA/Si interface, in that failure occurred more at the epoxy/SCA interface, but less at the stronger SCA/Si interface. For the DCB specimen bond geometry, different failure modes were observed depending on the thermal conditions. The SCA/Si interface was more sensitive toward the cyclic thermal condition, resulting from the stress build-up in the specimen. Bond failure occurred to a greater extent at the SCA/Si interface under thermal stress.

6.5 References

[1] R. K. Iler, in "The Chemistry of Silica", Wiley: New York, 1979, Chap 2.

7. Conclusions

This study has investigated the adhesion and durability of model epoxy/SCA/SiO_2/Si bonded specimens as a function of the type of surface preparation, pH of the media, temperature, cyclic thermal stress, and external applied stress. Bond degradation was caused principally by the diffusion of fluids through the bulk epoxy coating resulting in the formation of liquid containing blisters at the epoxy/Si interface. The bond durability (i.e., appearance of blister formation) depends critically on the nature of the epoxy/SCA/Si interface.

Bond durability increased for the model epoxy/SCA/O_2 plasma treated/Si bonded samples as the oxygen plasma pre-treatment time increased. However, the amount of silane deposited on the Si surface (as shown by the Si-O-Si/SiO_2 ratio) showed no correlation with the duration of oxygen plasma pre-treatment. However, the configuration of adsorption of hydrolyzed silanes and the SiO_2 surface may be affected by the oxygen plasma pre-treatment time, with the longer O_2 treatment yielding a cleaner, more uniform silicon oxide surface. The interfacial adhesion strength as measured by the critical strain energy release rate in the probe test for different silane-modified surfaces, correlated strongly with the nature of the amine functionalities on the silicon surface. The relative percentage of unprotonated (free) amine (compared to protonated amine) was significantly lower for a SCA-1 modified surface than for the SCA-2 and SCA-3 modified surfaces, leading to a less reactive silane surface toward the epoxy.

The durability of the model epoxy/SCA/Si bonded systems showed a general trend that depended on the silane coupling agent used to modify the adherend surface. Durability varied in the manner SCA-2 > SCA-3 > SCA-1 > no silane. Bond durability dependent on the pH of the aqueous environment. Better durability was observed in weakly acidic conditions (pH 4), a fact that is associated with the rate of hydrolysis of either the amine-epoxy linkage or the SCA-Si bonds. However, an opposite dependence on fluid pH was observed for durability tests in various formulated solutions; better

durability was noted at high pH (pH 9). This latter finding suggests that other solution components (i.e., surfactant, solvents, salts, etc.), influence bond durability to a greater extent than solution pH, either singularly or synergistically.

The in-situ probe test results showed no difference in debond profile for different water-solvent mixtures containing surfactant (a surfactant), diol-1, and diol-2 if the bond specimens were not pre-soaked in liquid solutions. For pre-soaked specimens, the solution composition containing diol-2 was more aggressive with respect to interfacial degradation. The surfactant component had a limited 'add-on' effect rather than a synergistic effect.

The subcritical debonding results obtained using the double cantilever beam specimen with the same bonded system showed diffusion controlled debond behavior and a $G_{threshold}$ when tested under static 70 ^{o}C conditions. Only limited crack growth was observed for 25 ^{o}C-70 ^{o}C cyclic loading. This difference suggests that thermal energy is an important factor that controls the rate of diffusion of water into the region at the crack tip.

The failure modes for the model epoxy/SCA/Si bonded samples with different bond geometries having been exposed to various pH and thermal conditions were determined using XPS. Because the silane interface is thin (mono to bilayer), uniform cohesive failure within the silane layer was not observed. Rather, failure usually occurred interfacially at the epoxy/SCA or at the SCA/Si interface. Long-term immersion at pH 9 led to a greater extent of debonding at the SCA/Si interface which was likely caused by hydrolysis of the Si-O-Si bond. For short-term immersion (~30 days), the effect of the chemical environment on the failure mode was not substantial. The location of the bond failure was largely influenced by mechanical stresses applied to the epoxy/SCA/Si interface, in that failure occurred more at the epoxy/SCA interface.

8. Future Directions

This research could be extended into two areas in future studies.

1) The in-situ probe test could be conducted at elevated temperatures (temperature of the chemical environment as well as the bonded specimen) while the crack front is under stress in the probe test. The results from this study will reveal the effect of temperature on debond profile/behavior resulting from the interaction of fluids at the stressed bond interface. To perform this study, modification/construction of a special heating stage is needed to generate an isothermal condition for the bonded specimen during the test.

2) A more accurate analytical model is needed to deduce the strain energy release rate. The experimental results showed that a pure bending based formulation is not sufficient for computing the strain energy release rate. Hence, an analysis considering both bending and stretching is required.

VITA

Dingying Xu was born on July 13, 1972 to Peiyuan and Fengmei Xu in Shanghai, China. He came to US in 1991 to join his parents who arrived several years earlier. After graduating from Liberty High School (Bethlehem, PA) in 1992, he began his undergraduate career at Allentown College (now DeSales University) in Center Valley, PA as a chemistry major under Dr. Rodger Berg as an academic advisor. During his senior year in college, he pursued undergraduate research in the area of conducting polymers under Dr. Michael S. Freund at Lehigh University. In May 1996, he graduated *cum laude* with a BS degree in Chemistry. He entered the graduate chemistry program at Lehigh University, and subsequently pursued polymer research involving the synthesis and characterization of composite latex polymer particles under the direction of Prof. Mohamed S. El-Aasser. After graduating from Lehigh with a MS degree in Polymer Science and Engineering in 1999, he was employed as an R&D Chemist at Electronic Specialty Chemicals (ESC) Inc. in Bethlehem, PA. In August 2000, he came to Virginia Tech in Blacksburg, VA to pursue his doctoral degree. Under the guidance of Prof. John G. Dillard, he performed research in the areas of adhesion, durability, and surface modification as related to microelectronics. Following the completion of his Ph.D. in June 2004, he will assume a position of Sr. Packaging Engineer at the Intel Corporation in Chandler, AZ.